ANALYSIS OF THE EFFECT OF REDUCING ACCIDENTS INVOLVING PEDESTRIANS THROUGH THE COORDINATION OF ACTIVE SAFETY AND PASSIVE SAFETY

Yuichi Omoda
Yuji Arai
Kazunori Kikuchi
Ryohei Homma
Hisashi Imanaga
Japan Automobile Research Institute
Japan

Nobuhiko Takahashi
Japan Automobile Manufacturers Association
Japan

Paper Number 23-0025

ABSTRACT

In order to efficiently reduce traffic fatal accidents, it is important that all parties involved in traffic safety (traffic participants, road infrastructure, and vehicles) work in unison to implement countermeasures. For this purpose, it is necessary to analyze the reduction effects of vehicle safety measures, the limitations of vehicle safety measures, and the accident patterns that remain after the vehicle safety measures are taken. In this study, the fatal accident reduction effect of vehicle safety measures combined with active and passive safety technologies was estimated for the accidents involving pedestrians, which are the most common type of fatal traffic accidents in Japan. In addition, the characteristics of fatal accidents in which vehicle safety measures are not currently addressed are summarized.

First, we estimated the extent to which pedestrian fatalities can be reduced through the AEB for pedestrians and improvement of pedestrian head protection performance. For the remaining fatal accidents, we estimated the number of fatal accidents that could be reduced by expanding AEB functions (additional fatal accident reduction effects are expected by increasing AEB corresponding scenarios) and by other vehicle safety measures (advanced emergency steering systems, etc.). This clarifies the extent of fatal accidents that have not yet been addressed by vehicle safety measures. This study used accident data collected by the Japan Institute for Traffic Accident Research and Data Analysis (ITARDA) from year 2015 to 2017. The analysis assumed a vehicle safety measure penetration rate of 100%.

It was found that the number of fatal accidents could be reduced by 20% and 29% by the AEB for pedestrians and improving the performance of pedestrian head protection in the daytime and nighttime, respectively. It could also be observed that AEB function expansion and devices other than AEB covered approximately 38% and 23% in the daytime and nighttime, respectively. The results suggest that the accident reduction effect of AEB for pedestrians is significant, but that 42% and 48% of accidents are left behind even when the functional enhancements of AEB and other vehicle safety measures are added up in the daytime and nighttime, respectively. In order to further reduce the number of accidents left behind, it is efficient to to promote not only vehicle safety measures but also measures for the society as a whole.

PURPOSE

The number of traffic accident fatalities in Japan was 2,636 in 2021 [1], and although it is steadily declining, the downward trend has slowed. In particular, the proportion of pedestrians in the number of traffic accident fatalities is increasing, and under the safety concept of putting people first, the safety of pedestrians must be ensured. To achieve a society without traffic accidents, more effective and efficient traffic safety measures must be strongly promoted throughout all parties involved in traffic safety (traffic participants, road infrastructure, and vehicles).

To that end, we first need to estimate the effect of currently anticipated measures (i.e., the number of traffic accident fatalities reduction effect), then, organize the issues for reducing the number of accidents further after the implementation of such measures, and propose new measures with a view towards cooperation that is based not only on vehicles but on people and the road as well. In terms of vehicle safety measures, there are active safety technologies and passive safety technologies, and when estimating the effects of such measures, the combination of both technologies are assumed to produce continuous effects in light of the chronological flow of accidents (Figure 1). Therefore, it is ideal to estimate accident reduction effects by combining the two technologies.

However, there are only a few cases in which the effects of combining the two technologies were estimated.

The purpose of this study is to promote initiatives aimed at eliminating traffic accident fatalities. To that end, we attempted an analysis to derive the traffic accident fatality reduction effect by combining active safety technologies and passive safety technologies, with a focus on fatal accidents involving pedestrians. Furthermore, we analyzed the characteristics of fatal accidents that are currently not addressed in vehicle safety, and organized the perspectives for future safety measures.
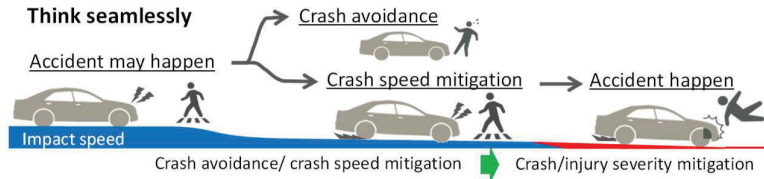
Figure 1. Concept of vehicle safety measures by combining active safety and passive safety with pedestrian accidents
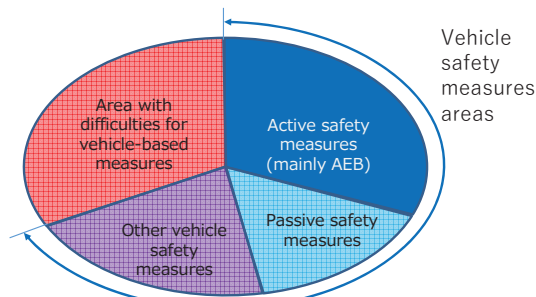
ANALYSIS METHOD

Overall policy

Figure 2 shows the basic concept of the analysis. In this study, we aimed to classify the areas that can be addressed by vehicle safety measures and those that are difficult to address with vehicle safety measures, and accidents corresponding to each area were aggregated using national traffic accident statistical data (macro accident data). The areas that can be addressed by vehicle safety measures were further subdivided into three areas: active safety measures (Advanced Emergency Brakes (AEB)), passive safety measures, and other vehicle safety measures. For the reduction effects of active and passive safety measures, we targeted the typical equipment in the pedestrian accident, and when estimating the reduction effect of passive safety measures, we aimed to avoid overlap with the reduction effect of active safety measures. This method is described in detail in two next Section. As for other vehicle measures, equipment that is not yet widespread but whose dissemination is expected in the future was selected, and the areas of the target accidents were indicated.

Figure 3 shows the analysis flow for pedestrian accidents. First, we focused on AEB for pedestrian (henceforth, "AEB"), a typical item of active safety measures for reductions that can be expected in vehicle safety measures against pedestrian accidents. The accidents within the scope of AEB operation were classified into those for which reductions can be expected and those for reductions would be difficult (fatal accidents that would be targeted by AEB but for which reductions could not be achieved owing to the decreased performance of the AEB = reduction difficulty). Next, we estimated the extent to which fatal accidents involving pedestrians among accidents for which AEB reduction is difficult and accidents that are not targeted by the AEB could be reduced by designing vehicles with improved pedestrian head protection performance. We also estimated the area of other vehicle safety measures. Specifically, we estimated the number of fatal accidents that could be reduced by enhancing the AEB functions (i.e., additional fatal accident reduction effects can be expected by widening the sensing range and thereby diversifying the AEB response scenarios) or other vehicle safety measures (e.g., device for pedal misapplication prevention, automatic high beam, Advanced emergency steering system). The remaining accidents are currently unaddressed fatal accidents that cannot be addressed through vehicle safety measures.

In this estimation, we targeted accidents from 2015 to 2017, when the AEB had just begun to spread, and assumed that the AEB dissemination rate was 0%. We estimated the number of fatal accidents that would be reduced if the AEB were 100% disseminated.
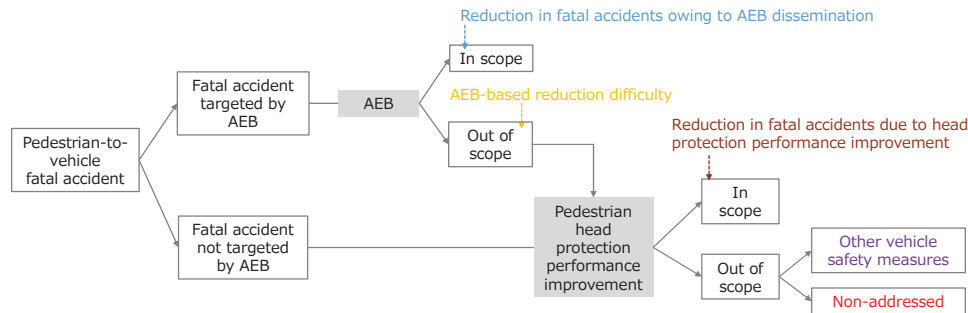

Figure 2. Accident classification method

Figure 3. Pedestrian accident analysis flowchart

Estimation of fatal accident reduction effect of AEB

We used the macro accident data to estimate the effect of the AEB on fatal accident reduction. The basic idea of estimating the accident reduction effect was to calculate the number of accidents that can be prevented by equipping the vehicle with an AEB. The target AEB-installed vehicles were four-wheeled vehicles (ordinary passenger + light(Kei) passenger + regular cargo + light(Kei) cargo) for which the Japan New Car Assessment Program (JNCAP) started evaluation tests from FY2016 and future installation was expected. Figure 4 shows the procedure for effect estimation. First, we extracted the accident scenes where accident reduction could be expected by the AEB according to its function (i.e., accidents targeted by AEB). The commercially available AEB applies brake control when the system determines that a collision is unavoidable based on the distance and speed of a pedestrian crossing the road as the vehicle is traveling straight ahead, and the conditions for extracting a specific accident were set as listed subsequently. Additionally, it is difficult to address scenes in which a pedestrian suddenly rushes out of a blind spot. Therefore, in addition to the extraction conditions, accidents involving a pedestrian "rushing out" in violation of the law were excluded as being out of the scope of support. Accidents within the extraction conditions were aggregated, regardless of whether four-wheeled vehicles driver's fault or not.

・Accident type: pedestrian-to-vehicle accident(as pedestrian crosses road)
・Action type: driving straight ahead
・AEB Operating speed range: driving speed (hazard recognition speed for four-wheeled vehicles) not exceeding 60 km/h
・Pedestrian law violations: other than rushing out

The 2021 JNCAP AEB for pedestrian test results indicate that most of the vehicle models tested earned perfect scores. Therefore, it is assumed that AEB could prevent fatalities in all extracted accidents. However, the JNCAP results were obtained under limited conditions, and in an actual traffic environment, the AEB may not operate normally even within the above extraction conditions (i.e., conditions in which it functions) owing to the weather or the state of the detection target (i.e., when the contour of the entire pedestrian's body is vague, such as when the pedestrian is slouching or wearing a raincoat) [2]. Excluding such conditions from the aggregate conditions of the macro accident data, although desirable for more precise prediction of effects, is difficult. Therefore, in this study, we estimated the extent to which the number of accidents were reduced after the introduction of AEB by applying a coefficient for converting the JNCAP evaluation results under limited conditions into performance under the actual environment (i.e., traffic environment application coefficient).

The Ministry of Land, Infrastructure, Transport and Tourism [3] evaluated the degree to which accidents were reduced by an AEB with average performance. In the study, macro accident data (2016) were used to estimate the accident rate of vehicles with and without an AEB (number of accidents per 1,000 vehicles per year), as shown in Table 1. The daytime accident reduction rate (which expresses the number of accidents that can be avoided by equipping a vehicle with pedestrian AEB) were 35.7%. However, this value was attributed to not only the AEB performance but traffic environment factors as well. Therefore, we investigated the JNCAP results, which indicated the AEB performance, to extract traffic environment factors. The JNCAP performance evaluation results of AEB in the same period as the evaluation' period are summarized in Table 2. For example, at a test speed of 30 km/h, 95.8% of the vehicles successfully stop in front of the pedestrian target (=accident reduction rate); however, at 60 km/h, the accidence reduction rate, at 33.3%, was different as a result of speed, and the range was 33.3–95.8%. The accident avoidance rate of the AEB was applied to the accident data from 2015–2017 and it was found that the AEB reduced the accident rate by 76.4% (=10687.39/13980) on the average. Therefore, the traffic environment application coefficient was calculated as 0.467 (=0.357/0.764). Strictly speaking, it is possible that the traffic environment application coefficients during the day are different from those at nighttime. However, in this study, we assumed that they were the same.

Omoda 3

Table 3 shows the final reduction effect of the AEB. In 2015–2017, there were a total of 3,441 accidents involving pedestrian fatalities, 1,855 of which were within the scope of AEB operation. Of this number, a total of 866.29 cases (=1855×0.467) were found to be reduction cases.
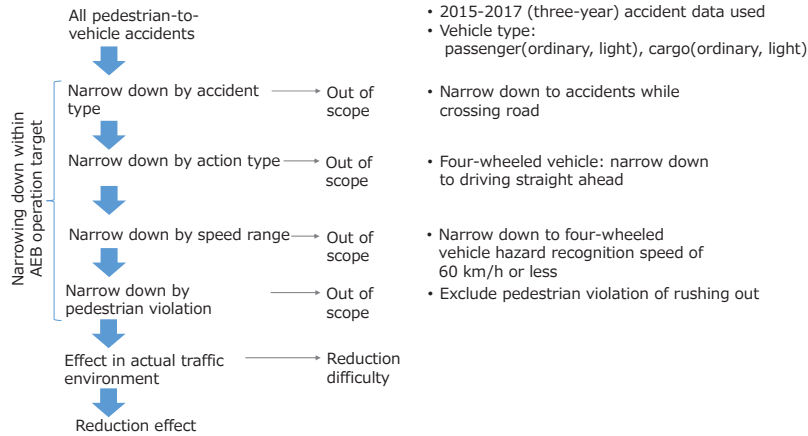

Figure 4. Reduction effect estimation flowchart for AEB for pedestrian

Table 1. Average AEB for pedestrian accident reduction rate (daytime)[3]

Accident rate	Equipped	0.09
(number of accidents per 1,000 vehicles per year)	Unequipped	0.14
Accident reduction rate		35.7%

（Accident reduction rate） ＝1 - (Accident rate of equipped vehicle) / (Accident rate of unequipped vehicle)

Table 2. Test results of AEB for pedestrian in JNCAP (daytime) and estimated number of accident reductions

		Collision speed (km/h)						
		Collision Avoidance	≤10	≤20	≤30	≤40	≤50	≤60
Initial speed (≒Hazard recognition speed) (km/h)	≤10	44.4%	55.6%	-	-	-	-	-
	≤20	81.9%	0.0%	18.1%	-	-	-	-
	≤30	95.8%	1.4%	0.0%	2.8%	-	-	-
	≤40	76.4%	1.4%	11.1%	6.9%	4.2%	-	-
	≤50	61.1%	0.0%	2.8%	8.3%	15.3%	12.5%	-
	≤60	33.3%	0.0%	19.4%	6.9%	4.2%	4.2%	31.9%

Hazard recognition speed (km/h)	Number of accidents	Accident reduction
≤10	2097	931.07
≤20	3761	3080.26
≤30	3741	3583.88
≤40	3142	2400.49
≤50	1004	613.44
≤60	235	78.26
Total	13980	10687.39

Table 3. Fatal accident reduction effect of AEB for pedestrian

Hazard recognition speed [km/h]	≤10	≤20	≤30	≤40	≤50	≤60	≤70	≤80	≤90	≤100	＞100	Others	Total
Total number of pedestrian to vehicle fatal accidents	248	327	276	720	921	648	195	66	15	10	8	7	3441
AEB targeting fatal accidents	4	24	120	515	693	499	–	–	–	–	–	–	1855
Fatal accidents reduction by AEB	1.87	11.21	56.04	240.51	323.63	233.03	–	–	–	–	–	–	866.29

Estimation of fatal accident reduction effect by pedestrian head protection performance improvement

A majority of injuries to pedestrians in fatal accidents are head injuries. Therefore, a shock-absorbing structure for the front part of the vehicle, such as a bonnet hood, has been adopted as a technology for pedestrians as a passive safety measure. In this study the reduction effect of this measure were analyzed.

Figure 5 shows the relationship between all pedestrian accidents and accidents where fatalities could be avoided by improved pedestrian head protection performance. The reduction effect (s) was obtained by multiplying the pedestrian head protection target accident (S) with the effect (E) arising from the improved pedestrian head protection. Pedestrian head protection performance is considered effective in accidents where fatalities cannot be prevented by the AEB. Therefore, it is crucial to prevent overlapping effects with AEB when estimating the effect of improved pedestrian head protection on fatal accident reduction. We estimated the effect through the following procedure.

1) Estimate the number of fatal accidents that could be prevented by improving head protection performance ($s_{\alpha+\beta+\gamma}$)

2) Estimate the number of fatal accidents that were avoided with AEB that could be avoided by improving head protection performance (s_β)
3) Estimate the number of fatal accidents that could be avoided by improving head protection performance, excluding the overlapping effect with AEB ($s_{\alpha+\beta+\gamma}$ - s_β)

Of all pedestrian accidents, those that are targeted by head protection $S_{\alpha+\beta+\gamma}$ were extracted by applying the following restrictions.
・collision site where a pedestrian collide : "front of four-wheeled vehicle"
・body part of a pedestrian mainly injured: "head"

Accidents where fatalities were prevented by the AEB and were subject to head protection (S_β) were obtained by limiting the AEB accident reduction effects in the previous section to those subject to head protection.
For improvement of the pedestrian head protection performance, we estimated the degree to which fatal accidents could be reduced if vehicles with performance equivalent to JNCAP Level 5 became widespread. The effect is assumed to the difference in the fatality rate between the average performance of vehicles from 2010 to 2017 and the performance of vehicles that acquired JNCAP Level 5 during the same period. Figure 6 shows the the results of fatality rates by speed (number of fatal accidents / (number of fatalities + serious injuries + minor injuries)), and Figure 6(b) shows the fatality rate by speed, as estimated by logistic regression, based on Figure 6(a). It can be confirmed that JNCAP Level 5 had a lower fatality rate over a wide speed range.
Table 4 shows the number of fatal accidents that were reduced by improving the pedestrian head protection performance. The estimated result after excluding the overlap with the final AEB was 41.50 cases.
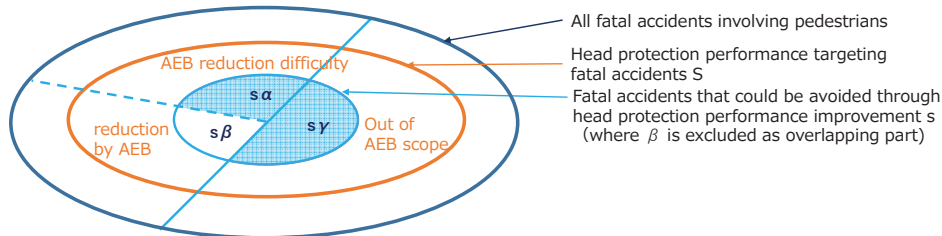
Figure 5. Relationship between AEB for pedestrian and number of fatal accidents that could be reduced by pedestrian head protection performance
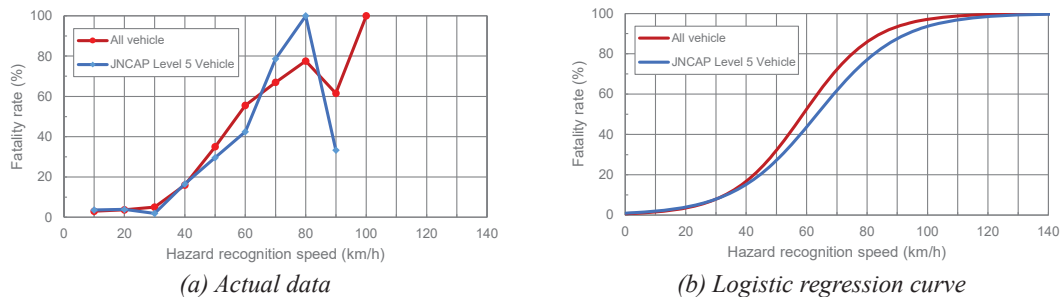
(a) Actual data   *(b) Logistic regression curve*
Figure 6. Fatality rate by hazard recognition speed

Table 4. Reduction effect of improved head protection performance

Hazard recognition speed [km/h]		≤10	≤20	≤30	≤40	≤50	≤60	≤70	≤80	≤90	≤100	Total
Number of fatal accidents	$S_{\alpha+\beta+\gamma}$	38	81	75	280	357	254	89	34	8	4	1220
	S_β	1.40	1.40	15.41	88.26	125.16	88.26	—	—	—	—	319.90
Fatality rate reduction %	E	-0.41	-0.43	-0.01	1.58	4.92	8.85	10.43	8.81	5.96	3.52	—
Fatal accident reduction	$s_{\alpha+\beta+\gamma}(=S_{\alpha+\beta+\gamma}\times E)$	-0.16	-0.35	-0.01	4.42	17.56	22.48	9.28	3.00	0.48	0.14	56.85
	$s_\beta(=S_\beta\times E)$	-0.01	-0.01	0.00	1.39	6.16	7.81	—	—	—	—	15.35
	$s_{\alpha+\gamma}(=s_{\alpha+\beta+\gamma}-s_\beta)$	-0.15	-0.34	-0.01	3.03	11.41	14.67	9.28	3.00	0.48	0.14	41.50

Survey of other vehicle safety measures
In this section, we summarize the initiatives for vehicle safety measures other than AEB and pedestrian head protection performance improvement. We made selections based on technologies that target pedestrian accidents among the technologies summarized in the ASV (Advanced Safety Vehicle) Technologies Overview [4] as initiatives of other vehicle safety measures. The selections were divided into two categories: enhancements of

AEB function and devices other than AEB. Devices that are mainly intended to reduce driving-related burdens (i.e., devices classified as driving load reduction control) were excluded from this study.

Enhancements of AEB function

In the ASV Technologies Overview, driving assistance technologies for passenger cars, which are positioned as an accident avoidance support control function with a function for controlling braking devices include low-speed vehicle peripheral collision mitigation braking devices (Peripheral sonar with brake) and rear obstacle collision mitigation braking devices(Rear cross traffic advanced emergency brake). It was not clearly specified that the target accident is a pedestrian-vehicle accident for any of the devices. However, it is expected that the devices will be expanded in the future.

Current AEB were designed mainly to respond to events in which a vehicle equipped with this function traveling "straight ahead" collides with a "pedestrian crossing the road" . However, improvements in pedestrian detection performance can expand the events that can be handled. Meanwhile, the NCAP in each country has started to evaluate AEB performance for bicycle accidents and intersection accidents [5], [6]. For example, if the device can respond to rear-end collisions with bicycles, then it can be expected to reduce the number of collisions with pedestrians facing or backing to a vehicle, and collisions when vehicle are overtaking or passing a pedestrian. Additionally, the ability to respond to accidents at intersections is expected to detect pedestrians when the vehicle is turning left or right at intersections. Table 5 shows the expected accident reduction areas by the AEB function expansion.

Table 5. Areas expected to benefit from AEB function expansion

Device name	Accident type	Vehicle behavior type	Vehicle speed range
Low-speed vehicle peripheral collision mitigation braking device	・While working on road, ・While playing on road	・Other than backing up	・Low-speed range
Rear obstacle collision mitigation braking device	・Other than while lying on road	・Backing up	・Low-speed range
Expanded AEB pedestrian detection range (rear-end collision)*	・While crossing road, ・Facing to vehicle / back to vehicle, ・While standing on road	・Straight ahead, ・Overtaking / passing, ・Changing course,	・Low- / medium-speed range
Expanded AEB pedestrian detection range (intersection)*	・While crossing road ・Facing to vehicle / back to vehicle ・While stationary on road	・Left / right turn, ・While turning	・Low-speed range

Low-speed range: 30 km/h or less; medium-speed range: 30 km/h –60 km/h; high-speed range: >60 km/h
*Not name of device

Devices other than AEB

Accident types that are difficult to address using AEB include "accidents in which the brake pedal is mistaken for the accelerator" and "accidents when the speed range is high". In both cases, there may be interference between the AEB brake control and the driver's operation, such that the device may be unable to actively intervene in braking. To avoid interference with the driver's operation, driving support system generally prioritize the intention of the driver [7], and in the event of an accident in which the driver accidentally steps on the accelerator instead of the brake, the device may prioritize the driver's accelerator position. Therefore, it is difficult for the system to intervene in braking even if the driver operates the accelerator pedal by mistake. Pedal misapplication prevention device compatible with pedestrians detection is expected to spread in the future [8].

On high speed, avoidance by steering is more effective than avoidance by braking [9]; therefore, braking interventions by the device are delayed to avoid interference with the driver's steering avoidance operation. An advanced emergency steering system, which was commercialized in 2017 [10], may be able to respond to accidents in the high-speed range. The device enables pedestrian accident avoidance by intervening in steering when pedestrians are in front of the vehicle and it is impossible to avoid an accident using AEB alone.

Another type of accident that is difficult for AEB to address is "the accidents when pedestrian lies on the road (road-lying accidents)". In road-lying accidents, the pedestrian who is lying on the road can have a variety of postures, and it is currently considered technically difficult to respond to such pedestrians using AEB [11]. Advanced lights may enable drivers to better detect pedestrians, thus avoiding road-lying accidents. Advanced lights include four devices related to headlights, high-intensity headlights, variable orientation headlights, automatic switching headlights, and automatic anti-glare headlights. Among these devices, automatic anti-glare headlights will reduce accidents, considering that the "majority of nighttime pedestrian accidents occurred while driving with low beams, and that it has been indicated that in many cases, such accidents may possibly have been avoided if driving with high beams" [12]. It is difficult to obtain the effects of high beams at low-speed ranges. Therefore, there are many vehicle models in which the device operates at medium-speed ranges (over 30 km/h)

Omoda 6

and higher.

From the above results, the pedal misapplication prevention device, advanced emergency steering system, and automatic anti-glare headlights are considered specifically effective for accident types that are difficult to address using AEB. Table 6 shows the accident areas in which devices other than AEB are expected to have an effect. The area where the effects of these devices are expected may overlap with the area of AEB function expansion. However, in the case of overlap, we decided to prioritize the AEB function expansion.

Table 6. Areas where vehicle safety measures other than AEB are expected to be effective

Device name	Accident type	Vehicle behavior pattern	Speed range etc.
Pedal misapplication prevention device	Unlimited	Unlimited	・Low-speed range ・Operational error
Advanced emergency steering system	・Other than during crossing	・Straight ahead	・Medium-/high-speed range
Automatic anti-glare headlights	・Lying on road	・Straight ahead	・Medium-/high-speed range ・Night

Low-speed range: 30 km/h or less, medium-speed range: between 30 km/h and 60 km/h, high-speed range: over 60 km/h

RESULTS AND DISCUSSION OF THE STATUS OF INITIATIVES TO REDUCE FATAL ACCIDENTS INVOLVING PEDESTRIANS THROUGH VEHICLE SAFETY MEASURES

Results

Figure 7 shows the results of categorizing fatal accidents involving pedestrians according to daytime and nighttime. These data were the total number of fatalities from 2015 to 2017. The accident reduction estimation were carried out in case that the dissemination of AEB and improvement of pedestrian head protection performance is 100%. Meanwhile, the areas of other vehicle safety measures are areas where not all accidents can be reduced by the other vehicle safety.

Figure 7 shows that, the rate of fatal accidents can be reduced by approximately 20% and 29%, respectively, by dissemination of AEB and improvement of pedestrian head protection performance in the daytime and nighttime. It could also be observed that AEB function expansion and devices other than AEB covered approximately 38% and 23% during the daytime and nighttime, respectively. Meanwhile, when combining the areas where accident reduction with AEB is difficult and those that are not addressed (by current vehicle safety measures), the areas that it is difficult for the vehicle safety measure to prevent fatal pedestrian accident are left approximately 42% and 48% of fatal accidents in the daytime and nighttime, respectively.

Characteristics of non-addressed areas

Figure 8 shows the categorization of fatal accidents involving pedestrians by hazard recognition speed and by day/night. Three areas with many accidents can be observed as characteristics of the "non-addressed" areas: (1) low-speed range (30 km/h or less) in daytime; (2) high-speed range (over 60 km/h) at night; and (3) low-speed range (30 km/h or less) at night. Therefore, we further analyzed the characteristics of accidents in each area according to the accident location.

(1) Low-speed range in daytime

Figure 9 shows the number of fatal accidents in non-addressed areas according to accident location and speed range. Figure 9(a) shows that there were 153 cases at the low-speed ranges of 30 km/h or less during the day, which accounted for approximately 77% of the total. Of these, approximately 45% (=69/153) occurred in other locations used for public traffic, which include parking lots of stores, as well as squares, vacant lots. In the future, it is important to take measures against accidents that occur in such locations. However, in the macro accident data classification, the types of accidents that occur in other locations used for public traffic are often classified as "other", which makes it difficult to glean details from such data.

(2) High-speed range at night

Figure 9(b) shows that there were 215 cases at high-speed ranges exceeding 60 km/h during the night, which accounted for approximately 53% (=215/406) of the total. Of these, 205 occurred in areas equivalent to arterial roads with a road width of 5.5 m or more (henceforth, referred to as "arterial road"). Furthermore, of the 205 cases, 67% (=138/205) occurred within the speed range of 60 km/h– 70 km/h; fatalities can be avoided by increasing the operating speed range of the current AEB or by individual and technical approaches to make drivers keep speed limit.

(3) Low-speed range at night

During the nighttime, 119 cases within the low-speed ranges, accounting for approximately 31% (=119/385) of the non-addressed areas at night. Furthermore, of the 119 cases, 73 were road-lying accidents, which are difficult to address using the current AEB [11]. Fatal accidents can be further reduced by considering safety measures that are not dependent on the vehicle only.
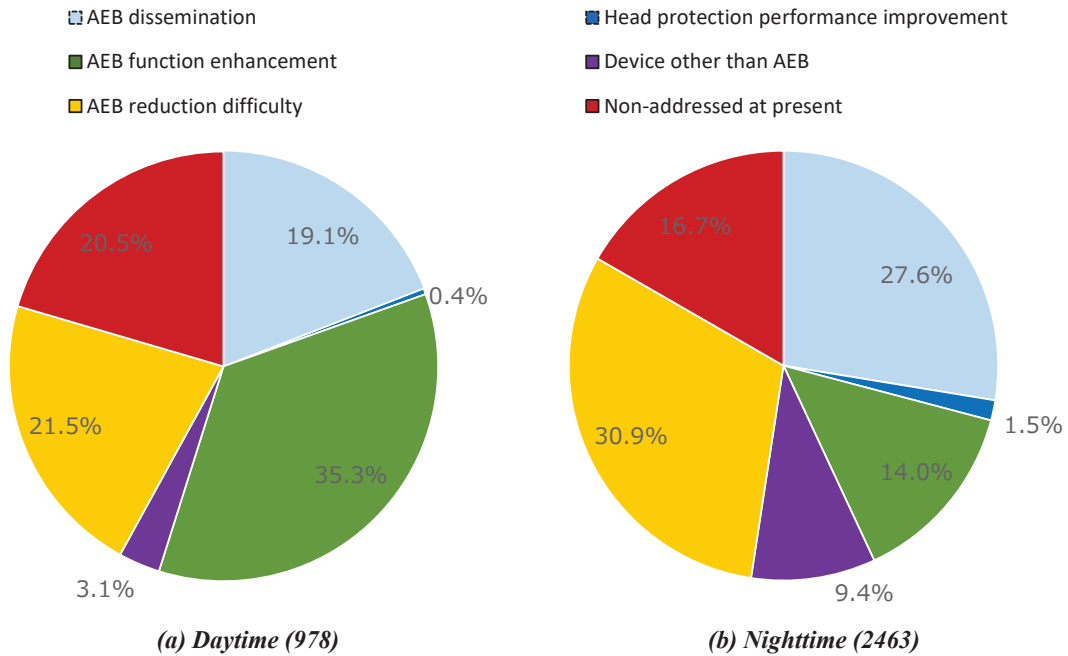

(a) Daytime (978)   *(b) Nighttime (2463)*

Figure 7. Ratio of vehicle safety measures against pedestrian accidents (at 100% dissemination)

(a) Daytime (978)   *(b) Nighttime (2463)*
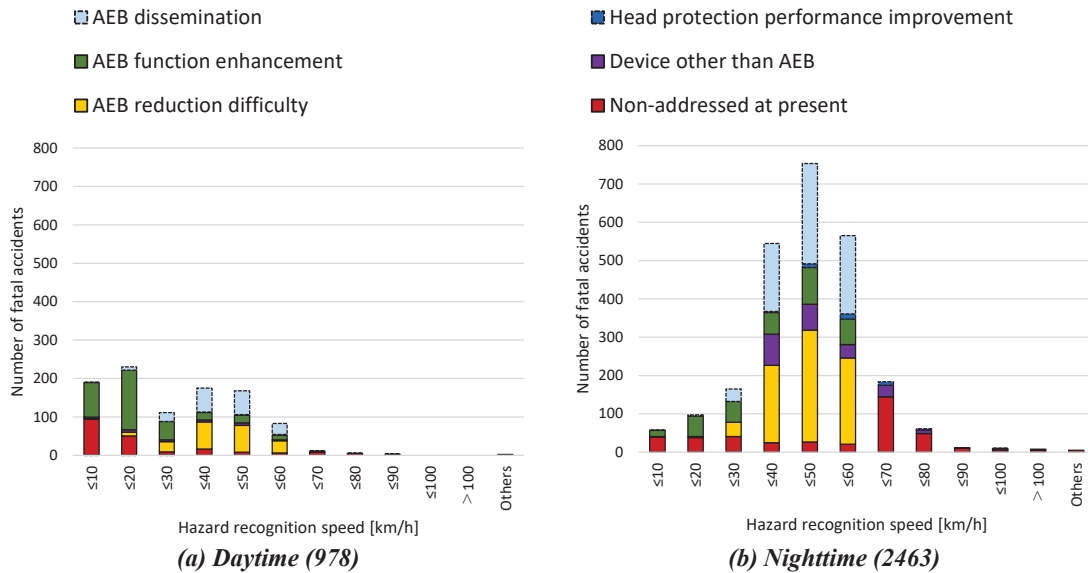
Figure 8. Ratio of vehicle safety measures against pedestrian accidents by speed (at 100% dissemination)

(a) Daytime (198)   **(b) Nighttime (406)**
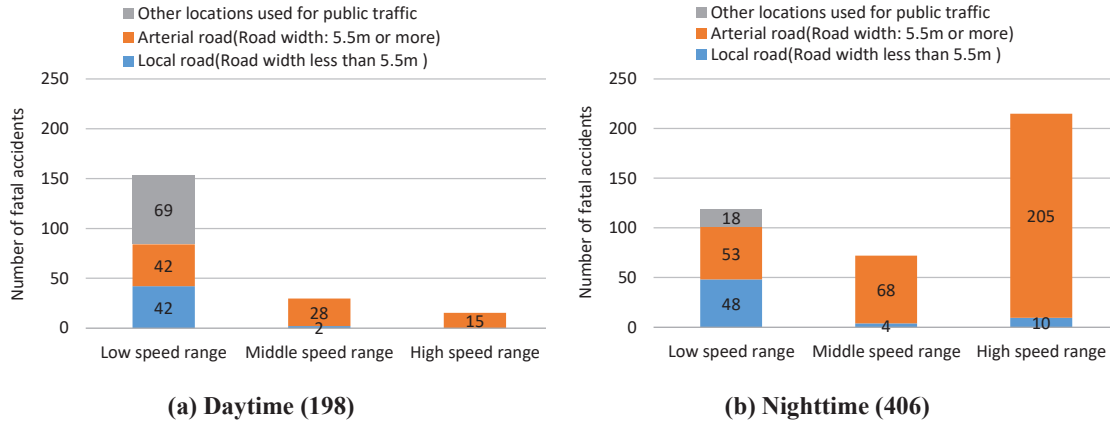
Figure 9. Non-addressed areas by accident occurrence location and speed range (speed range = other excluded)
Low-speed range: 30 km/h or less; medium-speed range: 30 km/h– 60 km/h; high-speed range: > 60 km/h

Analysis issues

In this study, we expressed situations where the AEB could not operate normally owing to the weather or the state of the detection target, even if the conditions are favorable, using the traffic environment application coefficient that was calculated from the evaluation results of AEB. The results showed that there were many areas (AEB reduction difficulty) where pedestrian accident reduction with AEB was difficult within the speed range of 30 km/h– 60 km/h. To investigate the safety measures in this area, it is important to investigate the actual conditions under which these accidents occurred. It is necessary to collect data that enables the analysis of situations where AEB does not function.

CONCLUSION

In this study, we organized the status of initiatives for vehicle safety measures for pedestrian traffic accidents to promote not only vehicle safety measures but also measures for the society as a whole to achieve zero traffic accident fatalities. The status of initiatives refers to such as AEB and pedestrian head protection performance, as well as other vehicle safety measures whose effects are unknown but which are taken to reduce fatal accidents. These were then organized by day/night and speed. These analyses showed that areas in which vehicle safety measures are currently not implemented account for approximately 42% and 48% of fatal accidents in the daytime and nighttime, respectively.

In the future, it is expected that such quantitative results serve as a basis for not only considering additional vehicle safety measures but also for collaborations with such as road and traffic administrators, to efficiently achieve goals toward zero fatalities. In particular, there are increasing expectations for safety measures that utilize communication technology (vehicle to everything: V2X), and it is necessary to specifically investigate the direction of measures that utilize V2X. Furthermore, although this study was the analysis of pedestrian accidents, similar studies are necessary for bicycle accidents, which are also related to vulnerable road users.

REFERENCES

[1]   National Police Agency: Occurrence of Traffic Accidents in 2021 (2022)
[2]   ITARDA: ITARDA information No. 133 (2019)
[3]   Ministry of Land, Infrastructure, Transport and Tourism of Japan: FY2017 3rd Vehicle Safety Measures Study Group, Document 6 (2018)
[4]   Ministry of Land, Infrastructure, Transport and Tourism of Japan: ASV Technologies Overview (2022)
[5]   Ministry of Land, Infrastructure, Transport and Tourism of Japan: New Car Assessment Roadmap (2018) FY2018 1st New Car Assessment and Evaluation Study Group, Document 1-2 (2018)
[6]   Euro NCAP: Euro NCAP 2025 Roadmap (September 2017), For Engineers, Technical Papers (2017)
[7]   Ministry of Land, Infrastructure, Transport and Tourism of Japan: 6th Advanced Safety Vehicle (ASV) Promotion Plan Report (2021)
[8]   Automobile Traffic Subcommittee, Land Transport Committee, Council for Transport Policy: The Future of Vehicle Safety for a Traffic Accident-Free Society (2021)
[9]   Kikuchi, K. et al.: Investigation of Driver Steering Avoidance Characteristics for Designing Avoidance Support Device, Proceedings of the Fall Meeting of the Society of Automotive Engineers of Japan, No. 100–04 (2004)
[10] ITmedia: Collision Avoidance with Automatic Steering in the New Toyota Lexus LS, https://www.itmedia.co.jp/business/articles/1706/26/news090.html (2017)
[11] Council of Transport Policy: 3rd Technical Safety WG Material 4-3 (2021)
[12] Ministry of Land, Infrastructure, Transport and Tourism of Japan: FY2016 3rd Vehicle Safety Measures Study Group, Document 8 (2017)

AN OVERVIEW OF ROAD TRAFFIC INJURIES AMONG CHILDREN IN SWEDEN OVER 20 YEARS

Maria Klingegård,
Folksam
Sweden
Anders Kullgren
Folksam
Sweden
Helena Stigson
Folksam
Sweden
Anders Ydenius,
Folksam
Sweden

ABSTRACT

This register study, focusing on children from (0-17 years), aimed to investigate traffic injuries (AIS1-5) among children on roads in Sweden between 2000 and 2019. The Swedish national database (STRADA) was used. It includes road traffic crashes reported by the police and by emergency care centers. The data included road user group, age, gender, injury type, AIS level, and use of seatbelt or child restraint. Descriptive statistical analysis and simple linear regression were performed to investigate significant changes in injury distribution between 2010 and 2019. A total of 14 731 registered crashes during the last 20 years involved 15 045 injured children (0-17 years). Six thousand six hundred forty-three were girls and 8088 boys. The total number of injuries decreased over time (40% since 2010). Most injured children (80%) sustained minor injuries (AIS1). Most were 12 to 17 years old (80%). A change in injury distribution was found according to age; for 0-9-year-olds, most injured children were pedestrians, while for 9-13 years old's, bicyclists were most common. For 14-16-year-old children, moped riders were most common. Most injured children (62%) were vulnerable road users (2000-2019). A 15% increase in the proportion of injuries between 2010 and 2019 was found. A 24% decrease in the proportion of injuries for children as vehicle occupants (excl. motorcycle and moped riders) between 2010 and 2019 was found; still, in 2019, 35% of the injured children were vehicle passengers. The most frequently injured body region was the head (26%), followed by the neck (19%). Eleven percent of the injured children in cars were unbelted. Twenty-two percent of the 0-12 years old children did not use a proper child restraint. The study confirms that Sweden's traffic safety for children (0-17 years) has improved since 2000. A 40% reduction in the number of injuries was found between 2010-2019 (including minor injuries that account for 80% of all reported injuries). The study also highlights that for vulnerable road users, the proportion of child injuries (0-17 years) increased by 15%, which was lower than vehicle occupants (24% decrease). Moped riders account for the largest road user group (35%) (2000-2019). Therefore, it is important to improve protection for children as vulnerable road users both regarding severe injuries as well as minor injuries leading to long term consequences for a safe (sustainable) traffic environment.

INTRODUCTION

Traffic safety is on the global agenda. Target 3.6 in the UN Sustainability Development Goals state the ambition to reduce fatalities and injuries by at least 50% by 2030 [1]. UNICEF is the global custodian for children, responsible for 7 of the UN sustainability goals [2]. Knowledge of accident and injury distribution is important for designing a safe road transport system and prioritizing countermeasures that minimize the risk of traffic accidents and injuries (e.g., recommendations on speed limits, separation of road user groups, helmets, and restraint use). A total of 390 children were killed on European roads, and more than 6000 were seriously injured in 2020 [3]. Children have physical and cognitive limitations that make them more at risk., Children are less visible to drivers due to their small stature and when in traffic, have a lower field of view than adults. Their posture and size also influence the type of injuries they sustain in crashes. Over the past decade (2011-

2020), road safety for children has improved more rapidly than road safety for the rest of the population (46% and 36% decrease in mortality, respectively) [3]. Serious injuries for children in traffic crashes account for approximately 5% of all serious road traffic injuries in the EU [3]. There are, however, large differences within the EU countries. The mortality rate for children in traffic is ten times higher in Romania compared to Norway, Cyprus, or Sweden [3]. The proportion of child road traffic deaths compared to all causes of death varies from less than 2% in Norway to over 11% in Latvia, and about 10% in Israel, Czechia, and Romania [3]. In 2020 a total of 204 road traffic fatalities occurred in Sweden, of which 15 were under the age of 18 [4]. Approximately 100 000 children are born each year in Sweden, and 23% of the Swedish population is under the age of 19. Approximately 500 children under 19 died of any cause in Sweden in 2020, a decrease from 670 fatalities in 2000. Sweden has a strong safety culture manifested in national programs such as Vision Zero [5] and the annual road traffic safety targets [6, 7]. Since 2005 children under 15 must use a helmet while biking. Since 2008 it has been mandatory to have a driving license for a moped, which can be obtained from the age of 15. A driver's license for cars can be obtained by age 18 (from 16, it is allowed to drive with an educated supervisor). The use of child restraints has been regulated by law since 1988, and in 2007 a requirement to use child restraints up to a height of 135 cm was implemented. Focused regional efforts have increased the awareness of child safety in traffic [8, 9]. During the last decade, Sweden has had a 23% reduction in deaths on roads, meaning that the national target of a 50% reduction over the period 2007-2020 has been reached [10]. Sweden is now working towards target 3.6 adopted in the UN sustainability goals for 2030, targeting a 50% decrease in mortality over the decade. Typically, mortality and serious injury rates are used as safety targets in the EU for international comparison, e.g.,[1, 3, 11]. However, there is less knowledge regarding the development of minor injuries. Moreover, many minor injuries could lead to long-term consequences [12]. Children, as a road user group, are not analyzed separately on the same regularity as adults. Hence, this study takes advantage of 20 years (2000-2019) of data covering road traffic accidents in Sweden, where accident and injury distributions are studied for children 0-17 years of age as various road users. This study thus targets children specifically, includes all injury severity levels, and complements official statistics on fatality and serious injury rates. The result can guide preventive actions for children of various ages and road user groups to reach the UN Agenda 2030 goals.

METHOD

Material

This study is based on the registry STRADA, the Swedish national system for traffic injury data collection (for a full description of STRADA, see [13]. The Swedish Transport Agency hosts STRADA with restricted access. For example, ethical approval is needed for access. STRADA includes information from two separate sources; traffic accidents reported by the police and medical reports provided by Swedish emergency hospitals. Only accidents within the road transport environment are included. The road environment is defined as a street, pedestrian and cycle path, sidewalk, separate parking, market square, public transport stop, or petrol station. A road accident is defined as a sudden event (collision) within the traffic environment that leads to a personal injury. Fall (e.g., falling when walking on pavement) is typically not included within the dataset in line with the international definition of an accident in the road system. The information in the registry is pseudonymized. Extracted dataset for this study includes all unintentional injuries (i.e., excluding suicide) of children aged 0-17 years during the study period 2000-2019, which can be found in both data sources (police reports and hospital data). For each injury, extracted variables from police reports include accident number, reference number, accident date, accident description, seatbelt use, child restraint use, road characteristics, speed limit, road user group (pedestrian, cyclist, moped rider, car occupant, bus occupant, light/heavy truck occupant, etc.), and injury severity as set by the police in two categories (minor and serious injury). Extracted variables from medical reports include accident number, reference number, accident date, diagnostic code, road user group (the same categories as in the police report), injury type, AIS level, age, and gender. Body region was derived from the injury diagnosis. One accident can include more than one child, and each child can sustain multiple injuries. One child can be involved in several accidents during the study period. The Swedish ethical review authority approved the research via the regional ethical board in Stockholm (DRnr 2018/711-31/5).

Analysis

The analysis was performed with descriptive statistics, including frequencies and proportion (percentages) of all available variables for children 0-17 years old (excluding. suicide) for 2000-2019. The studied variables

were road user group, age, gender, injury type, body region, AIS level, seatbelt, and child restraint use. Excel Power Pivot (v. 2108) and SAS Enterprise Guide (v. 8.3.0.103) were used for statistical analysis. 95% confidence intervals (CI) were used to identify significant changes between variables, Eq. (1). The road user groups included: pedestrians, cyclists, moped riders, car occupants, bus occupants, light/heavy truck occupants, and others (tractors, snowmobiles, horse riders, off-road vehicles, etc.). The road user groups were also divided into two categories according to their degree of protection in traffic; (1) vulnerable road users (VRU) include unprotected road users such as pedestrians, cyclists, motorcycle riders, and moped riders, and (2) vehicle occupants refer to passengers who are protected inside a car, bus, or heavy/ light vehicle. Changes over time were highlighted by calculating relative change (Eq. 2) and by estimating the trend with simple linear regression between 2010 and 2019 to ensure a none-overlapping 95% CI (Eq. 2). By 2010, all hospitals in Sweden were included in STRADA and by excluding 2020, the covid pandemic year is accounted for in the analysis.

$$95\% \text{ confidence interval:} \quad CI \qquad \underline{\qquad\qquad} \qquad \text{(Eq. 1)}$$

$$\text{Relative change:} \quad C = \frac{x_2 - x_1}{x_1} \quad \text{(Eq. 2)}$$

RESULTS

During the study period, 2000-2019, a total of 13 139 registered traffic accidents occurred that involved 14 731 (unique) injured children (0-17 years old). Six thousand six hundred forty-three were girls, and 8088 were boys. A total of 34 776 injuries are included in the data set. The descriptive statistics are presented (Figures 1 to 6), and corresponding frequencies include 95% CI for the included variables. A visualization of the simple regression analysis is presented in the Appendix.

Age and gender distribution of injured children

The majority (80%) of the reported injured children between 2000 and 2019 (including all severity levels and road user groups) were 12 to 17 years old, Figure 1. Over time, a general decline in injured children (0-17 years old) was found (2000-2019). Subsequent simple linear regression analyses for the accident years 2010 to 2019 (when all hospitals were included) estimates a significant negative trend for injured children in the 12 to 17 age group (a 40% decrease). The trend estimates a 95% CI for mean 2010 and 2019 is non-overlapping. See Appendix, Figure A1.
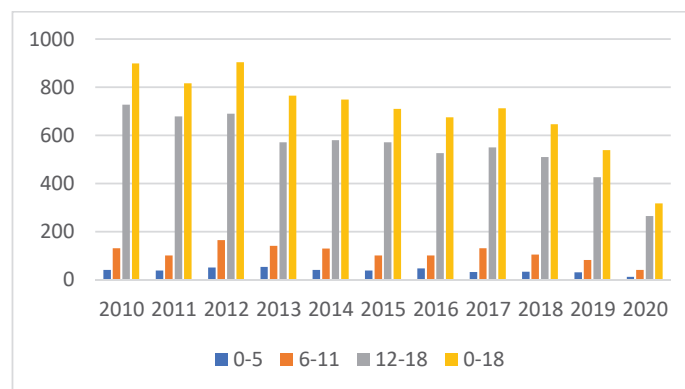

Figure 1. The number of injuries across age groups during the study period (2010-2019). The corresponding

table, including CI 95%, can be found in the Appendix, Table A2.

Children in the 0-5-year-old age group were most often injured as pedestrians (23%), while 9-13-year-olds were mostly injured as bicyclists (22%). Between 12-17 years old, children were mostly injured as moped riders (44%), Figure 2. The proportion of injured children as car occupants decreased by age: 0-5 years (68%),

7-11 years (55%), and 12-17 (28%). Boys accounted for 55% of the number of injured and girls 45% (accidents 2000-2019). For moped riders, a larger proportion of boys were injured than girls (64% and 36%, respectively).
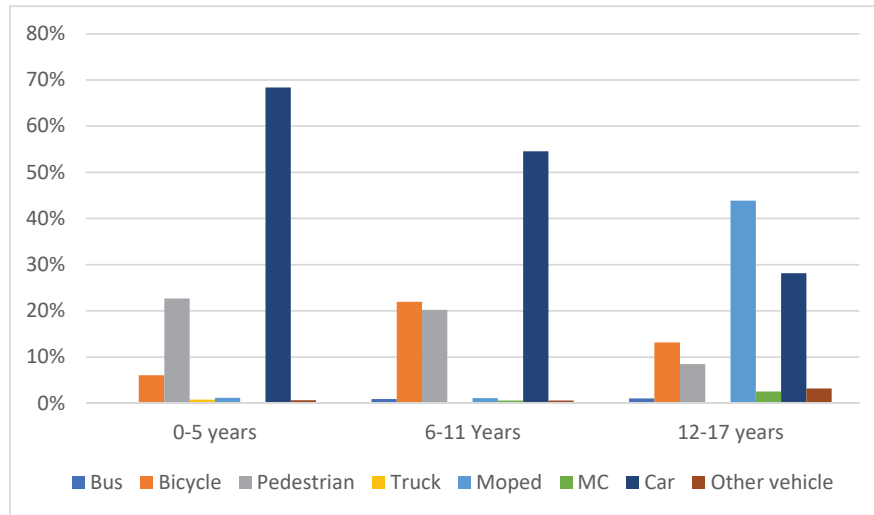

Figure 2. The Proportion of injured children per road user group by age. The corresponding table, including frequencies, proportions, and CI 95%, can be found in the Appendix, Table A3.

The distribution between different road user groups

A majority (62%) of the injured children 0-17 years old (including all severity levels) were injured as vulnerable road users during the study period (2000-2019) Figure 3, where eight percent were traveling as pedestrians, 13% as a bicyclist (13%), and 35% as moped riders. Children 0-17 years old traveling as vehicle occupants (bus, car, light/heavy vehicle) accounted for 38% of all road traffic injuries during the study period (2000-2019). Car occupants specifically accounted for 35% of all injuries. Simple linear regression analysis estimated significant trends (decreases) for the following groups (children 0-17) between the accident year 2010 and 2019 (Appendix, Figures A2-A5): vulnerable road users (30%), vehicle occupants (54%), car occupants (57%), moped riders (35%). Indications of decreases in the number of injured children between 2010 and 2019 for pedestrians and bicyclists were found (not significant). Considering the proportion of injuries among children as vulnerable road users and vehicle occupants between 2010 and 2019, a 15% increase could be seen for vulnerable road users, during a 24% decrease in injuries for vehicle occupants. Based on police data, the proportion of injured children using child restraints increased during the same period (from 14% in 2010 to 25% in 2019). Nevertheless, 11% of the children injured as car occupants did not wear the seatbelt, and as high as 14% of the 12-17 years old were unbelted. Twenty-two percent of 0-12-year-old children did not use proper child restraint.
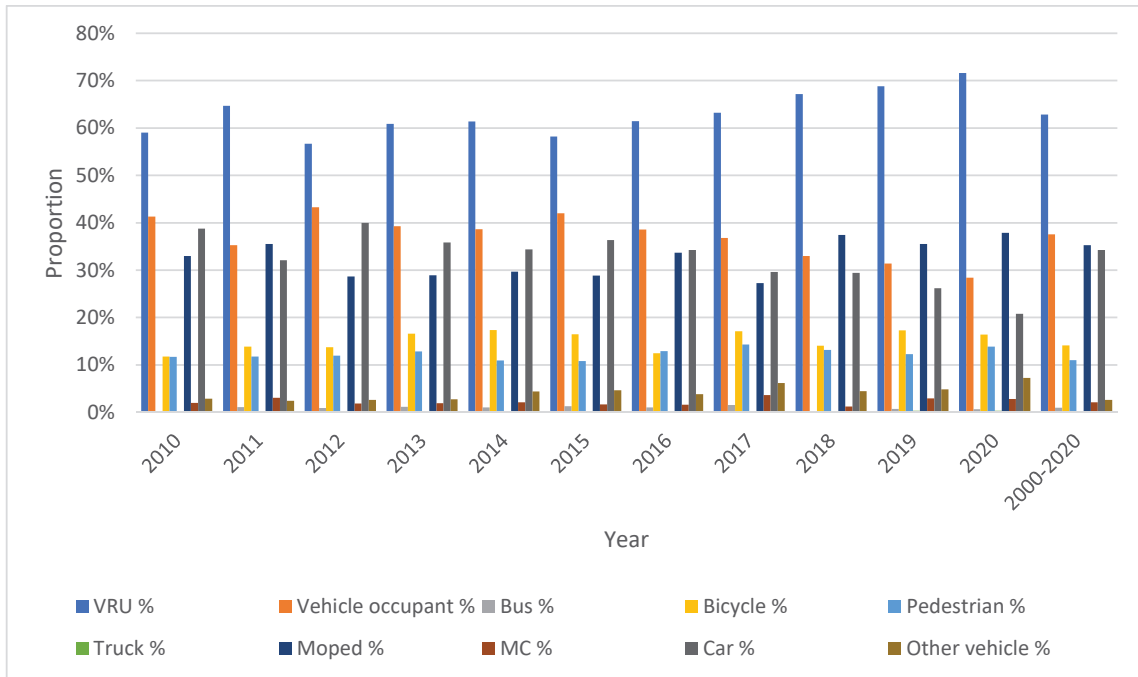
Figure 3. The proportion of injured children per road user group and accident year. The corresponding table, including frequencies, proportions, and 95% CIs, can be found in the Appendix, Table A4.

Injured body region

The main injured body regions for injured children aged 0-17 years (2000-2019), including all road user groups and injury severity levels, were the leg and pelvis (35%), followed by upper extremities (22%) and head/face (20%), Figure 4. However, the injury distribution varied according to the road user groups. For vulnerable road users, the most injured body regions were leg and pelvis injuries (36%), followed by the arm (25%) and head/face (22%). For pedestrians and bicyclists specifically, head/face (30-31%) is the second largest body region. The major injured body regions for vehicle occupants were the head (26%) and neck (19%). No major trends were found over 2010-2019 when comparing relative changes for injured body regions except for car occupants. Head/throat injuries were reduced to a larger extent (300%) than other body regions (total mean of 176%).
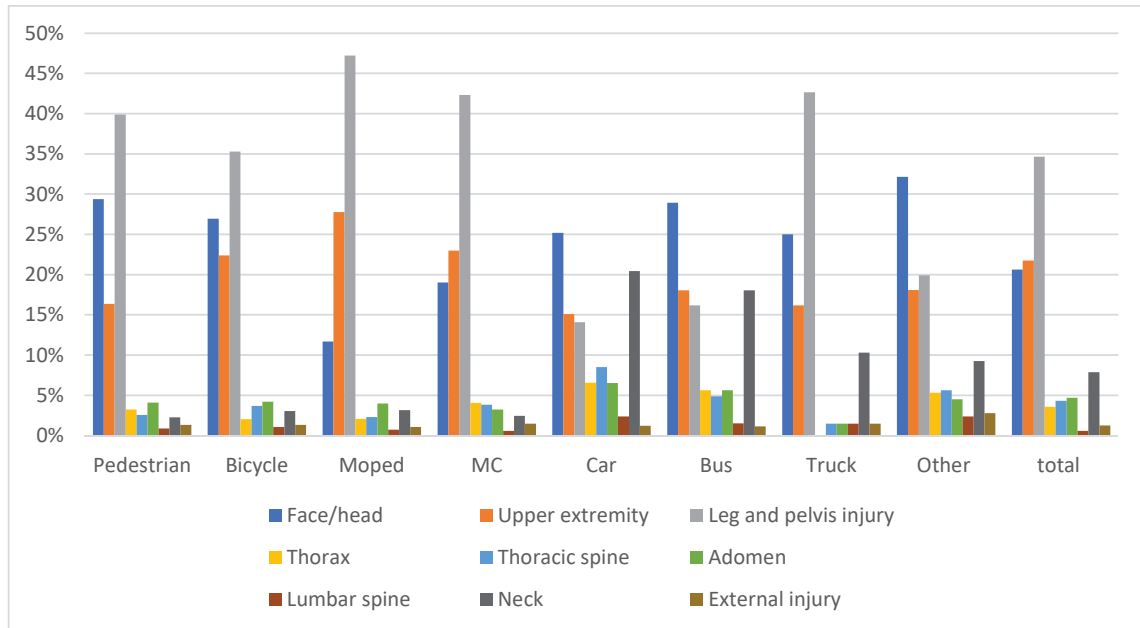
Figure 4. The overview of injured body regions per road user group, including all ages and severity levels. The corresponding table with frequencies, proportions, and 95%CIs can be found in the Appendix, Table A5.

Injury severity level

Over the 20 years investigated, most injuries sustained by children (0-17 years old), including all road user groups, were minor injuries (80%) (AIS1), Figure 5. Moderate to serious injuries (AIS 2+) accounted for 20 %. Most of those receiving moderate to serious injury (AIS2+) were 15 years old or older. The injury severity for children (0-17) varied among the road user groups during the study period (2000-2019). Motorcycle riders sustained the most severe injuries (AIS3+: 9%). Large road user groups sustained moderate injuries (AIS2) includes motorcycle riders (27%), moped riders (15%), pedestrians (18%). Only a small variation could be seen in severity levels between vulnerable road users (AIS1: 80%; AIS2:16%; AIS3+4%) and vehicle occupants (AIS1: 82%; AIS2: 13%, AIS3+: 5%). Over time, the number of injuries has decreased by 40% for children (0-17 years) (2010-2019). However, a larger decrease is seen for minor injuries (AIS1: 47%) than moderate to severe ones (AIS2+: 24%). The linear regression analysis indicated significant changes in the estimated trends between 2010-2019 for minor injuries but not for moderate to severe injuries, see Appendix Figure A10-A11.
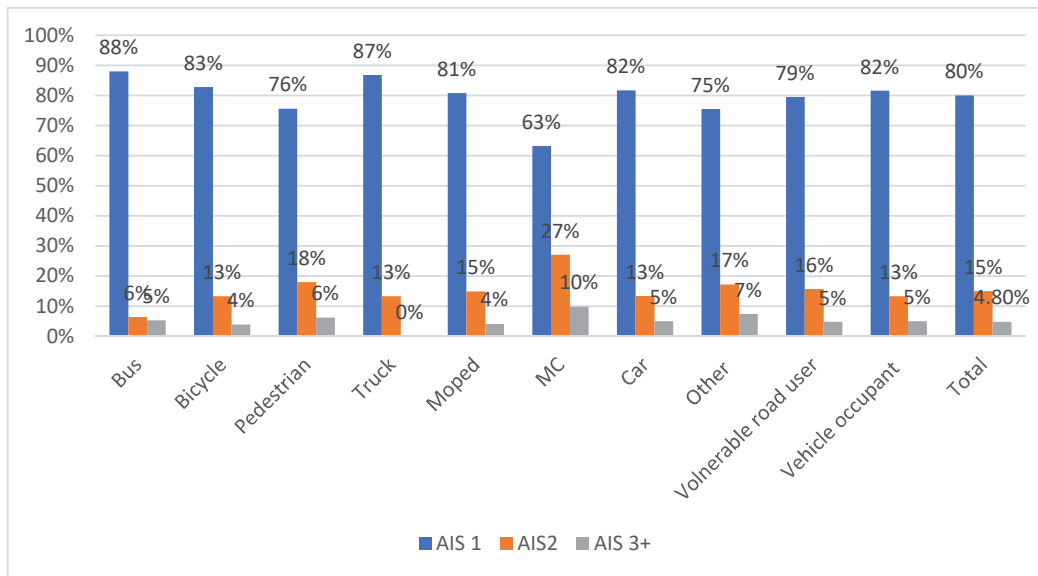
Figure 5. The overview of the severity of injuries according to the AIS scale as reported by the hospitals divided into road user groups (2000-2019). The corresponding table with frequencies, proportions, and 95% CIs can be found in the Appendix, Table A6.

Type of accident

The vulnerable road users were most often struck by a vehicle (73%), and approximately 20% were involved in single-vehicle crashes (with no (human) counterpart). Forty-seven percent of vehicle crashes involved another vehicle, and about 30% were single-vehicle crashes.

DISCUSSION

Over time, an overall decrease in road fatalities has been reported for children and adults[10, 11]. However, this study shows a significant decrease in the number of injuries (including minor injuries) sustained by 12-17-year-old children, while there is no significant trend for the other age groups. There may be many reasons for this trend. Children travel increasingly independently as they age. Their choice of transportation changes accordingly. This point is also reflected in the injury distribution of this study as in other studies on fatal child injuries. Children in the 0-5-year-old age group were most often injured as pedestrians (23%), while 9-13-year-olds were mostly injured as bicyclists (22%). Twelve to 17-year-olds were mostly injured as moped riders (44%). Hence, the decrease in injuries for car occupants by age is probably a result of traveling by other means of transportation. Therefore, it is important not to consider children (0-17) as one homogenous group. In this study, moped riders are the most frequently injured road user group for children 0-17 years (35%) and as much as 74% of the 15 years old children. A significant decline in the number of injuries when traveling by moped was found during the study period (2010-2019). In 2008, a driver's license was introduced for moped riders. Despite that fact, moped riders were the largest road user group involved in crashes in 2019, indicating the need for more preventive actions.

Official statistics on fatality rates for the year 2020 show that car occupants accounted for more than 50% of the fatalities (106 out of 204), while the numbers for pedestrians and moped riders are lower (25 and 2, respectively) [10, 11]. This study has shown that vulnerable road users account for the majority (62%) of the injuries, while children injured as car occupants account for about 35%. Historically preventive actions for car occupants have been prioritized. The national goals for reducing fatality rates among car occupants have been fulfilled in Sweden. However, the fatality rates for vulnerable road users do not show the same positive trend. This fact is also true for children. This study shows that 0-17-year-old children injured as vulnerable road users

increased by 15% during the study period 2010 to 2019, while children injured as car occupants decreased by 59%. Carlson et al. [14]showed that fatalities among 0-14-year-old children as passengers decreased by 83% from 1980 to 2010, while for vulnerable road users, the decrease was only 30%. Another report[11] also shows a mortality rate reduction between 29% and 74% for different road user groups over time. This study shows the need for more preventive actions to reduce injuries sustained by children traveling as vulnerable road users, especially as moped riders.

Knowledge of accident and injury distributions among road users and age groups for children is important to design a safe road system and prioritize preventive actions. Sweden has successfully adopted the Vision Zero program, a strategic approach for a safe system where no one should be fatally or seriously injured while using the road transport system. This study identifies that motorcycle riders (AIS3+) are the largest group for serious and sever injuries. The long-term national goal, Vision Zero, regarding a 50% reduction in fatality rates, has been fulfilled for car occupants and children in cars. However, for vulnerable road users, the goals have not been fulfilled, urging more preventive actions.

Even though 0-17-year-old children only represent 23% of Sweden's population and only 4% of those people were fatally injured in traffic in 2019, this study shows that an average of 750 children are injured each year, and 80% are minor. In Sweden, a serious injury is defined as an injury leading to any kind of permanent medical impairment. Out of all injuries (for all ages) leading to permanent medical impairment, 81% are initially reported as minor by the police and regarded as minor according to the AIS scale [12]. The figure for the corresponding proportion of injuries to children 0-12 years old is 67% [15]. Future studies must identify injuries leading to permanent medical impairment for children as road users and in different age groups. This information is important for finding effective preventive actions.

Limitations

The nationwide coverage of STRADA varies over time, and the inclusion process has changed (e.g., due to GDPR 2018). The COVID pandemic (2020) influences the number of reported cases. This situation has been accounted for in the analysis by (1) focusing on the last ten years of data (because by then, most hospitals had been included in the data set) and (2) excluding the COVID pandemic year 2020. Furthermore, people suffering from a minor injury requiring only primary care, without being directed to a hospital, are not recorded in STRADA. However, road users with minor injuries known by the police are reported in STRADA. Fatalities are excluded from the data set because the hospitals stopped reporting them in 2018. The injured road user must be reported by the police and a hospital to be included in the analysis. In some cases, only one source could report an injured road user. Therefore, the number of injured children presented is an underestimation of the total number of injured children, especially from 2000-2010. Falls on the road system (e.g., a pedestrian falling while walking on the pavement) are not typically included in STRADA because they are not covered by the definition of traffic accidents and are, therefore, most often not reported. Studies have shown that falls are a major pedestrian accident category (influencing perceived traffic safety). Including a fall as a road traffic accident could impact the distribution of injuries among road user groups [16].

CONCLUSION

This study confirms that traffic safety for 0-17-year-old children in Sweden is improving over time, with a 40% reduction in the number of injuries (AIS1-AIS3) during the last decade. The improvement varies by age and means of travel. Therefore, it is important not to consider 0-17-year-old children as one homogenous group. Studies have shown that most fatally injured children are injured as car occupants. However, this study shows that the majority of injured children were vulnerable road users (i.e., pedestrians, bicyclists, moped and e-scooter, and horse riders). Moped riders were in 2019, despite the large reduction due to the introduction of a driving license in 2008, the most frequently injured road user group for children. Even though there is a general decline in the number of injured children, the proportion of vulnerable road users is increasing (15%) and does not follow the same positive trend as vehicle occupants (24% decrease). Therefore, more effort is needed to protect children as vulnerable road users to fulfill the UN sustainability and the national Swedish Vision Zero goals. Future studies should identify injuries leading to permanent medical impairment for children as different road users and in different age groups. This information is important for finding effective preventive actions.

ACKNOWLEDGEMENT

REFERENCES

1. United Nations General Assembly. 2019. "The global sustainable report development report 2019: The future is now science for achieving sustainable development". September 2019. Retrieved from: https://sustainabledevelopment.un.org/content/documents/24797GSDR_report_2019.pdf Retrieved: 2022-08-01

2. UNICEF. 2021. "The State of the World's Children 2021: On My Mind – Promoting, protecting and caring for children's mental health". 2021: New York, https://www.unicef.org/media/114636/file/SOWC-2021-full-report-English.pdf Retrieved: 2022-08-01

3. ETSC. 2022. "Reducing child deaths on European roads". Pin Flash Report 43. September 2022. https://etsc.eu/wp-content/uploads/ETSC_PINFLASH43-1.pdf Retrieved: 2022-11-15

4. TRAFA. 2019. "Vägtrafikskador 2020" (in Swedish), Retrived from: https://www.trafa.se/globalassets/statistik/vagtrafik/vagtrafikskador/2020/vagtrafikskador-2020.pdf Retrieved: 2022-08-01

5. Johansson, R., 2008 "Vision Zero – Implementing a policy for traffic safety". Safety Science, 2008. **47**: p. 826-831. Doi: https://doi.org/10.1016/j.ssci.2008.10.023 Retrieved: 2022-08-01

6. STA. 2019. "Analysis of road safety trends 2018". Report, April 2019. Borlänge, Sweden. Retrieved from: http://trafikverket.diva-portal.org/smash/get/diva2:1389250/FULLTEXT01.pdf Retrieved: 2022-08-01

7. STA. 2019. "Saving Lives Beyond 2020: The Next Steps Recommendations of the Academic Expert Group for the Third Ministerial Conference on Global Road Safety 2020". October 2019. Retrieved from: https://www.roadsafetysweden.com/contentassets/c65bb9192abb44d5b26b633e70e0be2c/200113_final-report-single.pdf Retrieved: 2022-08-01

8. De Leon, A. P., Svanström, L., Welander, G., Schelp, L., Santesson, P., & Ekman, R. 2007 "Differences in child injury hospitalizations in Sweden: the use of time-trend analysis to compare various community injury-prevention approaches". Scand J Public Health, 2007; 35(6): 623-630 doi:10.1080/14034940701431163

9. Ekman, R., L. Svanström, and B. Långberg. 2005. "Temporal trends, gender, and geographic distributions in child and youth injury rates in Sweden". Injury Prevention, 2005. **11**(1): p. 29. doi:10.1136/ip.2003.005074

10. ETSC. 2021. "Ranking EU progress On road safety 15th Road safety performance index report, in Pin award 15" ETSC: Bryssel. https://etsc.eu/wp-content/uploads/15-PIN-annual-report-FINAL.pdf

11. OECD. 2021. "Road safety report: Sweden". 2021. https://www.itf-oecd.org/sites/default/files/sweden-road-safety.pdf Retrieved: 2022-10-10

12. Malm S, Krafft M, Kullgren A, Ydenius A, Tingvall C. 2008. "Risk of permanent medical impairment (RPMI) in road traffic accidents". Annu Proc Assoc Adv Automot Med. **52**: p. 93-100. PMID: 19026226; PMCID: PMC3256772.

13. Howard, C. and A. Linder. 2014. "Review of Swedish experiences concerning analysis of people injured in traffic accidents". Report VTI notat 7A-2014; Diarienr: 2013/0487-8.3. Retrieved from: https://www.diva-portal.org/smash/get/diva2:699198/FULLTEXT01.pdf

14. Carlsson A, Strandroth J, Bohman K, Stockman I, Svensson M, Wenäll J, Jakobson L. 2013. "Review of Child Car Occupant Fatalities in Sweden During Six Decades". in Int. IRCOBI Conf. on the Biomechanics of Injury 2013. Gothenburg, Sweden. Retrieved from: http://www.ircobi.org/wordpress/downloads/irc13/pdf_files/104.pdf Retrieved: 2022-11-11.

15. Bohman, K., H. Stigson, and M. Krafft. 2014. "Long-term medical consequences for child occupants 0 to 12 years injured in car crashes" Traffic Inj Prev, 2014. **15**(4): p. 370-8. doi:10.1080/15389588.2013.826799

16. Amin, K., Skyving, M., Bonander, C., Krafft, M., & Nilson, F. 2022. "Fall- and collision-related injuries among pedestrians in road traffic environment - A Swedish national register-based study". J Safety Res, 2022. **81**: p. 153-165. Doi: https://doi.org/10.1016/j.jsr.2022.02.007

Table A1. The overview of the total number of injured children from 2000-2020. One child can be injured several times during the study period. Other vehicles include, e.g., tractors, snowmobiles, and 4-wheelers.

	Vulnerable road users (VRU)				Vehicle occupants (excluding Moped/MC)				
	Pedestrians	Cyclists	Mopeds	Motor bikes	Cars	Buses	Heavy / light vehicles	Other vehicles	Total
Age									
0-5	179	48	9	2	540	2	6	5	791
6-11	447	501	25	13	1233	21	3	16	2259
12-17	1019	1585	5266	305	3380	125	19	386	12020
Gender									
Girl	843	921	1958	48	2799	88	10	133	6268
Boy	800	1213	3341	272	2352	60	18	274	8058
Unbelted									
0-5					9%				
5-11					6%				
12-17					13%				
Child Restraint									
0-5					10%				
6-11					28%				
12-17					10%				

Table A2. The corresponding table to Figure 1. The number of injuries across age groups during the study period (2010-2019), including frequencies and 95% CIs.

	Number of injured children				% (CI 95%)		
Year	0-5	6-11	12-17	0-17	0-5	6-11	12-17
2010	41	130	727	898	5±6.4%	15±6.0%	81%±2.9%
2011	38	100	678	816	5±6.7%	12±6.4%	83%±2.8%
2012	50	164	689	903	6±6.3%	18±5.9%	76%±3.2%
2013	53	140	571	764	7±6.8%	18±6.4%	74%±3.6%
2014	40	129	579	748	5±7.0%	17±6.5%	77%±3.4%
2015	38	101	571	710	5±7.2%	14±6.8%	80%±3.3%
2016	47	101	526	674	7±7.3%	15±7.0%	78%±3.5%
2017	32	130	550	712	5±7.2%	18±6.6%	77%±3.5%
2018	33	104	509	646	5±7.5%	16±7.1%	78%±3.6%
2019	30	82	426	538	6±8.2%	15±7.8%	79%±3.9%
2000- 2020	**414**	**1222**	**6090**	**7726**	**5.25%**	**15.01%**	**79.89%**

Table A3. The corresponding table to Figure 2. The proportion of injured children (0-17) by age group per road user group for 2000-2020, including frequencies and 95% CIs. Other vehicles include, e.g., tractors, snowmobiles, and 4-wheelers.

	Number of injured children				% (CI 95%)			
	0-5	**6-11**	**12-17**	**0-17**	**0-5**	**6-11**	**12-17**	**0-17**
Buses	2	21	125	148	0.3±7.0%	0.9±4.1%	0.9±1.8%	1±1.6%
Cyclists	48	496	1583	2127	6±6.8%	22±3.6%	22±1.6%	13±1.5%
Pedestrians	179	456	1022	1655	23±6.1%	20±3.7%	20±1.6%	9±1.5%
Trucks	6	3	19	28	1±6.9%	0.1±4.1%	0.1±1.8%	0.2±1.6%
Mopeds	9	25	5269	5302	1±6.9%	1±4.1%	1±1.8%	44±1.3%
MCs	2	13	305	320	0.3±7.0%	0.6±4.1%	0.6±1.8%	3±1.6%
Cars	540	1233	3381	5152	68±3.9%	54±2.8%	55±1.2%	28±1.3%
Other vehicles	5	13	382	400	0.6±7.0%	0.5±4.1%	0.6±1.8%	3±1.6%

Table A4. The corresponding Table to Figure 3. The proportion of injured children per road user group and accident year 2010-2019, including frequencies and 95% CIs. VRU refers to vulnerable road users not protected by a vehicle (e.g., pedestrians, cyclists, and moped riders). Vehicle occupants include those people who are protected inside a vehicle (e.g., buses, cars, trucks). Other vehicles include, e.g., tractors, snowmobiles, and 4-wheelers.

	VRUs	Vehicle occupants	Buses	Cyclists	Pedes trians	Trucks	Mopeds	MCs	Cars	Others
Number of injured children										
2010	530	371	1	106	105	1	296	18	348	26
2011	528	288	9	113	96	1	290	25	262	20
2012	512	391	8	124	108	2	259	17	361	24
2013	465	300	9	127	98	1	221	15	274	21
2014	459	289	8	130	82		222	16	257	33
2015	413	298	9	117	77	1	205	12	258	33
2016	414	260	7	84	87	1	227	11	231	26
2017	450	262	11	122	102	2	194	26	211	44
2018	434	213	2	91	85		242	8	190	29
2019	370	169	4	93	66	2	191	16	141	26
% (CI 95%)										
2010	59±4.2%	41±5.0%	0±6.5%	12±6.1%	12±6.1%	0.1±6.5%	33±5.4%	2±6.5%	39±5.1%	3±6.4%
2011	65±4.1%	35±5.5%	1±6.8%	14±6.4%	12±6.4%	0.1±6.9%	36±5.5%	3±6.8%	32±5.7%	2±6.8%
2012	57±4.3%	43±4.9%	1±6.5%	14±6.1%	12±6.1%	0.2±6.5%	29±5.5%	2±6.5%	40±5.1%	3±6.4%
2013	61±4.4%	39±5.5%	1±7.0%	17±6.5%	13±6.6%	0.1±7.1%	29±6.0%	2±7.0%	36±5.7%	3±7.0%
2014	61±4.5%	39±5.6%	1±7.1%	17±6.5%	11±6.8%	0.0±0	30±6.0%	2±7.1%	34±5.8%	4±7.0%
2015	58±4.8%	42±5.6%	1±7.3%	16±6.7%	11±6.9%	0.1±7.4%	29±6.2%	2±7.3%	36±5.9%	5±7.2%
2016	61±4.7%	39±5.9%	1±7.5%	12±7.1%	13±7.0%	0.1±7.5%	34±6.1%	2±7.5%	34±6.1%	4±7.4%
2017	63±4.5%	37±5.9%	2±7.3%	17±6.7%	14±6.8%	0.1±7.3%	27±6.3%	4±7.2%	30±6.2%	6±7.1%
2018	67±4.4%	33±5.8%	0±7.7%	14±7.1%	13±7.2%	0.3±0	37±6.1%	1±7.7%	29±6.5%	4±7.5%
2019	69±4.7%	31±6.3%	1±8.4%	17±7.7%	12±7.9%	0.4±8.4%	36±6.8%	3±8.3%	26±7.3%	5±8.2%
2000-2020	**63%**	**38%**	**0.98%**	**14.14%**	**11.00%**	**0.19%**	**35.24%**	**2.13%**	**34.24%**	

Table A5. The corresponding Table to Figure 4. The overview of injured body regions per road user group, including all ages and severity levels (2000-2020). One child can have multiple injuries. VRU refers to vulnerable road users not protected by a vehicle (e.g., pedestrians, cyclists, and moped riders). Vehicle occupants include those people who are protected inside a vehicle (e.g., buses, cars, trucks). Other vehicles include, e.g., tractors, snowmobiles, and 4-wheelers.

	VRUs	Vehicle occupants	Buses	Cyclists	Pedestrians	Trucks	Mopeds	MC	Cars	Other vehicles
Number of injuries										
Head/face	4634	2723	77	1469	1262	17	1663	193	2363	313
Upper extremity	6136	1617	48	1221	704	11	3944	233	1416	176
Leg and pelvis	10828	1536	43	1925	1714	29	6710	429	1320	194
Thorax	597	671	15	111	139		293	41	617	52
Thoracic spine	697	849	13	201	110	1	329	39	798	55
Abdomen	1013	663	15	229	176	1	566	33	612	44
Throat	70	141	2	21	7	2	37	5	133	4
Lumbar spine	208	248	4	58	38	1	102	6	224	23
Neck	680	1911	46	145	91	5	413	20	1785	86
External injury	299	144	3	73	57	1	154	15	113	27
% (CI 95%)										
Head/face	18±1.1%	21±1.5%	29±10.1%	27±2.3%	29±2.5%	25±20%	12%±1.5%	19%±5.5%	25±1.8%	29±5.2%
Upper extremity	24±1.1%	15±1.8%	18±10.9%	22±2.3%	16±2.7%	16±21%	28±1.4%	23±5.4%	15±1.9%	18±5.7%
Leg and pelvis	43±0.9%	15±1.8%	17±11%	35±2.1%	40±2.3%	43±18%	47±1.2%	42±4.7%	14±1.9%	16±5.6%
Thorax	2±1.2%	6±1.9%	6±11.7%	2±2.6%	3±2.9%	0,00±0	2±1.6%	4±6%	7±2.0%	6±6.1%
Thoracic spine	3±1.2%	8±1.8%	5±11.7%	4±2.6%	3±3.0%	1±24%	2±1.6%	4±6%	9±1.9%	5±6.1%
Abdomen	4±1.2%	6±1.9%	6±11.7%	4±2.6%	4±2.9%	1±24%	3±1.6%	3±6.1%	6±2.0%	6±6.1%
Throat	0.3±1.2%	1±1.9%	0.8±12%	0.3±2.6%	0.2±3.0%	3±24%	0.3±1.6%	0.5±6.1%	1±2.0%	0.8±6.3%
Lumbar spine	0.8±1.2%	2±1.9%	1.5±11.9%	1±2.6%	0.9±3.0%	1±24%	0.7±1.6%	0.6±6.1%	2±2.0%	1±6.2%
Neck	2.7±1.2%	18±1.7%	17±10.9%	3±2.6%	2±3.0%	7±23%	3±1.6%	2±6.1%	19±1.8%	17±6%
External injury	1.2±1.2%	1±1.9%	1±11.9%	1±2.6%	1±3.0%	1±24%	1±1.6%	1±6.1%	1±2.0%	1±6.2%

Table A6. The Corresponding Table to Figure 5. The overview of the severity of injury according to the AIS scale reported by hospitals divided into road user groups from 2000-2020. VRU refers to vulnerable road users not protected by a vehicle (e.g., pedestrians, cyclists, moped riders). Vehicle occupants include those people who are protected inside a vehicle (e.g., buses, cars, trucks). Other vehicles include, e.g., tractors, snowmobiles, and 4-wheelers.

	Buses	Cyclists	Pedestrians	Trucks	Mopeds	MCs	Cars	Othesr	VRUs	Vehicle occupants
					Number of injuries					
AIS1	234	4504	3248	59	**11483**	640	7649	734	**19986**	**8565**
AIS2+	31	935	1039	9	**2701**	373	1713	239	**5122**	1918
AIS3+	14	212	267	0	**584**	99	463	72	1187	524
					% (CI 95%)					
AIS 1	88±4.2%	83±1.1%	76±1.48%	87±8.7%	81±0.7%	63±3.7%	82±0.9%	75±3.1%	79±0.5%	82±0.8%
AIS2	6±11.6%	13±2.47%	18±2.71%	13±22.2%	15±1.5%	27±5.2%	13±1.9%	17±5.7%	16±1.1%	13±1.8%
AIS 3+	5±11.7%	4±2.61%	6±2.9%	0±0%	4±1.6%	10±5.8%	5±2%	7±6.1%	5±1.3%	5±2.1%
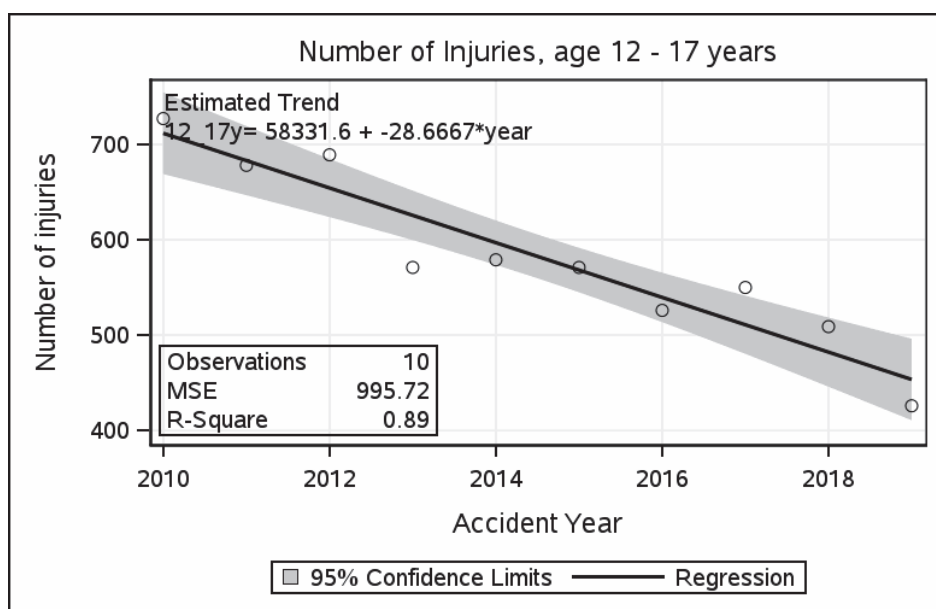
Figure A1. A simple linear regression analysis with an estimated trend for the number of injuries (2010-2019) for children 0-17 years old.
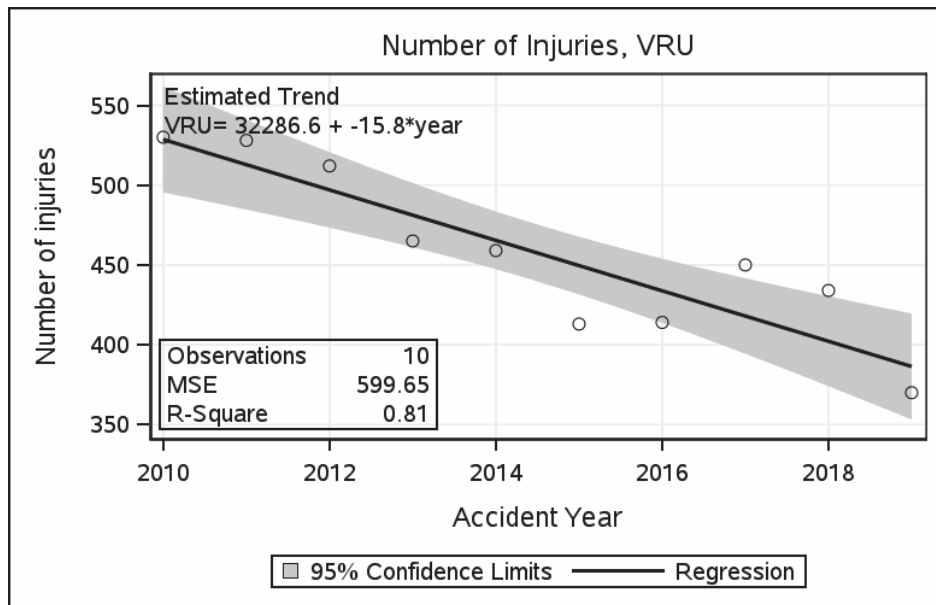
Figure A2. A simple linear regression analysis with an estimated trend for the number of injured VRU (2010-2019) for children 0-17 years old.
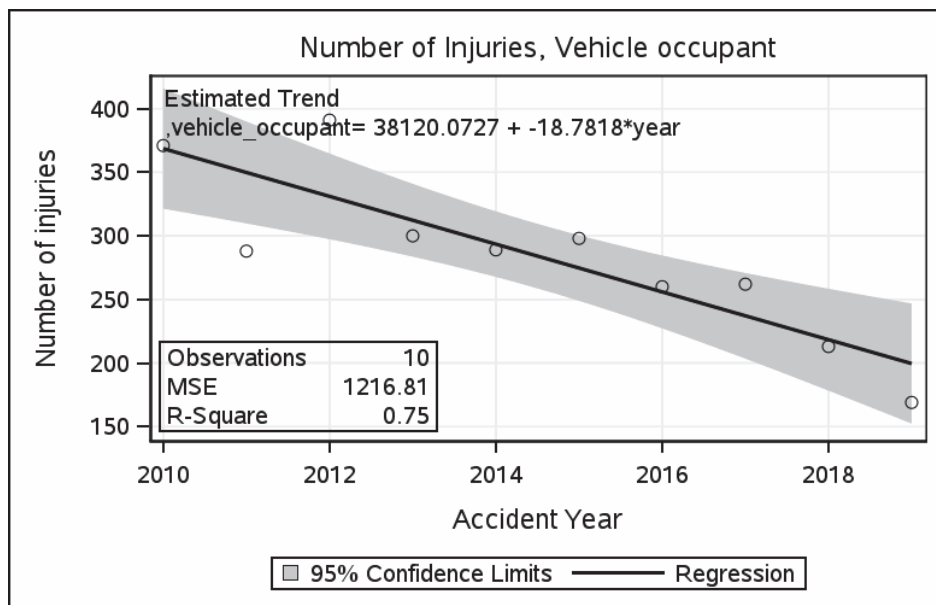
Figure A3. A simple linear regression analysis with an estimated trend for the number of injured vehicle occupants (2010-2019) for children 0-17 years old.
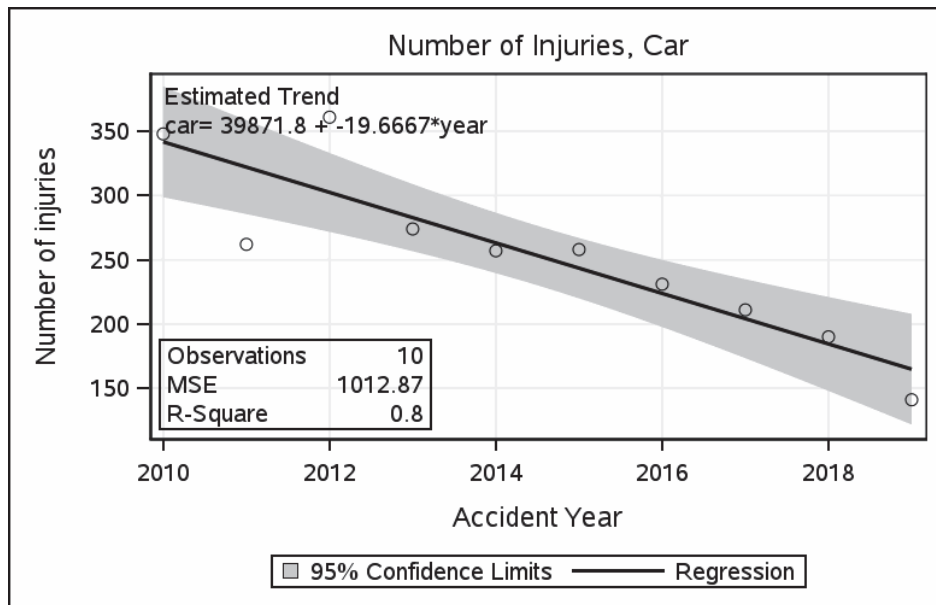
Figure A4. A simple linear regression analysis with an estimated trend for the number of injured children (0-17) traveling by car (2010-2019).
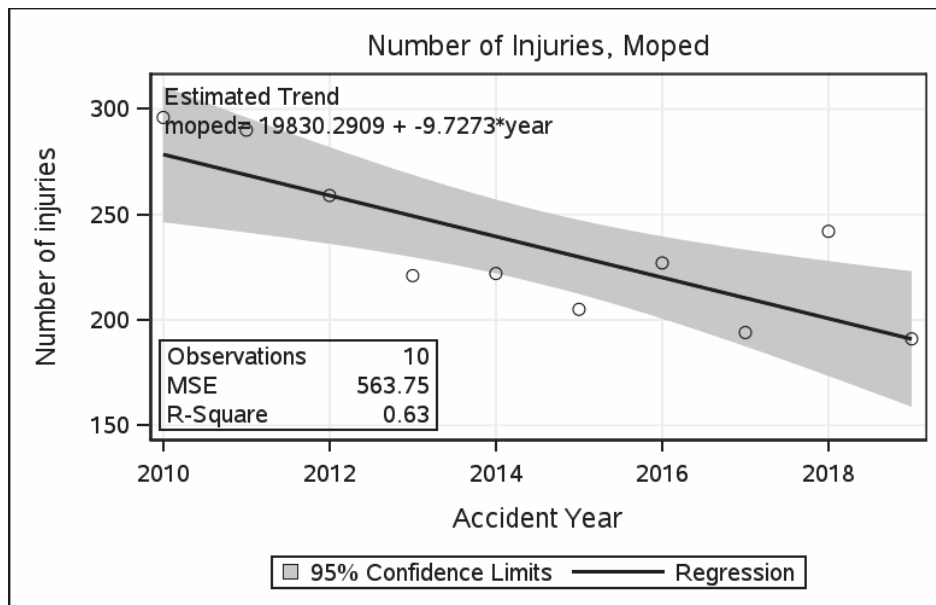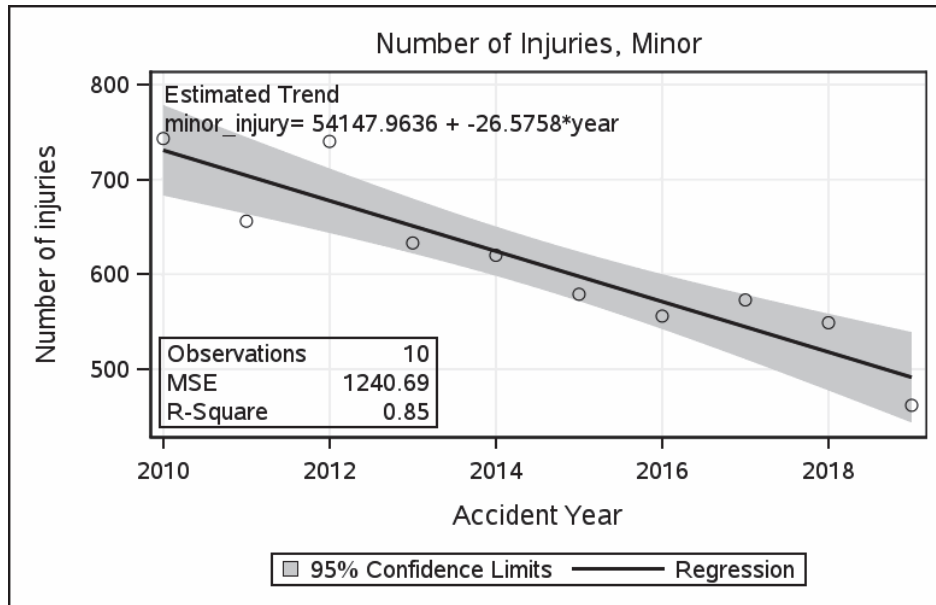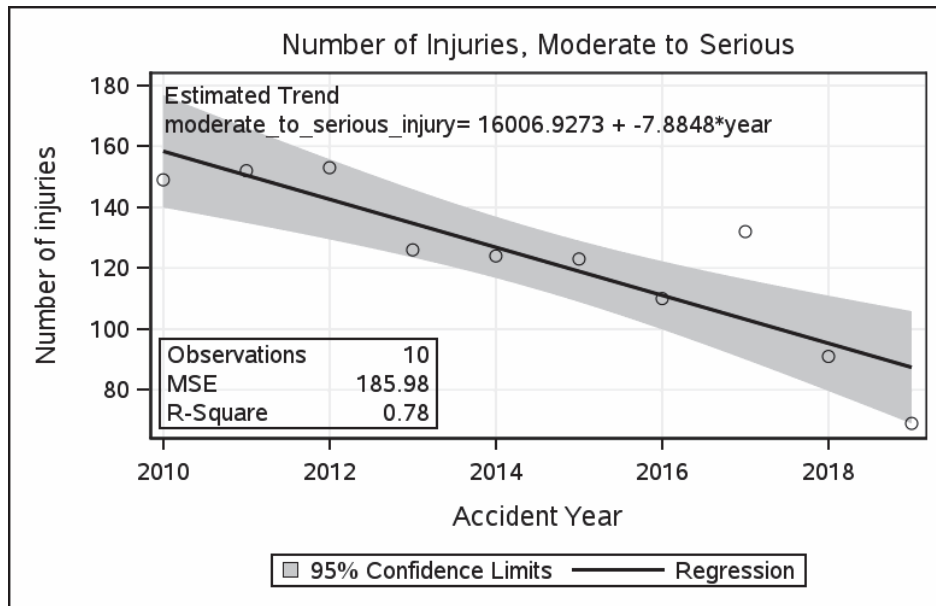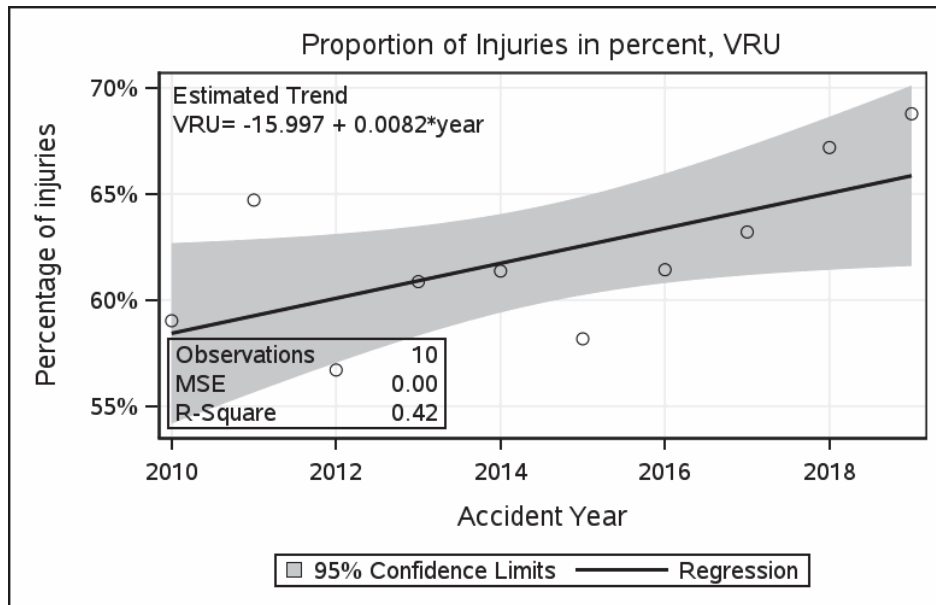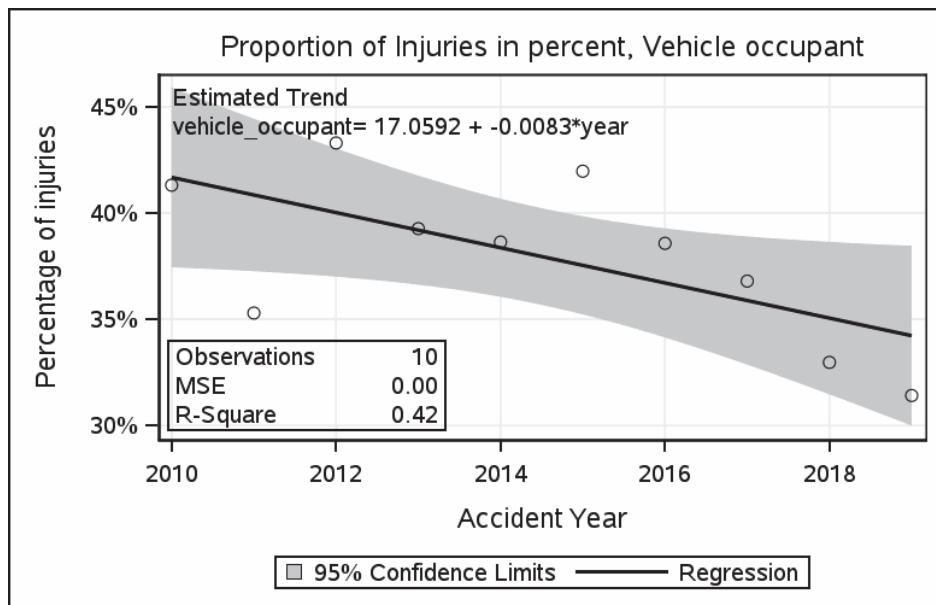

Figure A5. A simple linear regression analysis with an estimated trend for the number of injured children (0-17) traveling by moped (2010-2019).
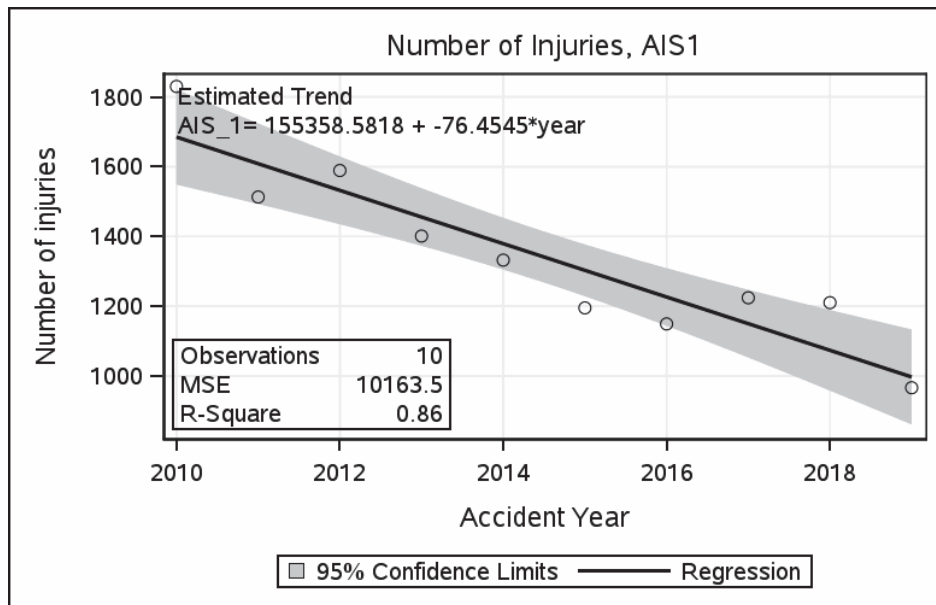
Figure A6. A simple linear regression analysis with an estimated trend for the number of minor injuries (2010-2019) for children 0-17 years old.

.

Figure A7. A simple linear regression analysis with an estimated trend for the number of moderate to serious injuries (2010-2019) for children 0-17 years old.

.

.

Figure A8. A simple linear regression analysis with an estimated trend in the proportion of VRU injuries (2010-2019) for children 0-17 years old.

Figure A9. A simple linear regression analysis with an estimated trend of the proportion of vehicle occupant injuries (2010-2019) for children 0-17 years old.

Figure A10. A simple linear regression analysis with an estimated trend in the number of AIS1 injuries (2010-2019) for children 0-17 years old.
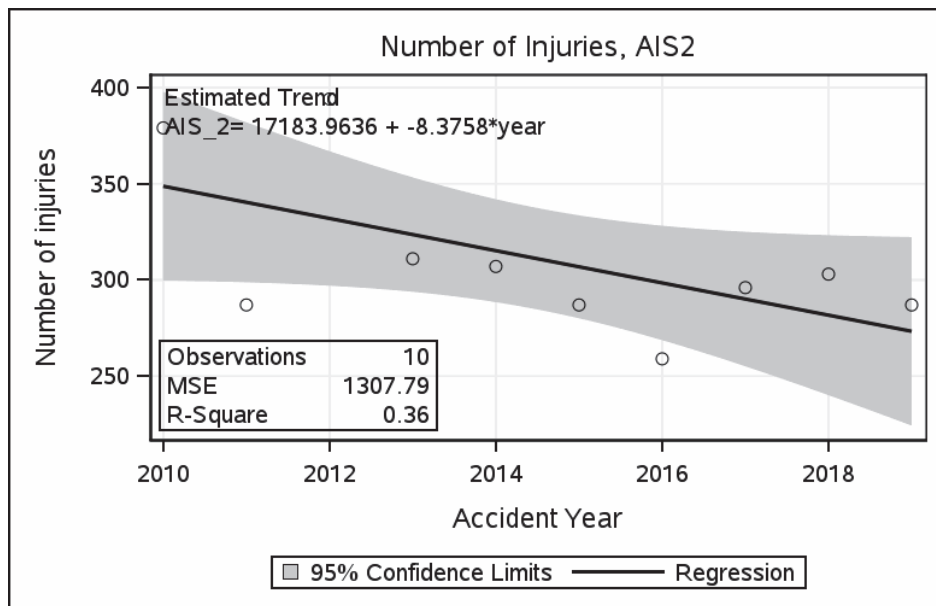

Figure A11. A simple linear regression analysis with an estimated trend in the number of AIS2+ injuries (2010-2019) for children 0-17 years old.

DEVELOPMENT OF A STANDARD FOR DEPLOYABLE PEDESTRIAN PROTECTION SYSTEMS (DPPS) FOR AMENDMENTS TO UN GLOBAL TECHNICAL REGULATION NO. 9 AND UN REGULATION NO. 127

Oliver Zander
Federal Highway Research Institute (BASt)
Germany

Irina Dausse
Renault
France

Peter G. Martin
National Highway Traffic Safety Administration (NHTSA)
United States of America

Jin Seop Park
Korea Automobile Testing & Research Institute (KATRI)
Republic of Korea

Paper Number 23-0144

ABSTRACT

World-wide test and assessment procedures for passive pedestrian protection have been in place for many years. Passive safety requirements within global technical regulation no. 9 (UN-GTR9) are prescribed through tests to the front ends of stationary vehicles with instrumented impactors representing the pedestrian's head, pelvis and lower extremities. However, no specific requirements are included for vehicles equipped with active bonnets and other deployable pedestrian protection systems (DPPS). This paper describes the work of the UN informal working group (IWG) to develop procedures on DPPS that are intended to be incorporated into UN-GTR9 and UN-R127 as amendments.

DPPS must work as intended during actual vehicle-to-pedestrian accidents. Therefore, test methods and conditions need to reflect the challenges DPPS are facing during actual and representative accident scenarios, but without being design restrictive. Several prerequisites need to be met in order to assure that DPPS operate properly and offer at least the same level of pedestrian protection as conventional passive pedestrian protection systems. These prerequisites include system requirements providing pedestrian detection and the timely and safe DPPS deployment. Also, headform tests are run at impact speeds below the DPPS deployment threshold on the undeployed system to confirm the undeployed bonnet is sufficiently safe.

Draft amendments intended for UN-GTR9 and UN-R127 are being finalized by the IWG on DPPS to harmonize testing under the agreements of 1958 and 1998 while preserving contracting parties' options for domestic standards. Results reported herein include IWG investigations of: (1) An appropriate impactor to assure a pedestrian is detected by the front-end sensing system; (2) Real world pedestrian accidents to determine the needed width of the detection test area; (3) Qualification procedures for Human Body Models (HBM) for use in simulations to determine head impact times (HIT) and impact locations; (4) An empirical formula to determine HIT in lieu of HBM computer simulations; (5) Experimental determination of the total response time of the DPPS. Altogether, the amendments provide for headform impact test conditions on deployable systems against established performance requirements to reduce head injury risk.

A DPPS is expected to offer a sufficient level of pedestrian protection while preserving vehicle design freedom. Several shortcomings of the developed procedure are discussed and limitations are identified which could reduce the actual pedestrian protection during a crash: The FlexPLI does not mimic the hardest to detect pedestrian. The detection test area does not fully account for all pedestrian impact trajectories. The bonnet clearance afforded by a DPPS could be compromised by the upper body load. The deployment height and the oncoming speed of the

deploying bonnet could differ between testing and real-world scenarios. A valid HIT determination using a HBM simulation on a given vehicle model requires good CAE correlation with the actual vehicle. The alternatives, experimental testing or an empirical formulation to determine HIT, could increase objectivity.

The draft procedures are being developed by the IWG for consideration as amendment to UN-GTR9 and UN-R127. It will offer an approach for compliance testing of vehicles equipped with DPPS. Since UN-R127 and the European New Car Assessment Programme (Euro NCAP) have extended their scopes to the head protection of bicyclists, the DPPS head protection potential should be investigated accordingly in future studies.

INTRODUCTION

Test and assessment procedures for vehicle-related passive pedestrian protection have been in place internationally for many years. These procedures evolved from Working Groups 10 and 17 of the European Enhanced Vehicle-safety Committee (EEVC, 2002) and the pedestrian working group within the International Harmonization of Research Activities (IHRA) (Mizuno, 2001). Then, the European Directive 2003/102/EC introduced the first mandatory requirements with effect from October 2005 (European Union, 2003). These were followed by Regulation (EC) No 78/2009 on pedestrian protection in January 2009 (European Union, 2009). The global technical regulation on pedestrian safety (UN-GTR9) under the parallel agreement of 1998 was published in January 2009 (UNECE, 2009) and United Nations Economic Commission for Europe Regulation on pedestrian safety (UN-R127) under the umbrella of the agreement of 1958 entered into force in November 2012 (UNECE, 2013).

More recently, since July 2022, Regulation (EU) 2019/2144 on type-approval requirements for motor vehicles as regards their general safety and the protection of vehicle occupants and vulnerable road users governs the legal passive pedestrian protection requirements for obtaining a European whole vehicle type approval (European Union, 2019).

Deployable Pedestrian Protection Systems (DPPS)

The most common type of DPPS to date is an active bonnet. It incorporates actuators and lever arms to automatically lift the bonnet upon detecting that a pedestrian has been struck by the front-end of the vehicle. The system acts to pre-position the bonnet before the secondary impact takes place with an oncoming pedestrian. In doing so, space is created between the bonnet and rigid components in the engine bay, thus reducing the risk of injury to the pedestrian. A second type of DPPS is an airbag e.g. deploying from the cowl area and partially covering hard structures of the windscreen periphery (e.g. lower frame, A-pillars).

DPPS are not directly addressed in UN-GTR9 or UN-R127. The GTR9 regulatory text merely states that "all devices designed to protect vulnerable road users when impacted by the vehicle shall be correctly activated before and/or be active during the relevant test" and furthermore adds the manufacturer's responsibility to demonstrate any devices acting as intended during a pedestrian impact.

The current preamble of UN-GTR9 offers a guideline to Contracting Parties for performing headform tests on vehicles with DPPS. The "Certification Standard for Type Approval Testing of Active Deployable Systems of the Bonnet/Windscreen Area" (UNECE, 2005), prepared by the International Organization of Motor Vehicle Manufacturers (OICA), provides a broad overview for determining whether a headform test on the deployed system, on the deploying system, or another type of test should be carried out. It contains a decision tree analysis devised for a type approval system of compliance in which the vehicle manufacturer and a type approval authority agree on the test parameters. However, the guidelines serve only to specify terminology for defining the timing of a launch as provided by the manufacturer, without specifying the timing itself. They do not cover requirements for the deployment threshold or the detection test area.

IWG on DPPS

Soon after UN-GTR9 was adopted, Euro NCAP introduced more sophisticated test provisions and requirements for deployable bonnets (Euro NCAP, 2010). Similar to those provisions, the IWG on DPPS is develop-

ing amendments to UN-GTR9 and UN-R127 with regards to the prerequisites and modified test provisions that are indispensable for assessing the safety level provided to pedestrians' heads by deployable systems during accidents. The prerequisites mainly comprise of (1) sufficient protection of a pedestrian at vehicle speeds below the deployment velocity threshold of the system, (2) the capability to detect a pedestrian during an impact, and (3) appropriate timing for a DPPS to be in the correct position for providing head protection during the impact. Each of these prerequisites is discussed in this paper. Depending on the degree of fulfillment of those prerequisites, the draft amendment will require headform tests to be performed either statically on the fully deployed DPPS, dynamically on a deploying DPPS, or statically on the DPPS in fully stowed position. A certain level of head protection also at vehicle speeds beyond 40km/h and the actual protection level of the DPPS during real world pedestrian accidents being sufficiently reflected by experimental impactor tests are further aspects for a proper functionality of the system and may be additionally considered in the future.

PROTECTION AT SPEEDS BELOW THE DEPLOYMENT THRESHOLD

DPPS are technical systems which are designed to increase head protection for a pedestrian in the event of an impact by a four-wheeled power-driven vehicle. This safety benefit is usually implemented by means of additional clearance between the bonnet and the underlying structure for sufficient energy absorption before any possible hard contact. Since DPPS do not activate below the "lower deployment velocity threshold," head protection at an impact velocity corresponding to this vehicle speed must be demonstrated to an equal level of protection of a passive, non-deployable system. This is done by performing a number of component tests with the headform impactors at the defined velocities.

Previous studies have suggested that head impact velocities of a pedestrian may correspond to not more than in average 0.9 times the vehicle speed (UNECE, 2003). However, wide variations of head impact velocities can be observed depending on the position of the pedestrian prior to impact, the pedestrian's stature, shape of the vehicle, random effects of different body parts and the chosen surrogate (Hardy et al., 2007). A range of head impact velocities with k-factors (the ratio between head velocity and vehicle speed) between 0.68 and 1.5 for a car impact speed of 40km/h were reported by Lawrence et al. (2004). Since those estimations were also taken into account when defining the test provisions for the legal headform tests at 35km/h, the same factor of 0.9 has been applied by the IWG for head impacts below the lower deployment threshold.

For UN-R127, the draft amendment calls for three headform tests, one to each third of the headform test area, are to be performed at an impact velocity of 0.9 times the corresponding vehicle's lower deployment velocity threshold. The GTR draft amendment will not place restrictions on the number of headform tests. The markup for the performance zones where the head performance criterion (HPC) must not exceed values of 1000 or 1700 may differ from that for the headform tests at the nominal impactor velocities of 35km/h.

PEDESTRIAN DETECTION

In order to take into consideration the safety benefit provided by a DPPS in the event of a collision, the pedestrian must be appropriately detected. To account for a range of real-world accident scenarios covering the most common and frequent cases, the draft amendment requires tests with a pedestrian surrogate representing a broad variety of pedestrian statures and stances. According to the draft amendment, the tests have to be carried out on the area of the vehicle front where a pedestrian impact can be expected. It is assumed that a vehicle-to-pedestrian impact at the vehicle speed corresponding to the lower deployment threshold of the DPPS represents the most challenging case to be detected (referred to as "hardest to detect", or HTD) by the sensing system.

Pedestrian surrogate

During the discussions among members of the IWG on DPPS, it was recognized that most of the currently available impactors show several shortcomings when acting as pedestrian surrogates for the purpose of detection and sensor activation. The pros and cons of available pedestrian legform impactors were investigated in

terms of scope, certification procedures, contact biofidelity, representativeness, and applicability during component or full-scale tests (see Table 1.

Table 1.
Comparison of candidate Sensing Impactors (Zander et al., 2020)

	EEVC WG 17 Lower Legform Impactor	EEVC WG 17 Upper Legform Impactor	Flexible Pedestrian Legform Impactor	Pedestrian Detection Impactor 2
State of the art / Current Usage	Tool for homologation in Regulation (EC) No. 78/2009 50th percentile Pedestrian surrogate in Euro NCAP Pedestrian Testing Protocol (++)	Tool for homologation in Regulation (EC) No. 78/2009 and UN-R127/UN-GTR9 (+++)	Tool for homologation in UN-R127/UN-GTR9 50th percentile Pedestrian surrogate in Euro NCAP Pedestrian Testing Protocol (+++)	Tool for HTD Pedestrian surrogate in Euro NCAP Pedestrian Testing Protocol (+)
Dynamic Certification (Injury Criteria)	Procedure and verification of 3 criteria (internal biofidelity) (+)	Procedure and verification of 5 criteria (internal biofidelity) (+)	2 procedures and verification of 7 criteria each (internal biofidelity) (++)	Not available (-)
Contact Biofidelity	not verified (-)	not verified (-)	not verified (-)	verified (+)
Mass	13.4kg	9.5-18kg	13.2kg	6.7kg
Representativeness	50th male	50th male	50th male	Various statures (++++)
Applicability	Yes (moving car) Feasibility in low speed testing with propelled impactor (+)	No (needed mass reduction to 7.4kg for HTD approximation not feasible. New guiding system would be needed) (-)	Yes (moving car) Feasibility in low speed testing with propelled impactor (+)	Yes (moving car) Feasibility in low speed testing with propelled impactor (+)
Summary	+++	++	+++++	++++++

According to the summary table, the pedestrian detection impactor 2 (PDI-2) would be the first choice as pedestrian representative. However, while its very conservative and demanding requirements seem appropriate for consumer tests, it sometimes underestimates the loads that are emanated from a pedestrian onto a sensing system.

Figure 1 shows that the mean intrusions, forces, and energy levels (i.e. the internal energy of the expanded polypropylene foam block at the middle loadpath, considering intrusions and horizontal and vertical deformation) induced by the PDI-2 (evaluated only at the approximate height of the sensor system, i.e. in the middle loadpath) are very often at the lower end of the scale when being compared to Human Body Model simulations, the FlexPLI, and the EEVC WG 17 pedestrian legform impactor (Pauer et al., 2018).
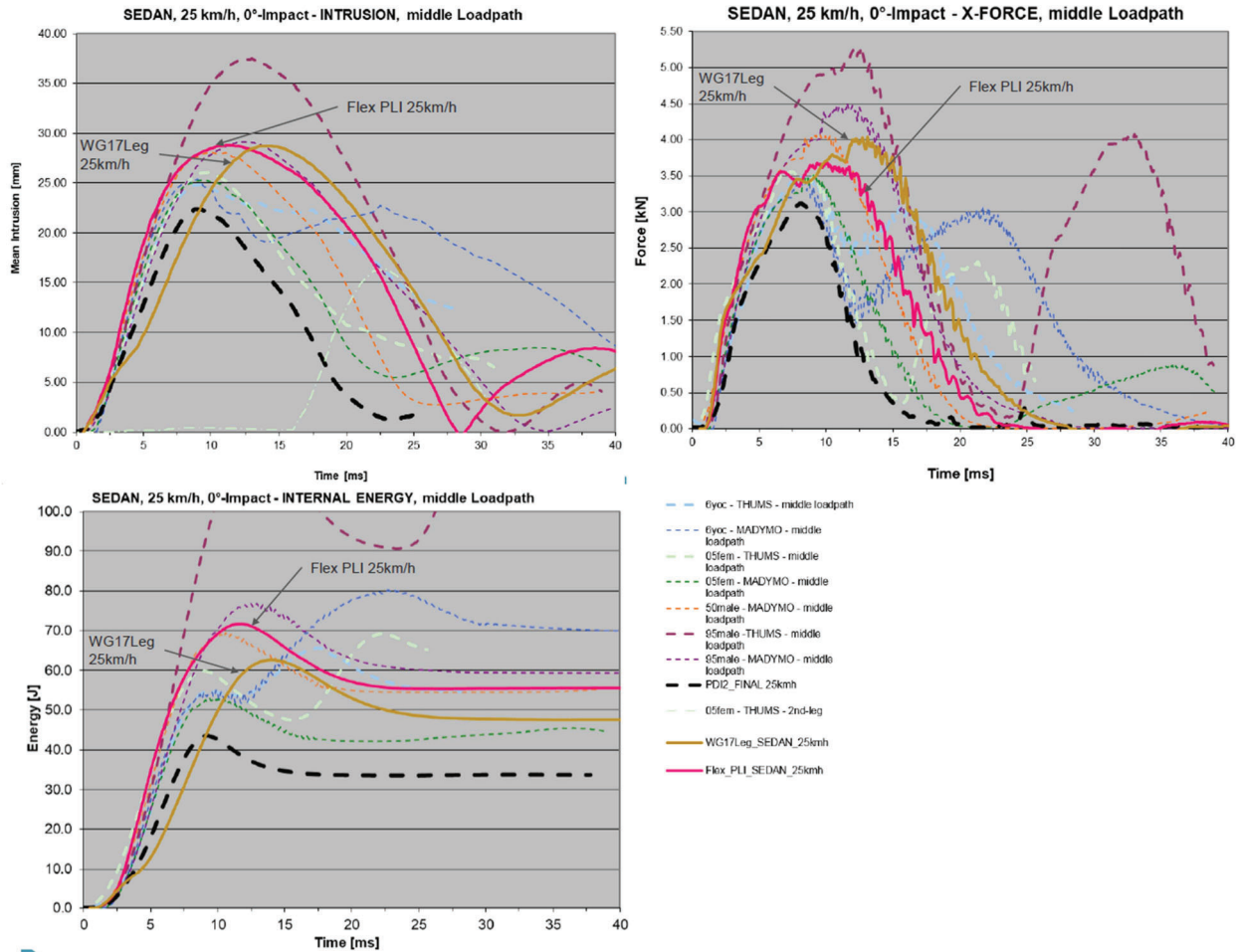
Figure 1. Loadings from pedestrian Human Body Models, PDI-2, FlexPLI and EEVC WG17 PLI on the vehicle frontend – Example Sedan 2D test frame, 25km/h, perpendicular impact at mid loadpath (Pauer et al., 2018).

The FlexPLI, on the other hand, provides good representativeness and contact biofidelity. Furthermore, it has already been established as a tool for injury assessment in UN-GTR9, UN-R127, as well as consumer tests. It was demonstrated to have good repeatability for injury assessment. Dynamic certification tests were established to assure the reproducibility of the device and repeatability during testing. The device is fully specified within UNECE Mutual Resolution No. 1, including a complete set of engineering drawings (UNECE, 2020).

For a validation of its contact biofidelity, properties of the FlexPLI that are relevant for the sensor signals need to stay within defined tolerances. When meeting the tolerances as defined within the impactor specifications (UNECE, 2018), its total mass, the mass distribution, moments of inertia, centers of gravity, lateral dimensions for all load paths and the bending stiffness around the y axis can be considered very robust. Furthermore, the stability of the impactor local stiffness / compression behavior in the longitudinal direction at height of the vehicle mid cross beam were evaluated by the intrusion which can be approximated by integrating twice the channel filter class (CFC) 180-filtered (to account for the test specification) acceleration signal. The double integral then needs to stay within a narrow range.

The results of a number of dynamic inverse tests, derived from the inverse test as described in UN-GTR9 and UN-R127, were evaluated with regards to the repeatability of the acceleration signal. Acceleration, as described above, is the most convenient criterion for ensuring high quality contact biofidelity. The acceleration measurement needs to be done at the impactor itself, and not on the impacting aluminum honeycomb, as speci-

fied in Figure 2, in order to get the full path of travel of the impactor and to damp the effect of scatter of the folding honeycomb. The tests were performed at a common DPPS lower deployment velocity threshold of 25km/h. Two inverse tests, each with halved honeycombs, were carried out with ten certified FlexPLI impactors (UNECE, 2018). One impact height matched the inverse certification test at the knee, the second one was 64mm lower on the tibia, altogether representing "worst case" heights of typical cross beam structures around the requirement of the Research Council for Automotive Repairs (RCAR, 2010), see Figure 2. The accelerations were measured with the standard accelerometer positioned at the knee location, 523mm above ground level, and an additional accelerometer positioned at the uppermost tibia segment, 459mm above ground level:
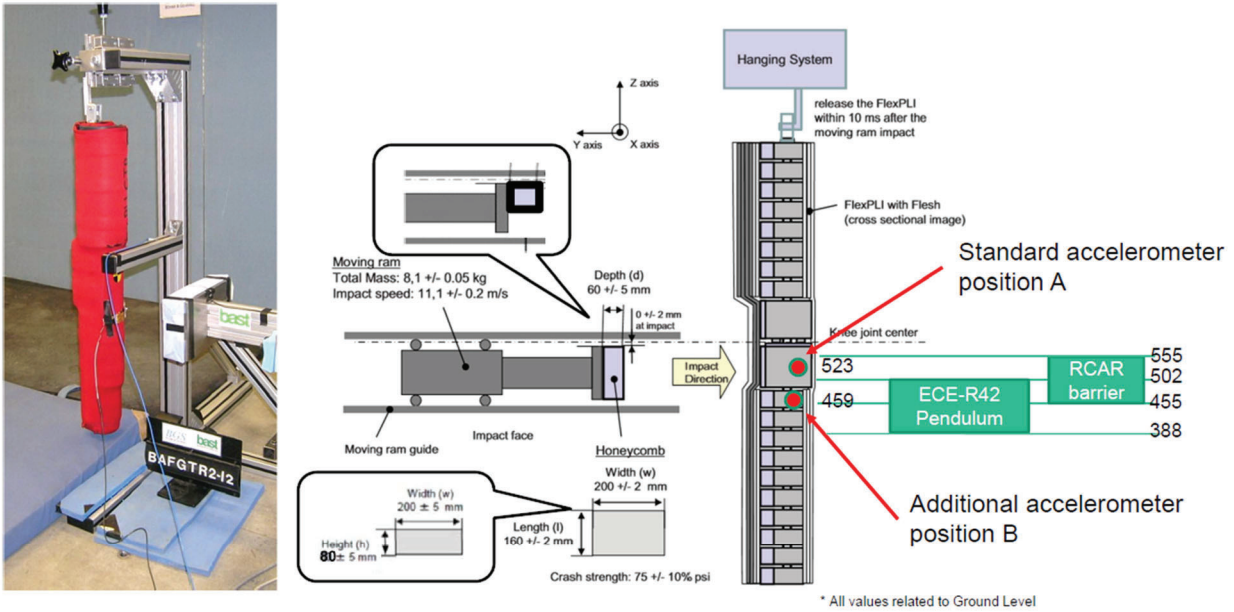
Figure 2. Test setup and positioning of the accelerometers for FlexPLI contact biofidelity check (Zander et al., 2020-2).

The determined displacement vs. time results of the inverse tests are plotted in Figure 3 for the honeycomb alignment with the knee (left) and with the tibia (right). The coefficients of variation were calculated at different time steps at 20, 25, 30 and 35ms after the impact with 2.4-2.8% for the knee impact and 5.7-6.2% for the tibia impact. Altogether, the repeatability of the displacement was good or acceptable.
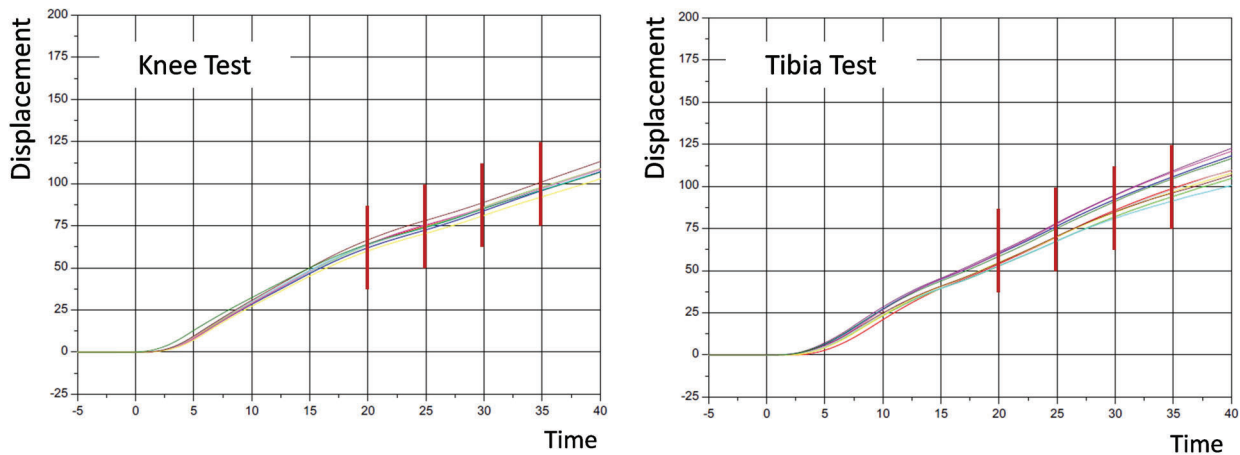
Figure 3. Displacement vs. time for the knee test (left) and the tibia test (right) (Gehring et al., 2021).

Altogether, it could be demonstrated that the FlexPLI represents a pedestrian surrogate that can be used for the sensing verification of a DPPS. However, the impactor can only represent a limited range of typical load cases. The authors recommend including the corresponding language within the preamble of UN-GTR9 and in UN-R127.

Detection test area

As one of the fundamental prerequisites to account for the potential safety benefits of a DPPS, any pedestrian needs to be detected during an accident prior to head impact on the vehicle. The IWG discussed the required width of the area on the vehicle front where a pedestrian needs to be detected in order to purposefully initiate the DPPS. The area definition should balance the zone where a pedestrian contact with the vehicle front could occur as well as the technical feasibility and limitations of an impactor test.

In a study of the German In Depth Accidents (GIDAS), Zander et al. (2014) found that first contact of pedestrians take place, in principle, over the entire width of the vehicle, where thus a detection would be needed. A Laboratory of Accidentology and Biomechanics (LAB) study of the In-Depth Database of only injured or fatal accidents in France (LAB, 2022) revealed no head impacts to the bonnet for cases in which a pedestrian was struck outside the longitudinal frame rails of the vehicle, while approximately 1/3 of cases resulted in a pelvis impact to the bonnet. The LAB study found that the area outside the frame rails accounts for approximately 15-20% of the vehicle width.

A pedestrian may tend to spin off at the outer widths of typical angled or V-shaped vehicle front end surfaces, without a head-to-bonnet impact. This effect may be even more pronounced when using a leg impactor as pedestrian surrogate without attaching additional mass representative of the pedestrian's hip, torso, arms, neck and head. The lower mass reduces the load on the sensing system and is therefore not representative of a pedestrian.

Several possible definitions for a detection test area were discussed by the IWG. Based on the laboratory results from post-mortem human subject (PMHS) tests, HBM simulations and full-scale dummy tests, there was mainly a longitudinal wrap-around of the pedestrian, with low lateral offset, and thus a detection area with lateral dimensions identical to the width of the activated part of the DPPS was suggested (JASIC, 2021). On the other hand, GIDAS data showed a number of real-world cases with a significant lateral offset between the first leg impact and the subsequent pedestrian head impact (Zander et al., 2021). Among the proposals for the detection test area were:

(a) to use the existing lower leg bumper test area (BTA) as defined in UN-R127 and UN-GTR9;

(b) to use the corner reference points (CRPs) as specified in UN-R127 (the intersections of the side reference lines (SRLs) and the bonnet leading edge reference line (BLERL)) as outer boundaries;

(c) to use a percentage of the relevant vehicle width (RVW), where RVW is defined as the width at the cross-section of the front axle, without rear view mirrors or rear-view mirror substitute systems. Under this setting, the detection test area is taken from reference points on the vehicle front-end that are (12.5% * RVW) inboard from the outer boundaries of the RVW. Thus, all vehicles would be equally treated, regardless of their effective width;

(d) in addition to (c), to account for wider vehicles, a subtraction of no more than 250mm on either vehicle side would be allowed;

(e) to exclude any structure-based criterion such as the cross beam with possible additional structures which are appended to fulfill crash test requirements for different markets.

In subsequent deliberations, the IWG decided against the use of the corner reference points. It was noted by IWG participants that when a vehicle has multiple or continuous intersections between the BLERL and the SLR, the most outboard point is used as the CRP. It was also noted that the distance between right and left CRPs can be narrowed easily by a minor, cosmetic redesign of the vehicle front end. Such a redesign would

have no effect on the legform test zone, but could lead to large differences in CRP locations and thus greatly affect the DPPS detection test area.

The IWG also deliberated on the use of the BTA, which is defined as the wider of the width defined by the corners of the bumper (CoB, determined by contacting the vehicle front with a corner gauge maintaining an angle of 60° to the vehicle longitudinal centre plane) and the width of the underlying bumper beam. The IWG decided to exclude the bumper beam, reasoning this to be consistent with a performance-based standard. If a bumper beam requirement had been included, it would have partly acted to prescribe the currently prevalent sensing tube technology and the form of the bumper beam itself. A regulation should not prescribe a particular design nor stand in the way of new technologies, such as different sensing technologies or bumper beams that utilize different materials, shapes and functions.

While discussing the various definitions, the IWG also examined a survey of current vehicles with DPPS on the market, see Table 2 (VDA, 2022). The survey revealed the 12.5% stipulation would determine the width of the detection test area in all but one case. It also showed that the reported width of sensing of some (but not all) vehicles would exceed the width of the detection test area.

Additionally, the survey demonstrated that the width of sensing, i.e. the area in which a detection of a pedestrian is potentially covered, can also extend outboard into an area where the front-end is highly curved and a glancing blow of the impactor could occur. Furthermore, subtracting 12.5% of the relevant vehicle width at each side could also still result in an area with potential impactor spin-off. In general, new vehicles are expected to have a greater width of sensing relative to vehicles not fulfilling any of the requirements associated with a detection test area.

Table 2. Survey of current vehicles with DPPS (VDA, 2022).

OEM	RVW* (mm)	RVW - 2*12,5% (mm)	Corner gauge - 2*42mm	Width of Sensing (mm)	Type of sensing system	Vehicle Category
# 1	1985	1488.75	1108	1390	single pressure tube	SUV
# 3	1954	1465.5	1012	1544	pressure tube + 3 accel.	SUV
# 4	1922	1441.5	1452	1672	single pressure tube	Sedan
# 5	1880	1410	1110	1316	single pressure tube	Sedan
# 1	1878	1408.5	1328	1600	single pressure tube	SUV
# 3	1876	1407	1234	1380	single pressure tube	SUV
# 5	1871	1403.25	972	1472	pressure tube + 3 accel.	Sedan
# 1	1838	1378.5	1120	1400	7 accelerometers	Sedan
# 2	1820	1365	1258	1410	single pressure tube	Sedan
# 3	1798	1348.5	1304	1424	single pressure tube	Compact
# 4	1790	1342.5	1170	1430	pressure tube + 3 accel.	Compact
# 5	1777	1332.75	1200	1276	single pressure tube	Compact

*The 250 mm stipulation did not apply to any of the vehicles in the survey.
Dark green: Determination of the Detection Test Area
Light Green: Width of Sensing larger than Detection Test Area

The IWG finally agreed upon that the minimum width of the detection test area would be the relevant vehicle width minus 12.5% (but not more than 250mm) on each side. Additionally, the width must extend to at least 42 mm inboard of each corner of bumper (CoB), see Figure 4:
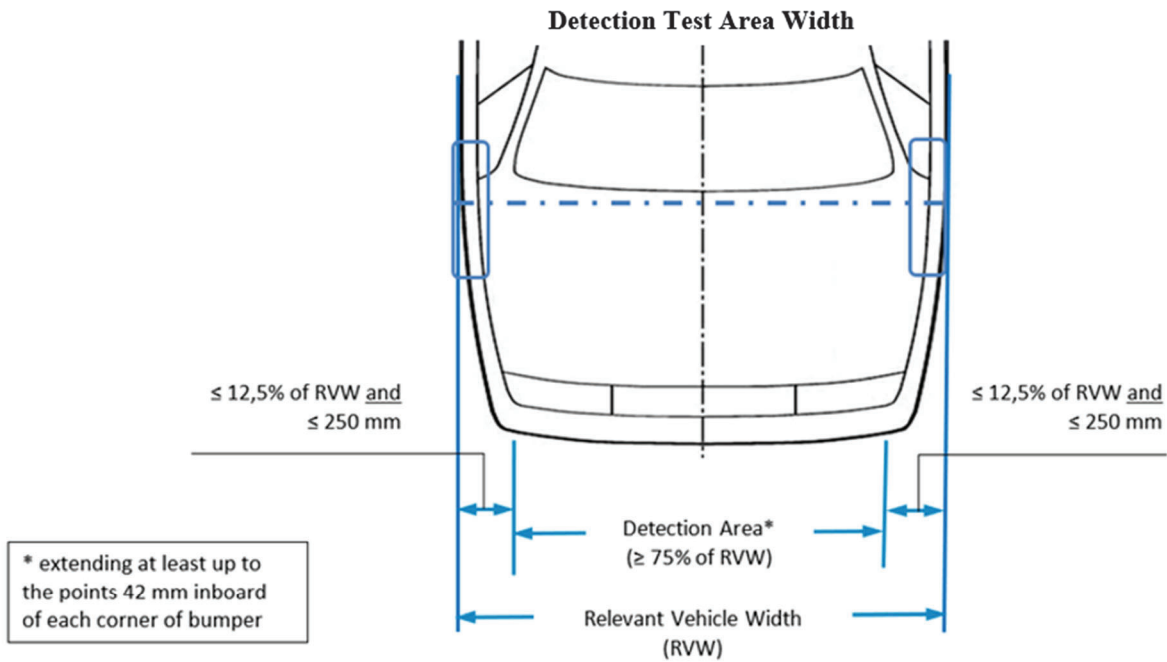
Detection Test Area Width

≤ 12,5% of RVW <u>and</u>
≤ 250 mm

≤ 12,5% of RVW <u>and</u>
≤ 250 mm

Detection Area*
(≥ 75% of RVW)

* extending at least up to
the points 42 mm inboard
of each corner of bumper

Relevant Vehicle Width
(RVW)

Figure 4. Definition of the Detection Test Area (based on Gehring et al., 2020).

Depending on the outer contour of the vehicle frontend, the detection test area is either determined by the CoB -42mm on either side (compare Figure 5 left), or the relevant vehicle width -12,5% on either side (Figure 5, right):

CoB -42mm (l+r) > 75% of RVW

CoB -42mm (l+r) < 75% of RVW

CoB (r)   CoB (l)

CoB (r)   CoB (l)

Relevant Vehicle Width (RVW)

Relevant Vehicle Width (RVW)

75% of RVW

75% of RVW

CoB -42mm (l+r)

CoB -42mm (l+r)

Detection Test Area

Detection Test Area
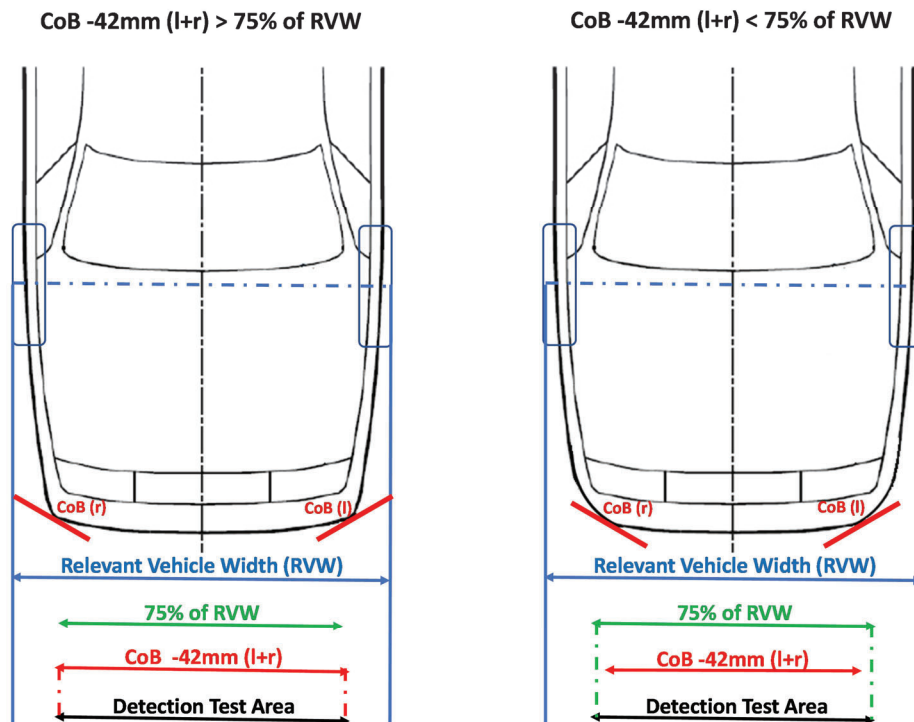
Figure 5. Factors for the determination of the detection test area.

Sensor activation tests

The draft amendment specifies sensor activation tests for UN-R127 and UN-GTR9. For UN-R127, the detection test area will be subdivided into thirds of equal width, measured with a flexible tape along the outer bumper contour at a height of the upper bumper reference line. A minimum of one test per third with the FlexPLI, with a distance of at least 50mm to adjacent points, will be performed at the lower deployment velocity threshold. For UN-GTR9, there will be no mandates on the number of tests or where along the bumper reference line testing is carried out.

When tested with a moving vehicle against a stationary impactor, a vehicle velocity tolerance of ±0.6m/s and an impact accuracy of ±50mm must be met. During the inverse test with the FlexPLI propelled against the stationary vehicle, all tolerances on impact velocity and impact location specified in the UN-R127 / UN-GTR9 injury assessment tests must be fulfilled. Tests must be repeated if they do not meet the prescribed test specifications and the DPPS does not deploy. If the DPPS does not activate in any of the tests, the subsequent headform tests will be performed with the DPPS in the undeployed position.

TIMING OF DPPS DEPLOYMENT

As one of the indispensable prerequisites for consideration of the safety benefits provided by a DPPS, its position must be in its intended position during the pedestrian's head impact. For testing the DPPS statically in the fully deployed position, the total response time (TRT) of the system must be smaller or equal to the head impact time: $TRT \leq HIT$. If the $TRT > HIT$, the test is to be performed dynamically on a deploying DPPS or statically on a completely undeployed system. For contracting parties not considering static tests on the fully deployed system, the determination of the TRT is not necessary; however the sensing time (ST) as part of the TRT as well as the HIT must be determined in order to appropriately synchronize the firing times of the head impactor and the DPPS during dynamic headform tests.

Total response time

The total response time is the first benchmark for deciding upon the state of the DPPS during static headform tests. It is the sum of the sensing time (ST) and the deployment time (DT): $TRT = ST + DT$. The sensing time is understood as the duration from the time of first contact of the pedestrian (excluding forearms and hands) with the vehicle outer surface until the initiation of the deployment. The deployment time means the duration from the initiation of the deployment until the DPPS reaches its deployed position. The sensing time is experimentally determined during an impactor test with the FlexPLI at 40km/h. It starts with the first contact of the impactor with the vehicle frontend. As with the sensor activation tests, this test can be performed either as a driving test with a stationary FlexPLI or as an inverse test with the FlexPLI being propelled horizontally against the vehicle frontend. The same test specifications as for the sensor activation tests apply.

The IWG discussed several aspects that need to be taken into account when determining the TRT. The TRT can, in principle, be considered as the elapsed time from the point of first contact with the pedestrian until the operating condition of the DPPS. However, a full deployment is not necessarily equal to the required deployment height (RDH), i.e. the height which is required in order to provide sufficient clearance under the bonnet for head energy absorption. Furthermore, a full deployment / final state can differ from the maximum deployment height since, after having reached the maximum, the DPPS may oscillate and fade out around the final state. For each test point on the bonnet, the RDH, maximum deployment height (MDH), and final state and their corresponding timings will need to be compared with the HIT of the pedestrian. Figure 6 illustrates possible different states of the DPPS during its deployment:
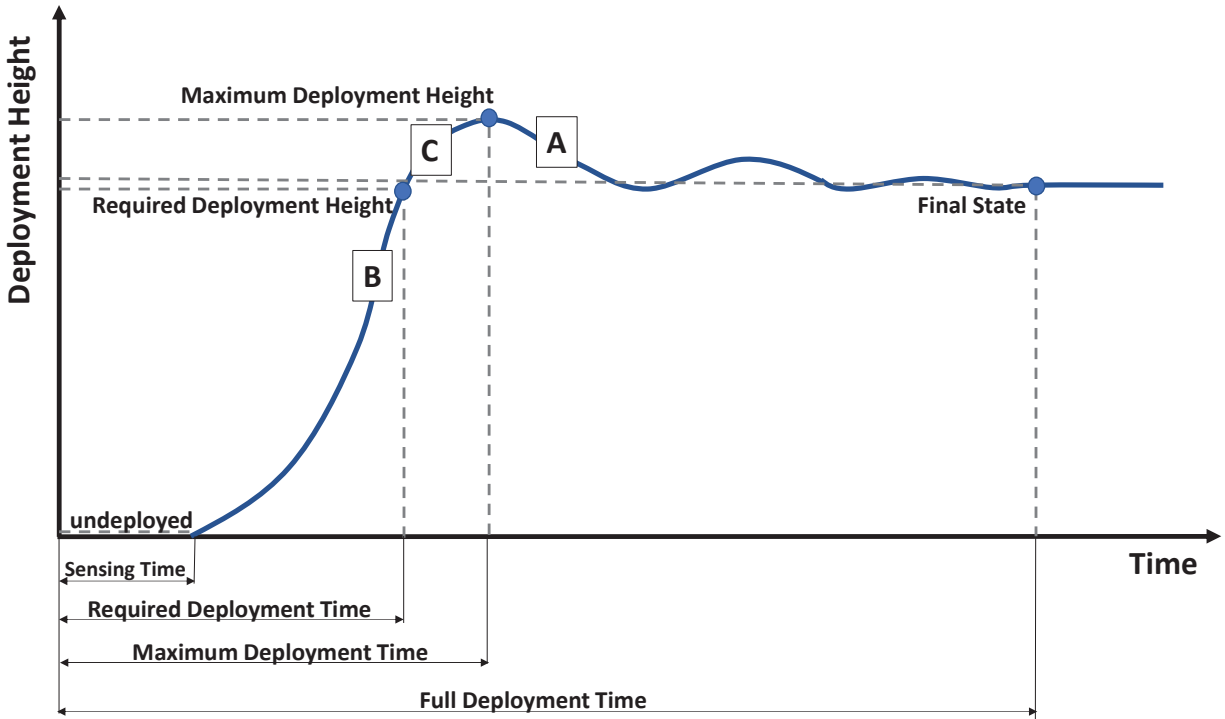
Figure 6. DPPS deployment height vs. time (Zander, 2022-2).

Subsequent to the required deployment time (RDT), i.e. the duration from the time of first contact of a pedestrian with the vehicle front until the DPPS reaches (stops at or passes) the RDH, the system may continue moving upwards until it has reached the MDH at the maximum deployment time (MDT). Afterwards, it may continue to oscillate around the full deployment height which will be the final state of the DPPS.

According to the draft procedure, depending on the HIT of the pedestrian, the DPPS may be tested in the fully deployed state (HIT ≥ MDT, in area "A") or in the dynamic mode while the DPPS is deploying (HIT < RDH, in area "B"). The test conditions for RDT ≤ HIT < MDT in area "C" depend on the effects of the oncoming, not yet fully deployed, DPPS on loads to the headform. If the effects are negligible, the DPPS may be tested statically at a height no more than the RDH. Otherwise, a dynamic test at the time of head impact must be performed. However, since a study of the possible effects of an oncoming DPPS did not result in unambiguous evidence for a neglectable influence, the draft test procedure tentatively specifies to perform all tests with HIT < MDT with the DPPS in the dynamic mode.

Head impact time

For a decision upon the boundary conditions of headform impact tests, the TRT is to be compared with the HIT of the pedestrian. The IWG discussed several alternatives for HIT determination: (a) by means of numerical simulations with HBMs on vehicle models, (b) by performing experimental full-scale tests using pedestrian dummies and the actual vehicle (c) by applying an empirical formula to calculate a generic HIT.

The IWG intends to present the draft procedures in multiple phases. For the first phase of legal DPPS testing, HITs are determined by means of numerical simulations, only. The method for including full scale dummy tests and the generic approach with empirical formula are being further evolved for subsequent phases of UN-GTR9 and UN-R127.

Simulation-based approach

A simulation-based determination of pedestrian HITs on vehicle frontends requires high quality HBMs and vehicle models. Euro NCAP already developed a procedure for the certification of HBMs with regular updates and revisions (Euro NCAP, 2021). The IWG transposed this procedure into the draft amendment's regulatory text for the HBM qualification, including the documentation of the validation of the reference HBMs. Figure 7 illustrates the process for determination of the HIT based on simulations with qualified HBMs:
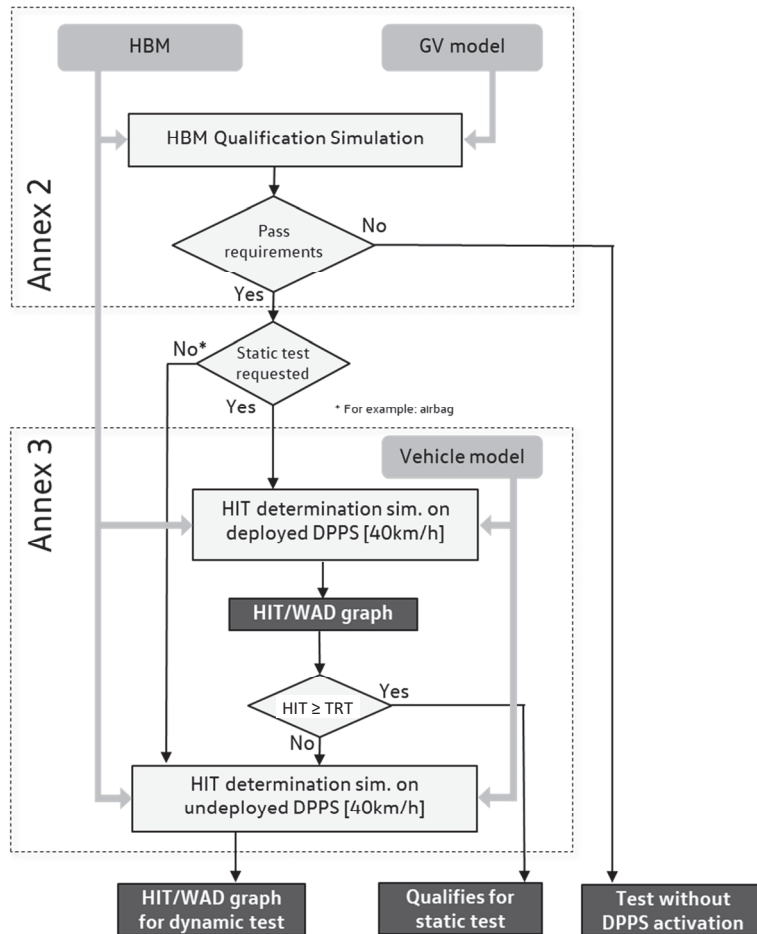
Figure 7. Flowchart for HIT determination based on numerical simulations (Besch, 2022).

Qualification of the HBM is performed on Generic Vehicle (GV) models representing a roadster (RDS), a family car (FCR) and a sports utility vehicle (SUV). A multi-purpose vehicle (MPV) had been evaluated and used for several years by Euro NCAP (2021). Since its shape was found to be represented by FCR and SUV, it was removed from the simulation matrix. Those findings were transposed to the legal procedure.

Vehicle speeds are 30km/h, 40km/h and 50km/h. All relevant HBM statures are used at predefined initial postures, with the Head Centre of Gravity (CoG) located on the vertical longitudinal vehicle centre plane. The static and dynamic coefficients of friction are 0.3 each.

During the qualification simulations, HIT values, the height of the centre of the left and right acetabulum centres (AC), the head CoG (HC) relative to the ground level and their relative horizontal distance at HIT need to fulfill the corridors drafted with reference values from HBMs that were validated against PMHS by Forman et al. (2015). The calculated HIT from the simulations is the elapsed time between the first time where the

contact force deviates from 0 (neglecting shoulder and upper arm) and the contact time of the head to the vehicle.

The HBMs for the six-year-old child (6YO), the 5th female (AF05) and the 50th male (AM50) need to be specifically qualified. For the 95th male (AM95), no qualification simulations are needed because the AM95 HBM was derived directly from the AM50 HBM. The 6YO, AF05, and AM50 HBMs were developed independently. Only HBMs qualified according to the described procedure can be subsequently used to determine the HIT with simulations on the actual vehicle models.

If headform compliance tests are targeted to be run statically on a deployed DPPS, the HIT determination simulations are to be performed on the deployed DPPS. If the requirement HIT ≥ TRT is met, the headform compliance tests may be done statically on the deployed system; otherwise, further HIT determination simulations have to be performed on the undeployed DPPS for setting up the firing times and WAD values during dynamic compliance tests on the deploying DPPS.

If no static but only dynamic headform compliance tests on the deploying DPPS are requested, the HIT determination simulations will be altogether performed on the undeployed DPPS only, for firing times and WAD values (compare Figure 7, "Annex 3"). In either case, for simplification, the vehicle speed during all simulations is 40km/h.

All HBMs with their heads properly hitting the actual DPPS need to undergo HIT determination simulations. In case of only one HBM properly hitting the DPPS with its head, the next tallest HBM should also be used for the purpose of drawing a HIT vs. WAD graph. Based on the results of HBM simulations on the deployed DPPS, the HITs of all relevant HBMs are plotted as a function of the WADs and the connecting line (drawn by means of linear interpolation) is compared with the TRT of the DPPS, see Figure 8 (left):
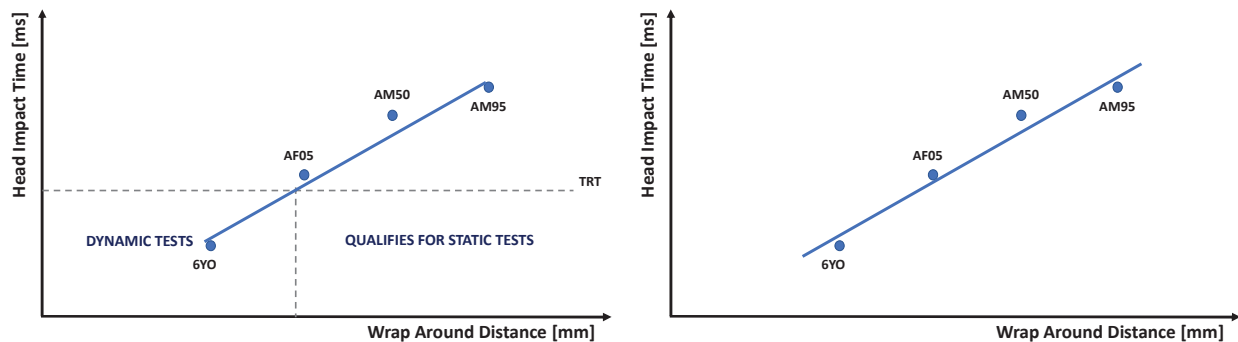
Figure 8. HIT vs. WAD graph for HBM simulations on deployed DPPS (left) and on undeployed DPPS (right).

If HIT ≥ TRT, compliance headform tests may be performed statically on the deployed DPPS. In case of HIT < TRT, compliance headform tests must be performed dynamically on the deploying DPPS. In some situations, only portions of a given DPPS may be tested in static mode since HIT varies depending on the point of impact.

For the determination of the firing times related to WAD of points to be tested dynamically, additional HBM simulations on the undeployed DPPS must be performed, the HIT for all relevant HBM statures plotted vs the corresponding WAD and the regression line marked in the diagram and extrapolated to all WADs within the DPPS (see Figure 8 (right)). To obtain the HIT for a dynamic test, the known WAD can be associated to the corresponding HIT by means of the regression line.

HIT determination by experimental dummy testing

As an alternative to finite element (FE) simulations, the IWG plans to develop a procedure wherein pedestrian head impact times can be determined with full scale vehicle crash tests against stationary pedestrian dummies. Specifications for a midsize pedestrian dummy are outlined in SAE J 2782 (2019), with focus on biofidelic

whole body kinematics during a vehicle to pedestrian impact. It may be assumed that additional performance specifications for other pedestrian sizes will be developed in the future. Thus, at this point in time, the experimental determination of the HIT is possible for the 50th male, only. The applicability of alternative dummies such as the biofidelic dummy (Schäuble et al., 2019) needs to be further investigated. A full-scale testing procedure can be found in SAE J 2868 (2020), but it is understood to be a guideline rather than a mandatory set of requirements.

HIT determination by a generic approach

The IWG on DPPS is also planning on developing an option for HIT determination using an empirical formula. This formula will make use of geometry information of the vehicle with potentially significant influence on the pedestrian's impact kinematics: height of different load paths such as BLE, bumper, lower stiffener, bonnet angle etc. Geometry information such as BLE height, bonnet angle, WAD or HIT will be collated in a database. An algorithm will be developed in order to determine the HIT based on the available geometry information and WAD of the test point. A correction factor will account for possible inaccuracies. The database will be updated regularly for further improvement of the approximations. Due to its objectivity and independency, the generic approach seems advantageous, in particular, for self-certification.

ADDITIONAL PREREQUISITES TO BE CONSIDERED FOR FUTURE DPPS AMENDMENTS

The IWG discussed the need for two other system requirements that are not covered by the DPPS amendments: (1) Assurance that a DPPS system will deploy safely at pedestrian impact speeds above 40 km/h; (2) Certainty that pedestrian body loading to a DPPS will not compromise its effectiveness prior to head impact. These requirements are discussed below. Additionally, future accidentology may reveal a prominent safety need exists in current DPPS due to body loading and impacts at higher speeds. In either case, the GTR will be reviewed and adapted if and where necessary.

Protection at higher vehicle speeds

Headform compliance tests are means for representing head injury assessment during vehicle to pedestrian accidents at vehicle speeds of 40km/h. However, passive systems are expected to also provide some protection during accidents with higher vehicle speeds. Since DPPS are to provide at least the same level of protection as passive systems, they need to ensure measures to meet this requirement. For that purpose, its deployment should be at least initiated at vehicle speeds beyond 40km/h, or sufficient clearance be provided for energy absorption during head impacts at impact velocities higher than 35km/h.

Body loading: Actual DPPS protection level

In case of meeting the defined prerequisites, DPPS may undergo headform compliance tests in a deployed state or during deployment. The generated clearance underneath the bonnet provides for energy absorption of the impacting headform, decreased impactor accelerations and a lower head injury criterion, linked to a lower injury risk. However, provisions need to take care of the additional clearance not being reduced before pedestrian head impact. In the regulatory impact analysis conducted for the European Directive 2003/102/EC (European Union, 2003), a failure mode and effects analysis found that the actuators used to raise the bonnet pose one of the greater risks to failure of the entire active bonnet system (Hardy et al., 2006). Nuß et al. (2013) also investigated the effect of upper body contact on the deformation of the bonnet:

Figure 9 shows a passive vehicle front with undeformed (left) and with deformed (middle) bonnet due to loadings induced from the upper body of the pedestrian (right), at the location of and prior to head impact:
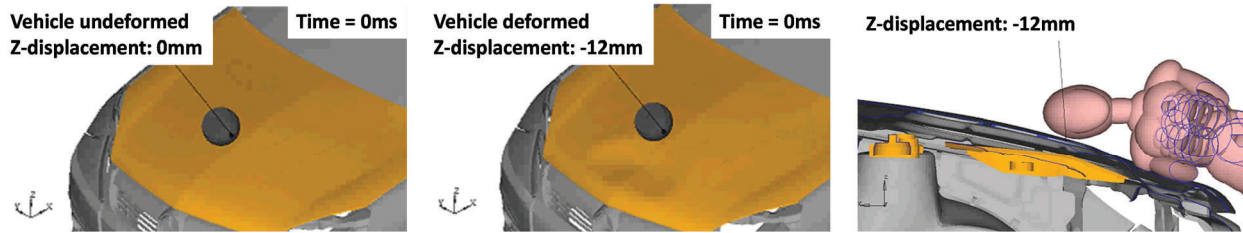
Figure 9. Deformation of the bonnet due to upper body prior to head impact (Nuß et al., 2013).

The influence of the deformation is depicted in Figure 10: The peak headform acceleration during head impact on the deformed bonnet exceeds the acceleration on the undeformed bonnet by approx. 40 percent; the HIC increases by almost 44 percent.
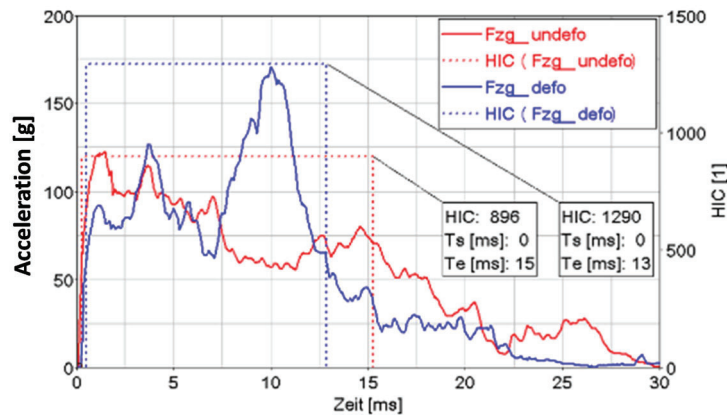

Figure 10. Head acceleration during impact on undeformed and deformed bonnet (Nuß et al., 2013).

Notwithstanding concerns with higher speeds and body loading, the IWG agreed that a regulatory need is not known with enough certainty to warrant the development of test procedures and requirements. However, further research or the development of future DPPS may result in insights for which the effect of pedestrian body loading and protection at higher speeds may require special attention. Test procedures may be needed to assure that the lifting linkages are strong enough for not only the initial lift but also to support the weight of the pedestrian's torso so that the bonnet does not collapse prior to head-to-bonnet impact. The IWG furthermore acknowledged that corresponding requirements have already been implemented within the Euro NCAP test procedures (Euro NCAP. 2010).

Non-contact pedestrian detection sensors

In current DPPS, only contact sensors are taken into consideration for pedestrian detection. Procedures for forward-looking and non-contact-based sensing systems that will contribute to a time shift of the initiation of the deployment and the TRT and allow for actuators with larger deployment times may need to be elaborated.

IMPACTOR COMPLIANCE TESTS

Prior to headform testing, the vehicle markup, including the allocation of the performance zones "HPC 1000" and "HPC 1700" and test point selection, is always done on the undeployed DPPS. UN-R127 specifies a minimum of 18 headform tests, thereof 9 to the child headform test area and 9 to the adult headform test area. Furthermore, UN-R127 prescribes that 3 impacts for each impactor be tested to each third of the bonnet (UNECE, 2013). UN-GTR9 does not define a number of tests.

With the introduction of the General Safety Regulation (EU) No 2019/2144, cyclists as the second big group of vulnerable road users will be protected by extending the head impact area up to a maximum of WAD 2500, adding a windscreen test area and a cowl monitoring area (European Union, 2019). Thus, according to the respective amendment to UN-R127, wherever possible, at least one out of the nine tests each with the child and the adult headform impactor should be performed within the windscreen test area and within the cowl monitoring area (UNECE, 2022).

Depending on the degree of fulfillment of the prerequisites, the compliance tests with adult and child headform impactor are performed on either the undeployed or the deployed DPPS, or dynamically on the deploying DPPS. The firing times for the headform impactor and the DPPS during dynamic tests are to be derived from the generated HIT vs. WAD regression line in Figure 8 (right). Head impact velocity is 35km/h. HPC values are calculated from the recorded headform accelerations. The HPC requirements remain unchanged.

PROCEDURE

The flowchart in Figure 11 summarizes all steps that need to be passed for the assessment of DPPS according to the test procedures drafted by the IWG. The DPPS assessment is divided into the verification of the prerequisites, followed by the compliance testing.

Prerequisites

As first prerequisite the DPPS needs to demonstrate a pedestrian protection at vehicle speeds below the deployment threshold. There will be a slight difference in the draft amendments. For UN-R127, a minimum of three headform impactor tests are to be performed on the part of the vehicle front being affected by the DPPS, at headform impact velocities equivalent to the vehicle speed at lower deployment threshold. HPC 1000 must be fulfilled at 2/3 of the affected part of the vehicle front. For the remaining test area, HPC 1700 shall not be exceeded. For UN-GTR9, unlike UN-R127, the amendment does not specify a minimum number of tests, but it does maintain the HPC requirements. If those are fulfilled, the proper functionality of pedestrian detection is checked as second prerequisite, otherwise, the DPPS fails.

To demonstrate that a pedestrian is detected in case of an accident, UN-R127 will require three tests with the FlexPLI with an impact speed equivalent to the vehicle speed at lower deployment threshold and one test at 40km/h in the detection test area. UN-GTR9 will not specify a number of tests. If, during all tests, the FlexPLI is re-cognized by the sensing system of the DPPS and its deployment initiated, HBMs will be qualified to fulfill the third prerequisite; otherwise, all headform compliance tests are to be performed with the DPPS in undeployed position.

During numerical simulations of generic vehicle frontends, all HBMs that are used to determine HIT for the compliance testing must be qualified and fulfill reference corridors for AC, HC and HIT. In case of meeting the corridors, clearance provided by DPPS may be taken into consideration during compliance testing; otherwise all headform tests must be performed against the DPPS in undeployed position.

Flowchart DPPS Assessment[1]

OEM information on DPPS

I) Prerequisites

Protection at lower vehicle speeds

Low speed protection
3 x headform tests
@ 0.9*LDT speed[1]
1 test to each third[1]
HPC 1000 / 1700

→ no → **Fail**

↓ yes

Pedestrian detection

Pedestrian detection
Tests in detection area:
3 x FlexPLI @ LDT[2]
1 x FlexPLI @ 40 km/h[2]

→ no

↓ yes

Qualification of HBM

HBM Qualification
Annex 2:
Corridors met?

→ no → **Headform tests with DPPS @ undeployed position**

↓ yes

II) Compliance Testing

Timing of DPPS deployment

Selection of head impact points

↓

CP opts to consider static tests

→ no

↓ yes

System/surrogate stability check for lab testing

→ no

↓ yes

HIT vs WAD regression line
Annex 3:
HBM simulations on deployed bonnet, 40 km/h

↓

TRT, as determined

↓

HIT
(WAD, head impact point)
≥ TRT

→ no → **HIT vs WAD regression line**
Annex 3:
HBM simulations on undeployed bonnet, 40 km/h

↓

ST, as determined

↓ yes (left)

Test Assessment

Static test @ deployed [required] position

Dynamic test @ HIT

↓

HPC criterion
HPC 1000 / 1700

→ no → **Fail**

↓ yes

Pass

[1]: Will be updated with DPPS Phase 2 (Generic approach)
[2]: Minimum number of tests specified for Contracting Parties of the 1958 Agreement, only

Figure 11. Flowchart for the assessment of DPPS under consideration for UN-R 127 and UN-GTR9 (Zander, 2022).

Compliance testing

Prior to headform compliance testing, the vehicle markup, allocation of the HPC 1000 and HPC 1700 performance zones and the selection of head impact points are done with the DPPS in the undeployed position. Based on the fulfillment of all prerequisites, the amendment will permit Contracting Parties (CP) to the agreements of 1958 and 1998 to perform headform compliance tests on a statically deployed (static tests) or on a deploying (dynamic tests) DPPS, see Figure 11.

For static tests, a stability check is needed to verify that the resisting force of the pre-deployed DPPS is equivalent to the force in a real-world situation when the DPPS deploys just before the head of a pedestrian makes contact with it. Depending on the outcome of the stability check, a time constraint may be needed, i.e. the test must be run within a certain time period after deployment. Otherwise, an unlimited period of time is allowed in which the test may be conducted on a static, pre-deployed DPPS.

As demonstration of HIT ≥ TRT of the DPPS, simulations with all relevant statures of the qualified HBMs are performed on the deployed DPPS of the actual vehicle model and the HIT vs. WAD regression line plotted (compare Figure 8, left). For all selected impact points with the HIT greater than or equal to the TRT, static tests on the deployed DPPS may be performed. For the remaining impact points dynamic tests on the deploying DPPS are conducted. In the latter case, prior to headform testing, for the correct timing of the DPPS and the headform impactor, additional HBM simulations with the qualified HBMs are performed on the undeployed DPPS of the actual vehicle model and the HIT vs WAD regression line plotted and extended to all relevant WADs within the DPPS (see Figure 8, right).

In case of the CP opting for dynamic tests only, the stability check, the HBM simulations on the deployed DPPS and TRT determination are not necessary. HBM simulations with the qualified HBMs are performed on the undeployed DPPS to create the HIT vs WAD regression line that is extended to all relevant WADs. For the determination of the correct timing during testing, the sensing time (ST) needs to be previously determined.

For the first phase of implementing the DPPS procedures, HITs will be determined by means of numerical simulations, only. The formerly described method for including full scale dummy tests and the generic approach with empirical formula are being further explored by the IWG for subsequent phases.

DISCUSSION

A draft procedure for assessing DPPS systems as part of whole vehicle type approval or self-certification is being developed by an informal working group of UNECE. Depending on the degree of fulfillment of several prerequisites, the procedure specifies that the DPPS may be tested statically in the deployed state or dynamically during deployment. The procedure is intended to enable authorities to fully integrate the DPPS within compliance testing according to UN-R127 and UN-GTR9.

However, several shortcomings and limitations of the procedure have been identified which could decrease the actual pedestrian protection during an accident. The FlexPLI has proven to be a robust test tool for the assessment of the sensing system with a high repeatability of the generated intrusions. However, it represents a typical rather than the hardest to detect pedestrian. For pedestrians that remain undetected, the DPPS does not offer any safety benefit. Since, due to feasibility reasons, the detection test area does not cover the entire vehicle width, not all pedestrian trajectories can be accounted for and not all head impacts can be mitigated.

Furthermore, the clearance between the surface of the DPPS and the underlying structure may be compromised due to upper body contact prior to head impact. Also, the deploying DPPS may have a negative influence on the pedestrian's head that differs from the laboratory test conditions with an isolated headform impact. The quality of the determined HITs as basis for DPPS conditions during compliance testing strongly depend on the correlation of the HBMs with actual pedestrians as well as the vehicle models with the actual vehicles. Experimental dummy tests and the generic HIT determination are expected to increase the objectivity of the proce-

dure. Finally, procedures for forward-looking and non contact-based sensing systems that will contribute to a time shift of the initiation of the deployment and the TRT need to be elaborated.

CONCLUSIONS

A set of procedures and requirements for DPPS is in the final stages of development. These are intended to enable authorities to approve and certify systems with a deployable unit for head protection. Including a generic approach for HIT determination in the future is expected to increase objectivity of the procedure. However, further research is needed to also consider the influence on, and possible injury mitigation to body parts other than the head. The upcoming scope extension of UN-R127, taking into account the head protection of cyclists, will bring new challenges to the sensing system and possibly require modifications of the sensing impactor and the simulation procedures for HBM qualification and HIT determination.

DISCLAIMER

The authors of this paper are members of the IWG on DPPS who have helped to create the draft procedures. IWG members (including the authors) do not have the authority to approve the procedures for regulatory use. Although the authors may represent their respective contracting parties within the deliberations of the IWG on DPPS, the views expressed in this paper are not necessarily those of the contracting parties to which they belong. Authorship of this paper does not guarantee that a contracting party will completely agree with the positions taken or will vote to affirm adoption of the DPPS procedures into GTR9 or UN-R127.

REFERENCES

Besch A. 2022. "Qualification process of Human Body Models for pedestrian HIT determination." 19th Meeting of the Informal Working Group DPPS (IWG-DPPS). Doc IWG-DPPS-19-09, 08-09 November 2022.

European Enhanced Vehicle-safety Committee. 2002. "EEVC Working Group 17 Report Improved test methods to evaluate pedestrian protection afforded by passenger cars." December 1998 with September 2002 updates. www.eevc.net.

European New Car Assessment Programme. 2011. "Pedestrian Testing Protocol Version 5.2." Euro NCAP, November 2010.

European New Car Assessment Programme. 2021. "Pedestrian Human Model Certification Version 3.0.1." Euro NCAP Technical Bulletin 024, November 2021.

European Union. 2003. "DIRECTIVE 2003/102/EC OF THE EUROPEAN PARLIAMENT AND OF THE COUNCIL of 17 November 2003 relating to the protection of pedestrians and other vulnerable road users before and in the event of a collision with a motor vehicle and amending Council Directive 70/156/EEC." Official Journal of the European Union, 06 December 2003.

European Union. 2009. "REGULATION (EC) No 78/2009 OF THE EUROPEAN PARLIAMENT AND OF THE COUNCIL of 14 January 2009 on the type-approval of motor vehicles with regard to the protection of pedestrians and other vulnerable road users, amending Directive 2007/46/EC and repealing Directives 2003/102/EC and 2005/66/EC." Official Journal of the European Union, 04 February 2009.

European Union. 2019. "REGULATION (EU) 2019/2144 OF THE EUROPEAN PARLIAMENT AND OF THE COUNCIL of 27 November 2019 on type-approval requirements for motor vehicles and their trailers, and systems, components and separate technical units intended for such vehicles, as regards their general safety and the protection of vehicle occupants and vulnerable road users, amending Regulation (EU) 2018/858 of the European Parliament

and of the Council and repealing Regulations (EC) No 78/2009, (EC) No 79/2009 and (EC) No 661/2009 of the European Parliament and of the Council and Commission Regulations (EC) No 631/2009, (EU) No 406/2010, (EU) No 672/2010, (EU) No 1003/2010, (EU) No 1005/2010, (EU) No 1008/2010, (EU) No 1009/2010, (EU) No 19/2011, (EU) No 109/2011, (EU) No 458/2011, (EU) No 65/2012, (EU) No 130/2012, (EU) No 347/2012, (EU) No 351/2012, (EU) No 1230/2012 and (EU) 2015/166." Official Journal of the European Union, 16 December 2019.

Gehring D., Zander O. 2020. "Detection area width." 7th Meeting of the Informal Working Group DPPS (IWG-DPPS). Doc IWG-DPPS-7-10, 05-07 September 2020.

Gehring D., Zander O. 2021. "Sensing impactor evaluation: FlexPLI low speed inverse testing." 9th Meeting of the Informal Working Group DPPS (IWG-DPPS). Doc IWG-DPPS-9-11, 20-21 January 2021.

Forman, J. L., Joodaki H., Forghani A., Riley P., Bollapragada V., Lessley D., Overby B., Heltzel S., Crandall J. 2015. "Biofidelity Corridors for Whole-Body Pedestrian Impact with a Generic Buck." Paper no. IRC-15-49 of the 2015 IRCOBI Conference in Lyon, France.

Hardy B., Lawrence G., Carroll J., Donaldson W., Visvikis C., Peel D. 2006. "A study on the feasibility of measures relating to the protection of pedestrians and other vulnerable road users – Final Report." Project report no. UPR/VE/045/06, E.C. contract no. ENTR/05/17.02, TRL Limited, October 2006.

Hardy B., Lawrence G., Knight I., Simmons I., Carroll J., Coley G., Bartlett R. 2007. "A study of possible future developments of methods to protect pedestrians and other vulnerable road users." Report for the European Commission. Transport Research Laboratory, 2007.

Japan Automobile Standards Internationalization Center (JASIC). 2021. "Relationship of impact location between leg and head in lateral cat to pedestrian impact." 10th Meeting of the Informal Working Group DPPS (IWG-DPPS). Doc IWG-DPPS-10-04, 09-10 March 2021.

Laboratoire d'accidentologie y de biomécanique (LAB). 2022. "Pedestrian against passenger car in front collision. Initial leg impact on the corner of the bumper: Check distribution of head impacts on vehicle."

Lawrence G., Hardy B., Carroll J., Donaldson W., Visvikis C., Peel D. 2004. "A study on the feasibility of measures relating to the protection of pedestrians and other vulnerable road users – Final Report." Report for the European Commission, EC Contract No. FIF.20030937. Transport Research Laboratory, 2004

Mizuno Y, Ishikawa H (2001), Summary of IHRA pedestrian safety WG activities – proposed test methods to evaluate pedestrian protection afforded by passenger cars, Paper No. 280, The 17th International Technical Conference on the Enhanced Safety of Vehicles, Amsterdam, The Netherlands, June 4 - 7, 2001.

Nuß F., Eckstein L, Berger L. 2013. "Aktive Systeme der passive Fahrzeugsicherheit: Bewertung im Rahmen einer Prüfvorschrift zum Fußgängerschutz". BASt Project Report F90, 2013.

Pauer G. et al. 2018. "ACEA impact simulations on test frames." 3rd Meeting of the Informal Working Group DPPS (IWG-DPPS). Doc IWG-DPPS-3-02, Geneva, 10 December 2018.

Research Council for Automotive Repairs (RCAR). 2010. " RCAR Bumper Test". Issue 2.0, September 2010.

Schäuble A., Weyde M. 2019. "Biomechanical validation of a new biofidelic dummy." Paper no. 19-0197 of 26th ESV conference proceedings. Eindhoven, 2019.

Society of Automotive Engineers. 2019. "Performance specifications for a midsize male pedestrian research dummy". SAE Standard J2782.

Society of Automotive Engineers. 2020. "Pedestrian dummy full scale test results and resource materials". SAE Standard J2868.

United Nations Economic Commission for Europe (UNECE). 2003. "Contents of Headform Test Procedure." Document INF GR/PS/58 of the Informal Working Group on Pedestrian Safety. United Nations, 2003.

United Nations Economic Commission for Europe (UNECE). 2005. "Certification Standard for Type Approval Testing of Active Deployable Systems of the Bonnet Area." Document INF GR/PS/141 Rev. 1 of the Informal Working Group on Pedestrian Safety. United Nations, 2005.

United Nations Economic Commission for Europe (UNECE). 2009. "Global registry: Created on 18 November 2004, pursuant to Article 6 of the Agreement concerning the establishing of Global Technical Regulations for wheeled vehicles, equipment and parts which can be fitted and/or be used on wheeled vehicles (ECE/TRANS/132 and Corr.1). Done at Geneva on 25 June 1988. Addendum: Global technical regulation No. 9: PEDESTRIAN SAFETY (Established in the Global Registry on 12 November 2008)." UNITED NATIONS, 2009.

United Nations Economic Commission for Europe (UNECE). 2013. "Agreement Concerning the adoption of uniform technical prescriptions for wheeled vehicles, equipment and parts which can be fitted and/or be used on wheeled vehicles and the conditions for reciprocal recognition of approvals granted on the basis of these prescriptions* (Revision 2, including the amendments which entered into force on 16 October 1995). Addendum 126: Regulation No. 127. Entry into force: 17 November 2012. Uniform provisions concerning the approval of motor vehicles with regard to their pedestrian safety performance." United Nations, 2013.

United Nations Economic Commission for Europe (UNECE). 2018. "Addendum 9: United Nations Global Technical regulation No. 9 – Amendment 2." (Established in the Global Registry on 14 November 2018)." UNITED NATIONS, 2018.

United Nations Economic Commission for Europe (UNECE). 2020. "Mutual Resolution No. 1 (M.R.1) of the 1958 and the 1998 Agreements – Amendment 2." UNITED NATIONS, 2020.

United Nations Economic Commission for Europe (UNECE). 2022. "Proposal for the 03 series of amendments to UN Regulation No. 127 (Pedestrian Safety)" Working Document ECE/TRANS/WP.29/2022/70 to the 187th session of the World Forum for harmonization of Vehicle Regulations, 2022.

Verband der Automobilindustrie (VDS). 2022. "Anonymised examples for sensing widths (Compact, Sedan, SUV)." 18th Meeting of the Informal Working Group DPPS (IWG-DPPS). Doc IWG-DPPS18-07, 18-20 October 2022.

Zander O. 2022. "Overall flowchart DPPS aligned with Annexes 2&3". 17th Meeting of the Informal Working Group DPPS (IWG-DPPS). Doc IWG-DPPS-17-10, 02-03 June 2022.

Zander O. 2022-2. "Proposal overshoot phase". 20th Meeting of the Informal Working Group DPPS (IWG-DPPS). Doc IWG-DPPS-20-06, 15-16 November 2022.

Zander O., Wisch M., Gehring D. 2014. "Proposal for a modification of the lower/upper legform to bumper test area in GTR9-PH2 and UN-R 127.01 Series of Amendments." 6th Meeting of Task Force Bumper Test Area (TF-BTA). Doc TF-BTA-6-07, Paris, 15 May 2014.

Zander O., Wisch M. 2021. "Detection Area for DPPS: Lateral offset lower extremities vs. head." 10th Meeting of the Informal Working Group DPPS (IWG-DPPS). Doc IWG-DPPS-10-09, 09-10 March 2021.

Zander O., Gehring D. 2020. "Proposal for sensing impactor." 6th Meeting of the Informal Working Group DPPS (IWG-DPPS). Doc IWG-DPPS-6-04, 04-05 March 2020.

Zander O., Gehring D. 2020-2. "FlexPLI as sensing impactor for UN-R 127: Contact biofidelity." 7th Meeting of the Informal Working Group DPPS (IWG-DPPS). Doc IWG-DPPS-7-09, 15-17 September 2020.

A SIMULATION-BASED STUDY ON DISTRACTIONS AND BENEFITS OF SIGNAL LIGHT PROJECTIONS WITH DIRECTIONAL INDICATORS

Hyeran Kang,   Hyensou Pak,   Han Eol Seo,   Nahyeon Kim,   Jemok Lee,   Chan-Su Lee

Department of Electronics Enigneering, Yeungnam University, Rep. of Korea

ABSTRACT

To prevent accidents, the signaling function of automotive exterior lighting is essential to provide other road users with information on the presence of the vehicle and/or changes in its moving direction. Recently, dynamic turn signal indicators, backup indicators, and other light projections with directional indicators have been proposed and studies are being conducted to evaluate their safety enhancement and visibility in different lighting conditions. However, previous studies had limitations since most of them had not been studied or verified under dynamic driving situations. In addition, there aren't any studies on the distraction caused by turn signal projection lamps. Therefore, it is necessary to provide an assessment of the distraction and benefits of turn signal projection lamps under several dynamic scenarios. For this reason, we investigated whether the signal projection lamps, which work simultaneously with directional indicators and project a simple geometric pattern of a certain color and size on the left and right road surfaces in front of the vehicle, are beneficial or distracting to other drivers and VRUs (Vulnerable Road Users) such as cyclists and pedestrians. Twenty participants participated in the experiment. The results showed that the signal projection lamp hardly distracts drivers, cyclists, and pedestrians, but rather helps predict the presence of oncoming vehicles and the moving direction of the vehicles. Particularly with the signal projection lamp, the cyclist test showed a 14% and 9% decrease in detection time when the vehicle turned right and left, respectively. These differences were statistically significant. Our results suggest that a signal projection lamp is more beneficial than a distraction to drivers, cyclists, and pedestrians.

INTRODUCTION

Driving at night has many visual limitations to maintaining safe driving. If the turning of the vehicle cannot be properly predicted, it can cause accidents. Therefore, to prevent accidents, the signaling function of automotive exterior lighting is essential to provide other road users with information on the presence of the vehicle and/or changes in its moving direction. Projection lamps on the road have enabled new interactions between vehicles and VRUs (Vulnerable Road Users). Therefore, the projection lamp can make a positive contribution to the VRU.

According to the previous study, visibility improved when using turn signal projection lamps for both young and middle-aged participants [1]. The backup guide lamp, which implements a guideline in the form of a dotted line pattern on the rear road surface when reversing after parking, improves safety [2, 3] and is already applied to commercial vehicles. There is also a light that projects a bicycle-shaped image forward to improve cyclist safety [4]. Currently, studies on the effect of projection distance and contrast on people's acceptance [5], safety improvements by lighting for pedestrians and cyclists [6], and the requirement of the performance of road projection lamps [7] are also being conducted.

However, previous studies have limitations since most of them have not been studied or verified under dynamic driving situations. We evaluated scenarios where the multiple signal lights of nearby vehicles projected a pattern on the road surface or the signal light of a passing vehicle is projected to the driving path and the effects they had on the drivers of vehicles passing through the intersection, the cyclists following the cycle path, and the pedestrians crossing the crosswalk.

In this experiment, three situations one for the drivers, one for the cyclists, and one for the pedestrians were created. The situations were all intersections and T-junction roads under dynamic conditions. These situations were implemented with a VR head-mounted display using a driving simulator, a bicycle riding simulator, and a

locomotion simulator by walking pad. Each situation had two different scenarios with different conditions. The result shows the statistically significant benefits and limited distractions of signal projection lamps.

METHODS

This experiment was conducted to evaluate the effect of a projection lamp in a VR environment. A driving simulation program was used to implement the road environment, and HMD (Head Mounted Display) was used to show the actual road environment to the participants. In addition, we investigated the interaction between the vehicle and the VRU by applying different simulators according to driving, riding, and walking situations.

Experimental set-up

We implemented the intersection with the driving simulation program SCANeR studio 2022. To select the proper cases of cyclist and pedestrian scenarios, cases with a high number of accidents were selected by referring to the case-by-case analysis of car-to-cyclist and car-to-pedestrian accidents in Germany by the EU-funded project PROSPECT (Proactive Safety for Pedestrians and Cyclists) [8]. Six scenarios were configured according to two driving conditions (left turn and straight in the intersection scene, turn left and right in the T-junction scene) with three kinds of road users (driver, cyclist, and pedestrian). For each scenario, we evaluate the performance of the test driver, cyclist, and pedestrian with/without turn signal projection lamp conditions.

Figure 1 shows examples of experiment environments from the participant's perspective. In the driver situation (scenario 1&2), five vehicles with turn signals stopped at the intersection, and the participant becomes the driver, following the preceding test vehicle and waiting for the signal to turn left or go straight. In the cyclist situation (scenario 3&4), a test vehicle approaches a cyclist with the turn signals on. In the pedestrian situation (scenario 5&5-1), the test vehicle approaches the participant's walking path with turn signals on as he/she crosses the crosswalk.

Figure 1. Examples of experiment environments in the participant's perspective. Scenario 1: driver test, left turn (left), Scenario 4: cyclist test, right turn (center), Scenario 5: pedestrian test, right turn (right).

Data collection

A driving simulator, a bicycle riding simulator, and a locomotion simulator were connected to the driver, cyclist, and pedestrian scenarios, respectively, to collect participants' data.

In the driver situations, the average speed, passing time of the ego vehicle, and time required for the ego vehicle to brake after the preceding vehicle brakes were analyzed. In the cyclist situation, participants are riding on a bicycle path and were ordered to press a button when they recognize a vehicle turning left or right to enter in front of their path. The speed of the bicycle was calculated by measuring the number of wheel rotations using a pedaling cadence sensor from Giant™. The horizontal distance between the cyclist and the vehicle, the time which is taken to press the button after detection of entering the vehicle (detection time), TTC (Time to Collision), and the distance from the cyclist to the vehicle when the button is pressed were analyzed. In pedestrian situations, participants crossed the crosswalk and pressed a button when they recognize a vehicle approaching the crosswalk. The pedestrian speed was fixed at 3.5km/h by the fixed constant speed of the walking pad. The horizontal distance between the pedestrian and the vehicle, TTC, the remaining time to the

accident, and the distance from the pedestrian to the vehicle when the button was pressed were analyzed. Figure 2 shows typical experiment scenes on simulators in different experimental situations.

Figure 2. Participant driving a vehicle using a driving simulator (left), riding a bicycle on a bicycle simulator (center), walking on the walking pad (right).

Experimental procedure

Participants practice the experiment environment with simplified scenarios for about 5 minutes before the driver, cyclist, and pedestrian situation test. The experiment was continued according to the following procedure:

1) In the driver situation, the participant becomes the driver, stops at an intersection and follows the proceeding vehicle to go straight or turn left.

2) In the cyclist situation, the participant becomes a cyclist and rides on a bicycle path as a test vehicle passes. Presses the button which is mounted on the handle of the bicycle when starting off, and press the button again when recognizing the approaching vehicle.

3) In the pedestrian situation, the participant walks and waits while facing the front, then presses the start button when the experiment starts and presses the end button as soon as he/she recognizes an approaching test vehicle while walking on the crosswalk.

All sessions of each scenario were randomized to minimize order effects. It took approximately 1 hour to complete each situation, including the time to complete the questionnaire, with additional break time whenever participants requested.

Participants

Twenty undergraduate and graduate students from Yeungnam University (male: 11, female: 19, average age: 24.6 years) participated in this experiment. All participants in the experiment were Korean, had a driver's license, had visual acuity of 0.7 or higher, and self-reported with no color blindness or color weakness. They wore an HMD during the experiment. Experiments with wearing HMD for more than 1 hour may cause other effects. Therefore, the experiment was performed for each situation separately. Each participant come to the test site three times.

RESULTS

The experimental data were analyzed using ANOVA and t-test using IBM SPSS Statistics (ver. 25).

Scenario 1: driver test, left turn

The average driving speed, passing time, and brake response time of participants with the projection lamp was 17.08 ± 1.20 km/h, 5.69 ± 0.33 sec, and 0.58 ± 0.25 sec. And they were 14.23 ± 2.06 km/h, 6.99 ± 0.93 sec, and 0.95 ± 0.53 sec respectively without the projection lamp. In scenario 1, the average speed with the projection lamp was 2.85 km/h, which is statistically significantly faster [t(19)=5.644, p=.000] than without the projection lamp. The passing time of 1.30 sec with the projection lamp was statistically significantly faster [t(19)=-6.101, p=.000] than that without the projection lamp (see Figure 3).
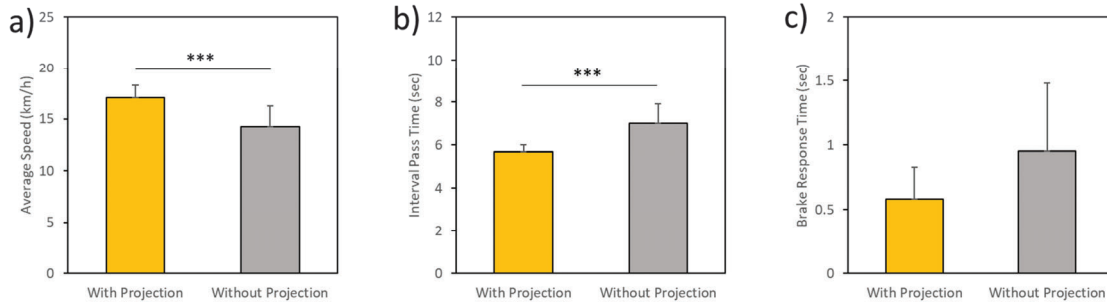
Figure 3. Data for scenario 1. a) Average driving speed. b) Passing time. c) Response time which is the braking time interval of the ego vehicle after breaking the test vehicle. ***p<.001.

Scenario 2: driver test, straight

Figure 4 show the average driving speed and passing time with and without the projection lamp. The average driving speed, and passing time were 26.48 ± 1.15 km/h and 5.18 ± 0.22 sec with the projection lamp. And they
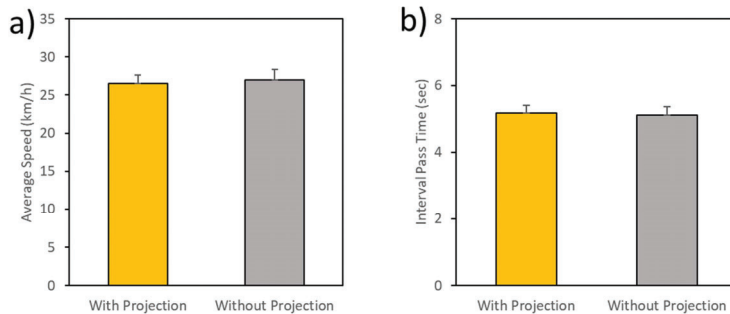
were 26.99 ± 1.34 km/h and 5.11 ± 0.26 sec without the projection lamp. There were no significant differences.

Figure 4. Data for scenario 2. a) Average driving speed. b) Passing time from starting point to finishing point.

Scenario 3: cyclist test, left turn

Detection time is the time when the participant detects an oncoming vehicle that is going to make a left turn and, TTC is computed assuming that the vehicle and cycle keep the current speed at the detection time, and the distance between the vehicle and the participant was also computed when the vehicle was detected. They were 8.65 ± 0.81 sec, 1.86 ± 1.12 sec, and 4.03 ± 2.24 m respective with the projection lamp and 9.45 ± 0.38 sec, 0.97 ± 0.38 sec and 5.30 ± 0.53 m without the projection lamp (see Figure 5). With the projection lamp, detection time was significantly faster [t(19)=-9.792, p=.000] than without the projection lamp. TTC with the projection

lamp was also significantly faster [t(19)=9.792, p=.000], and the distance was significantly longer than without the projection lamp[t(19)=-5.170, p=.000] (see Figure 5).
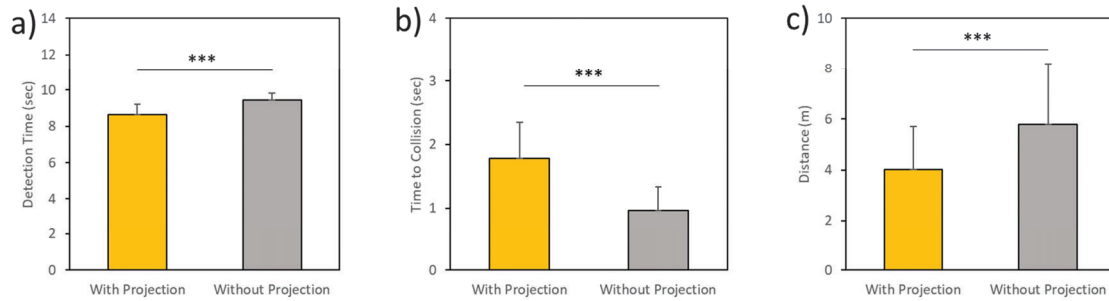
*Figure 5. Data for scenario 3. a) Detection time for the participant to recognize the test vehicle turning after the experiment started. b) TTC. c) Distance from the cyclist to the detected vehicle. ***p<.001.*

Scenario 4: cyclist test, right turn

In scenario 4, the detection time is the time when the participant detects that an oncoming vehicle is going to make a right turn. The detection time, TTC, and distance were 6.12 ± 0.49 sec, 3.93 ± 0.49 sec, and 1.77 ± 1.28 m with projection lamp. And they were 7.15 ± 0.69 sec, 2.90 ± 0.69 sec, and 4.15 ± 1.55 m without projection lamp (see Figure 6). With the projection lamp, detection time was significantly faster [t(19)=-14.454, p=.000], TTC was significantly faster [t(19)=14.454, p=.000], and distance was significantly longer [t(19)=8.783, p=.000] than without the projection lamp (see Figure 6).
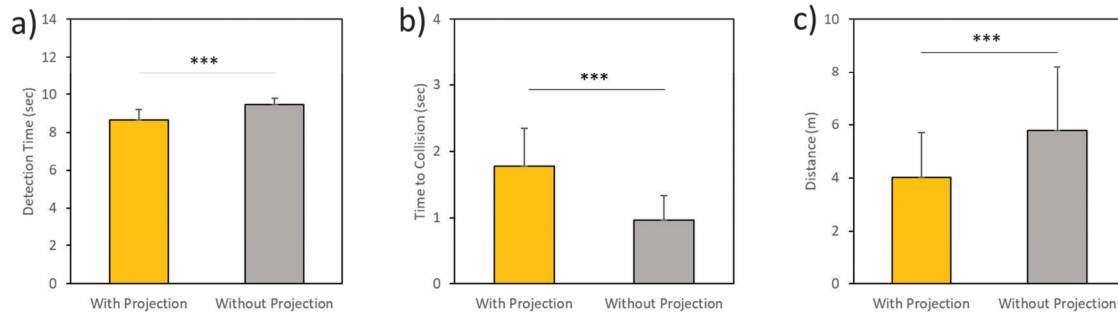
*Figure 6. Data for scenario 4. a) Detection time for the participant to recognize the test vehicle turning after the experiment started. b) TTC. c) Distance from the cyclist to the detected vehicle. ***p<.001.*

Scenario 5: pedestrian test, left turn, pedestrian & vehicle in the same direction

In Scenario 5, the detection time is the time when the participant detects an oncoming vehicle to make a left turn. The detection time, the TTC, and the distance between the vehicle and the participant when the vehicle was detected were 8.15 ± 0.74 sec, 1.28 ± 0.74 sec, and 12.24 ± 1.46 m with the projection lamp. And they were 8.44 ± 1.08 sec, 0.99 ± 1.08 sec, and 11.60 ± 1.89 m without the projection lamp (see Figure 7). With the projection lamp, the distance when the participant found the test vehicle was 0.64 m faster, and this difference was statistically significant [t(19)=2.397, p=.027].
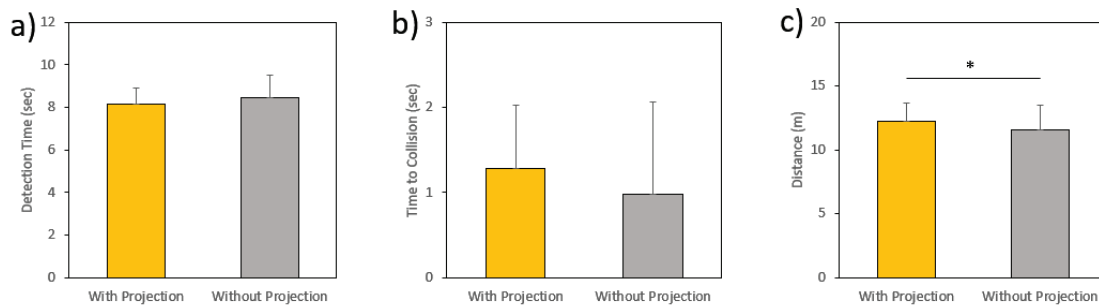
Figure 7. Data for scenario 5. a) Detection time for the participant to recognize the test vehicle turning after the experiment started. b) TTC. c) Distance from the pedestrian to the detected vehicle. *p<.05.

Scenario 5-1: pedestrian test, left turn, oncoming vehicle

In Scenario 5-1, the detection time, TTC, and the distance between the vehicle and the participant when the vehicle was detected was 7.51 ± 1.33 sec, 2.02 ± 1.33 sec, and 13.91 ± 6.14 m with the projection lamp. And they were 7.74 ± 1.24 sec, 1.79 ± 1.24 sec, and 12.96 ± 5.54 m without the projection lamp (see Figure 8). There was no significant difference.
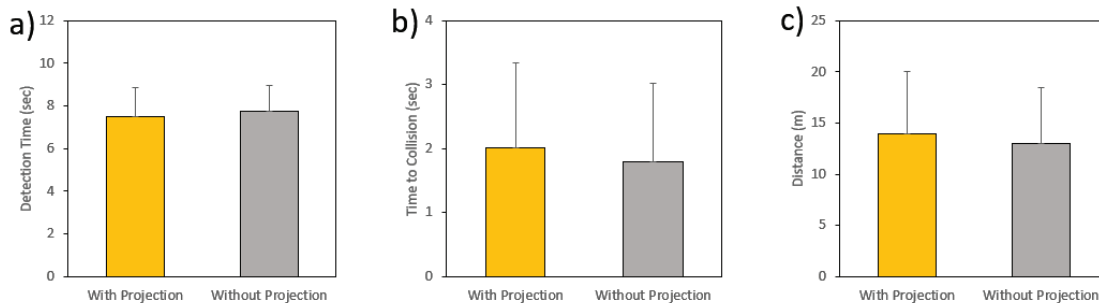
Figure 8. Data for scenario 5-1. a) Detection time for the participant to recognize the test vehicle turning after the experiment started. b) TTC. c) Distance from the pedestrian to the detected vehicle.

CONCLUSION

In this experiment, evaluations were performed by six scenarios for drivers, cyclists, and pedestrians situations. The result shows that the driver's driving speed and brake response time were faster with the projection lamp than without the projection lamp, and it was found that the detection time of the approaching vehicle was also decreased for cyclists and pedestrians.

This experiment result will be helpful to develop a safer road environment tailored to road users in the future by providing quantitative data showing significant benefits and limited distraction of turn signal projection lamps. Further study may be necessary to find the proper length or direction of the projection lamp to minimize distraction and maximize visibility. In addition, this study was conducted in the evening of a sunny day, additional research under adverse weather conditions or daytime seems to be necessary.

Since the results of our study were not obtained from field studies such as actual driving and walking situations, sufficient discussion and review will be required in the actual application process. Nevertheless, these results will be an important empirical basis for determining whether to adopt signal projection lamps for automotive lighting in the future.

REFERENCES

[1] H, Pak., H, Kang., D-W, Song., J-H, Lee., H, Park., C-S, Lee. (2022). Evaluation of direction judgements based on turn signal guide lamp and behavioural responses. *Lighting Research and Technology*, online first publication, https://doi.org/ 10.1177/14771535221076171

[2] H, Pak., J-W, Hwang., K-B, Lee. (2019). Safety enhancement effect of back-up guide lamps: A field experiment with North American consumers, *Proceedings of the 13th International Symposium of Automotive Lighting*. Darmstadt, Germany, 25-27 September 2019; 123-132.

[3] S, Azouigui., S, Saudrais., B, Barbedette., S, Bordel. (2021). Road Projections: Impact on Road Users and Potential to Enhance Awareness of Backing Situation in Parking Lots. *SAE Technical Paper*, https://doi.org/10.4271/2021-01-5078.

[4] S, Greenshields., & D, Tindall. (2015). A report on the use of the Blaze Laserlight on cycle hire scheme bicycles near buses [Brochure]. https://www.whatdotheyknow.com/request/367618/response/898056/attach/3/TRL%20Report%20CPR2036%20final%20v1%20Redacted.pdf?cookie_passthrough=1

[5] A, H, Shah., X, SUN., & Y, Lin. (2022). Study the Effect of eHMI Projection Distance and Contrast on People Acceptance in Blind-Spot Detection Scenario. *Applied Sciences,* 12(13), 6730. https://doi.org/10.3390/app12136730

[6] M, Hamm., & C, Hinterwaelder. (2020). Investigation on Safety Improvements by Lighting for Pedestrians and Cyclists (No. 2020-01-0633). *SAE Technical Paper,* https://doi.org/10.4271/2020-01-0633

[7] Y, Shibata. (2019). Requirement Performance of Road Projection Lamp in Conjunction with Turn Signal Lamp, *Proceedings of the 13th International Symposium of Automotive Lighting*. Darmstadt, Germany, 25-27 September 2019; 123-132. 362-373.

[8] M. Kunert. (2016). Specification of the PROSPECT demonstrators. *Deliverable D3.2 of Horizon 2020 project PROSPECT*, http://www.prospect- project.eu/download/public- files/public_deliverables/PROSPECT-Deliverable- D3.2.-Specification-of- PROSPECT- demonstrators.pdf

REAL-WORLD PROTECTION OF BOOSTER-SEATED CHILDREN – NEEDS AND CHALLENGES IN FUTURE TRANSPORTATION

Lotta Jakobsson[1,2], Katarina Bohman[1], Isabelle Stockman[1]
[1] Volvo Cars
[2] Chalmers University of Technology
Sweden

ABSTRACT

Driven by sustainability goals, passenger cars' design and ownership setups are changing. Vehicle safety is constantly improving, yet a trend of larger belt-positioning boosters is seen. The objective is to discuss the challenges of child passenger protection in the current and future mobility context. The study focuses on children who can use the vehicle seatbelt together with a booster, typically 4 to 10-12 years.

The study is based on protection principles of booster-seated children, with a vehicle-booster-user entity focus. Studies on restraint awareness and usage today, users' perceptions on future mobility and evolutions of vehicle design and mobility trends, are summarized and reflected on. Real-world protection needs are formulated based on in-vehicle crash testing/simulations, and studies on child passenger sitting postures during drive and evasive maneuvers. This is put in the context of regulatory and booster development trends.

In a real-world crash, children are protected by the vehicle and booster in combination. Crash tests/simulations highlight the importance of the seatbelt interaction, influenced by initial beltfit and the dynamic properties of the booster. On-road driving studies show that awake child passengers spend a non-neglectable duration of the trip with a forward head position, due to visibility and activities. A forward head position could also be a result of a pre-impact braking as well as the added space by the booster seat's backrest. In case of a frontal impact, a more forward head position at time of impact will result in a more forward excursion. Real-world side-impact data shows that the booster-seated child's head is protected similar to an adult, assisted by the vehicle safety systems.

The booster serves as an adapter, not as a primary restraint for the child. Booster-seated children benefit from the vehicle safety systems, given they are raised in position for good beltfit and posture. Addressing the changing trends of passenger cars' design and ownership setups, the role of the booster should be clearly communicated. Future designs must address issues of usability, portability, and acceptance. As examples, the streamlined roof designs driven by sustainability goals, reduce the roominess in the rear-seat, whereby the booster seat backrest's width and height might require larger space than needed for an adult; and the trend from personal mobility towards increased degree of shared mobility, emphasizes the need of the booster to be portable or integrated into the vehicle.

Real-world child passenger safety involves protection aspects beyond standardized crash testing scenarios. Most importantly, the booster should be used in every trip, irrespectively of passenger car ownership setup. This study provides insight into modern vehicles' protection capacity in relation to the booster-seated children. It outlines some areas that are affected by the current booster developments, such as the increased size and complexity of booster seats, and the booster cushion ban in some parts of the world. In relation to the current and future transportation context, a booster cushion with appropriate characteristics serves as an essential complement to booster seats (of reasonable size) and will help maintain a positive child safety global trend.

THE DEVELOPMENT, EXPERIENCE AND CONTEXT OF BOOSTERS

Smaller children need infant or toddler seats with internal harness. For optimal protection they should be placed rearward facing to ensure that their neck has better chances to cope with high severity frontal impacts (Tarriere, 1995; Jakobsson, 2017). When outgrown of the toddler seats, and at approximately 4 years old, the children can benefit from the vehicle restraints, given they are raised into a good position for the vehicle seatbelt, using a belt-positioning

booster. There are three design principles of boosters; booster seat which includes a backrest, booster cushion with no backrest and integrated boosters which are built into a vehicle. Recently, several new products have been developed targeting the group of booster-seated children. Such products include, e.g., so called "inflatable cushions", "height-less boosters" and different types of "belt straps restraints". These products are not addressed in this study, since unless the products elevate the child in a stable manner (during ride as well as during a crash), and shorten the seat cushion length, they should not be categorized as boosters, nor should they be used as child restraints in passenger cars.

This study focuses on children who can use the vehicle restraint together with a stable boosting belt-positioning booster, typically 4 to 10-12 years old (appr. 140 cm stature).

The Development

In 1978, the world's first booster was introduced (Norin et al., 1979). The idea of boosters for children sprung from a study initiated by the discussion of enforcing rear-seat seatbelt use, where it was questioned whether seatbelts were safe for small adults (Norin et al., 1977). The first booster was a booster cushion, shown in Figure 1a. Important features of the booster cushion are the belt-positioning guides for the lap-belt, one on each side. Their purpose is to help keep the seatbelt in position during a crash and to restrain the booster itself. Modern boosters have belt guides protruding upwards, improving accessibility, and they vary in height and design. The lap-belt guides can also serve to help position the shoulder portion of the seatbelt, by placing the shoulder belt over or under the guide on the buckle side. The same booster cushion can then help to obtain the desired mid-shoulder belt position for shorter and taller children, respectively. The booster helps to put the child in an upright position, allowing the legs to bend and providing thigh support, so the child will not slouch forward in the seat to find a more comfortable leg position. Slouching may result in sub-optimal belt geometry (DeSantis Klinich et al., 1994).

Figure 1a. World-first booster cushion 1978. The belt guides are positioned low on the side of the booster.

Figure 1b. Early version of a booster seat (1985). The belt guides are of similar design as in Figure 1a, although difficult to see in the photo.

Figure 1c. A booster seat from 1989. As the prior version (Figure 1b), it is a booster seat with removable backrest.

The backrests were initially intended to provide head support in vehicles without head restraints, as shown in the example from 1985 (Figure 1b). The backrest was also a way of adjusting the length of the cushion to accommodate the shorter thigh length of the smallest children. When removed, the cushion length better accommodates the larger children. It can include shoulder belt-positioning devices with the ambition to help guide the shoulder belt into a comfortable and safe mid-shoulder position (Reed et al., 2009). The backrest of the booster in Figure 1c allows for height adjustment, enabling the shoulder belt guide to adjust to different sizes of children. Backrests can potentially provide sleeping support and help to control the lateral position of the child's upper body during ride.

In 1990, the world's first integrated (built-in) booster was introduced addressing accessibility, acceptance, and reduced risk of misuse (Lundell et al., 1991), Figure 2a. A comfort cover can be used with the integrated booster (Figure 2b), providing side support when travelling, but not interfering during a potential crash. In 2007, a second-generation integrated booster was introduced providing two levels in height (Figure 2c), adapting beltfit to the growing child (Jakobsson et al., 2007). The acceptance of the integrated booster was greater, shown by the relative higher usage of

the integrated boosters, in comparison to accessory boosters, among the older children aged 8 to 10 (Jakobsson et al., 2012 and 2015). Osvalder and Bohman (2008) provided evidence that misuse was almost eliminated when using integrated boosters. A follow-up study in China, conducted with users without previous experience of integrated boosters and limited experience with boosters overall, showed similar findings of reduced risk of misuse when buckling up on an integrated booster compared to an accessory booster cushion (Bohman et al., 2016). On-road driving studies comparing integrated booster and a booster seat indicated a more positive attitude on comfort, as well as a higher degree of upright sitting posture towards the seatback for the integrated booster (Osvalder et al., 2013).

Figure 2a. World's first integrated booster, 1990.

Figure 2b. Comfort cover for an integrated booster.
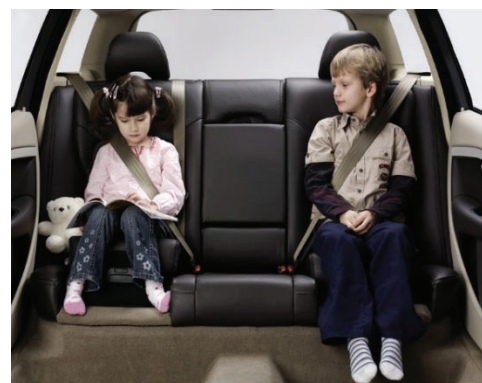
Figure 2c. Two stage integrated booster; high position (left) and low position (right).

Real-World Data

Real-world safety is about real children in real vehicles. Real-world crash data provides a foundation of knowledge, which will help address future challenges as well. User studies on child sitting postures, self-selected or by evasive maneuvers, provide insight into head and seatbelt positions at start of a potential crash. These studies help interpret different crash outcomes, as well as help identify important areas of real-world safety.

Crash data studies

Real-world crash data shows that the use of boosters substantially reduces injury risk compared to seatbelt only, and that boosters are effective to help protect children in frontal impacts as well as other crashes (DeSantis Klinich et al., 1994; Isaksson-Hellman et al., 1997; Warren-Bidez and Syson, 2001; Jakobsson et al., 2005; Arbogast et al., 2005 and 2009; Anderson et al., 2017). In frontal impacts, seatbelt syndrome related injuries to the abdomen and spine were nearly eliminated for children using boosters (Durbin et al., 2003). Children aged 4 to 8 using boosters were 45% less likely to sustain injuries than similarly aged children using the vehicle seatbelt only (Arbogast et al., 2009). Children in side-impacts derived the largest relative protection from boosters, with a reduction in risk of 68% and 82% for near-side and far-side side-impacts, respectively. No difference in booster seats versus booster cushions were seen (Arbogast et al., 2005 and 2009; Jermakian et al., 2007; Arbogast, 2010). No major differences in head injury patterns were seen between booster-seated children and adults, exposed to near-side side-impacts in similar passenger cars. This provides evidence of comparable mechanisms and indicates similar protection needs for both groups (Jakobsson et al., 2005).

User studies

Tests with children of different ages in different restraints provided data on head excursion during emergency braking of 1g (Stockman et al., 2013; Baker et al., 2017; Graci et al., 2019). During the braking, the head of the child moved 15-20 cm forward even when the child was restrained properly using a booster seat or a booster cushion (Stockman et al., 2013). An example of head position, as a result of the braking event, is shown in Figure 3a. Figure 3b shows the areas of head trajectories of the two child groups in the two booster types. Baker et al. (2017) showed that extent of head excursion was influenced by the degree of initial shoulder belt contact, due to differences in routing of the lower part of the shoulder belt. Using a booster cushion as compared to an integrated booster, a gap between the belt and lower torso was more frequently seen, in addition to a further outboard initial shoulder belt position on the shoulder (Baker et al. 2017).

Figure 3a. Maximum forward head position of a child restrained in a booster seat during an emergency braking event (Stockman et al., 2013).
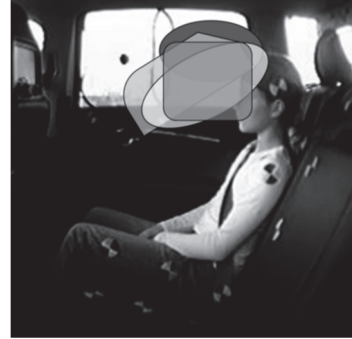
Figure 3b. Schematic plot representing trajectories of forehead markers for child volunteers from the emergency braking event study by Stockman et al. (2013).

Stockman et al. (2013) stated that in case of a subsequent side-impact, any of the head positions in Figure 3b could be a potential position at impact. This is in line with the study by Maltese et al. (2007), who identified evidence of a variety of head impact locations for restrained children (4 - 15 years old) in real-world side-impacts. As a consequence of a braking event, the head will be more forward than the coverage of most booster seat's head side supports. Also, in a side-impact, the struck vehicle is in many cases subject to an angled acceleration due to its speed at impact, which will add to a more forward head impact point as well.

A more forward head position at time of crash may increase head excursion in frontal impacts (Bohman et al., 2018; Maheshwari et al., 2020 and 2021). The forward excursion due to a braking event (Figures 3a-b) will reduce the distance to potential head impact areas in case of a subsequent frontal impact. If the child is using a booster seat, the backrest will further reduce this distance by the more forward head position as compared to using a booster cushion, as shown in Figure 4. The backrest will position the child's head forward due to the thickness of the backrest, as well as potential fitment incompatibility with the vehicle seat.

| Booster cushion | Booster seat | Booster cushion | Booster seat |
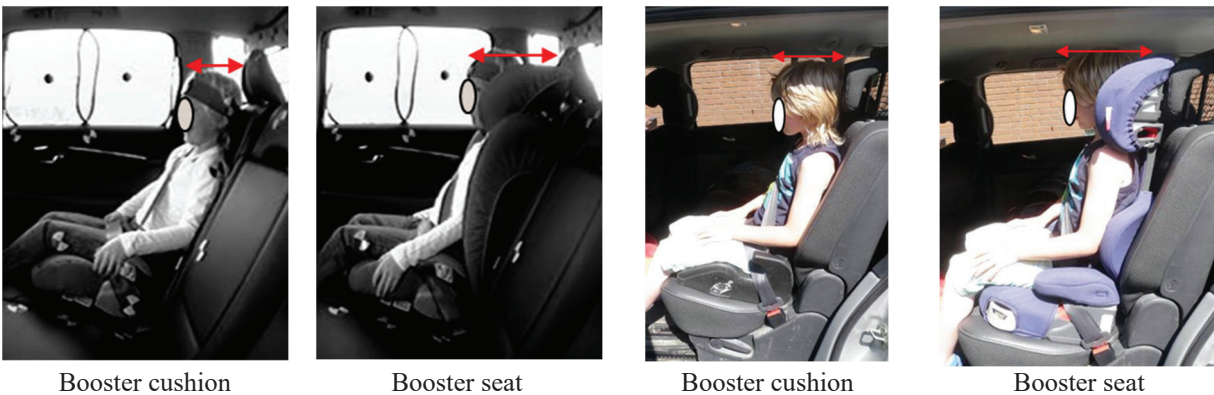
Figure 4. Illustrating influence of a booster seat's backrest on head position in relation to the vehicle. Left: 6 years old child (123 cm) in the rear-seat of a Volvo XC70. Right: 7 years old child (133 cm) in the rear-seat of a Renault Grand Espace (Jakobsson et al., 2012).

A forward head position may also be a result of a forward leaning posture due to visibility, activities or other reasons. Figure 5 shows self-selected postures due to visibility or activities. Andersson et al. (2010) showed that children were more prone to lean forward in the booster seat equipped with the more protruding head side supports, when studying children's sitting postures riding in two different types of booster seats (Figure 5a). The children were seated with the main part of the head in front of the front edge of the head side supports more than half the time, often due to visibility reasons. Another on-road user study identified that comfort related aspects influenced the sitting posture. Osvalder et al. (2013) found that the side supports of the booster seat's backrest restricted the children's possibilities to use their

arms when interacting with a tablet. This caused a forward leaning of the whole upper body, in addition to the head bending forward when looking at the tablet (Figure 5b).

| More protruding | Less protruding | Integrated booster | Booster seat |
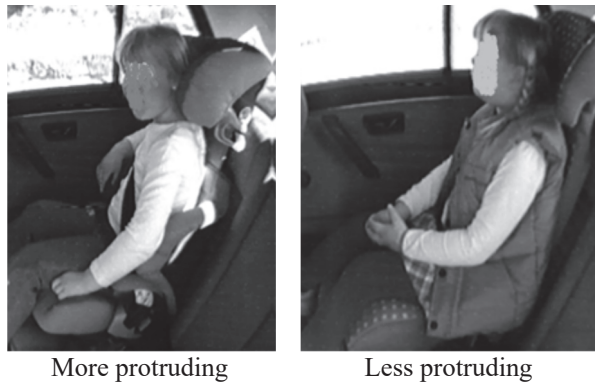
Figure 5a. The most common sagittal sitting posture for two types of booster seat head side supports (Andersson et al., 2010).
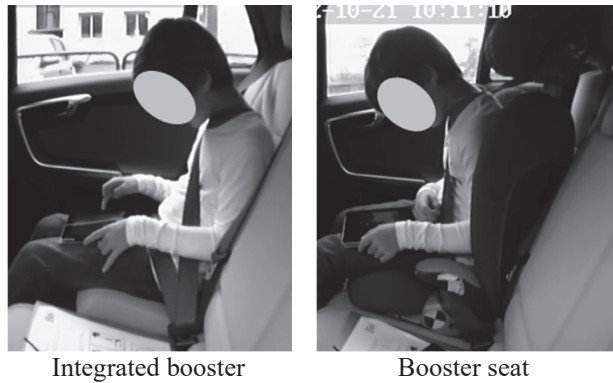
**Figure 5b. Comparing influence of backrest when interacting with a tablet (Osvalder et al., 2013).**

In a swerving vehicle motion, the children will move sidewise (Bohman et al., 2011; Baker et al., 2018; Graci et al., 2019). Bohman et al. (2011) conducted a maneuver study with children restrained in the rear-seat of a passenger car. Exposed for a sharp turn (lateral acceleration of approximately 0.8g) resulting in an inboard motion of the child, the kinematics were compared when seated on a booster, with and without a backrest. The backrest showed potential to maintain the shoulder belt on the shoulder during the swerving maneuver (Figure 6a). Whether the belt guide of the booster seat's backrest will continue to keep the shoulder belt in position during a frontal impact when the booster seat and the child are in such a pre-impact inboard tilted position is not obvious, as illustrated by Figure 6b. Figure 6b shows initial position and position at head impact from a frontal impact crash test with initial inboard tilted position of the anthropometric test device (ATD) and the booster seat.

| Booster cushion | Booster seat | Initial position | At time of head impact |
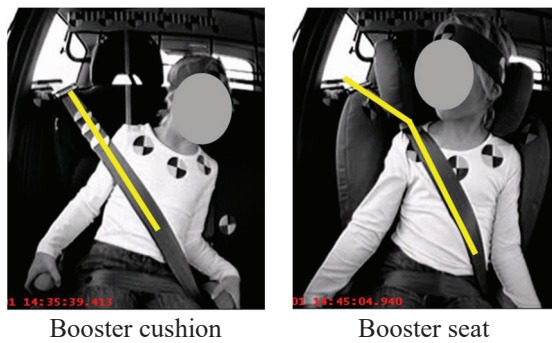
Figure 6a. Lateral inboard motion of a child during a swerving maneuver (Bohman et al., 2011).
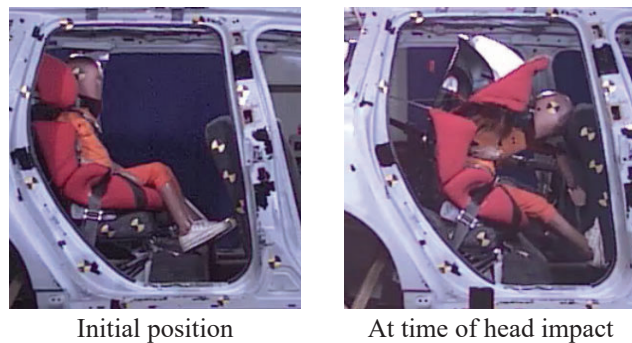
Figure 6b. Frontal impact crash test with initial inboard tilted position of the ATD similar to the child in the booster seat in Figure 6a.

Protection Principles

Regardless of crash configuration, children benefit from the vehicle safety systems given they are raised in position using a booster, and the booster is supportive in retaining a good seatbelt interaction throughout the crash. As for adults, the general protection principles of balancing the torso and head movements applies. This is irrespective of crash configuration, exemplified by an even support by the vehicle interior if exposed to a rear-end or side-impact.

The specific protection principle of a seatbelt is to restrain the strong parts of the body; the pelvic bones, and across the chest and over the shoulder in a crash (Adomeit and Heger, 1975; Bohlin, 1977). The lap-belt position is crucial in helping to avoid lap-belt interaction with the abdomen in frontal impacts. The anterior superior iliac spines of the

pelvis are important for good lap-belt positioning and they are not well developed until a child is about 10 years old (Burdi et al., 1968). In addition, the size of the pelvis grows with age, having influence on the height of the anterior superior iliac spines in relation to the seat cushion. By elevating the child, the lap-belt will be routed low on the pelvis, as for adults, instead of toward the abdomen. When positioned across the chest and in a mid-shoulder position, the shoulder belt helps provide a desired head and upper body kinematics during a frontal impact (Kent and Forman, 2015). A tight and early coupling of pelvis and upper body, maximizes the use of the available space in the vehicle, used to reduce the occupant motion, often referred to as the "ride down". Furthermore, a seatbelt performs best when routed as straight as possible. When extensively re-routed, its protective functions will be influenced due to introduction of slack, as exemplified in Figure 6b.

Figure 7 shows an animation of a frontal impact using PIPER6y which is a human body model representing a 6-year-old child. It illustrates how the lap-belt holds back the pelvis and allows the upper body to flex forward. Initially, the seatbelt pretensioner tightens the seatbelt, by reducing the belt slack, and offers an early and tight coupling of the pelvis. As can be seen, the booster elevates the child model, whereby the lap-belt is helped to interact with the pelvic bone reducing the risk of the child's pelvis to slide under the lap-belt, referred to as submarining.
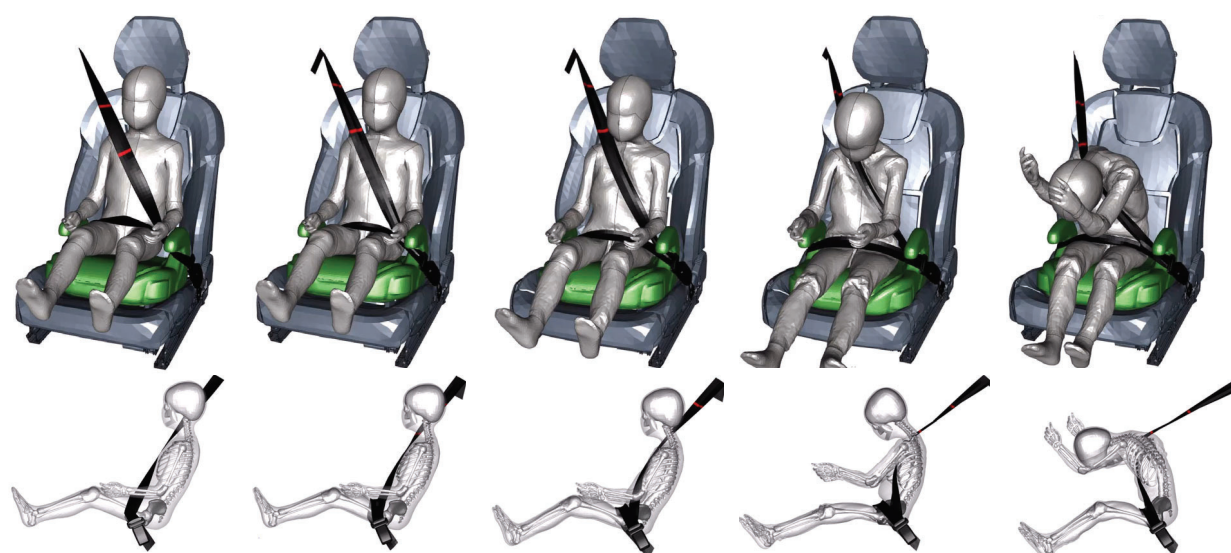
Figure 7. A frontal impact simulation with PIPER6y on a booster cushion restrained by a seatbelt with pretensioner, from start of impact to time of maximum forward head excursion. Time sequences (left to right): 0ms, 25ms, 50ms, 75ms and 110ms. Whole body in oblique frontal view (top) and skeleton in a side view (bottom). The red lines on the shoulder belt help to visualize the initial tightening of the pretensioner, occurring during the first 25ms.

The Child Passenger Protection Context

The booster is a part of a whole system, the vehicle-booster-user entity. In a real-world crash, children are protected by the vehicle and booster in combination. Crash tests and simulations highlight the importance of the seatbelt interaction with the occupant and the booster. This includes initial beltfit, the influence of belt guide design and potential re-routing due to those, in addition to the booster's shape and stiffness. The user aspect includes the sitting posture of the child, the potential movements prior to a crash, in addition to the safety awareness and possibilities to use the booster and the seatbelt correctly when riding as a car passenger.

The vehicle

Regardless of crash configuration, booster-seated children benefit from the vehicle safety systems. In frontal impacts, the seatbelt is the main protection system, as shown in Figure 7. By using the vehicle's seatbelt, the child will benefit directly from the vehicle's structural safety design and collision mitigation systems, as well as any advanced seatbelt functionality (e.g., belt pretensioners and load limiters). Depending on the vehicle model, modern frontal impact

passenger airbags may add to the protection of the booster-seated child in the front passenger seat, see further in Heurlin et al. (2016).

Using crash testing, Bohman et al. (2006) and Lopez-Valdes et al. (2009) illustrated the benefits of seatbelt pretensioners and load limiters for a child ATD in a frontal impact. For the load limiter to be effective for the child, the load levels need to be adapted to the size and weight of the child. Such systems were introduced on the market in 2007 (Jakobsson et al., 2007) and have increased in availability. The primary purpose of seatbelt pretensioners is to reduce seatbelt slack. Although manually tightened on an occupant wearing tight clothes, there is still some slack to remove (see Figure 7). If wearing bulky clothes or if the seatbelt has not been tightened manually the importance of the pretensioner is even more significant, for children as well as adults. Due to the high loads in a crash, the seatbelt will always strive to take the shortest path between its anchorage points. This was exemplified in the crash test shown in Figure 6b, in which the initial position of the shoulder belt was re-routed by the belt guide of the inboard tilted booster seat's backrest. In this case, the belt guide did not manage to retain the initial routing when lap-belt forces increased up to 4 kN. When the shoulder belt was straightened it resulted in a path outside the shoulder of the ATD. Generally, re-routing of the seatbelt, although attaining an initial visually appropriate position on the body, may result in slack when the webbing is straightened, having consequences on pelvis retention and the preferred torso flexion. If no pretensioner, the addition of the initial slack will further add to the outcome.

The purpose of the inflatable curtain (IC) is to cover the open area of the side windows, in case of a side-impact, rollover crash or other crash configurations, when needed. As for an adult, the IC, in addition to the interior side structure of the vehicle, including panels and energy absorption, will also help protect a child by distribution and reducing the loads. The torso side-impact airbags are designed not to be harmful to the child and studies suggest that they may add protection for the child as well, when seated on the struck side in a side-impact crash (Andersson et al., 2012; Bohman and Sunnevång, 2012). If seated on the non-struck side, the pretensioning of the seatbelt will help to further restrain the child and limit head excursion (Tylko et al., 2015; Jakobsson et al., 2017). With the pretensioner activated, no difference in extent of lateral head excursion were seen for the ATD, comparing restrained on an integrated booster and on a booster seat, irrespectively if attached to the ISOFIX anchorages or not (Jakobsson et al., 2017).

The user

In most motorized countries there is a high awareness of the need to use boosters for children in passenger cars. In a Swedish survey in 2021, 94% of children aged 4 up to 8 report always using appropriate restraints (Bergfors et al., 2021). This observation has been stable since 2016, while an increase from 77% and 69% in 2014 and 2015, respectively. In US in 2019, 69.5 % of children aged 4-7 were using child restraints (Enriques, 2021). The usage frequency varies between countries and the age of the child, with a decreasing trend with increased age. In addition, the type of booster varies with age. For Sweden, booster cushions represent an increasing share of boosters with increased age, as well as a proportionally higher use of integrated boosters with increased age, as compared to add-on boosters (Jakobsson and Lindman, 2015). More recent Swedish data from 2021 shows that 88% use booster cushions and 23% use booster seats (multiple choice possible) among booster restrained children aged 8 to 11 (Bergfors et al., 2021). Among those aged 4 to 8, the booster cushion usage was 40%.

The reasons for non-use or part-time booster use are several: such as lack of knowledge, the child thinks it is childish or claims it to be uncomfortable and refuses, or the booster is too big (Ramsey et al., 2000; Simpson et al., 2002; Ebel et al., 2003; Bingham et al., 2006). Lack of access and inconvenience are other reasons for non-use. The boosters may not be easily available e.g., when travelling with others, or when in a hurry (Bingham et al., 2006). Compared to private vehicles, the use of child restraints is lower in taxis, which was seen attributable to the inconvenience of carrying them to and from the taxi (Keshavarz et al., 2006).

Another important safety challenge is misuse. The most frequent misuse modes for boosters relate to the belt routing; incorrect lap-belt path or non-optimal shoulder belt routing (O'Neil et al., 2009; Bohman et al., 2016). Discomfort caused by the shoulder belt being too close to the neck may be handled by placing the belt off the shoulder, away from the neck or even placing the shoulder belt under the arm or behind the back (Ebel et al., 2003; Jakobsson et al., 2011). These actions will likely increase risk of injury if exposed to a crash.

The booster

The booster is as an adapter, not a primary restraint for the child. The booster serves the purpose to adapt the child to the vehicle seat and seatbelt, addressing the protection principles for the child passenger protection. The main characteristics of a booster can be summarized as follows:

- **Boost**! – Raise the child to ensure the lap-belt is positioned low on the pelvis and the shoulder belt is positioned on a mid-shoulder position.

- Design to **position the lap-belt low on the pelvis,** ensuring contact with the boney parts of the pelvis and prevent placement too far forward on the thigh or too high on the abdomen.

- Provide **comfortable cushion length**, allowing the child to bend the legs comfortably over the seat edge.

- **Move in a controlled manner** together with the child during crash.

In addition, **lateral support** for comfort and upright lateral sitting posture, to keep the shoulder belt on the shoulder by avoiding lateral leaning, especially for the younger children and during longer trips. The lateral supports could be provided by the booster seat's backrest, but only if it does not obstruct the vehicle safety system to work. A lateral support could just as well be an add-on comfort cover, providing sleep support and restricting the lateral movement, but not influencing during a crash.

During the crash, the booster should have **stable performance**; excessive deformation of the booster has been shown to alter lap-belt positioning and increase the risk of submarining (Tylko and Bussières, 2012; Forman et al., 2022). Forman et al. (2022) evaluated the effect of 17 different parameters in a large-scale simulation study. They identified booster stiffness being the most influential parameter, together with sitting posture, for predicting submarining risk. In another simulation study on different booster cushion parameters, although no submarining occurred, the booster with reduced stiffness resulted in less favorable overall kinematics as the pelvis was not restrained as efficiently as for the boosters with more stable performance (Bohman et al., 2020).

Tight attachment to the vehicle (e.g., to the ISOFIX anchorages) should only be made when the vehicle-booster system is developed together, such as integrated boosters, or used only when there is a seatbelt pretensioner available to reduce belt slack. This is to ensure that the child will not slide off the booster in a frontal impact. Non-tight attachments can be used allowing the booster to move with the child forward, and still serve as a booster restraint when no child is using the booster.

CURRENT AND FUTURE MOBILITY CHALLENGES

Although there is a high awareness of the need to use boosters for children in vehicles, the usage varies between countries, and decreases with the child's age. For optimal protection, children up to approximately 140 cm should use a booster when riding in a passenger car. This is not the case in current mobility. Driven by sustainability goals, passenger cars' design and ownership setups are changing. These trends in combination with the current booster development trend pose challenges for child occupant protection. The challenges include ensuring booster usage at current levels and even more so, to increase future usage reaching the optimal situation. A summary of the three trends is provided.

Passenger Car Development Trends

Passenger cars are becoming more streamlined having implications on space between the outboard rear-seat passenger's head and the vehicle's side structure. Although an adult might fit well, as well as a child using a booster cushion, it is not as obvious for a large booster seat due to its large head and torso side supports, and thereby potential interaction with the vehicle's roof or side structure, see Figure 8. This interaction of tight fitment might even cause problems for the vehicle's safety systems to function as intended. For example, the IC is positioned within this area of interaction. In the event of a side-impact, the IC is intended to inflate and serve as a part of the protection system for both front- and rear-seat occupants. Incorrect inflation of the IC might influence protection of the child in the booster seat as well as the front-seat occupant.

Figure 8a. A mid-sized male adult in the rear-seat of a modern passenger car.

Figure 8b. A booster seat with a 6-year-old-sized ATD in the rear-seat of a modern passenger car.

Figure 8c. A booster seat with a 10-year-old-sized ATD in the rear-seat of a modern passenger car

.

Autobrake systems were introduced more than a decade ago and have evolved over the years, as well as increased in availability in modern passenger cars. Based on data prior to auto brake system introduction, approximately 40% of the crashes were preceded by an avoidance maneuver by the driver (Stockman, 2016). This number is likely higher when adding the maneuvers made by the vehicle, to help mitigate the severity of a crash. Hence, there will be a higher likelihood for children to be exposed to maneuvers in future crashes, having potential influence on their forward position or lateral sitting posture, including shoulder belt position at time of impact.

Mobility Trends

Passenger car ownership setups are changing. Ridesharing and car sharing (shared mobility) are increasing trends all over the world. An overview of 47 countries showed that, in October 2018, car sharing businesses included 32 million users, sharing 198 000 vehicles (Shaheen and Cohen, 2020). In 2018, online car hailing accounted for 36% of the total traffic volume in China (Sohu, 2019). Shared mobility services have also grown in popularity as a family transportation option (Ehsani et al., 2021; Koppel et al., 2021). The use of taxi services, car-pool systems, and other car sharing, such as remote activation of borrowing your friend's car on short notice, are examples of not using the same car every day. In addition, an increase of multiple transportation modes during one trip; using cars only part of the trip, becomes a consequence of city planning as well as changes in mobility trends. These changes pose challenges for child passenger protection in relation to the traditional way of car ownership/usage. For example, although child restraint usage is high in privately owned vehicles in high-income countries, child restraint usage is substantially lower in shared mobility services such as taxis, rideshare vehicles, and car sharing (Koffsky et al., 2018; McDonald et al., 2018; Prince et al., 2019; Owens et al., 2019; Koppel et al., 2021; Reed et al. 2022). Parents were most likely to report none usage of child restraint while travelling in a rideshare vehicle because: lack of child restraint in the rideshare vehicle, they did not bring a child restraint with them, or the trip was of a short distance (Owens et al., 2019; Koppel et al., 2021).

Booster Development Trends

The booster design development has been driven separately from the vehicle development, which has influenced the regulatory and consumer information tests. The test rigs lack important state-of-the-art vehicle protection characteristics, including IC, which are standard in the vast majority of current vehicles. Such test rig designs may drive optimized side structures of the booster seat.

The role of the ATD and its assessment criteria is important too. As an example, the ATD assessment in the side-impact tests are acceleration-based, which directly drives the design of the side supports in the booster's backrest. The relevant structure in the test rig is limited, whereby the backrest's side supports serve as the energy absorption, driving wider booster seats. Even more so, chest accelerations are optimally reduced by early contact, whereby thicker side

support structures are more likely rewarded with higher scores. On top of that, adjustable features such as "lateral impact devices" can further reduce contact time. Such features are typical examples of optimization for the ATD criterion in the test rig, though questionable with respect to real-world relevance. While regulatory tests provide a limit for approval, consumer information tests serve the purpose to differentiate between boosters, and therefore are motivated to include stringent targets.

Booster cushion banning

Several parts of the world are banning booster cushions, claiming lack of head protection in side-impacts. European child restraint consumer information tests disqualify booster cushions, claiming the side support of the backrest being essential for the child's protection in side-impacts. The reasoning for this is not in line with decades of real-world experience, which shows that the vehicle protection is serving to protect the booster-seated child's head, similar to an adult (Jakobsson et al., 2005) and no evident difference between booster seat and booster cushion is seen (Arbogast, 2010). The Australian regulation, as well as the UN Regulation No. 129 type-approval, require head side structure on the booster to pass the side-impact test. UN Reg No. 129 still includes booster cushions by allowing exception of the side-impact test. However, this is only for children 125 cm and taller. Booster height specifications, with the ambition to get the child's head into a certain height position, make it difficult, if not impossible, to design an attractive booster cushion for the children it targets (Jakobsson et al., 2020).

Booster seat development trend

Booster seats are becoming larger and with increased complexity. This trend is beyond the ban of booster cushions, although also likely related to a lack of understanding the vehicle-booster-user entity. This trend is about adding features in the booster seat design. In combination with a created consumer belief and demand for these features, the booster seats become large, heavy, and bulky, while lacking substantial arguments on the features' real-world safety relevance. Instead, this may have serious implications on usage for all trips, which evidently is negative for child passenger protection. The features relate to several areas, such as an extensive backrest, devices influencing the seatbelt, and attaching the booster seat to the vehicle, as exemplified in Figure 9.
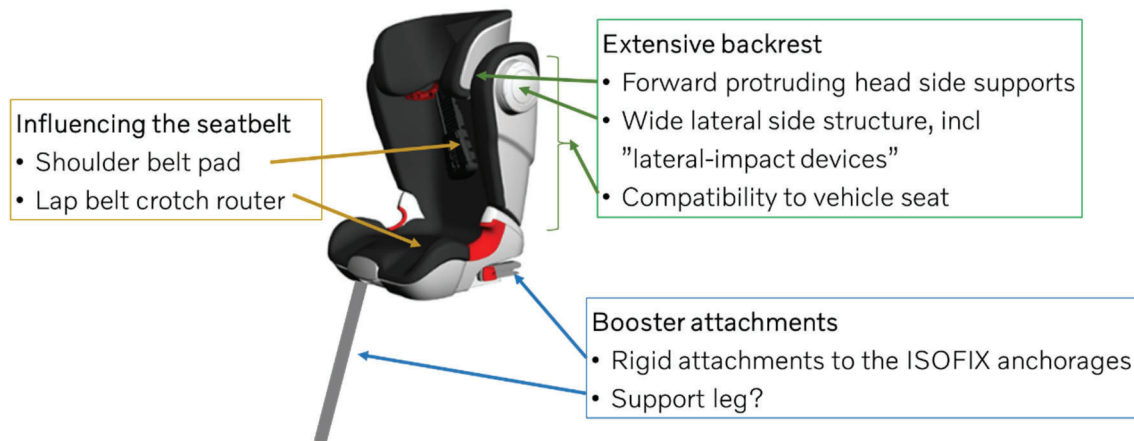
Figure 9. Examples of the booster seat design trend.

The extensive backrest

The backrest designs have evolved towards large side supports both at the torso and head area. The child restraint manufacturers emphasize two reasons for this; to provide comfort for children by keeping them upright when relaxed or asleep, and to provide improved side-impact protection (Bendjellal et al., 2011). Supporting the child to remain in lateral upright position is favorable in helping to keep the shoulder belt in a mid-position on the shoulder. This is essential for the child's protection in case of a frontal impact or in complex crashes in general.

Although developed for crash protection, it is not evident that a backrest with forward protruding head side supports offers lateral protection for the child in all real-world situations. As exemplified in Figures 3 and 5, several reasons may influence the child's head position at time of impact, resulting in a position more forward than of the coverage of most booster seat's head side supports. The forward protruding head and torso side supports could even contribute

to drive a more forward sitting posture due to visibility and comfort related aspects (Figure 5). In addition, there are relatively few real-world occasions in which the child's head will interact with the head side support as in the test rig methods for which it is assessed for, when considering the variety of side-impact configurations and the forward trajectories of a child sitting in a moving vehicle when exposed to such impact.

The lateral width of the side support, as exemplified in Figures 8b-c is substantial in some booster seats. Although likely scoring well in test rig setups, it is questionable whether they are beneficial in the real-world context. Adding the adjustable "lateral-impact devices" it becomes even more questionable. In addition, the backrest as such has compatibility challenges in the vehicle seats. It is difficult to make it fit in a contoured vehicle seat back and the interaction with the vehicle head restraint may force it into a forward position, resulting in an unnecessarily upright sitting posture of the child. Although likely not a safety problem, the upright posture might be uncomfortable, whereby a better solution is to use a booster cushion together with the vehicle seat back and head restraint. Removal of the head restraint, which is often incorrectly recommended, is not a safe alternative. The vehicle's head restraint is designed and assessed for high severity rear-end impacts, while the booster seat's backrest is likely not.

Influencing the seatbelt

As previously described, the seatbelt is the primary restraint for a booster-seated child. Booster belt guides should be designed with care to secure the performance by the seatbelt at crash. This includes the lap-belt guides on the cushion part as well as the shoulder belt guides on the backrest. An example of design for good guiding is shown in Figure 10a. Some boosters guide the lap-belt too far forward on the thighs, not touching the pelvis, which may result in slouching (Jones et al., 2020), and in delayed coupling of the pelvis. Extensive shoulder belt routing might add slack and provide a sense of "false" protection expectations, as exemplified in Figure 6.

Figure 10a. A booster seat designed to guide the seatbelt without adding slack or risk for the belt to get stuck. Same design as shown in Figure 1c.	**Figure 10b. A booster seat with a shoulder belt pad.**	**Figure 10c. A child in a booster seat with the lap-belt routed through a lap-belt crotch router strap.**

Recent trends include adding pads to the shoulder belt and connecting the lap-belt to a lap-belt crotch routers, exemplified in Figure 10b and Figure 10c, respectively. The shoulder belt pad in Figure 10b was introduced to help reduce the ATD's responses in the chest and neck, by damping the head-to-torso impact. Hence, this is a device that is designed for ATDs and does not necessarily provide any benefits to real children. If used correctly, it might not harm. However, if not positioned correctly it might risk getting stuck and to hinder the seatbelt functionality, especially in a vehicle with seatbelt pretensioner. Hence, it adds an unnecessary misuse aspect, rather than protection for the child. Unfortunately, this is not understood by the users, who are told the opposite and perceives it therefore as a safety device. The lap-belt crotch router was introduced in 2015 and is now also perceived by the users as an important safety device. This lap-belt crotch router introduces slack into the lap-belt, which may reduce the overall protection effect due to delayed coupling of the pelvis. Poor lap-belt fit, due to inadequately designed belt guides, may be improved by this feature, however that aspect should be addressed by improvements to the booster design, rather than introducing an additional feature.

Attaching the booster to the vehicle

Restraining the booster seat when not used by the child will help to protect other occupants in the vehicle, in case of a crash. This can be done by the seatbelt or, as recently introduced, by attachments to the vehicle's ISOFIX anchorages. With vehicle restraints reducing potential seatbelt slack in case of a crash, this attachment might not be a problem for the child passenger in those conditions. However, it adds weight and complexity to the booster seat. In addition, crash tests in a vehicle environment have shown that with a tight attachment of the booster in combination with slack in the seatbelt, the ATD slides off the booster (Tylko et al., 2016). Hence, there might be a potential real-world protection issue, which is not detected in standardized test rig methods.

Recently, the question on allowing a support leg for the category of booster seats was raised at UNECE Working Party on Passive Safety (GRSP) (United Nations, 2022). The main argument addressed the convertible or multi-purpose type of child restraints, accommodating the use of the support leg also when in a booster seat mode. Currently, the booster seat envelope in UN Reg No. 16 does not allow for a support leg. If including the possibility of a support leg for a booster seat, there is an obvious risk that this becomes a popular feature among booster seat designs as well. Hence, it may contribute to drive the already large booster seats to become more complex, bulky and heavier. Bohman et al. (2022) showed that minor and non-consistent differences were seen when adding a support leg to a booster seat in frontal impact simulations, with two different child occupant models in a vehicle interior, when including activated seatbelt pretensioner. Although somewhat larger differences were seen in the configurations without seatbelt pretensioner activation, it was concluded that no kinematical nor response aspects provided evidence of enhanced real-world protection needs of a support leg for the booster seat (Bohman et al., 2022).

DISCUSSIONS

Children aged 4 to 10-12 are well protected if using boosters that elevate them, shorten the seat cushion length, position the lap-belt in contact with the pelvis and position the shoulder belt across the chest and shoulder. The protection is a combination of the vehicle design, the booster design and how the child is using the restraints. Integrated boosters benefit from being designed together with the vehicle restraints, optimizing their protective performance. Studies have confirmed integrated boosters to reduce the likelihood of misuse, being comfortable, and a way to attract the older children to use boosters (Osvalder and Bohman, 2008; Jakobsson et al., 2012; Osvalder et al., 2013; Bohman et al., 2016). However, integrated boosters are available in a limited number of vehicle models and never in all passenger seat positions, whereby there is a need for a non-integrated booster matching the principles of the integrated booster, while being portable and easy to use.

The Mismatch

There is a mismatch with respect to the booster trend and the challenges in current and future mobility. The current booster trend includes banning booster cushions and promoting booster seats with large designs and several features adding weight and complexity. This is also a mismatch in relation to overall real-world protection. Not allowing booster cushions causes issues as illustrated in Figure 8, showing that a booster-seated child may require more space in the vehicle seat than an adult. The potential incompatibility between a large booster seat's backrest and the vehicle interior will increase with the trend of more streamlined roof designs, as driven by sustainability goals. The reasons behind the development of the extensive side supports are partly clear. Backrests with forward protruding head side supports were introduced approximately in year 2000 and was driven by an ambition to help protect the child's head in a side-impact (Bendjellal et al., 2011). At the same time, vehicles were starting to be equipped with ICs. A decade later, the side supports of the booster seat have increased in width, mainly driven by introduction of side-impact tests using test rigs, with no vehicle-like head protection included. Likely an adult-sized ATD would be just as poorly protected in such a test rig method. Isolated from the vehicle-context, it was perceived that a booster cushion was not capable alone to protect the child without the protruding head side supports as part of the booster seat. This perception spread widely, and similar test methods were included in regulatory updates, leading to banned booster cushions in some parts of the world. Unfortunately, there was a misconception that the booster seat should serve as the main protection for the head despite real-world data that showed that the child's head was likely mainly protected by the vehicle (as for adults), prior the introduction of extensive side supports and ICs. The compatibility issues of fitment and vehicle safety systems are essential motivators for allowing use of booster cushions.

User studies show several reasons for children having a forward leaning head position at impact, such as being engaged in electronic devices or due to visibility reasons, or because of an evasive braking. Studies also show that children in boosters with forward protruding side supports were more prone to attain a forward head position, resulting in the head being out of the head side supports. In such cases, the effect of the booster's head side support will be limited. The backrest as such adds distance to the vehicle seatback and thereby positions the child more forward and closer to the structure in front, as exemplified in Figures 4 and 5b. In case of a frontal impact, a more forward initial head position, relative to the vehicle, will result in a more forward head excursion and thereby increasing the risk of head impact. Although developed for head protection using test rig methods, it is not evident that a backrest with head side supports offers head impact protection for the child in real-world situations.

More recently, shoulder belt pads and belt routing straps (Figures 10b-c), in addition to attachments of the booster to the vehicle by using the ISOFIX anchorages, have been added to serve as anticipated improvements for frontal impact protection. These features are not shown as safety enhancements in real-world situations, although there are likely situations in which they might not do any harm. Nevertheless, the seatbelt re-routing by the belt routing straps, and the tight attachment of the booster to the ISOFIX anchorages are concrete examples of a lack of understanding the booster-vehicle context and may be counterproductive. Overall, these over-engineered products drive the complexity of the boosters, likely having impact on usage.

Another mismatch is about the test rigs for booster assessment and how the results are analyzed and communicated, not acknowledging the limitations of the test rigs' real-world resemblance. Based on the simplified test setup, lacking representative vehicle and user context, safety perceptions are communicated which are not aligned with real-world safety performance. Too many consumers today are told that a booster with all the features is the safest alternative, while likely that is not the case.

A main challenge today is the increased degree of shared mobility services and to help ensure the use of a booster at every trip. The current booster offer is not aligned with this development. The trend of changing from the habit of using one vehicle from start to destination to flexible use of several different vehicles is a challenging task when addressing the needs of families. The sketch in Figure 11a illustrates some choices addressing how to make sure the whole system is in place when using the vehicle. Can they carry a booster with them; large or small? Or, could there be one available when reaching the vehicle? How can we help the users to always use a booster even in shared mobility situations? Another challenge of large booster seats is illustrated in Figure 11b, in which two mid-sized male adults are sitting together with a booster seat in a rear-seat of a modern large family car.

Figure 11a. A sketch illustrating shared mobility challenges for a family

Figure 11b. Fitting two mid-sized male adults together with a booster seat in the rear-seat of a large family car

Real-World Protection

Real-world data shows that boosters, irrespectively of backrest or not, provide protection for the child.

The fundamentals for real-world protection for the category of booster-seated children are:
- The seatbelt is the primary restraint, as for an adult.
- The booster's main purpose is to raise the child in position for good lap-belt geometry, for reduced risk of submarining in frontal impacts.
- By raising the child, the booster will also provide a more comfortable and safe mid-shoulder shoulder belt position.
- The booster shortens the cushion length, improving comfort and thereby reducing risk of slouching.
- The booster-seated child will benefit from the advanced seatbelt technologies, such as the pretensioners.
- In a side-impact, the vehicle safety systems will help protect the child, as for an adult.
- Lateral support for comfort and upright sitting posture could be provided by the booster, but only if obstruction of vehicle safety systems is avoided. It could just as well be an add-on comfort cover.

In addition, not to jeopardize real-world protection of the child these guidelines should be followed:
- Don't let the booster introduce excessive re-routing of the seatbelt. Re-routing may have negative impact on the seatbelt's performance during crash.
- Avoid extensive side supports. This may have negative impact on vehicle safety systems' function.
- The boost should maintain stable during the whole crash.
- Be careful when attaching the booster to the vehicle (by other means than the seatbelt), when the child is using it. The booster should move with the child, if needed.

Most importantly, a booster should be used at every trip.

What is Needed?

Allowing booster cushions for children from 4 years of age is essential for safe shared mobility. The consequences of banning the booster cushion could result in children not using a child restraint, due to the hassle of bringing a booster seat along to the car sharing service or limited access to boosters by the car services. The trend of decreased use of booster seats by increased age is seen already today, while the use of booster cushions is relatively greater among the older booster-seated children. Today in conventional car ownership, there is a relatively high share of seatbelt-only-restraint among the oldest children required to use boosters. If no safe and convenient alternative is available, the share of incorrectly restrained children is likely to increase when car ownership changes and multiple transport modes during one trip will increase. This will influence the protection in a crash and have negative impact on the overall traffic safety.

Banning a well-performing booster cushion based on arguments not substantiated by real-world data, is not in line with the users' needs. Instead, efforts should be focused on providing information on the importance of beltfit and sitting upright, whereby the child could fully benefit from the vehicle safety systems. This is in line with the proposed joint efforts by the vehicle, the booster and the user for the protection of the child in the vehicle. For the younger booster-seated children, they may need support for lateral restriction to ensure good shoulder belt fit throughout the ride. This need varies by individual and by the trip. Likely more support is needed during longer trips to support the child when sleeping, as compared to shorter trips. Other strategies, than a backrest with large protruding side supports, can be applied to address this, such as adding low-weight comfort support helping to stabilize the child laterally into an upright sitting posture when resting. These supports should not be rigidly attached to the booster, nor the seatbelt and they should not influence the vehicle safety systems during a crash.

As a safety community we need to ensure that parents and caregivers are educated on what a booster does. Consumer misunderstanding the role of a booster, such as considering it as a restraint and not as an adapter, may contribute to encourage the designs to be larger and have more extraneous features, that do not positively contribute to occupant safety. This is to be expected as these consumers are graduating from harness-based child restraints, which are not as

dependent of the vehicle restraint in its protective design. We need to re-orient the consumer to how a booster works, driving simple solutions that positively impact safety, as well as the other key characteristics of accessibility and affordability.

There is also a need to address the test methods for booster assessment, in addition to the interpretations and messages provided from the tests. This includes the certification tests by UN Reg No. 129 and in Australia, which today are restricting real-world safe booster cushions. It also includes the consumer information rating tests, in addition to the child seat manufactures, and their role in communicating the benefits of different features. Since the test rig has limitations in reflecting the vehicle-booster-user entity, care should be taken when communicating safety benefits of features evaluated via this method, in relation to a real-world protection context. This was also emphasized by Arbogast et al. (2022), summarizing discussions at an international workshop on child occupant protection.

The rear-seats of passenger cars are constantly improving. Therefore, there is a need to investigate how the test methods for booster assessment can be further developed, to improve the representation of modern vehicles. In addition, the child occupant's representation by the child ATDs also needs to be further addressed. In the absence of a complete understanding of the ATD limitations, the interpretation of the response can contribute to conflicting safety countermeasures (Arbogast et al., 2022). In line with the concept of a booster as an adapter, rather than a stand-alone restraint, it is important that the methods and tools for testing reflect that the booster is part of a system that includes the vehicle environment as well as the child context. To capture the full protective effect of a booster, the context should be as realistic as possible.

The Way Forward

Today there is a reluctance among families to use car sharing services, of which one of the main reasons is their concerns regarding the child restraints (Koppel et al., 2021). The journey towards increased shared mobility, being one of the enablers for a more sustainable traffic situation, is a collaborative task by all involved stakeholders. The car manufacturers, as well as the child seat manufacturers and the users, in addition to rulemaking and organizations influencing the design of the different parts, such as consumer information testing, need to work together and be aligned towards the common goal of sustainable and safe transportation.

The trend in recent booster developments is likely a result of lack of cooperative efforts between the involved stakeholders. Obviously, the booster regulation methods are done with the best intentions for the children. However, there seems to be a lack of understanding of the larger context, such as the environment in which the child will be using the booster. When used, the booster is always positioned in a passenger car seat. A car seat is designed to protect car passengers. The vehicle safety systems, e.g., the seatbelt, the vehicle interior and airbags, will help protect the booster-seated child as well. Hence the booster's main purpose is to complement with the child specific needs, i.e., being an adapter to raise the child in position for the seatbelt. From the user's perspective, different types of boosters, complementing each other, are needed to benefit overall protection of children in vehicles.

Real-world crash data includes data over many years, although not the most recent years. During these years, the basic booster designs, are included and many of the vehicles are likely without advanced seatbelt technology and ICs. Regardless of this, the real-world data clearly shows that booster-seated children are well protected. For the booster design, it is essential that we acknowledge the real-world evidence and experience and adhere to the protection principles. The protective performance of a well-designed booster cushion is proven, and there is evidence that booster cushions, as well as integrated boosters, increase usage especially among the older child age group. Adapting these to the protection needs of children aged 4 to 10-12 and making them portable, focusing size and weight still adhering the protection principles, will help keep children safe in the increased trend of shared mobility. By going back to the fundaments and learnings from the past, we should align towards a common goal of sustainable and safe transportation for children aged 4 to 10-12.

CONCLUSIONS

There is a mismatch between booster development and assessment, and the needs for child passenger protection in current and future vehicles. Driven by sustainability goals, passenger cars' design and ownership setups are changing requiring practical solutions for child passenger protection. At the same time the boosters are becoming larger and more complex, including a ban of booster cushions. While passenger cars encompass more advanced safety systems, the boosters are assessed using test rig methods without resemblance of these characteristics, nor consideration of the large range of sitting postures in the real-world context. Real-world child passenger safety involves an understanding that the booster is an adapter and not a restraint. Most importantly, irrespectively of passenger cars' design and ownership setups, the booster should be used in every trip.

Real-world child passenger protection is achieved by the vehicle and booster together. Children benefit from the vehicle safety systems, given they are raised in a position for good beltfit: over the pelvis and across the chest and shoulder. This is exemplified by vehicle's head protection of the forward leaning child in side-impacts, and pretensioner reducing seatbelt slack when wearing bulky clothes. Hence, the design of boosters should focus the necessary elevation of the child to achieve a good initial beltfit and maintain a good seatbelt interaction during the whole crash.

This study urges all stakeholders to be aligned towards a common goal of sustainable and safe transportation for booster-seated children, typically aged 4 to 10-12. The way forward is to focus on the essential protection principles and always consider the real-world context, which includes the vehicle, the booster, and the user as an entity, and to use this as the foundation for all tests, assessments, and communication. This joint effort is an essential part to help maintain, and potentially even enhance, current real-world protection level of booster-seated children into future transportation.

ACKNOWLEDGEMENT

REFERENCES

Adomeit D, Heger A. Motion sequence criteria and design proposals for restraint devices in order to avoid unfavorable biomechanic conditions and submarining, *19th Stapp Car Crash Conf*, SAE-751146, 1975

Andersson M, Bohman K, Osvalder AL. Effect of booster design on children's choice of seating position during naturalistic riding. *Annu Proc Assoc Adv Automot Med*. 54:171-80, 2010

Andersson M, Pipkorn B, Lövsund P. Parameter study for child injury mitigation in near-side impacts through FE simulations. *Traffic Inj Prev*, Vol 13:2, 2012:182-192

Anderson M, Carlson LL, Rees DI. Seat effectiveness among older children: Evidence from Washington state, *Am J Prev Med*. 53(2), Aug 2017:210–215.

Arbogast KB, Ghati Y, Menon RA, Tylko S, Tamborra N, Morgan R. Field investigation of child restraints in side impact crashes. *Traffic Inj Prev*. Vol 6:4, 2005:351–360

Arbogast K, Jermakian JS, Kallan M, Durbin DR. Effectiveness of belt positioning booster seats: An updated assessment. *Pediatrics* 124, 2009:1281–1286

Arbogast KB. Injury Risk – Side impacts; 4-8 year olds, rear rows, PCPS dataset 12/1/98-11/30/07, presentation as Invited Speaker at *2010 Stapp Car Crash Conf.*, Personal communication, 2010

Arbogast KB, Bohman K, Jakobsson L, Jermakian J, Koppel S, Tylko S. A Safety framework for the evolution of boosters: Current and future mobility, *20th Int. Conf. Protection of Children in Cars*, Munich, Germany, Dec 2022

Baker G, Stockman I, Bohman K, Jakobsson L, Osvalder AL, Svensson M, Wimmerstedt M. Kinematics and shoulder belt engagement of children on belt-positioning boosters during emergency braking events. *IRCOBI Conf.* Antwerp, Belgium, 2017

Baker G, Stockman I, Bohman K, Jakobsson L, Osvalder AL, Svensson M, Wimmerstedt M. Kinematics and shoulder belt engagement of children on belt-positioning boosters during evasive steering maneuvers. *Traffic Inj Prev.* 28;19(sup1), Feb 2018:S131-S138

Bendjellal F, Scicluna G, Frank R, Grohspietsch M, Whiteway A, Flood W, Marsilia R. Applying side impact cushion technology to child restraint systems, *22nd Int. ESV Conf.*, Paper no. 11-0138, Washington DC, USA, 2011

Bergfors S, Lundberg H, Jakobsson L, Bohman K. Child restraint use in Sweden, *19th Int. Conf. Protection of Children in Cars*, Munich, Germany, 2021

Bingham CR, Eby DW, Hockanson, HM, Greenspan AI. Factors influencing the use of booster seats: A state-wide survey of parents, *AAP* 38, 2006:1028-37

Bohlin N. Fifteen years with the three point safety belt. *IAATM 6th Int. Conf.*, Melbourne, Feb 1977; https://group.volvocars.com/company/safety-vision/research-1970-1980 (accessed 16/12/2022)

Bohman K, Boström O, Olsson J, Håland Y. The effect of a pretensioner and a load limiter on a HIII 6y, seated on four different types of booster cushions in frontal impacts. *IRCOBI Conf.,* Madrid, Spain, 2006:377-380

Bohman K, Stockman I, Jakobsson L, Osvalder AL, Bostrom O, Arbogast K. Kinematics and shoulder belt position of child rear seat passengers during vehicle maneuvers. *Ann Adv Automot Med*. 55, 2011:15-26

Bohman K, Sunnevång C. Q10 child dummy performance in side and frontal sled tests. *10th Int. Conf. Protection of Children in Cars*, Munich, Germany, 2012

Bohman K, Jorlöv S, Zhou S, Zhao C, Sui B, Ding C. Misuse of booster cushions among children and adults in Shanghai - An observational and attitude study during buckling up, *Traffic Inj Prev* 18:0, 2016

Bohman K, Arbogast KB, Loeb H, Charlton JL, Koppel S, Cross SL. Frontal and oblique crash tests of HIII 6-year-old child ATD using real-world, observed child passenger postures. *Traffic Inj Prev*. 19(Suppl 1), 2018:125–130.

Bohman K, Östh J, Jakobsson L, Stockman I, Wimmerstedt M, Wallin H. Booster cushion design effects on child occupant kinematics and loading assessed using the PIPER 6-year-old HBM and the Q10 ATD in frontal impacts, *Traffic Inj Prev*. 24, 2020:1-6. DOI: 10.1080/15389588.2020.1795148

Bohman K, El-Mobader S, Jakobsson L, Lundgren D. Influence of support leg for booster seats. 20th Int. Conf. Protection of Children in Cars, Munich, Germany, Dec 2022

Burdi AR, Huelke DF, Snyder RG, Lowrey GH. Infants and children in the adult world of automobile safety design: Pediatric and anatomical considerations for design of child restraints, *J. Biomechanics*, Vol. 2, 1968:267-280

DeSantis Klinich K, Pritz HB, Beebe MB, Welty KE. Survey of older children in automotive restraints. *Proc. 38th Stapp Car Crash Conf.* SAE-942222, 1994:245-264

Durbin RD, Elliott MR, Winston FK. Belt-positioning booster seats and reduction in risk of injury among children in vehicle crashes, *JAMA* 289(21), June 2003:2835-2840, doi:10.1001/jama.289.21.2835

Ebel B, Koepsell T, Bennett E, Rivara F. Too small for a seatbelt: Predictors of booster seat use by child passengers, *Pediatrics*, 111 (4), 2003:323–327

Ehsani JP, Michael JP, Gielen A. Rideshare use among parents and their children. *Inj. Epidemiol*. 2021, 8, 1–3, doi:10.1186/s40621-021-00302-4.

Enriques J, The 2019 National Survey of the Use of Booster Seats, DOT HS 813 033, *NHTSA*; May 2021

Forman J, Miller M, Perez-Rapela D, Gepner B, Edwards M, Jermakian JS. Parametric study of booster seat design characteristics. *Transportation Research Board*, 2022. https://trid.trb.org/view/1928889. (accessed 16/12/2022)

Graci V, Douglas E, Seacrist T, Kerrigan J, Mansfield J, Bolte J, Sherony R, Hallman J, Arbogast KB. Characterization of the motion of booster-seated children during simulated in-vehicle precrash maneuvers, *Traffic Inj Prev*. 20:sup2, 2019:S75-S80, DOI: 10.1080/15389588.2019.1639160

Heurlin F, Jakobsson L, Nilsson H. Front passenger airbag benefits for restrained forward-facing children, *IRCOBI Conf.,* IRC-16-43, Malaga, Spain, 2016

Isaksson-Hellman I, Jakobsson L, Gustafsson C, Norin H. Trends and effects of child restraint systems based on Volvo's Swedish accident database. *Child Occupant Protection 2nd Symposium Proc.*, P-316, SAE-973299, SAE Int, Warrendale, PA, USA, 1997:43-54

Jakobsson, L, Isaksson-Hellman I, Lundell B. Safety for the growing child – Experiences from Swedish accident data, *19th Int. ESV Conf.*, Paper no. 05-0330, Washington DC, USA, 2005

Jakobsson L, Wiberg H, Isaksson-Hellman I, Gustafsson J. Rear seat safety for the growing child – A new 2-stage integrated booster cushion, *20th Int. ESV Conf.,* Paper no. 07-0322, Lyon, France, 2007

Jakobsson L, Bohman K, Stockman I, Andersson M, Osvalder A-L. Older children's sitting postures when riding in the rear seat, *IRCOBI Conf.,* IRC-11-44, Krakow, Poland 2011

Jakobsson L, Lechelt U, Walkhed E. The balance of vehicle and child seat protection for the older children in child restraints, *10th Int. Conf. Protection of Children in Cars*, Munich, Germany, 2012

Jakobsson L, Lindman M. Booster usage in cars 2000-2013, in Sweden, *13th Int. Conf. Protection of Children in Cars*, Munich, Germany, 2015

Jakobsson L. Rearward facing child seats – past, present and future, *15th Int. Conf. Protection of Children in Cars*, Munich, Germany, 2017

Jakobsson L, Bohman K, Svensson M, Wimmerstedt M. Rear seat safety for children aged 4-12: Identifying the real-world needs towards development of countermeasures, *25th Int. ESV Conf.*, Paper no. 17-0088, Detroit, USA, 2017

Jakobsson L, Bohman K, Stockman I, Simmons S, Johansson C. Boosters for shared mobility, *18th Int. Conf. Protection of Children in Cars*, Munich (virtual), 2020.

Jermakian JS, Kallan MJ, Arbogast KB. Abdominal injury risk for children seated in belt-positioning booster seats, *20th Int. ESV Conf.,* Paper no. 07-0441, Lyon, France, 2007

Jones MLH, Ebert S, Manary MA, Reed MP, Klinich KD. Child posture and belt fit in a range of booster configurations*, Int. J. Environ. Res. Public Health* 17(3), 810, 2020, doi:10.3390/ijerph17030810

Kent R, Forman J. Restraint biomechanics, In: Yoganandan N. *Accidental Injury*, Springer, 2015:116-118

Keshavarz R, Patel R, Bachar R, Laddis D. Children in taxis: An opportunity for pediatricians and emergency physicians to save lives?, *Pediatric Emergency Care*, 22(11), 2006:704-9.

Koffsky S, Pham T, Gutman A, Ng C, Goldman JM, Milanaik R. Underuse of proper child restraints in taxis: Are weak laws putting children in danger? *Pediatrics* 141, 81, 2018.

Koppel S, Peiris S, Aburumman M, Wong C, Owens J, Womack K. What Are the Restraint Practices, Preferences, and Experiences When Australian Parents Travel with Their Children in a Rideshare Vehicle? *Int J Environ Res Public Health*. 25;18(17):8928, Aug 2021. doi: 10.3390/ijerph18178928.

Lopez-Valdes F, Forman J, Kent R. A comparison between child-size PMHS and the Hybrid III 6 yo in a sled frontal impact, *Ann Adv Automot Med* 5;53, Oct 2009:237-246.

Lundell B, Carlsson G, Nilsson P, Persson M, Rygaard C. Improving rear seat safety – A continuing process. *13th Int. ESV Conf.* Paper no. S9-W-35, Munich, Germany, 1991:1194-1200

Maheshwari J, Sarfare S, Falciani C, Belwadi A. Pediatric occupant human body model kinematic and kinetic response variation to changes in seating posture in simulated frontal impacts – with and without automatic emergency braking, *Traffic Inj Prev.* 21:sup1, 2020:S49-S53. DOI: 10.1080/15389588.2020.1825699

Maheshwari J, Sarfare S, Falciani C, Belwadi A. Analysis of kinematic response of pediatric occupants seated in naturalistic positions in simulated frontal small offset impacts: With and without Automatic Emergency Braking, *SAE Technical Paper* 2020-22-0002, 2021. https://doi.org/10.4271/2020-22-0002.

Maltese MR, Locey CM, Jermakian JS, Nance ML, Arbogast KB. Injury causation scenarios in belt-restrained nearside child occupants, *Stapp Car Crash J.* Vol 51, 2007:299–311

McDonald CC, Kennedy E, Fleisher L, Zonfrillo M. Situational use of child restraint systems and carpooling behaviors in parents and caregivers. *Int. J. Environ. Res. Public Health* 15(8), 2018:1788.

Norin H, Andersson B. The adult belt – a hazard to the child? *IAATM 6th Int. Conf.,* Melbourne, Feb 1977; https://group.volvocars.com/company/safety-vision/research-1970-1980 (accessed 16/12/2022)

Norin H, Saretok E, Jonasson K, Andersson Å, Kjellberg B, Samuelsson S. Child restraints in cars – An approach to safe family transportation. *SAE Congress and Exposition*, SAE-790320, SAE Int., Warrendale, PA, USA, 1979

O'Neil J, Daniels D, Talty J, Bull M. Seat belt misuse among children transported in belt-positioning booster seats, *AAP*, 21(3), 2009:425–429

Osvalder A-L, Bohman K. Misuse of booster cushions – An observation study of children's performance during buckling up, 52nd AAAM Annual Conference, *Annals of Advances in Automot Med*, 2008

Osvalder A-L, Hansson I, Stockman I, Carlsson A, Bohman K, Jakobsson L. Older children's sitting postures, behaviour and comfort experience during ride – A comparison between an Integrated Booster Cushion and a high-back booster. *IRCOBI Conf.,* IRC-13-105, Gothenburg, Sweden, 2013

Owens J, Womack K, Barowski L. Factors surrounding child seat usage in rideshare services. Final Report. Safe-D National UTC. *Virginia Tech Transportation Institute*, Texas A&M Transportation Institute, Report No 01-005, Sept 2019. https://rosap.ntl.bts.gov/view/dot/63050. (accessed 16/12/2022)

Prince P, Hines LH, Bauer MJ, Liu C, Luo J, Garnett M, Pressley JC. Pediatric restraint use and injury in New York City taxis compared to other passenger vehicles. In *Proceedings of the Transportation Research Board's Annual Meeting*, Washington, DC, USA, 13–17 January 2019.

Ramsey A, Simpson E, Rivara F. Booster seat use and reasons for nonuse, *Pediatrics*, 106(2), 2000:20

Reed MP, Ebert SM, Sherwood CP, Klinich KD, Manary MA. Evaluation of the static belt fit provided by belt-positioning booster seats, *AAP* 41, 2009:598-607

Reed MP, Ebert SM, Jones MLH, Hallman JJ.A naturalistic study of passenger seating position, posture, and restraint use in second-row seats. *Traffic Inj Prev*. 15, Jun 2022:1-6.

Simpson E. Moll E, Kassam-Adams N, Miller G. Winston F. Barriers to booster seat use and strategies to increase their use, *Pediatrics*, 110(4), 2002:729– 36

Shaheen S, Cohen A. Innovative mobility: Carsharing outlook. In carsharing market overview, analysis, and trends; Transportation Sustainability Research Center, University of California: Berkeley, CA, USA, 2020, https://escholarship.org/uc/item/61q03282 (accessed 16/12/2022)

Sohu. The proportion of online car hailing passenger traffic in total taxi passenger traffic increased from 9.5% to 36.3% from 2015 to 2018. Sohu news. 2019 March 15 [cited 17 Sep 2019]; (in Chinese) https://www.sohu.com/a/301430490_274290

Stockman I, Bohman K, Jakobsson L, Brolin K. Kinematics of child volunteers and child anthropomorphic test devices during emergency braking events in real car environment. *Traffic Inj Prev*. 2013;14(1):92-102

Stockman I. Safety for children in cars – Focus on three point seatbelts in emergency events. *Doctoral Thesis*, Dept. of Applied Mechanics, Chalmers University of Technology, Sweden, 2016, ISBN: 978-91-7597-468-2

Tarrière C. Children are not miniature adults, *IRCOBI Conf.,* Brunnen, Switzerland, 1995:15-27

Tylko S. Bussières A. Dynamic responses of Hybrid III 6 & 10-year-old ATDs seated on inflatable booster cushions. *10th Int. Conf. Protection of Children in Cars*, Munich, Germany, 2012

Tylko S, Bohman K, Bussières A. Responses of the Q6/Q6s ATD positioned in booster seats in the far-side seat location of side impact passenger car and sled tests. *Stapp Car Crash Journal*, Vol. 59, 2015:313-335.

Tylko S, Bussières A, Starr A. Evaluating child safety innovations: have we got the right tools and the right test methodologies? *14th Int. Conf. Protection of Children in Cars*, Munich, Germany, 2016.

United Nations. Working party on Passive Safety (GRSP), World Forum for Harmonization of Vehicle Regulations (WP.29), United Nations Economic Commission for Europe (UNECE), Geneva, Switzerland, 2022 https://unece.org/transportvehicle-regulations/working-party-passive-safety-introduction (accessed 16/12/2022)

Warren Bidez M, Syson S. Kinematics, injury mechanisms and design considerations for older children in adult torso belts. *SAE World Congress*, SP-1573, SAE Paper No. 2001-01-0173, SAE International, Warrendale, PA, USA, 2001

ACCIDENT SIMULATIONS OF A NOVEL RESTRAINT SAFETY CONCEPT FOR MOTOR-CYCLISTS

Steffen Maier, Jörg Fehr
Institute of Engineering and Computational Mechanics, University of Stuttgart
Germany

Paper Number 23-0189

ABSTRACT

Except for personal protective equipment, riders of powered two-wheelers are currently unprotected when impacting into an accident opponent. This work investigates a motorcycle safety concept that proposes a combination of thigh seat belts, airbags, and leg impact protectors. It gives a virtual prediction of the accident behavior using finite element models of the motorcycle with passive safety systems, an accident opponent, and an anthropometric test device as a rider surrogate in recommended frequent accident scenarios. It shows a meaningful graphical description of the functional and causal principles of a powered two-wheeler rider restraint and a quantified performance evaluation of the concept. The combination of several passive safety systems has shown to be promising in positively influencing accident behavior and mitigating consequences.

INTRODUCTION

From economic and environmental perspectives, powered two-wheelers (PTWs) are an efficient mode of transportation. Because of high traffic volume, many cities have already reached their capacity limits at peak traffic times. A shift to smaller vehicles can provide much-needed relief. A case study of the Leuven-Brussels motorway journey [1] examines the impact of a modal shift in which 10 % of cars are replaced by PTWs. The traffic flow model simulation states that traffic loss hours decrease by 63 % from 1925 hours in a reference scenario to only 706 hours lost. Also, regardless of the type of drive, PTWs consume fewer resources in production and have a lower energy consumption and use less space than cars. Considering the average occupancy (e-scooter: 1.1 persons vs., e.g., a mid class passenger car: 1.34 persons) in an evaluation of different transportation modes for urban areas [2], e-scooters perform among the best regarding the energy demand in use. They are more efficient than other electric vehicles, buses, and the tram; only bicycles and e-bicycles are more efficient than electric PTWs. However, their poor passive safety is their decisive disadvantage at considerable social costs.

A comparison of the fatality risks of various modes of transportation (cars & light trucks, pedestrians & bicycles, motorcycles, large trucks, buses, maritime, aviation, railroads, pipeline) in the US for 2000-2009 [3] shows that riding a motorcycle is by far the most dangerous. Riding a motorcycle accounts for 212 fatalities per billion passenger miles; driving or being a passenger in a car or light truck only accounts for 7.28 fatalities per billion miles traveled. This is because motorcycles do not provide any-where near the same level of crashworthiness and rider protection as automobiles do for their occupants. A car is much more stable and easier to see. In the event of an accident, a car has the advantage of significantly more weight and volume. It fully encloses the occupants in a safety cell and provides passive safety features such as seat belts and airbags. In contrast, the safety equipment of most mo-torcyclists is currently limited to personal-worn protective equipment. The current safety strategy of conventional motorcycles does not go beyond the intention or, even more so, hope that the vehicle user will be able to get as little as possible entangled with the motorcycle and will be thrown off quickly instead.

There are two main approaches to passive safety in motorcycle literature [4]. In the first principle, the rider is restraint to the motorcycle. In a collision, kinetic energy from the motorcycle is converted into

deformation work. The rider restraints, e.g., belts or airbags, aim to prevent direct contact between the motorcyclist and an accident opponent up to a certain collision speed. Production motorcycles that aim for that principle are rare. The Honda Goldwing is a large tourer equipped with a frontal airbag [5, 6, 7]. The BMW C1 is a city scooter with a rollover structure and belt restraint for an upright seated rider [8, 9].

In the second principle, the rider must be separated from the motorcycle as soon as possible, and a direct impact must be avoided. Here, the rider mustn't get tangled up in parts of the motorcycle. In the best case, a flyover of the motorcyclist over the accident opponent is initiated. The principle aims that the injuries of a flyover should be less than those of a direct impact. Most motorcycles aim for this safety principle. Several types of rider kinematics have been identified for impacts with these conventional motorcycles, see e.g. [10, 11], for experiments including a pillion passenger [12]. The observed patterns can be divided, as shown by [13], into one of the types illustrated in Figure 1: (a) a direct impact, (b) a rollover, or (c) a flyover of the rider. Before impact, this depends on the points of contact at the collision opponents; during the collision phase, it depends on the vehicle geometries and the structural properties. In a direct impact, the rider is decelerated the most; hence the resulting immediate energy input into the rider is the highest. For a rollover, the energy input is lower, and for a flyover even lower. In the case of a rollover or flyover, the rider detaches from the motorcycle, which remains the decisive safety principle of today's motorized two-wheelers. This assumes that injuries in the subsequent so-called secondary accident phase will be less than in a direct car impact. The chances of being injured less severely or not at all are promising only if the rider is wearing effective personal protective equipment and slides freely to the final position after impact without coming into contact with other vehicles or fixed objects.

(a) direct impact
   high energy transfer

(b) rollover with
   medium energy transfer

(c) flyover with
   low energy transfer
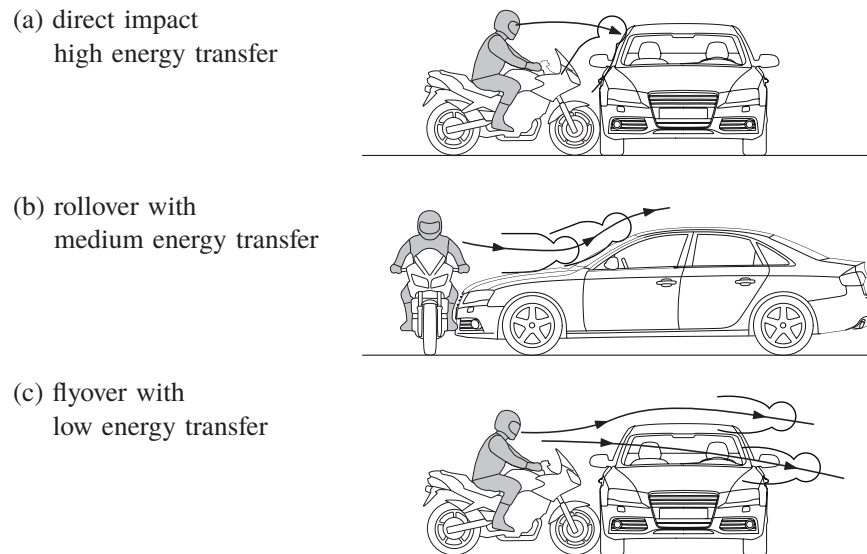
Figure 1: **Types of collisions of a conventional motorcycle and rider against an opposing vehicle.**

The safe motorcycle studied here aims at the first principle. It consists of a newly designed motorcycle frame and body, seat belts, multiple airbags, foam leg impact protectors, and a side impact structure; see full FE model in Figure 2. The concept, initially described in [14], envisages that in the event of an impact, the two belts around the thighs restrain the rider to the motorcycle. The surrounding airbags then decelerate the upper body rotation in a controlled manner and protect the rider from hard contact with an opposing vehicle, the road, or road-side structures. The foam impact protectors absorb the impact of the legs on the motorcycle cockpit and the side impact structure protects the lower extremities laterally. The concept's idea is to preserve the open design and superior all-around visibility and maneuverability of a two-wheeler without any rollover structure. The goal is to supersede a motorcycle rider's safety clothing and helmet entirely in the future and, therefore, significantly increase the suitability of motorcycles as commuter vehicles and/or shared mobility solutions.
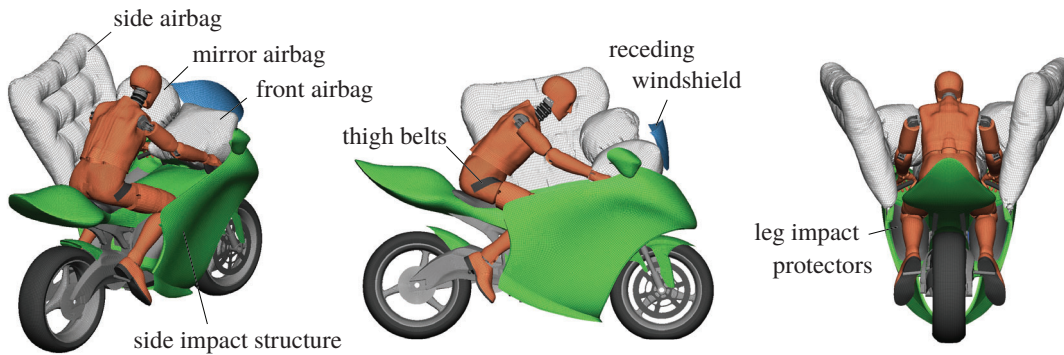
Figure 2: **FE motorcycle with restraint safety concept and Hybrid III 50th ATD as rider surrogate.**

This paper presents the tools and methods to design an optimal and robust novel safety concept for motorcycles. The safety concept combines well-established safety strategies of occupant protection onto a motorcycle to minimize the intrinsic unpredictability of PTW crashes. The novelty of this work is the investigation of the PTW safety concept in a full FE approach, as part of a modeling and simulation strategy with different levels of model fidelity. It aims for a meaningful description of the operating principles and their influence on the accident behavior in comparison to a conventional PTW based on the virtual models.

MODELING

The work presented here is part of a a multi-stage, multi-model approach with varying degrees of model fidelity, outlined in Figure 3.
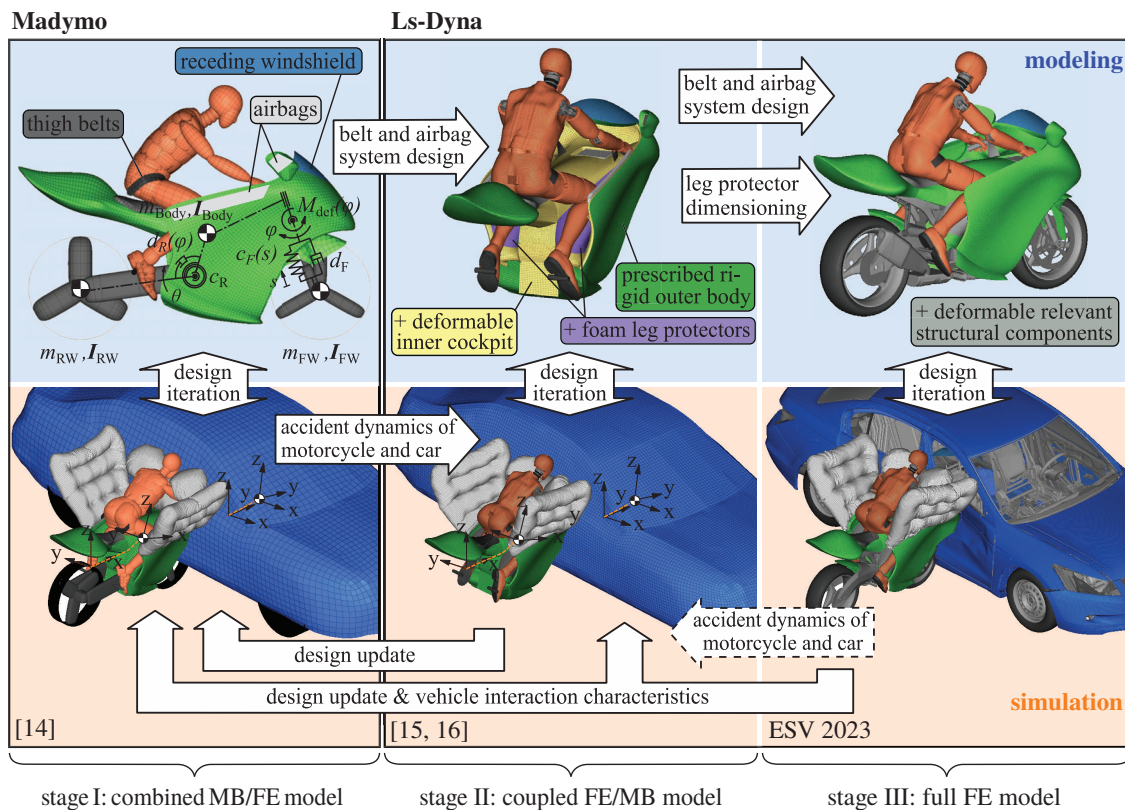
Figure 3: **Modeling and simulation strategy.**

81 parts
323,000 nodes
60 beam elements
243,000 shell elements
135,000 solid elements

12 joint connections
25 extra node set connections
67 nodal rigid body connections
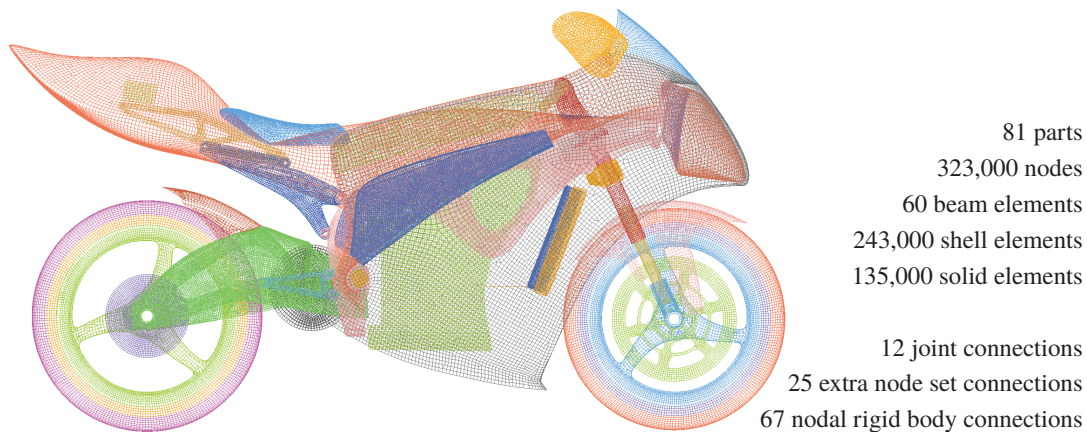
Figure 4: **Discretization of the FE motorcycle model, shown as wireframe elements.**

The modeling and simulation strategy consists of three stages (I) to (III): (I) In the MADYMO software environment[1], the motorcycle, airbags, belts, rider surrogate, and accident opponent are modeled in a combined multibody and FE approach, introduced in [14]. Vehicle deformation and contact characteristics, as well as an effectiveness assessment of the passive safety systems are based on fitted simulation models of full-scale crash tests of conventional motorcycles. (II) An equivalent FE model of the rider interaction surfaces, coupled to accident trajectories from MB simulations, includes the leg impact protectors in the LS-DYNA software environment[2], introduced in [15, 16] also used in [17]. (III) Simulations of a full FE approach in LS-DYNA that also includes the motorcycle's structurally relevant components as deformable parts.

In this work, the proposed motorcycle is investigated in the shown full FE model approach (stage III), shown in Figure 4.

The model aims to represent the interaction with the crash opponent, structural loading and deformation, and energy absorption of the motorcycle structure. As a result, its focus is on representing the crash-relevant structural components, which are the front wheel, front tire, and front suspension assembly. Components such as the drivetrain are modeled as rigid parts because they are assumed not to deform because they are very stiff or outside of the crash deformation. As a unique feature of the proposed motorcycle structure a foam crash box in the cockpit nose aims to control the energy transfer. This prevents a rollover in a frontal impact. The elevated side impact structures protect the lower extremities laterally. In total, the model consists of 81 parts from 378,000 elements with 323,000 nodes. The suspension is modeled with eight kinematic joints; front wheel rotation (2), telescopic front fork suspension (2), rear-wheel rotation (2), front fork steering, and rear swing arm rotation. The other kinematic joints are for the lids of the compartments behind which the airbags are located.

Recent other detailed FE models of PTWs for crash investigations are [7] (a large tourer), [18] (a three-wheeled scooter), [19] (a sport bike), and [20] (a sport tourer).

---

[1]SIEMENS Simcenter Madymo (version 2021.1 SMP): `https://www.plm.automation.siemens.com/global/en/products/simcenter/madymo.html`

[2]Ansys LS-DYNA (version R9.3.1 MPP): `https://www.ansys.com/products/structures/ansys-ls-dyna`

Impact configurations

As a set of representative impact scenarios, accident configurations from ISO1323 [21] are used. The standard isolates seven representative impact configurations ① to ⑦, shown in Figure 5. The set includes collisions between a motorcycle and a passenger car, with the motorcycle and car, either stationary or moving forward up to a speed of ≈48 km/h (13.4 m/s). The contact points on the motorcycle and car are at the front and side, respectively. There are no rear contacts included (either at the car or at motorcycle). The standard defines the opposing vehicle as a four-door saloon with a mass of 1,238-1,450 kg and an overall height of 137-147 cm. The set does not include scenarios with roadside barriers. As the accident opponent, the FE model of a 2001 Ford Taurus [22] is used. The model, developed and validated by the National Crash Analysis Center (NCAC), is publicly available in the NHTSA vehicle database [23]. With an overall height of 147 cm and a mass of 1477 kg the four-door passenger sedan complies with [24] specifications for the opposing vehicle height but slightly exceeds vehicle mass.
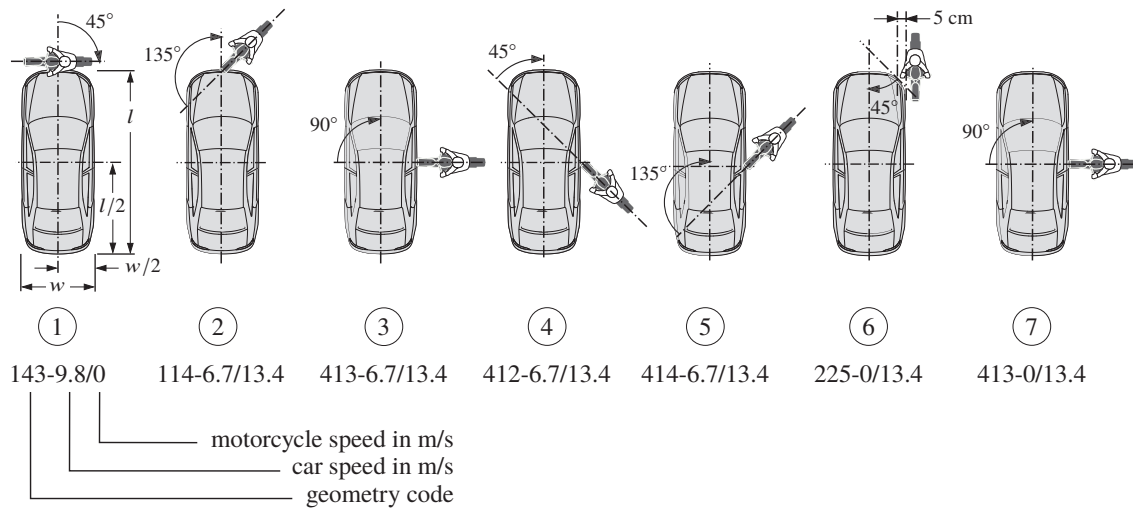
Figure 5: **Representative set of impact configurations according to [21].**

Injury criteria

For passenger vehicle occupant protection, there are national and international regulations, such as the ECE regulations by the United Nations Economic Commission for Europe (UNECE) or Federal Motor Vehicle Safety Standards (FMVSS) for the US that specifies injury criteria and respective maximal values for specific load cases. Also, consumer ratings such as the New Car Assessment Programs for the United States (US NCAP) and the European Union (Euro NCAP) provide constantly updated biomechanical criteria from the latest scientific findings of occupant protection. To the best of the authors' knowledge, for the passive safety of motorcyclists, such governmental regulations or consumer ratings currently do not exist. The most recent version of ISO 13232 recommends only a very limited set of criteria. The work presented here aims to assess many potential injury mechanisms for the whole body. The selection of injury criteria considered are summarized in Table 1. It is based on a comprehensive set of injury criteria and corresponding biomechanical limits for motorcyclists from an extensive literature review by [25]. This selection is extended to include the GAMBIT, which is recommended in the international standard [26], as well as the BrIC and the Nij criterium. For femur criteria, stricter thresholds from ECE-R 94 [27] are used.

body region	injury criterion		limit (Hyb III 50th)	ref.
head	resultant acceleration	$a_{t_{int}} = \max\limits_{t_1}\left(\min\limits_{t_1 \le t \le t_1+t_{int}} a_{res}(t)\right)$	80 g for t_{int} = 3 ms	[27]
	head injury criterion	$\text{HIC}(t_2-t_1) =$ $\max\limits_{t_1,t_2}\left\{(t_2-t_1)\left[\dfrac{1}{t_2-t_1}\displaystyle\int_{t_1}^{t_2} a_{res}(t)dt\right]^{2.5}\right\}$ with $a_{res}(t)$ in g and t in s	1000 for $t_2-t_1 \le 36$ ms	[28, 29]
	generalized acceleration model for brain injury threshold	$\text{GAMBIT} = \left[\left(\dfrac{a_{res}(t)}{a_C}\right)^{2.5}+\left(\dfrac{\ddot{\varphi}_{res}(t)}{\ddot{\varphi}_C}\right)^{2.5}\right]^{\frac{1}{2.5}}$ with a_C = 250 g and $\ddot{\varphi}_C$ = 25 krad/s^2	1	[30]
	brain injury criterion	$\text{BrIC(CSDM)} =$ $\sqrt{\left(\dfrac{\max|\omega_x(t)|}{\omega_{xC}}\right)^2+\left(\dfrac{\max|\omega_y(t)|}{\omega_{yC}}\right)^2+\left(\dfrac{\max|\omega_z(t)|}{\omega_{zC}}\right)^2}$ with ω_{xC} = 66.2, ω_{yC} = 59.1, ω_{zC} = 44.25 rad/s	1	[31]
neck	tensile force	$F_{z,tens,t_{int}} = \max\limits_{t_1}\left(\min\limits_{t_1 \le t \le t_1+t_{int}} F_z(t)\right)$	3.3 kN for t_{int} = 1 ms; 1.1 kN for t_{int} = 45 ms	[32, 29]
	compression force	$F_{z,compr,t_{int}} = \min\limits_{t_1}\left(\min\limits_{t_1 \le t \le t_1+t_{int}} F_z(t)\right)$	4 kN for t_{int} = 1 ms; 1.1 kN for t_{int} = 45 ms	
	shear force	$F_{xy,t_{int}} = \max\limits_{t_1}\left(\min\limits_{t_1 \le t \le t_1+t_{int}} \sqrt{F_x(t)^2+F_y(t)^2}\right)$	3.1 kN for t_{int} = 1 ms; 1.1 kN for t_{int} = 45 ms	
	forward moment	$M_{y,fwd,max} = \min M_y(t)$	190 Nm	
	rearward moment	$M_{y,rwd,max} = \max M_y(t)$	57 Nm	
	neck injury criterion	$\text{Nij}_{max} = \max\left(\left|\dfrac{F_z(t)}{F_{int}}\right|+\left|\dfrac{M_y(t)}{M_{int}}\right|\right)$ with $F_{int,C/T}$ = 6160/6806 N, $M_{int,F/E}$ = 310/135 Nm	1	[28, 33, 29]
thorax	resultant acceleration	$a_{t_{int}} = \max\limits_{t_1}\left(\min\limits_{t_1 \le t \le t_1+t_{int}} a_{res}(t)\right)$	60 g for t_{int} = 3 ms	[29]
	thorax compression	$\text{ThCC} = \max s(t)$	50 mm	[27]
	viscous criterion	$\text{VC}_{max} = \max\left(V(t) \cdot C(t)\right)$	1 m/s	[34, 27]
pelvis	resultant acceleration	$a_{t_{int}} = \max\limits_{t_1}\left(\min\limits_{t_1 \le t \le t_1+t_{int}} a_{res}(t)\right)$	60 g for t_{int} = 3 ms	[25]
femur	axial force	$|F_z|_{max} = \max|F_z(t)|$	9.07 kN	[27]
tibia	tibia index	$\text{TI}_{max} = \max\left(\left|\dfrac{\sqrt{M_x(t)^2+M_y(t)^2}}{(M_C)_{res}}\right|+\left|\dfrac{F_z(t)}{(F_C)_z}\right|\right)$ with $(M_C)_{res}$ = 225 Nm and $(F_C)_z$ = 35.9 kN	1.3	[35, 27]

Table 1: **Selected injury criteria with biomechanical limits for the Hybrid III 50th ATD.**

ACCIDENT SIMULATION

Conventional Motorcycle

For comparison, a full laboratory crash test of a conventional motorcycle against a passenger car is used. It is an impact according to ISO 12323 (7) with a helmeted Hybrid III 50th anthropometric test device (ATD) as part of investigations of [25], to which data we have access to. The laboratory tests are documented with a test protocol and high-speed video footage, a 15-channel sensor data set of the ATD, and accelerometers at multiple points on the motorcycle. The test is then simulated with the MBS approach, see [14], shown in Figure 6.
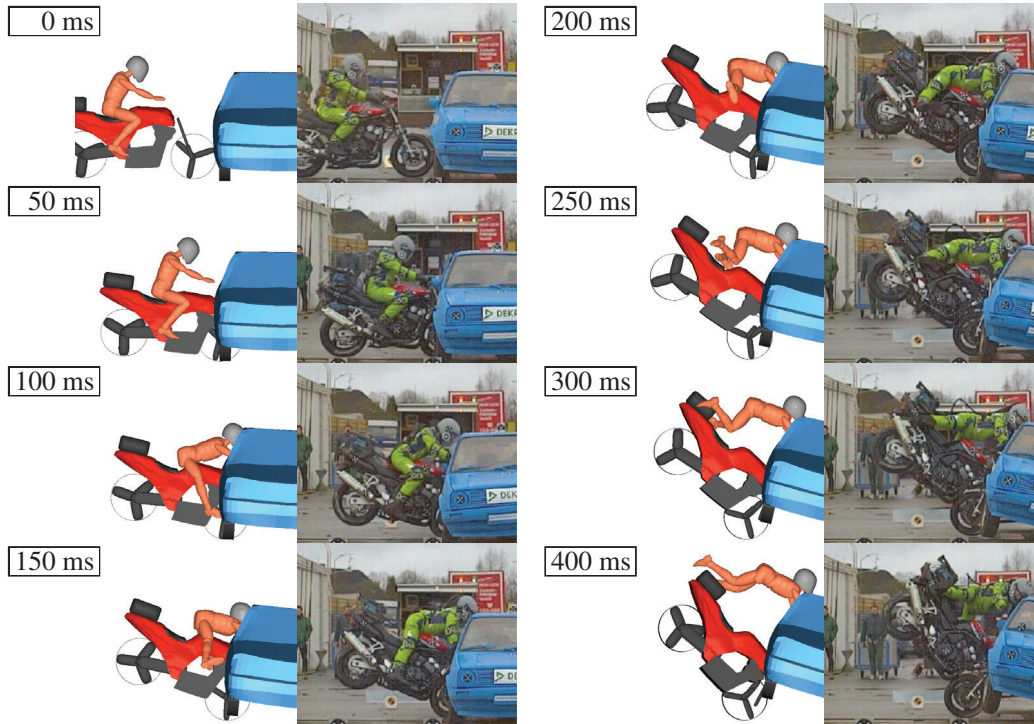
Figure 6: **MB simulation (stage I) of full-scale crash test SH01.01 [25] of a conventional motorcycle Yamaha FZS 600 Fazer and a helmeted Hybrid III 50th against a VW Golf II in scenario (7).**

Figure 7 illustrates the resulting deceleration from the MB simulation of the motorcycle, the opposing vehicle, and the main body parts of the rider for the conventional motorcycle impact by plotting the velocities. The velocities are filtered with a CFC (channel frequency class) filter, see [36]. The impact causes the motorcycle to decelerate relatively uniformly from the initial speed, initiating a forward rotation of the PTW. After the rider is not decelerated until about 40 ms, he is abruptly decelerated by the impact of the pelvis on the tank and the helmeted head on the car. According to the classification in Figure 1, the collision corresponds to a direct impact with a high energy transfer.

A classification into accident phases in Figure 8 reduces the accident occurrence to a chronology of significant events. It illustrates long dead times of the rider's head, pelvis, and legs. Tank impact and helmeted car impact are concentrated short-time events. These lead, i.a., to a high deceleration of the head (a_{3ms}), a very high neck axial compression ($F_{z,compr,1ms}$) and shear loading (F_{xy45ms}), and a high rearward (extension) moment ($M_{y,rwd,max}$), see the evaluation of the injuria criteria in Figure 15. The greyed fields ("N/A") are injury criteria that could not be determined with the ATD sensor channels of SH 01.01.
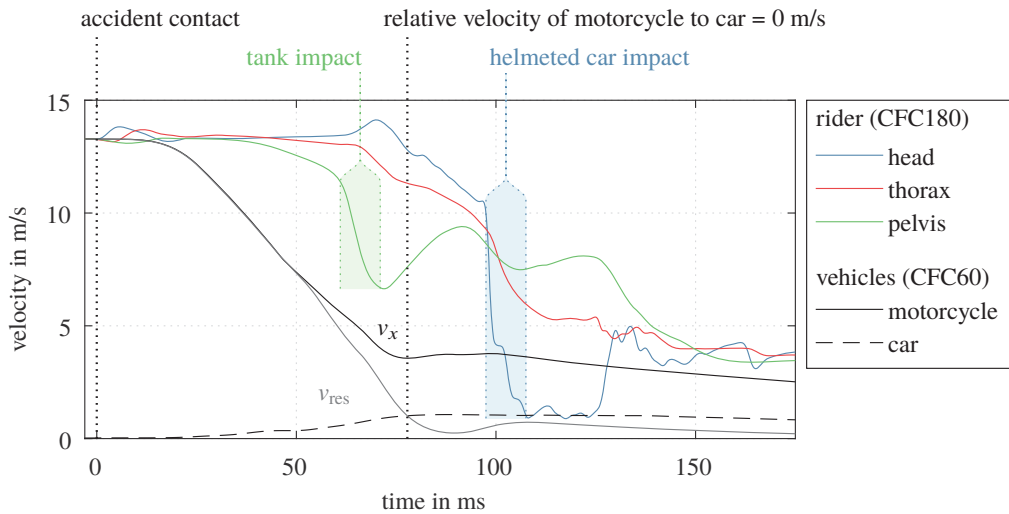
Figure 7: **Velocities of conventional motorcycle and motorcyclist's main body parts relative to car's velocity in a frontal collision according to scenario ⑦ (MB simulation shown in Figure 6).**
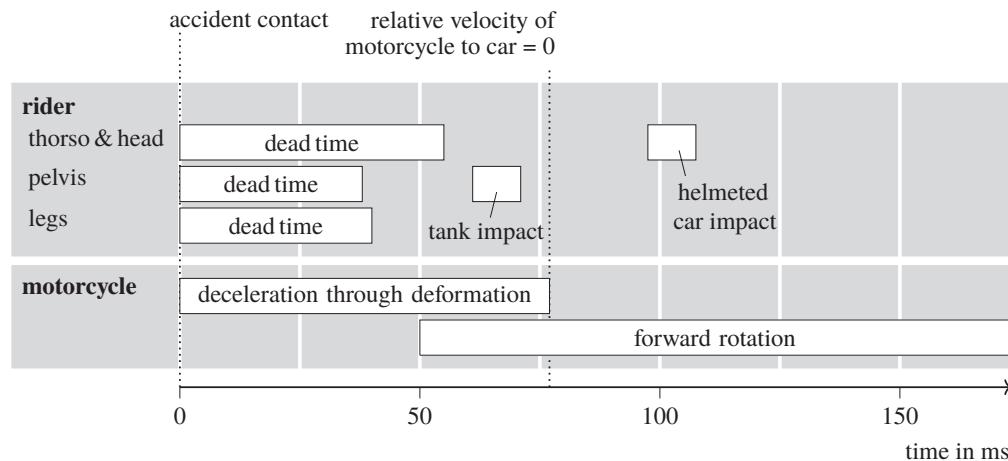
Figure 8: **Schematic chronology of conventional motorcycle and rider behaviour in a frontal collision according to configuration ⑦ (MB simulation of Figure 6).**

Motorcycle with Restraint System

To analyze the safe motorcycle with rider restraint, all seven ISO 13232 scenarios are simulated using the full FE model; see overview in Figure 9. It shows the accident kinematics up to 500 ms each, referred to as the primary impact phase. For the impacts shown, the effect of the safety system can be summarized as follows: The belts restrain the rider to the motorcycle, with the belt load-limiting devices limiting the pelvis accelerations. The belt restraint establishes a pivot point at the pelvis to guide the upper body in forward and sideward rotations and to keep the riders' bodies within the range of the airbags and within the leg protectors and side-impact protection structure. The surrounding airbags decelerate the upper body motion and prevent impact against hard structures, such as the uncushioned motorcycle cockpit surfaces and the accident opponent. The motorcycle cockpit and the accident opponent are reaction surfaces for the airbags.

solver run times:

59.9 h/16 CPUs/MPP/single precision/Ls-DYNA R9.3.1
with AMD Ryzen 9 5950X 16-Core CPU@3.4GHz
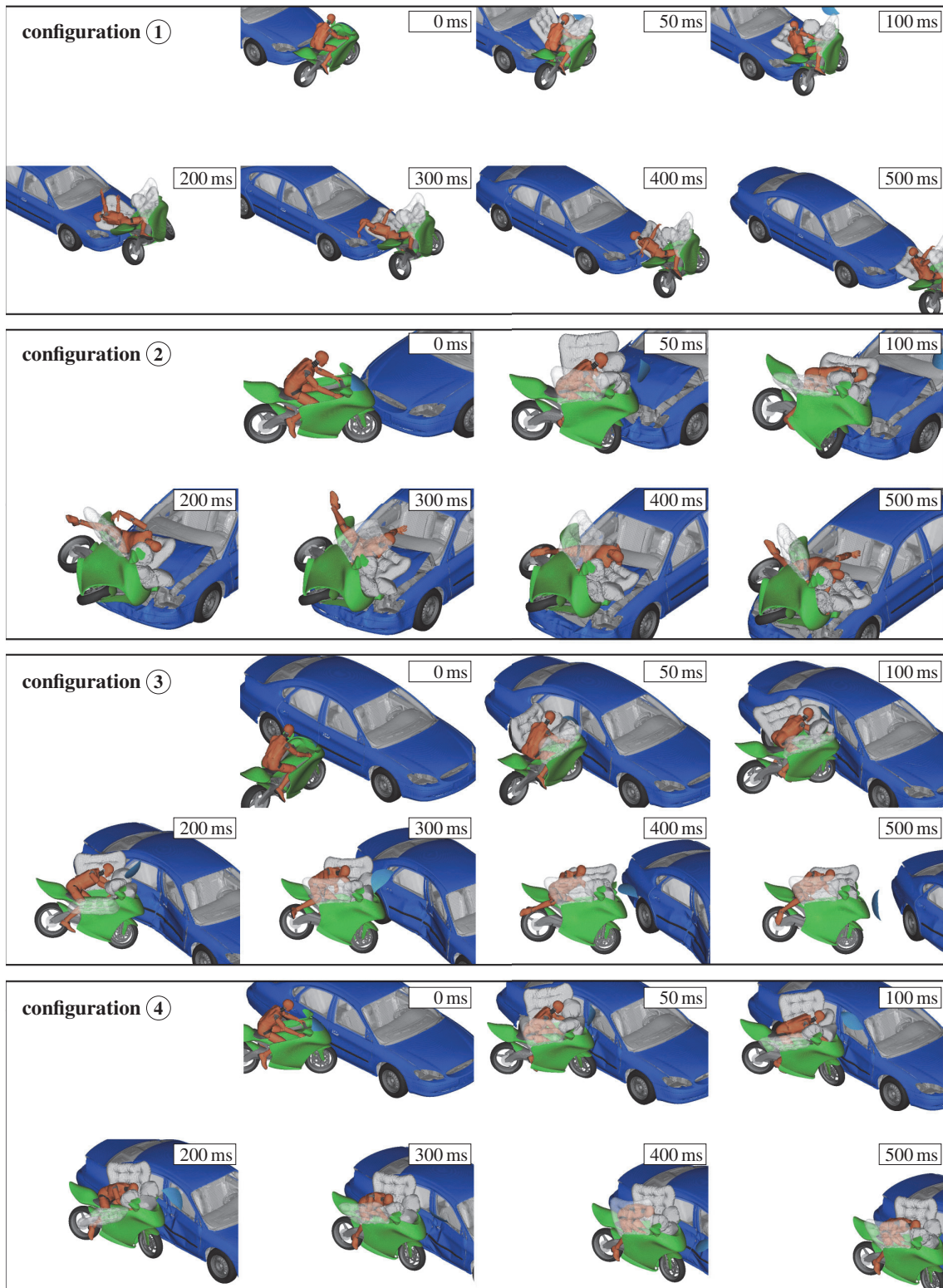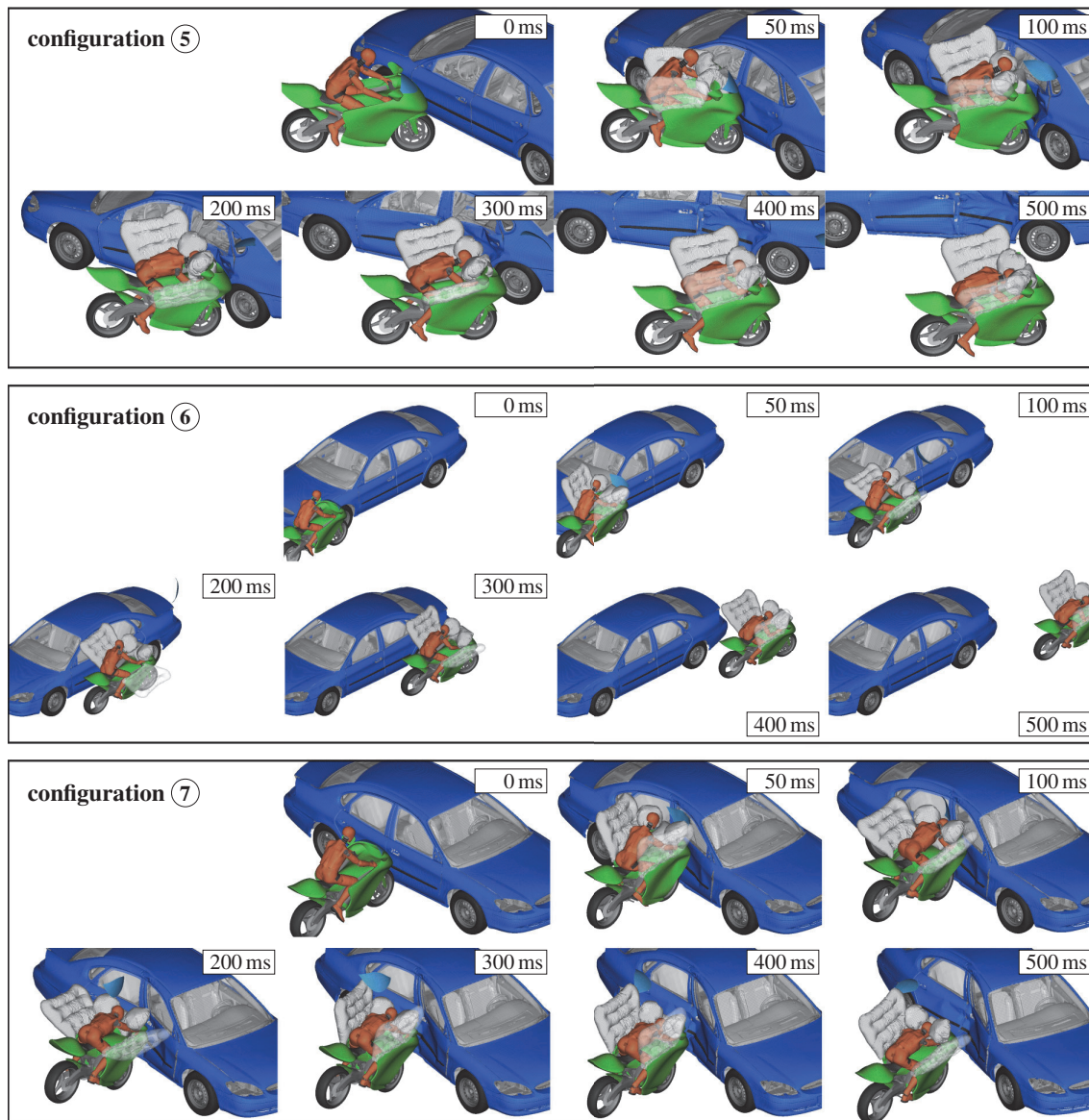
Figure 9: **Primary impact response of motorcycle with restraint system in full FE simulations of ISO 13232 configurations with a non-helmeted Hyb III 50th up to 500 ms.**

Scenarios ①–③, ⑤, and ⑦ are impacts where the motorcycle is particularly violently de- or accelerated. In scenario ④, the motorcycle bounces off at a shallow angle without losing much speed. In near miss scenario ⑥, the motorcycle grazes the car. The latter two scenarios are particulary interesting for analyzing the secondary accident behavior because much residual energy remains in the motorcycle and the passenger. This also applies to scenarios ① and ② because the car accelerates the motorcycle through the collision.

The heat map in Figure 10 illustrates an evaluation of the biomechanical injury criteria. The selected criteria from Table 1 are normalized to their respective biomechanical limit for the Hybrid III 50th ATD and are color-coded to indicate the severity of the body loads. Overall, only the tibia index (TI) from tibia forces and moments, the brain injury criterion (BrIC) based on head angular velocity, and the thorax acceleration a_{3ms} criterion exceed their biomechanical limits in some scenarios. Simulations of the safety

config	head				neck									thorax			pelvis	femur	tibia
	$HIC(36)$	a_{3ms}	$GAMBIT$	$BrIC(CSDM)$	$F_{z,tens,1ms}$	$F_{z,tens,45ms}$	$F_{z,compr,1ms}$	$F_{z,compr,45ms}$	$F_{xy,1ms}$	$F_{xy,45ms}$	$M_{y,fwd,max}$	$M_{y,rwd,max}$	$N_{ij,max}$	a_{3ms}	$ThCC$	VC_{max}	a_{3ms}	$\lvert F_z\rvert_{max}$	TI
①	0.38	0.59	0.21	1.06	0.52	0.97	0.07	0	0.15	0.24	0	0	0.32	0.36	0.07	0.01	0.49	0.24	0.69
②	0.21	0.49	0.23	1.08	0.37	0.35	0.04	0	0.15	0.17	0.02	0.4	0.24	0.74	0.39	0.14	0.93	0.23	1.02
③	0.26	0.73	0.43	1.14	0.35	0.06	0.08	0.02	0.33	0.12	0.03	0.12	0.24	1.24	0.5	0.35	0.7	0.25	0.79
④	0.13	0.39	0.19	0.66	0.21	0.24	0.07	0.02	0.12	0.13	0.04	0.19	0.13	0.44	0.19	0.04	0.36	0.16	0.68
⑤	0.12	0.52	0.26	0.64	0.47	0.23	0.07	0.04	0.23	0.08	0.01	0.06	0.31	0.74	0.29	0.11	0.43	0.19	0.47
⑥	0	0.13	0.08	0.21	0.12	0.01	0.04	0.01	0.08	0.14	0	0.11	0.08	0.12	0.06	0.01	0.29	0.13	0.53
⑦	0.33	0.69	0.28	0.87	0.54	0.54	0.02	0	0.3	0.09	0	0	0.37	0.72	0.34	0.09	0.62	0.23	0.49

Figure 10: **Injury criteria relative to biomechanical limits for primary impact up to 500 ms shown in Figure 9.**

concept with HBMs [17] also show high BrIC values, exceeding the recommended threshold. The high thorax a_{3ms} values in ③ are due to the arms getting caught in the cockpit fairing and being mechanically locked which transmits a shock trough the rigid arm joints into the torso. Apart from these, the highest values are the head and pelvis a_{3ms} acceleration and neck axial tension. These are concept-related mainly dependent on the belt restraint's load limit, which is a tradeoff between the feasible frontal displacement of the rider and tolerable body loads. A lower belt load limit reduces body loads from the rider restraint but also increases the risk of the head hitting the accident opponent. The leg protectors and side impact protection keep femur axial loading low.
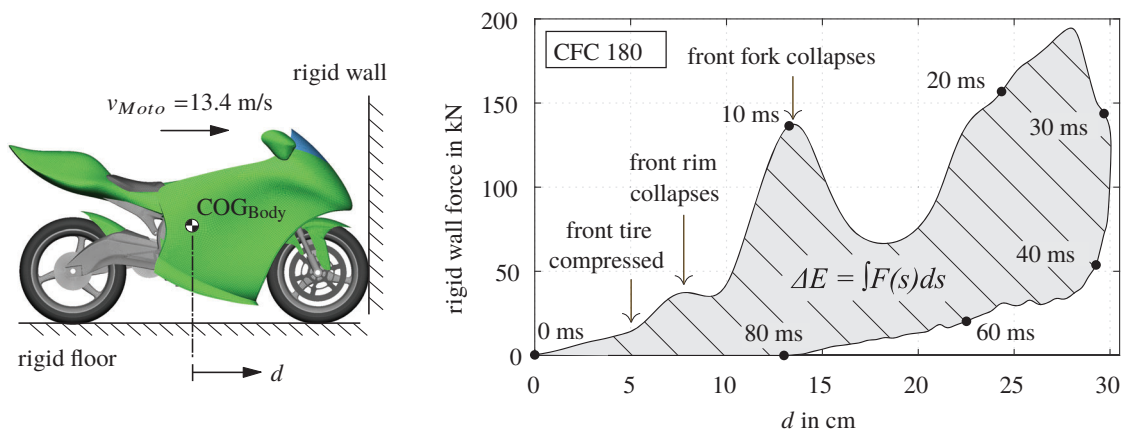
Figure 11: **Frontal deformation characteristics of motorcycle.**
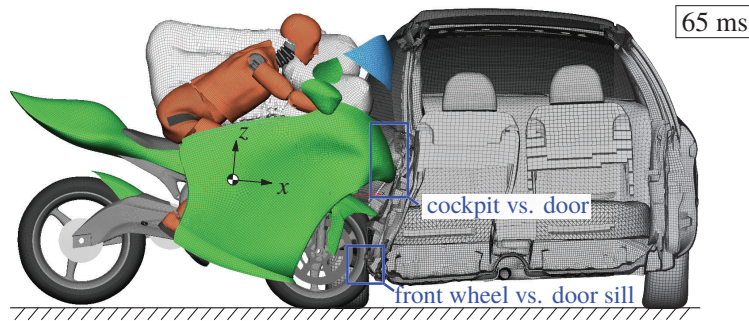
Figure 12: **Motorcycle to car structural interaction and intrusion behaviour in full FE simulation (right airbags are not displayed).**

Unlike the conventional motorcycle collision, the proposed motorcycle does not roll over about its transverse axis during a frontal impact. The voluminous cockpit and the resulting high contact point prevent pitching. Figure 11 illustrates the designed frontal deformation characteristics in impact with a rigid wall. It identifies subsequent phases of deformation: (i) compression of the front tire, (ii) collapse of the front rim, and (iii) collapse of the front fork. The area enclosed corresponds to the dissipated energy. Figure 12 reveals the structural interaction and intrusion of the motorcycle against the opposing vehicle. The motorcycle's front wheel collides with the sill of the car, and the motorcycle cockpit deforms the car door inward.

Figure 13 shows equivalent to Figure 7 the deceleration based on the velocities of the motorcycle and the main body parts of the rider in a frontal collision (scenario ⑦). It shows quite descriptive the benefits of the safety system concept. The belts interact early leading to a relatively continuous deceleration by restraining the pelvis. After about 80 ms, the front airbag decelerates the upper body rotation. Overall the main body parts are decelerated continuously over an increased time period, compared to the short-term impacts of the conventional motorcycle. Plotting a schematic chronology results in Figure 14. Extended by a safety systems layer, it shows the timing and operating phases of the seat belt and airbag systems as well as the leg impact protectors.
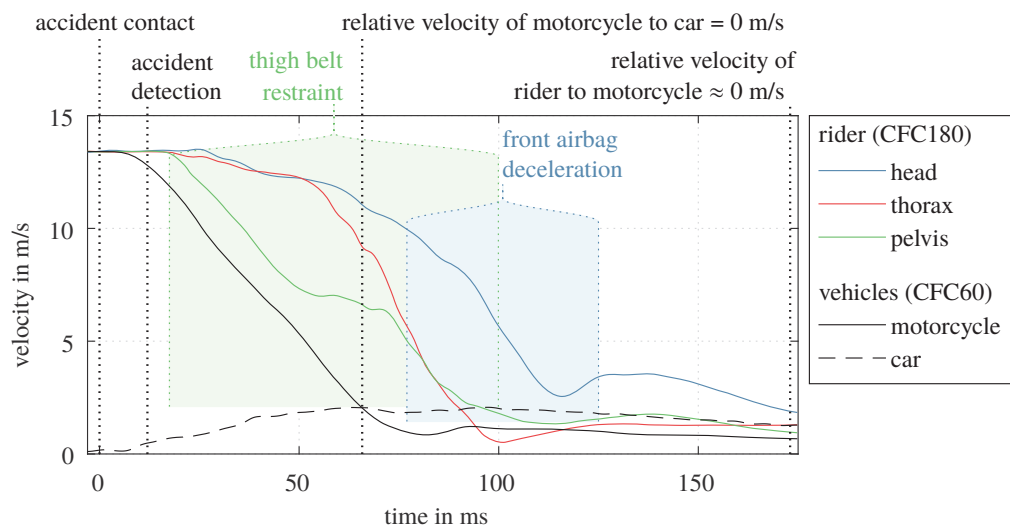
Figure 13: **Velocities of motorcycle with restraint safety systems and motorcyclist's main body parts in a frontal collision according to configuration ⑦ (Full FE simulation shown in Figure 9).**
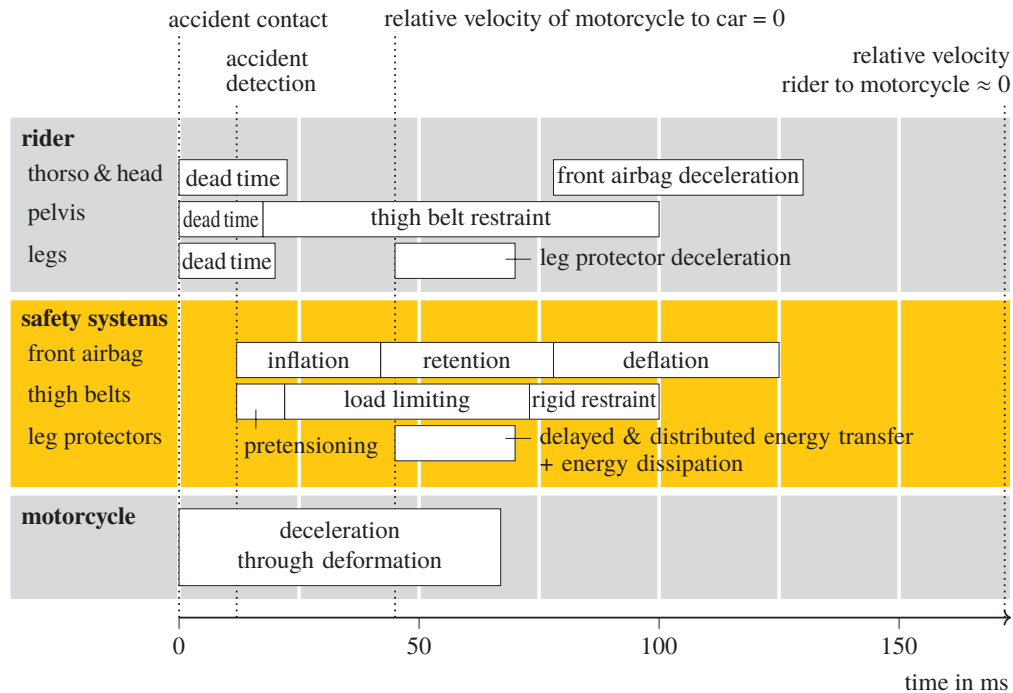
Figure 14: **Schematic chronology of motorcycle with restraint safety systems and rider behaviour in a frontal collision according to configuration ⑦ (Full FE simulation of Figure 9).**

Figure 15 is a comparison of the resulting injury criteria of the conventional motorcycle vs. the motorcycle with the rider restraint. The crash test criteria of the conventional motorcycle are based on the experimental sensor data of the laboratory test; for the motorcycle with rider restraint, they are from the full FE simulation. Change for the better or the worse is highlighted by green and red arrows. Overall, the number of critical values is reduced. Whereby with the current parameters fot the design varibles lead safety-concept related to higher loads for neck axial tension and pelvis and thorax acceleration.
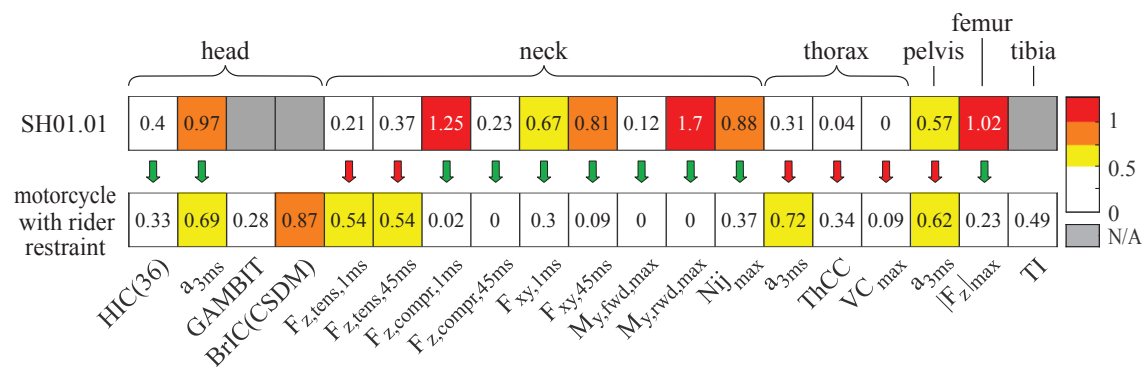
Figure 15: **Injury criteria relative to respective biomechanical limit for conventional motorcycle (top; experimental data of SH01.01) and motorcycle with rider restraint (bottom; full FE simulation).**

DISCUSSION

The work investigates the primary impact behavior of a recommended set of impact scenarios involving PTWs. The motorcycle's safety concept enables a guided rider trajectory and controlled energy dissipation through rider restraint with continuous deceleration during a motorcycle-to-car impact. With few exceptions, recommended injury criteria and respective biomechanical limits indicate tolerable rider loading. Some values for BrIC, TI, and thorax a_{3ms} are not within the recommended biomechanical limits. A comparison with a conventional motorcycle shows the advantages of controlled and continuous load application onto the body of the rider. The consequences of an accident depend less on the randomness and unpredictability of a conventional accident with multiple possible trajectories than on the design variables of the safety system.

The secondary impact behavior, impacts against other accident opponents, e.g., roadside barriers, and solo accident behavior, have not yet been considered. These types have prevalently long accident histories. The use of full FE models with long computation times is challenging since they are computationally costly, even when complex structural interactions with large deformations occur less in such secondary accident phases and solo accidents. Here, future use of hybrid variants that combine the structural impact response of a full FE model and the large rigid body motions of an MB model seems particularly desirable.

CONCLUSIONS

This work contains

- a virtual prediction of the accident behavior of a motorcycle with passive safety systems,

- a meaningful graphical description of the functional and causal principles of a PTW rider restraint,

- and a quantified performance evaluation of the concept.

Comparable to passive safety for car occupants, a combination of several passive safety systems has shown to be promising in positively influencing the accident behavior and consequences of PTW riders.

REFERENCES

[1] Yperman, I. (2011). Commuting by Motorcycle: Impact Analysis, Report No. 10.69. Transport & Mobility Leuven, Leuven, Belgium.

[2] Brunner, H., Hirz, M., Hirschberg, W., and Fallast, K. (2018). Evaluation of various means of transport for urban areas. Energy, Sustainability and Society, 8:117–121.

[3] Savage, I. (2013). Comparing the fatality risks in united states transportation across modes and over time. Research in Transportation Economics, 43(1):9–22. The Economics of Transportation Safety.

[4] Langwieder, K., Sporner, A., and Polauke, J. (1987). Stand der passiven Sicherheit für den Motorradfahrer und mögliche Entwicklungstendenzen (in German). In Gesellschaft Fahrzeugtechnik, Aktive und passive Sicherheit von Krafträdern: Tagung, Berlin, 8. u. 9. Oktober 1987, VDI-Berichte 657, pages 29–52, Düsseldorf. VDI-Verlag.

[5] Kobayashi, Y. and Makabe, T. (2013). Crash detection method for motorcycle airbag system with sensors on the front fork. In Proceedings of the 23rd International Technical Conference on the Enhanced Safety of Vehicles (ESV), number 13-0344, Seoul, Korea.

[6] Kuroe, T., Namiki, H., and Iijima, S. (2005). Exploratory study of an airbag concept for a large touring motorcycle: Further research second report. In Proceedings of the 19th International Technical Conference on the Enhanced Safety of Vehicles (ESV), number 05-0316, Washington, DC, USA.

[7] Namiki, H., Nakamura, T., and Iijima, S. (2005). A computer simulation for motorcycle rider injury evaluation in collision. In Proceedings of the 19th International Technical Conference on the Enhanced Safety of Vehicles (ESV), number 05-0309, Washington, DC, USA.

[8] Kalliske, I. and Albus, C. (1998). Safety potential of future two-wheel concepts – a challenge. In Proceedings of the 16th International Technical Conference on the Enhanced Safety of Vehicles (ESV), number 98-S10-O-15, pages 2279–92, Winsor Ontario, Canada.

[9] Osendorfer, H. and Rauscher, S. (2001). The development of a new class of two-wheeler vehicles. In Proceedings of the 17th International Technical Conference on the Enhanced Safety of Vehicles (ESV), number 01-S8-O-475, Amsterdam, Netherlands.

[10] Berg, F. A., Bürkle, H., and Schmidts, F. (1998). Analysis of the passive safety of motorcycles using accident investigations and crash tests. In Proceedings of the 16th International Technical Conference on the Enhanced Safety of Vehicles (ESV), number 98-S10-O-11, pages 2221–2236, Winsor Ontario, Canada.

[11] Lindenmann, M., Grandel, J., and Berg, F. (1986). Collision dynamics in experimental simulations of 90° motorcycle collisions against the side of moving passenger cars. In Proceedings of the IRCOBI Conference, pages 289–302, Zurich, Switzerland.

[12] Grandel, J. and Schapter, D. (1987). Investigation into motorcycle, driver and passenger safety in motorcycle accidents with two motorcycle riders. In Proceedings of the 11th International Technical Conference on the Experimental Safety of Vehicles (ESV), pages 888–900, Washington, DC, USA.

[13] Appel, H., Otte, D., and Wüstemann, J. (1986). Epidemiologie von Unfällen motorisierter Zweiradfahrer in der Bundesrepublik Deutschland - Sicherheitsaspekte (in German). In Koch, H., Der Motorradunfall: Beschreibung, Analyse, Prävention, Forschungshefte Zweiradsicherheit, pages 47–92, Bremerhaven. Wirtschaftsverlag NW.

[14] Maier, S., Doléac, L., Hertneck, H., Stahlschmidt, S., and Fehr, J. (2020). Evaluation of a novel passive safety concept for motorcycles with combined multi-body and finite element simulations. In Proceedings of the IRCOBI Conference, number IRC-20-38, pages 250–265, Munich, Germany.

[15] Maier, S., Doléac, L., Hertneck, H., Stahlschmidt, S., and Fehr, J. (2021). Finite element simulations of motorcyclist interaction with a novel passive safety concept for motorcycles. In Proceedings of the IRCOBI Conference, number IRC-21-17, pages 60–78, Munich, Germany.

[16] Maier, S., Helbig, M., Hertneck, H., and Fehr, J. (2021). Characterisation of an energy absorbing foam for motorcycle rider protection in LS-DYNA. In Proceedings of the 13th European LS-DYNA Users Conference, Ulm, Germany. DYNAmore GmbH.

[17] Maier, S., Kempter, F., Kronwitter, S., and Fehr, J. (2022). Positioning and simulation of human body models on a motorcycle with a novel restraint system. In Proceedings of the IRCOBI Conference, number IRC-22-22, pages 82–96, Porto, Portugal.

[18] Barbani, D., Baldanzini, N., and Pierini, M. (2014). Development and validation of an FE model for motorcycle–car crash test simulations. International Journal of Crashworthiness, 19(3):244–263.

[19] Schulz, N., Silvestri Dobrovolny, C., and Hurlebaus, S. (2016). Development of a finite element model of a motorcycle. In Proceedings of the 14th International LS-DYNA Users Conference, Detroit, MI, USA.

[20] Mongiardini, M., Walton, B., Grzebieta, R. H., McKay, M., Menictas, C., Berg, A., and Rücker, P. (2017). Development of a motorcycle FE model for simulating impacts into roadside safety barriers. In Proceedings of the First International Roadside Safety Conference, number E-C220, pages 657–673, San Francisco, CA, USA.

[21] ISO 13232-2:2005 (2005). Motorcycles – Test and Analysis Procedures for Research Evaluation of Rider Crash Protective Devices Fitted to Motorcycles – Part 2: Definition of Impact Conditions in Relation to Accident Data. International Organization for Standardization, Geneva, Switzerland.

[22] Marzougui, D., Samaha, R. R., Cui, C., and Kan, C.-D. S. (2012). Extended validation of the finite element model for the 2001 Ford Taurus passenger sedan. Technical Report NCAC 2012-W-004, The National Crash Analysis Center, The George Washington University, Ashburn, USA.

[23] NHTSA (2012). Mass Reduction for Light-Duty Vehicles for Model Years 2017–2025, Final Report, Report No. DOT HS 811 666. National Highway Transport Safety Association (NHTSA), Washington, DC, USA.

[24] ISO 13232-6:2005 (2005). Motorcycles – Test and Analysis Procedures for Research Evaluation of Rider Crash Protective Devices Fitted to Motorcycles – Part 6: Full-scale Impact-test Procedures. International Organization for Standardization, Geneva, Switzerland.

[25] Berg, F. A., Rücker, P., Bürkle, H., Mattern, R., and Kallieris, D. (2004). Prüfverfahren für die passive Sicherheit motorisierter Zweiräder: Bericht zum Forschungsprojekt FE 82.121/1997 (in German). Berichte der Bundesanstalt für Straßenwesen. F, Fahrzeugtechnik; 49. Wirtschaftsverlag NW, Verlag für neue Wissenschaft, Bremerhaven.

[26] ISO 13232-5:2005 (2005). Motorcycles – Test and Analysis Procedures for Research Evaluation of Rider Crash Protective Devices Fitted to Motorcycles – Part 5: Injury Indices and Risk/Benefit Analysis. International Organization for Standardization, Geneva, Switzerland.

[27] UNECE (2012). Regulation No 94 of the Economic Commission for Europe of the United Nations (UN/ECE) – Uniform Provisions Concerning the Approval of Vehicles with Regard to the Protection of the Occupants in the Event of a Frontal Collision. United Nations Economic Commission for Europe (UNECE), Geneva, Switzerland.

[28] Kleinberger, M., Sun, E., Eppinger, R., Kuppa, S., and Saul, R. (1998). Development of Improved Injury Criteria for the Assessment of Advanced Automotive Restraint Systems, NHTSA Docket No. 98-4405-9. National Highway Transport Safety Association (NHTSA), Washington, DC, USA.

[29] NHTSA (2011). 49 CFR, Section 571.208 – Standard No. 208; Occupant Crash Protection. National Highway Transport Safety Association (NHTSA), Washington, DC, USA.

[30] Newman, J. A. (1986). A Generalized Acceleration Model for Brain Injury Threshold (GAMBIT). In Proceedings of the IRCOBI Conference, pages 121–131, Zurich, Switzerland.

[31] Takhounts, E., Craig, M., Moorhouse, K., McFadden, J., and Hasija, V. (2013). Development of Brain Injury Criteria (BrIC). Stapp Car Crash Journal, 57:243–266.

[32] Melvin, J. W. (1985). The Engineering Design, Development, Testing, and Evaluation Of an Advanced Anthropomorphic Test Device, Phase 1: Concept Definition, Report to Contract No. DTNH22-83-C-07005. National Highway Transport Safety Association (NHTSA), Washington, DC, USA.

[33] Eppinger, R., Sun, E., Bandak, F., Haffner, M., Khaewpong, N., Maltese, M., Kuppa, S., Nguyen, T., Takhounts, E., Tannous, R., Zhang, A., and Saul, R. (1999). Development of Improved Injury Criteria for the Assessment of Advanced Automotive Restraint Systems – II, NHTSA Docket No. 99-6407-5. National Highway Transport Safety Association (NHTSA), Washington, DC, USA.

[34] Lau, I. V. and Viano, D. C. (1986). The viscous criterion – bases and applications of an injury severity index for soft tissues. SAE Transactions, 95:672–691.

[35] Mertz, H. J. (1993). Antropometric test devices. In Nahum, A. M. and Melvin, J. W., Accidental Injury: Biomechanics and Prevention, pages 66–84, New York, NY, USA. Springer New York.

[36] SAE J211-1:1995 (1995). Instrumentation for Impact Test – Part 1 – Electronic Instrumentation. SAE International, Warrendale, PA, USA.

ACTIVATING GLOBAL COLLABORATION TO DRIVE ADVANCEMENTS IN CHILD RESTRAINT SYSTEMS FOR CHILDREN WITH DISABILITIES

Helen Lindner
Emma Clarkson
Mobility and Accessibility for Children in Australia Ltd
Australia

Paper number 23-021

ABSTRACT

Research shows that children with disabilities face an increased risk of injuries and fatalities in a crash compared with other children. However, a recent literature review concluded that these particularly vulnerable road users continue to be inappropriately restrained in vehicles, constituting an ongoing road safety problem. This also impacts on their human right to safe and accessible transport. Although globally, there are established independent assessment programs for child restraint systems, there is no such program for special purpose child restraints or other restraint types used by children with disabilities. With the formation of a new Australian charity dedicated to advancing the rights of children with disabilities to safe and accessible transport, the objective of this project is to enhance the protection of children with disabilities travelling in child restraint systems in motor vehicles through the establishment of an independent safety and assessment program. The development of the Australian Safety Assessment Program (AuSAP) was supported with funding from the Victorian Transport Accident Commission, and in-kind support from NeuRA and Britax.

A mixed methods research approach was used, consisting of:

Desktop review
A review of the legislative and regulatory environment impacting on the supply, sale and use of special purpose child restraints and accessories in Australia was conducted. A global product scan identified restraints for inclusion.

Governance framework
Several governance framework options were developed, with the recommended option being a not-for-profit lead agency model supported by an Expert Committee.

Protocols
The Expert Committee developed the Test and Assessment Protocol based on a review of standards/regulations.

Assessments/crash testing
Fifty-four crash tests have been undertaken (forward and side impact testing), with results shared with relevant suppliers and manufacturers.

Communication/education
MACA is developing individual Product Guides that incorporate AuSAP findings to support allied health professionals in their prescribing role.

AuSAP is implementing a global approach to improve motor vehicle restraint systems for children with disabilities in line with the recommendations in the World Health Organization's global report on Assistive Technology and the Convention on the Rights of Persons with Disabilities. The program has rapidly stimulated the Australian market to supply special purpose child restraints by increasing the confidence of suppliers, prescribers, consumers, and government funders. This has expanded safe motor vehicle transport options for children with disabilities. It has also provided a unique opportunity for global collaboration with manufacturers to improve the design and safety of restraint systems for children with disabilities. AuSAP has facilitated international engagement about the suitability of current requirements in standards/regulations for special purpose child restraints and consideration of potential improvements for future reviews. This has the potential to remove barriers to access not only in Australia but globally. The first program of its kind, AuSAP has achieved early success in encouraging international cooperation and learning to advance the human rights of our most

vulnerable road users to safe and accessible motor vehicle transport. Access to such life changing assistive technology is a precondition for equal opportunities and participation.

INTRODUCTION

It is estimated that approximately 1 in every 10 (more than 150 million) children globally under the age of 18 has a disability [1].

Some children with disabilities and medical conditions, such as Cerebral Palsy and Autism Spectrum Disorder, require additional support and features not provided by conventional child restraints. Special purpose child restraints have been specifically designed to support the needs of these children.

However, children with disabilities and medical conditions in Australia face significant barriers in accessing special purpose child restraints when unable to travel in a conventional child restraint [2]. This situation is not unique to Australia, with the gaps greatest in low- and middle-income countries. This global inequity requires urgent collective attention and action [3].

A literature review in 2019 reflected little change in how children with disabilities are being transported since a previous literature review in 2001, noting that they "continue to be inappropriately restrained in vehicles, constituting an ongoing road safety problem" [4]. Further, 74 per cent of children with autism escape their child restraint, and more than 20 per cent of parents report their child demonstrates aggressive or self-injurious behaviour during travel, impacting on their safety and others [5].

More recently Australian families of children with disabilities and medical conditions have raised significant concerns about their child's safety during transport and reported that their transport situation restricts their child's participation [3]. Key safety concerns include having to pull over to reposition their child, becoming distracted as a result of their child becoming upset or distressed, and having difficulty physically getting their child in and out of the car. Over half of parents reported their child was getting out of their child restraint or vehicle seatbelt whilst the vehicle was moving and ten per cent reported their child had escaped the vehicle into the road environment. Over two thirds of parents reported never receiving information about how to safely transport their child and nearly half reported that their child was missing out on participating in everyday life [2].

Access to assistive technology, such as special purpose child restraints, is regarded as a precondition for achieving equal opportunities, enjoying human rights, and living in dignity [1]. This right is enshrined in Article 32 of the UN Convention on the Rights of Persons with Disabilities that calls for international cooperation to support national efforts to improve access to assistive technology across the world. Such cooperation can support efforts in areas of research, policies, regulations, fair pricing, market shaping, product development, technology transfer, manufacturing, procurement, supply, service provision and human resources [3].

Australian context

Mobility and Accessibility for Children in Australia Ltd (MACA) Established in 2019, MACA is a not-for-profit charity dedicated to advancing the rights of children (under 16 years) with disabilities and medical conditions to safe and accessible transport. MACA is the first Australian organisation of this type focused on addressing the significant gaps and barriers impacting on the motor vehicle transport needs of children with disabilities and medical conditions.

National Disability Insurance Scheme (NDIS) There has been a fundamental shift in the past decade in Australia's approach to supporting the everyday needs of people living with disability. People with a "permanent and significant" disability (under the age of 65) can now access full funding for any "reasonable and necessary" support needs related to their disability. This funding is accessed through the NDIS, the first scheme of its kind in Australia.

Funding includes access to *assistive technology*, which the NDIS defines as "items that help you do things you can't do because of your disability. Or things that help you do something more easily or safely." Special purpose child restraints are classified by the NDIS as high-risk assistive technology.

Due to the lack of knowledge about special purpose child restraints, including compliance with standards, safety and performance, the NDIS experienced challenges in approving funding applications, resulting in some children not benefiting from the scheme for their motor vehicle transport needs. Where funding approval was achieved, NDIS participants experienced long wait times, ranging from three weeks to three years [2].

Australian standards Australia has a long-established standard for child restraints (AS/NZS 1754 *Child restraint systems for use in motor vehicles*) however this standard does not cater for the restraint types used by children with disabilities - which include special purpose child restraints, harnesses/vests, and modified child restraints. This situation has resulted in Australian children travelling in either locally made products that do not comply with standards, (e.g., harnesses and modified child restraints), or special purpose child restraints from overseas which may comply with a relevant regulation or standard.

Australia's child restraint standard (AS/NZS 1754) is mandated through a national consumer protection notice and reflected in each of Australia's eight state and territory road laws. As this standard does not provide for special purpose child restraints, products can be legally supplied and sold in Australia from overseas, with exemption provisions in road laws for use in motor vehicles. AS/NZS 1754:2013 is currently under review, with a new section being drafted to consider allowing for some variations to Australian standard child restraints to cater for the needs of children with disabilities and medical conditions. However, this approach requires analysis of the potential benefits and barriers that may impact industry, families, and government policy if these changes are accepted for Australia and New Zealand.

In addition, Australia (and New Zealand) has a unique standard, AS/NZS 4370 *Restraint of children with disabilities, or medical conditions, in motor vehicles* (current version 2013), to guide allied health professionals when assessing and prescribing for children's motor vehicle transport needs. This standard however does not cover the safety and performance of the restraint types used by children with disabilities and medical conditions and is scheduled for review to ensure it reflects recent research and learnings.

Child restraint evaluation program Like many other countries, Australia has an established independent review program for its Australian standard child restraints. This program, aimed at consumers, is known as the Child Restraint Evaluation Program. It's funded by government and road safety focused organisations and tests child restraints to a higher level than the Australian standard.

However, until the establishment of AuSAP, no such program existed for special purpose child restraints (and other products) used by children with disabilities and medical conditions.

OBJECTIVES

MACA established the Australian Safety Assessment Program (AuSAP) to improve knowledge of the safety and performance of restraint types used by children with disabilities and medical conditions. This is the first independent assessment program for special purpose child restraints (and other restraint types) used by children with disabilities and medical conditions when travelling in motor vehicles.

AuSAP is a key program contributing to MACA's vision that *every child has access to safe and equitable transport*. The objectives of AuSAP are broad, invite collaboration, and encompass a whole-of-system approach:

AuSAP aims:

- To uphold the rights of children with disabilities to safe and accessible motor vehicle transport
- To improve knowledge and raise awareness of the motor vehicle transport needs of children with disabilities and medical conditions
- To influence the design and safety of vehicle restraint systems for children with disabilities and medical conditions
- To expand safe vehicle restraint options for families
- To support health professionals in their prescribing role.

METHODS

The establishment of AuSAP involved extensive development and research spanning three years, involving industry, government, researchers, and parents of children with disabilities and medical conditions.

Funding
MACA invested 12 months in developing the AuSAP scope and engaged in extensive stakeholder engagement to secure funding.

In 2020, the Transport Accident Commission (Victoria, Australia) provided establishment funding with MACA receiving in-kind support from Britax Childcare Pty Ltd (Victoria, Australia) and the Neuroscience Research Australia – Transurban Road Safety Centre (NSW, Australia).

In addition, AuSAP industry participants donated special purpose child restraints for crash testing.

Governance
Four governance options were considered in establishing AuSAP. The model implemented is coordinated and promoted by MACA and supported by an Expert Committee and Reference Group.

The Expert Committee consists of preeminent Australian child restraint experts and researchers, responsible for setting the aims of the program, developing and reviewing test and assessment protocols and reviewing results.

The Reference Group advises on the development and distribution of AuSAP resources. This group includes parents of children with disabilities, allied health professionals, communications and road safety experts.

Desktop review
Two desktop reviews were undertaken – a legislative and regulatory review and product/practice review.

The legislative and regulatory review investigated the environment impacting on the supply, sale and use of special purpose child restraint systems and other devices (e.g., harnesses) in Australia. This review identified significant complexity, inconsistency, and lack of clarity in rules, regulations, and interpretation in relation to special purpose child restraints and other devices.

The product and practice review used selected restraint types as outlined in AS/NZS *4370 Restraint of children with disabilities, or medical conditions, in motor vehicles* as a guide to investigate product types, allied health professional practice, and how these restraint types are used by families of children with disabilities and medical conditions. The selected restraint types (see Table 1), included:

- Australian standard child restraints
- Modified Australian standard child restraints
- Special purpose child restraints
- Customised restraints

Table 1.

AS/NZS 4370 Selected restraint types

AS/NZS 4370 Restraint category	Description	Details
Australian standard child restraint	Child restraint that complies with AS/NZS 1754	➢ Mandatory standard ➢ Independent safety and assessment program childcarseats.com.au ➢ Various government supported initiatives for consumer information, fitting and use ➢ Established evidence-base
Modified Australians standard child restraint	Australian standard child restraint that includes changes or add-on items such as postural supports, buckle covers, extended crotch strap, additional padding - not provided with the child restraint and not included in the manufacturer's instructions	➢ Voluntary accessory standard AS 8005:2020 (no products certified to this standard) ➢ No safety information available ➢ Common prescriber practice in Australia ➢ No evidence-base
Special purpose child restraint	Restraints made specifically for children with disability/medical condition that comply with one or more of the following standards: CMVSS 213; FMVSS 213; ECEr44; ECEr129	➢ No Australian standard requirements (new section being drafted in current review) ➢ Overseas child restraint standards and regulations ➢ New independent safety assessment program (AuSAP) ➢ Common prescriber practice ➢ Limited government supported initiatives ➢ Emerging evidence-base

Customised restraint	Designed or custom made for the individual child's needs and not compliant with any standard (e.g., bespoke harness)	➢ No standards ➢ No safety information ➢ No government supported initiatives ➢ Limited prescriber practice ➢ No evidence-base

It was identified that harnesses/vests are not included in AS/NZS 4370, however, these products were also considered in the desktop review.

The review identified the range of special purpose child restraints, harnesses/vests, and modification practices in Australia. It found there was a limited range of special purpose child restraints available in Australia, and they all complied with the US, Canadian or European standards/regulations.

The Expert Committee determined that special purpose child restraints be prioritised for assessment/testing, whilst further research was required to investigate modified Australian standard child restraints and harnesses/vests. Customised restraints were considered out of scope.

Protocol development
The development of the AuSAP Test and Assessment Protocol (protocol) [6] for special purpose child restraints involved extensive research over nearly 12 months.

Following a desktop review of relevant overseas standards and regulations (and test methods), including Canada, US, Europe, Brazil, China, and Japan, the Expert Committee agreed to use selected criteria (frontal and side impact) from the AS/NZS 1754:2013 for the protocol. This standard calls up test methods from AS/NZS 3629.1:2013 *Methods of testing child restraints, Method 1: Dynamic testing*.

The Expert Committee felt it was necessary to include side impact testing, even though most products selected for testing did not comply with standards/regulations requiring side impact protection. This decision reflected the fact that side impact protection is a key feature of Australian standard child restraints.

As well as frontal and side impact crash tests, the protocol includes a limited assessment of product design features to identify and evaluate potential sources of risk not covered by dynamic assessments, and any potential issues that may pose challenges to test set-up – for example, foot props.

The protocol includes a parameter assessment template which uses the criteria of 'good', 'acceptable', 'marginal' or 'not acceptable' for post-test reviews. The parameter assessments are for internal purposes only, used to guide assessment discussions with the Expert Committee. Direct comparisons between product parameter assessments are not undertaken due to the unique nature of special purpose child restraints, unlike some independent assessment programs that make direct comparisons, or use a star rating system.

Assessments/crash testing
Seven Australian importers (see Table 2) signed an agreement to participate in AuSAP. To date, fifty-four crash assessments have been completed, involving fifteen special purpose child restraints, with new products currently under testing and review.

Table 2.

Australian importer participation and product list

Australian importer	Products (Manufacturer/country)
Specialised Wheelchair Company Pty Ltd	Stabilo Multiseat (Stabilo – Poland)
Medifab Australia Pty Ltd and Medifab Global Pty Ltd	Carrot 3000 Carrot XL (Seeds – Japan) Hero NXT IPAI LGT Starlight NXT Kidsflex (Hernik GmbH – Germany)
Dejay Medical and Scientific Pty Ltd	Special tomato soft touch booster seat

	(Special Tomato – United States)
FAS Therapeutic Equipment P/L	Spirit Car Seat (Inspired by Drive) IPS 2000 series (Inspired by Drive – United States)
Active Rehab	Baffin.1 (LIW Care Technology – Poland)
Apex Mobility Pty Ltd	Thomashilfen Commander (Thomashilfen) Thomashilfen Defender (Thomashilfen – Germany)
Etac ANZ Pty Ltd	Quokka Wallaroo (Etac – United States)

The fifty-four tests were undertaken between June 2021 and August 2022 across three testing centres - Britax Childcare Pty Ltd, Victoria, Australia (see Image 1); NeuRA (Transurban Road Safety Centre), NSW, Australia; and APV-T Test Centre, Victoria, Australia.

Image 1. Carrot 3000 set-up for testing at Britax Childcare Pty Ltd, Australia.

RESULTS

The testing revealed mixed results. Whilst some products performed well against the AuSAP Test and Assessment Protocol for frontal testing, no product met the side impact test criteria (see Image 2). Other findings included products with significant submarining (see Image 3), ISOFIX/LATCH and top tether failures (see Image 4), and one product with a broken splitter plate (see Image 5).

Image 2. Side impact test example.

Image 3. Significant submarining.

Image 4. LATCH and top tether failure.

Image 5. Frontal test resulting in splitter plate breakage.

Following testing, meetings were held with Australian importers and overseas manufacturers to communicate AuSAP independent assessment findings. As a result, several products are undergoing further investigation and/or testing, and a few products have subsequently been withdrawn, or will not be introduced to the Australian market

Eight special purpose child restraints have progressed to publication on MACA's national product register with their status published on MACA's website (see Figure 1).

Figure 1. AuSAP product status www.macahub.org as at 11 December 2022.

Communicating AuSAP results

AuSAP outcomes are communicated through a range of practical tools and resources, including:

National product register MACA's national product register is a centralised register of restraint types used by children with disabilities and medical conditions in Australia, including special purpose child restraints, Australian standard child restraints and harnesses/vests.

The special purpose child restraint product register only includes products that have been independently assessed through AuSAP, and meet the AuSAP Test and Assessment Protocol.

Product Guides MACA has developed product guides for the special purpose child restraints published on the national product register. The guides bring together important independent information such as AuSAP testing outcomes, safe use, compliance with standards/regulations, and prescribing advice. The guides support allied health professionals who assess children's transport needs, as well as importers, product suppliers and government funders/regulators.

Training Knowledge and learning from AuSAP is incorporated in MACA's Australian-first on-line training course targeted at allied health professionals: *Transporting Children with Disabilities and Medical Conditions.*

DISCUSSION

This paper presents an overview of the development, aims, and outcomes of the Australian Safety Assessment Program (AuSAP), since its establishment in 2020. No other program has been identified that independently assesses the specialty restraint types used by children with disabilities and medical conditions when travelling in motor vehicles.

Although this program is a significant advancement and is demonstrating its potential as a catalyst for change, several areas require further investigation and research.

Instruction manuals

Special purpose child restraints often have multiple parties involved in their design and manufacture, with some products complying with standards and regulations in more than one country. This results in products often having more than one set of instruction manuals (with differing information).

To illustrate, where a conventional child restraint is modified for use by a third party as a special purpose child restraint, they develop their own instruction manual, often with no reference to the originating manual. In some cases, the product may also have accessories (e.g., swivel base) made by another organisation, with a separate set of instructions for use. Local importers may also produce their own branded instructions and include additional information.

This situation causes confusion about product installation and use. This may contribute to incorrect consumer advice and product misuse, impacting on safety. Through AuSAP, MACA's desktop review of the various instruction manuals identified the need for an intervention to reduce the risks associated with products having multiple and varied instruction manuals. In response MACA developed Product Guides (see Image 6), which include independent information about compliance with standards/regulations, AuSAP outcomes, and prescribing advice that clarifies key information relating to safe installation and use of products in Australian vehicles. The guides support allied health professionals, as well as importers, suppliers, government regulators and funders.

Image 6. Product Guides.

The role of standards/regulations
Although there are well established standards and regulations for child restraint systems throughout the world, not all have provision for special purpose child restraints, and other devices commonly used by children with disabilities and medical conditions. Where they are provided for, requirements are often inadequate, not informed by evidence and user needs - particularly for older and larger occupants.

The development of the new UNECE r129 did not consider the motor vehicle transport needs of children with disabilities, nor the impact on these road users of the changes being introduced by this new regulation. This situation has the potential to impact on the rights of children with disabilities and medical conditions to safe and accessible vehicle restraint systems.

MACA is convening a working group of global experts to discuss what steps are urgently needed to respond to this situation, and more broadly to discuss what type of standards and regulatory system is needed to ensure equitable access to affordable, durable, safe, and effective products.

Systems change
There are many barriers to people accessing assistive technology - including lack of awareness and affordability, lack of services, inadequate product quality, range and quantity, inadequate government policies, standards and procurement and supply chain challenges [3].

As discovered in Australia there has been a reluctance for suppliers to import products, and for government to fund products, due to the standard and regulatory environment being unclear, inconsistent, and inadequate. Whilst MACA (and AuSAP), is stimulating an increase in supply to Australia and informing government funding policy (e.g., the NDIS is reviewing the impact of MACA's work and AuSAP on its funding decisions) further mechanisms are needed to improve access for other small markets, and low- and middle- income countries.

Unlike access to conventional child restraints in Australia, family access to special purpose child restraints is also impacted by the silos of the disability, education, health, and transport sectors. This makes it easy to deflect responsibilities across the system, creating systemic barriers which impact on children's rights to safe and accessible transport.

AuSAP, with its tangible, evidence-informed outcomes, is an effective vehicle for MACA to engage across sectors and borders to influence change in policies, programs, and systems. However, this requires ongoing government commitment, investment, and global collaboration, for the benefits to be fully realised and systemic change to occur.

LIMITATIONS

AuSAP's outcomes are only relevant to the products tested to date, therefore not representative of all available special purpose child restraints in the world. In addition, the AuSAP Test and Assessment Protocol [6] is based on selected criteria from AS/NZS 1754, and provides an independent review, not certification, of each product.

At this stage, AuSAP has not been evaluated. Curtin University, in Western Australia, will be implementing a follow up national survey in July 2023 to evaluate the effectiveness of MACA's work to-date.

CONCLUSION

As the first program of its kind globally, AuSAP has achieved early success in encouraging international cooperation and learning to advance the human rights of our most vulnerable road users to safe and accessible motor vehicle transport.

AuSAP findings are bringing confidence to industry, government, parents, and health professionals, and influencing policy, legislation, research, products and standards development.

Access to life changing assistive technology, such as special purpose child restraints, is a precondition for equal opportunities and participation. MACA's work to date demonstrates an ongoing need for AuSAP to advance the rights of children with disabilities and medical conditions to safe and accessible transport.

ACKNOWLEDGEMENTS

REFERENCES

[1] World Health Organization & United Nations Children's Fund (UNICEF). (2015). Assistive Technology for Children with Disabilities: Creating Opportunities for Education, Inclusion and Participation. A discussion paper.

[2] Black, M. H., Hayden-Evans, M., Picen, T., Lindner, H., Clarkson, E., Vale, L., McGarry, S., & Falkmer, T. (Under review-a). *Experiences of caregivers on the safe transport of children with disabilities and medical conditions*.

[3] World Health Organization & United Nations Children's Fund (UNICEF). (2022). Global report on assistive technology. World Health Organization.

[4] Downie A, Chamberlain A, Kuzminski R, Vaz S, Cuomo B, Falkmer T. Road vehicle transportation of children with physical and behavioral disabilities: A literature review. Scand J Occup Ther. 2020 Jul;27(5):309-322. doi: 10.1080/11038128.2019.1578408. Epub 2019 Mar 11. PMID: 30856035.

[5] Yonkman, J., Lawler, B., Talty, J., O'Neil, J., & Bull, M. (2013). S*afely transporting children with autism spectrum disorder: Evaluation and intervention*. Am J Occup Ther, 67(6), 711-716. https://doi.org/10.5014/ajot.2013.008250

[6] Mobility and Accessibility for Children in Australia Pty Ltd, *AuSAP Test and Assessment Protocol*, Version 9, August 2022. maca | Assessment & Results (macahub.org)

SIMULATION-BASED EVALUATION OF A GENERIC AUTONOMOUS EMERGENCY BRAKING SYSTEM USING A COGNITIVE PEDESTRIAN BEHAVIOR MODEL

Lucas Fonseca Alexandre de Oliveira
Lars Schories
ZF Friedrichshafen AG
Germany

Lukas Brostek
cogniBIT GmbH
Germany

Martin Meywerk
Helmut-Schmidt-Universität
Germany

ABSTRACT

In 2020 pedestrians accounted for 21,4% of all deaths in the European Union. Considering all vulnerable road users (VRU: pedestrians, cyclists, motorcycles, and mopeds) they accounted for 51,4% of all deaths. To reduce the number of deaths and improve VRU safety, systems have been developed in the last decades. The autonomous emergency braking system (AEB) is one of these systems and aims to intervene in conflict situations by applying an emergency braking (in some cases only after the driver starts the brake itself). The performance evaluation of an AEB system via simulation reduces cost and time against real tests and allows better robustness evaluation because of the higher number of scenarios that can be simulated. In the virtual-world, safety-critical situations can also be tested without any problems. The modeling of pedestrian behavior plays an important role since the pedestrian is the vehicle's adversary in this context. Current studies use a simple pedestrian model, in which the pedestrian does not have any perception of the environment, moving on a pre-defined path with constant speed. Such trajectory-based models are available in the most common vehicle dynamic simulation tools. In reality, however, pedestrians usually react to the approaching vehicle in conflict situations by adjusting their trajectory, which can change the conflict situation and affect the performance assessment of AEB systems. This study compares the standard model with neuro-cognitive pedestrian model from cogniBIT and investigates if and how these models affect the performance assessment of AEB systems.

INTRODUCTION

Pedestrians are the road user group with the highest number of fatalities in Europe in 2021 with 51,4% of all fatalities [7]. Crashes involving pedestrians occur mainly, when pedestrians cross the road at not signposted cross-sections [16], [2]. In these situations, pedestrians change direction and speed generating paths with higher safety issues [14].

To protect pedestrians, the automotive industry has developed safety systems over the past decades. One of these is AEB-P, an active system, that activates braking maneuver in detected critical situations, with the aim of preventing or reducing the severity of a collision [12]. Figure 1 shows the reduction in the number of deaths on German roads since driver assistance systems (ADAS), like AEB, have been implemented in vehicles.
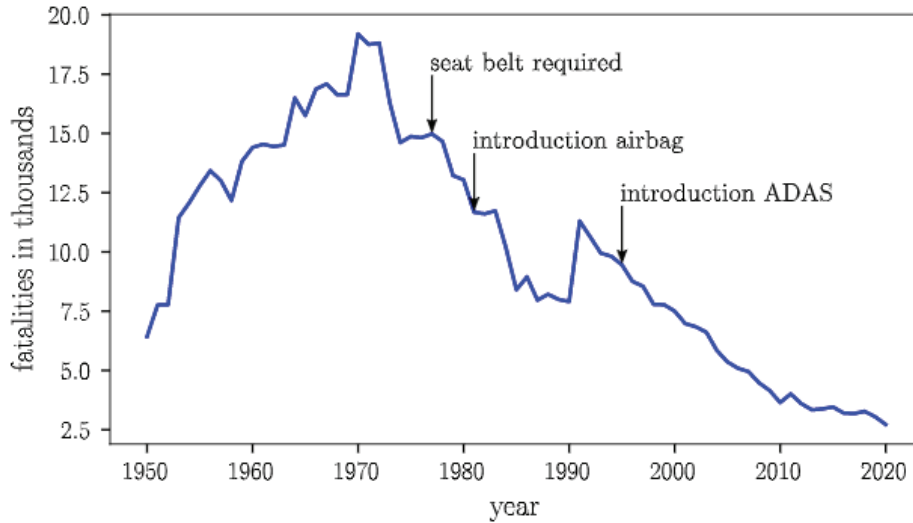
Figure 1. Fatalities on German roads since 1950 [12].

The evaluation of the AEB-P follows standards set by regulatory and consumer protection organizations such as Euro NCAP [10]. In the Euro NCAP test protocol for autonomous emergency braking for pedestrians (AEB-P) the pedestrian is represented by a dummy, which moves in a straight line with constant speed. However, real traffic situations are more complex and pedestrian crossing behavior is influenced by multiple factors such as road infrastructure (distance from the crosswalk, presence of traffic lights, number of lanes etc.), traffic situation (speed and flow), psychological and physiological characteristics, among other factors [16], [3], [14], [18] and [21].

To improve pedestrian safety, the next generation of active safety systems must be able to anticipate critical situations. For this, understanding pedestrian behavior and intentions in complex traffic situations is essential. Since simulation is used during the early stages of the development of new systems, it is necessary to use more realistic pedestrian behavior models for traffic situations which will allow the creation of more realistic scenarios.

This paper aims to evaluate a novel pedestrian behavior model for the evaluation of a generic autonomous pedestrian emergency braking system (AEB-P). First, we present a brief introduction to pedestrian behavior models and to the neuro-cognitive system architecture of the pedestrian model of CogniBiT (http://cognibit.ai). Next, the methods used to generate the scenarios and the metrics used to evaluate the performance of the AEB-P system are presented. Finally, the results are presented and discussed.

OVERVIEW PEDESTRIAN BEHAVIOR MODEL

The pedestrian model for use in simulations concerning ADAS falls into the category of microscopic models, since each pedestrian is modeled individually. [22], [6], [17], [23] present and discuss different microscopic pedestrian models. However, for the most part, the models do not consider intrinsic aspects of pedestrian behavior such as emotional state and intentions, and the influence of road infrastructure.

Commercial software also uses a simplified pedestrian model, in which the pedestrian follows a given trajectory, also called trajectory-based model. The pedestrian does not interact with the environment and does not consider other agents in its movement. In CARLA Driving Simulation the default pedestrian, used to populate the scene, walks randomly without considering other agents, which also cannot be considered a realistic model of pedestrian behavior. There are also commercial models that use other methods and can be integrated into third-party software. One promising approach uses Machine Learning, where the model is trained based on real data to reproduce pedestrian behavior in a specific scenario [11]. The approach looks promising but faces some limitations regarding scalability, once for each new scenario the model needs to be trained again.

A novel approach models the human cognitive process and will be referred to in this paper as the cognitive behavior model. The model is based on studies of pedestrian behavior and movement and reproduces the

cognitive decision-making process of humans. Since it is not based on a specific scenario, the model can be applied in different traffic situations.

NEURO-COGNITIVE PEDESTRIAN BEHAVIOR MODEL

The neuro-cognitive pedestrian behavior model developed by cogniBIT is based on the so-called cogniBOT system architecture, (see Figure 2). Pedestrian behavior in complex traffic situations results from a sequence of processes that take place in the central nervous system. The model divides this process into three major parts. The first stage of information processing is visual perception, representing how humans acquire information from their surroundings. The Cognition creates an internal representation of the outside world. Finally, in the motoric action stage a decision is made and translated into a desired trajectory and the corresponding control signals. These signals are fed back to a pedestrian locomotion model, resulting in a closed-loop interaction with the simulation environment.
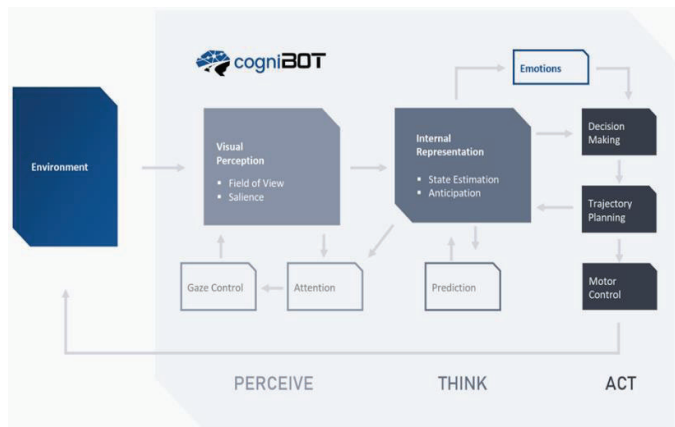

Figure 2. The cogniBOT neuro-cognitive system architecture.

The model considers different aspects of human sensorimotor information processing and their limitations focusing on the application in complex traffic situations.

Visual Perception
Sensory perception describes the intake of information from the environment, with the focus on visual perception in the simulation of traffic participants. The cogniBOT system architecture simulates relevant limitations of human road users, for example a restricted field of vision, which is compensated by eye movements. The simulated eye movements are controlled by a complex attention process that takes into account both top-down signals, such as the currently intended action, and bottom-up signals, for instance due to the recognition of other traffic participants in the peripheral field of vision.

Cognition
The information recorded in the perception modules is used to create an internal representation of the external world. Considering the objects that have been recognized, the cogniBOT AI architecture draws on previously identified information about the type, position and speed of other road users, as well as the internal map of the road course, to create a context-specific prediction from this information.

Motoric Action
The prediction of the situation forms the basis for decision making of the simulated traffic participant. For this purpose, the cogniBOT AI architecture implements a cost function that allows the simulated agent to make a trade-off for each traffic situation between speedy progress, distance to other road users, and the risk of an accident. Based on this decision, a desired trajectory is planned and translated into motor signals.

Emotions & Physiology
Human perception, cognition and action are under the influence of emotions and physiological states. Some emotions such as anger can lead to riskier behavior. These aspects are also considered within the model mainly through the behavior profile passed into the model.

Model usage
The user defines a starting position, a list of target destinations, initial and desired speed, and a behavior profile. It is possible to integrate a vehicle to be tested (VUT) or other external models of traffic participants into the simulation.

cogniBIT's models are stochastic as they simulate physiological processes such as perception and cognition which are probabilistic in nature. This allows automatic generation of variations of the same initial scene by different selection of the random seed. At the same time, cogniBIT's models are fully deterministic in the sense that exactly the same simulation results are reproduced when initial conditions and random seed are identical.

Behavior profile
Pedestrian behavior has many aspects that influences it, like age, emotional state and cultural background as internal aspects and traffic rules, surrounding traffic, road infrastructure and weather conditions as external ones. The behavior profile allows to define different types of behavior based on the intrinsic aspects, which in turn influence how the pedestrian interacts with his or her surroundings, the extrinsic aspects.

The behavior profile has five different parameters that can be defined by the user. The parameters are 'physical limitations', 'level of activity', 'rule adversity', 'cautiousness', and 'aggressivity'. Depending on the combination of these parameters, profiles ranging from very prudent and cautious to extremely risky and careless behavior can be generated.

Each parameter influences the pedestrian behavior differently. 'Physical limitations' simulates, for example, limitations caused by aging, handicap or intoxication and affects perceptive, cognitive, and motor skills. 'Level of activity' affects decision making and attention primarily. 'Rule adversity', along with 'cautiousness', are the parameters that most define pedestrian crossing behavior. Whereas the former defines the level of respecting traffic rules and signs, the latter rather refers to avoiding conflict situations with other traffic participants when jaywalking. The level of 'aggressivity' affects pedestrian-pedestrian interaction [15].

METHODS

The evaluation of ADAS and in vehicle safety system can be carried out in different ways. The method applied in this paper is based on [1], [20] and the ISO PDTR 21934 norm. The evaluation process consists of four main steps: (1) identification of the relevant traffic situations, (2) establishment of the baseline (3) establishment of the modified scenario, where the safety system is applied to the baseline and (4) the comparison of the results.

Relevant traffic situation
The relevant traffic situation represents the situation of interest where the application of the safety system could potentially be beneficial. According to ISO PDTR 21934, such situations can be derived from crash data analysis, naturalistic driving studies or from previous knowledge from technology development. As the focus of this paper is to evaluate the performance of the AEB-P system, scenarios involving the pedestrian were considered as relevant ones. The tests applied by Euro NCAP are already derived from crash data analysis, so the scenario chosen in this paper is also based on the Euro NCAP tests. Using the ISO PDTR 21934 nomenclature, the relevant scenario for this paper is **S**traight **C**rossing **P**ath, **p**edestrian from **r**ight (SCPpr), where the car is moving forward, and the pedestrian is crossing the path from right.

Figure 3 represents the baseline scenario. The road has two lanes and at one end, on the right side of the pedestrians' starting position, a signalized cross-section.
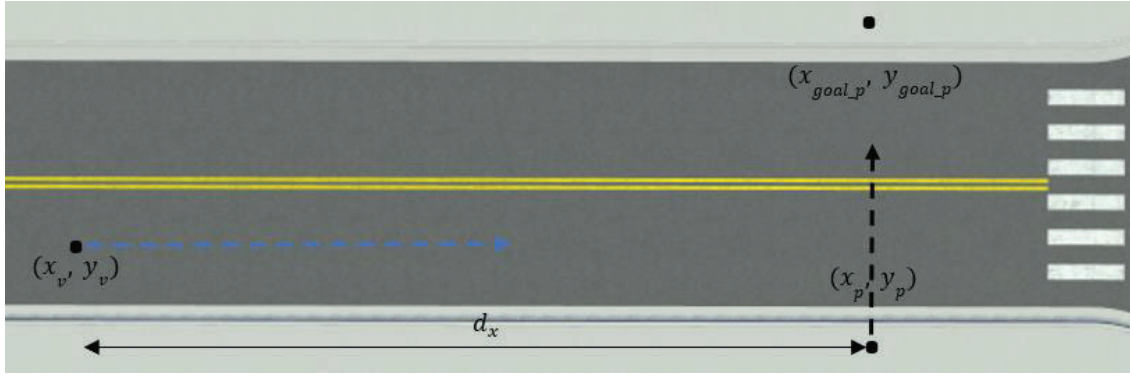

Figure 3. Relevant traffic situation.

(x_v, y_v) is the vehicle start position, (x_p, y_p) the pedestrian start position and (x_{goal_p}, y_{goal_p}) the pedestrian goal destination. The black dashed line indicates the direction of the pedestrian's movement. And the blue dashed line indicates the direction of movement of the vehicle. The distance between vehicle and pedestrian, d_x ,which was varied for the generation of the scenarios, is the distance in the x direction (see Equation 1).

$$d_x = x_p - x_v \quad \text{Equation (1)}$$

Baseline scenario

To generate the baseline scenarios, it is necessary to define the road infrastructure, as well as the number and type of road users, their starting speeds, and the vehicle trajectory. Following a similar approach as presented in [20] a parameter called 'initial vehicle waiting time' was implemented. By varying these three parameters in a virtual environment the baseline scenarios were generated. The parameters used and their distribution are listed in Table 1.

Table 1.
Baseline Scenario Input Parameters

Input name	value	step	unit
Vehicle speed	[10, 60]	5	km/h
Distance between vehicle and pedestrian	[10, 30]	5	m
Vehicle waiting time	[0.0, 1.0]	0.5	s

For a specific pedestrian behavior profile, 165 baseline scenarios were generated. In contrast to [20] the pedestrian trajectory was not predefined. Based on the pre-defined behavior profile and the specific situation, the neuro-cognitive pedestrian behavior model chooses a trajectory to reach the destination goal. The vehicle moves on a predefined trajectory.

Modified scenario

The modified situation is the baseline scenario, but with an AEB-P equipped vehicle. The AEB-P module contains two parts, an ideal sensor defined by a field of view and perception algorithm, and the braking module defined by time to collision (TTC), pedestrian detection status and braking profile. The used settings for the field of view are in Table 2, (see Figure 4). When the pedestrian enters the field of view, the TTC is calculated (see equation 2).

$$TTC = |\vec{r}_{rel}| / |\vec{v}_{rel}| \qquad \text{Equation (2)}$$
$$\vec{v}_{rel} := \vec{v}_{car} - \vec{v}_{ped} \qquad \text{Equation (3)}$$
$$\vec{r}_{rel} := \vec{r}_{ped} - \vec{r}_{car} \qquad \text{Equation (4)}$$

Where the $\vec{v}_{rel}$ represents the relative speed between vehicle and pedestrian, and $\vec{r}_{rel}$ the relative position, [11]. When the TTC is less than or equal to 1 s, the vehicle starts braking following the defined braking profile, (see Figure 5 and Table 3).
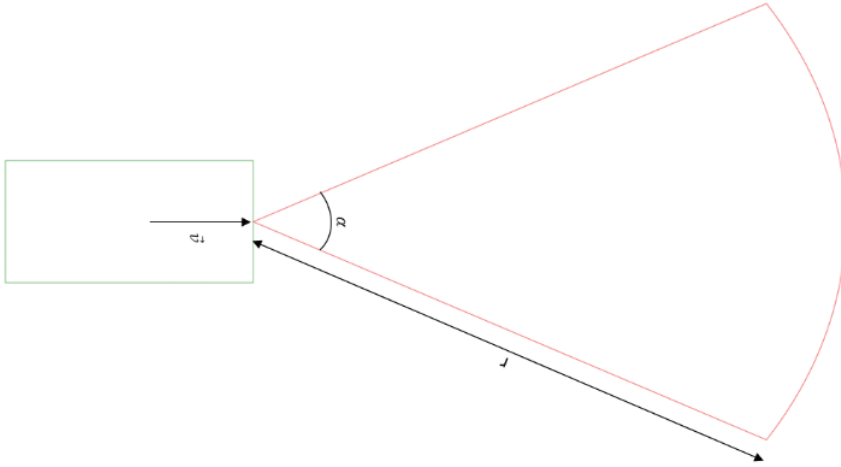
Figure 4. AEB Field of View [11].

Table 2.
Field of view parameters

Parameter	Value	Unit
Azimuth angle (α)	60	°
Range (r)	60	m

The braking profile used here is similar as in [20], (see Figure 4). It is divided into three parts: system delay, build up time, the time needed for full brake. During build up time the deceleration increases linearly over time.
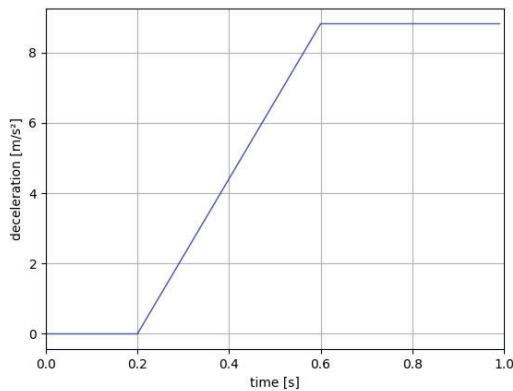

Figure 5. AEB Braking profile.

Table 3.
Braking profile settings

Parameter	Value	Unit
Delay	0.2	s
Build up time	0.4	s
Maximal deceleration	0.9	g

Safety Assessment

After simulating the baseline scenarios and the modified scenarios with the AEB-P system, the results were compared. The metric used in this paper is the reduction in frontal collision cases due to the AEB-P system. Figure 6 shows an overview of the process.
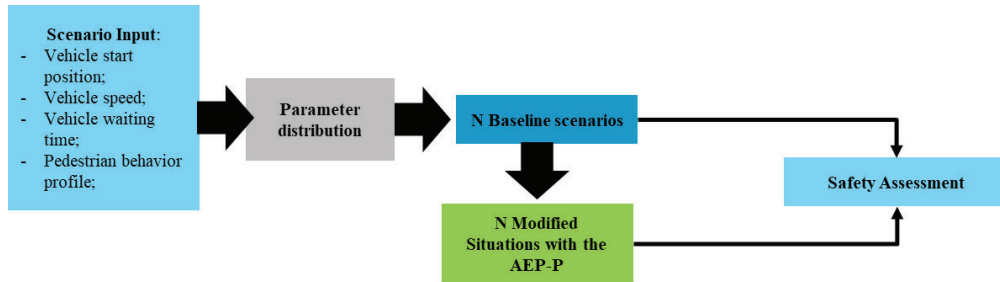
_____

Figure 6. Safety Assessment approach.

Simulation Environment

The choice of the platform used in this paper was based mainly on the integration with the pedestrian behavior model, support to OpenDrive file format and the quality of the 3D model, relevant for future studies. Therefore, open-source programs were prioritized. This paper uses the CARLA (Car Learning to Act) Driving Simulator platform, an open-source software built on top of Unreal Engine 4 (UE4) for autonomous car research, [9]. In CARLA vehicle dynamics is modeled using the standard UE4 vehicle model, PhysXVehicles, which is focused on the gaming market and is limited when compared to specific vehicle modeling software. But for the purpose of this paper, the model was sufficient.

RESULTS

Pedestrian Behavior model parameter analysis

Different combinations of the parameters were evaluated in pairs in the scenario used to evaluate the AEB-P system in this paper. The parameters which were not being varied had the default value of 0. The evaluated parameters were varied with a step of 0.2, from 0 to 1. The initial conditions of the scenario are listed in Table 4.

Table 4.
Initial condition by the simulation for the behavior profile evaluation

Parameter	Value	Unit
Vehicle initial speed	4	m/s
Vehicle goal speed	10	m/s
Distance to pedestrian	12	m

Each combination of parameters was simulated with eleven different random seeds. The results were evaluated considering whether the pedestrian had a collision with the vehicle or not. For the second case there are two possible reasons, either the pedestrian waited at the curb for the vehicle to pass or the pedestrian managed to cross the road without being hit by the vehicle. The results were plotted on the diagrams present in figure 7. Each point has a color ranging from blue to red. The results for seed 1, which was used in the study of the AEB-P system, are available in appendices.
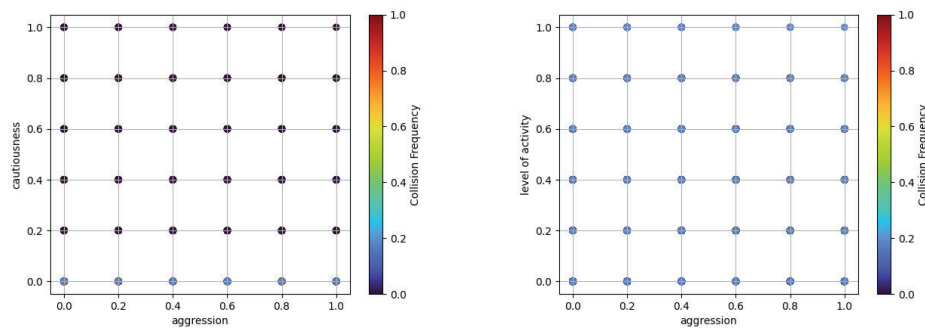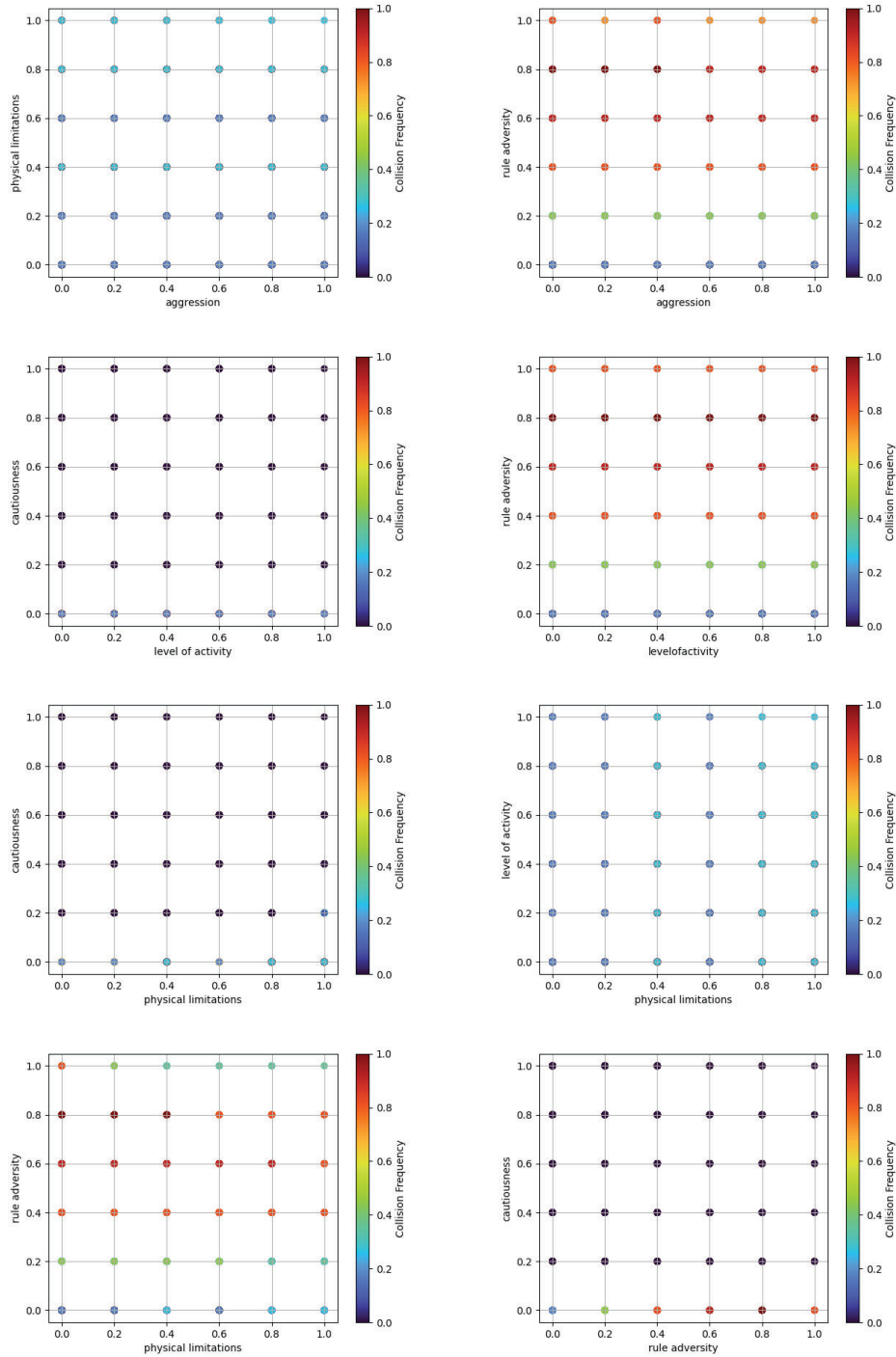
Figure 7. Pedestrian behavior profile parameter analyses. Dark blue means that in all cases the pedestrian was not hit by the vehicle, value of 0 on the scale, and dark red means that in all case there was a collision between the pedestrian and the vehicle, a value of 1 on the scale.

As was to be expected, the parameters "rule adversity" together with "cautiousness" were the parameters with the greatest influence on collision rate. With rule adversity greater than or equal to 0.4, in all cases (rule adversity vs physical limitation, rule adversity vs level of activity, rule adversity vs aggression) there were collisions between pedestrian and vehicle, once the pedestrian tried to cross the road without waiting at the curb. With "cautiousness" greater than 0.0 the pedestrian tends to wait at the curb, so in the cautiousness vs rule

adversity graph, for cautiousness values above 0.2 there were no collisions. A cautious behavior profile also led the pedestrian to cross at designated cross-sections.

Another parameter with greater relevance is physical limitations. The presence of light blue dots was observed for values of physical limitations higher than 0.4, indicating that in some seeds there was a collision, see the diagrams physical limitations vs aggression, level of activity vs physical limitations and cautiousness vs physical limitations. In these cases, the pedestrian chose to cross the road before the vehicle passed, but slowly due to the higher "physical limitations". In other seeds the pedestrian opted to wait at the curb, avoiding the collision.

The combination cautiousness = 0.0, rule adversity = 1.0, physical limitations=1.0, aggression = 1.0 and level of activity = 1.0 is the combination that leads to the riskiest behavior in the analyzed scenario and was used in the simulations to evaluate the AEB-P.

Using this setting, the neuro-cognitive model presented either one of the following behavioral patterns:

1. walk to the curb, wait, and walk or run across the road in front of the vehicle.
2. walk to the curb, wait, and walk or run across the road after the vehicle has passed.
3. cross the road without waiting at the curb.

In none of the above cases did the pedestrian use the crosswalk when crossing the road.

Performance assessment of the AEB-P system
A total of 165 cases were simulated, varying the initial distance between vehicle and pedestrian, vehicle initial speed, and vehicle waiting time. In 16 cases frontal collisions between vehicle and pedestrian occurred, which represents 9,7% of all cases. Of these 16 cases, 3 were prevented by the AEB-P system, which represents a reduction of 18.8%.

The avoided collisions can be divided into two groups. In two cases the vehicle was able to stop completely and therefore avoided the collision. In 1 case, with the application of AEB-P, the vehicle reduced its speed, giving the pedestrian enough time to leave the conflict region before colliding with the vehicle.

DISCUSSION

In [20] the application of an AEB-P system reduced the collision rate by was 24.1%. In that study, however, the braking profile had a larger maximum deceleration of $7\ m/s^2$ and a longer delay of 0.25 s. Other studies found collision reduction values ranging from 20% to above 50% [20], when using different approaches and virtual environments. [11] used a machine learning based pedestrian behavior model and found values between 19.4% to 38.8%, depending on the braking profile. The performance of 18.8% is slightly lower compared to previous results. However, this finding is unlikely to represent a significant difference due to the low number of positive test cases. Assuming that by using the neuro-cognitive model more valid simulation results are produced, the observed difference might indicate a lower performance of the AEB-P system in real life situations in comparison to previous simulations results.

In contrast to previous studies, the neuro-cognitive pedestrian model varied the road crossing path as well as the walking speed, and often waited at the curb before crossing. The high value in behavioral variation has probably led to more false-negative assessments of the AEB-P system than in previous studies, where the pedestrian usually crossed the road in straight line without speed adjustment or waiting.

The model also produced situations of a false-positive activation of the AEB-P system. In these cases, the system was activated by mistake as the pedestrian was just standing at the curb waiting. Such a situation is not atypical in everyday life, and activation of the system in these situations can lead to a low acceptance of the system by consumers. It therefore becomes obvious that active safety needs to interpret and predict the pedestrian's intentions in such situations.

[18] analyzed pedestrian crossing behavior on different road infrastructure (number of lanes, designated and non-designated cross-sections), weather conditions, and gap between pedestrian and vehicle. The main pedestrian reactions to the approaching vehicle were "stop", "clear path", "slow down", "speed up", "hand gesture" and "nod". "Stop" and "clear path" behaviors can be considered as cautious collision avoidance

strategies, and while "speed up" is representing greater rule compliance. Both behaviors were observed on the neuro-cognitive behavior model. "Hand gesture" and "nod" represents explicit communication between pedestrian and vehicle and are not yet implemented in the model. A "step-back" behavior was disabled due to limitations of the avatar in the simulation environment to handle it.

CONCLUSIONS AND FUTURE WORK

This paper aimed to evaluate the performance of a generic AEB-P system using the cogniBIT's neuro-cognitive pedestrian behavior model. The novel model is able to reproduce more complex behaviors with less effort than the conventional trajectory-based models, commonly used in commercial tools.

Of course, the study presented does not represent a complete evaluation of the neuro-cognitive pedestrian model. A more in-depth analysis evaluating for instance trajectories, gaze patterns, interactions should be considered in the future. The neuro-cognitive model in its current implementation is able to generate realistic pedestrian road crossing scenarios, but still limited in the types of pedestrian-vehicle interaction. By adding explicit and implicit communication mechanisms on both sides, pedestrians and driver [18] this limitation can be removed in the future.

ACKNOWLEDGMENTS

REFERENCES

[1] Alvarez, S., Page, Y., Sander, U., Fahrenkrog, F., Helmer, T., Jung, O.,Hermitte, T., Düering, M., Döering, S. Op den Camp, O. 2017. „Prospective Effectiveness Assessment of ADAS and Active Safety Systems via Virtual Simulation: A Review of the Current Practices." 25th International Technical Conference on the Enhanced Safety of Vehicles (ESV).
[2] Aoyagi, S., Hayashi, R., Nagai, M. 2011. "Modeling of Pedestrian Behavior in Crossing urban Road for Risk Prediction Driving Assistance System. 16th Asia Pacific Automotive Engineering Conference."
https://doi.org/10.4271/2011-28-0085
[3] Bandyopadhyaya, Ranja & Kumar, Chandan. 2022. "PEDESTRIAN CROSSING BEHAVIOUR IN MIXED TRAFFIC."
[4] Bechler, F., Fehr, J., Neininger, F.T., Knöß, S., Grotz, B. 2022. „Bipartite Graph Modeling of Critical Driving Scenarios - an Occupant Safety Perspective". ARGESIM Report 17, p 25-26, DOI: 10.11128/arep.17.a17060
[5] Bernhard, J., Schulik, T., Schutera, M., Sax, E. 2021. "Adaptive test case selection for DNN-based perception functions," 2021 IEEE International Symposium on Systems Engineering (ISSE), pp. 1-7, doi: 10.1109/ISSE51541.2021.9582499.
[6] Camara, F., Belloto, N., Cosar, S. et al. 2021. "Pedestrian Models for Autonomous Driving Part II: High-Level Models of Human Behavior". IEEE Transactions on Intelligent Transportation Systems, vol. 22, no. 9, pp. 5453-5472, doi: 10.1109/TITS.2020.3006767.
[7] Decae, R. 2022. "Annual statistical report on road safety in the EU, 2021". European Road Safety Observatory. Brussels, European Commission, Directorate General for Transport.
https://roadsafety.transport.ec.europa.eu/statistics-and-analysis/data-and-analysis/annual-statistical-report_e
[8] Dijkstra, J., Jessurun, A. J., & Timmermans, H. J. P. 2001. "A multi-agent cellular automata model of pedestrian movement". In M. Schreckenberg, & S. D. Sharma (Eds.), Pedestrian and Evacuation Dynamics (pp. 173-181). Springer.
[9] Dosovistikiy, A., Ros, G., Codevilla, F., Lopez, A., Koltun, V. 2017. "CARLA: An Open Urban Driving Simulator". Proceedings of the 1st Annual Conference on Robot Learning. PMLR Vol. 78 of Proceedings of Machine Learning research, pp 1-16. https://doi.org/10.48550/arXiv.1711.03938
[10] Euro NCAP, 2019. Test Protocol – AEB VRU Systems (Online). https://cdn.euroncap.com/media/53153/euro-ncap-aeb-vru-test-protocol-v302.pdf (Accessed 11 December 2022).
[11] Fonseca Alexandre de Oliveira, L. & Meywerk, M. & Schories, L. & Meier, M. & Nanjundaiah, R. & Victor, P. & Foglino, F. & Carroll, M. & Muralidharan, A. 2022. "Influence of different pedestrian behavior models on the performance assessment of autonomous emergency braking (AEB) systems via virtual simulation", Proceedings of the 7th International Digital Human Modeling Symposium 7(1): 7, 10 pages. doi: https://doi.org/10.17077/dhm.31753

[12] Hay, J. (2022). "A Surrogate Model-enhanced Simulation Framework for Safety Performance Assessment of Integrated Vehicle Safety Systems." [Doctoral Dissertation]

[13] Helbing, D. 1998. "Models for Pedestrian Behavior." arXiv: Statistical Mechanics.

[14] Jamil, R., Fang, Z., Kong, X. 2015. „Pedestrian Crossing Patterns Preference at Non-signalized Crosswalk". DOI: https://doi.org/10.1016/j.promfg.2015.07.496

[15] Knorr, A. G., Willacker, L., Hermsdörfer, J., Glasauer, S., & Krüger, M. 2016. „Influence of person-and situation-specific characteristics on collision avoidance behavior in human locomotion." Journal of experimental psychology: human perception and performance, 42(9), 1332. DOI: 10.1037/xhp0000223

[16] Naasah, N., Marzukhi, Marlyana A., Leh, Oliver L. H., Zaharah, M. Y., Nurul, S. K. 2020. "Modelling Pedestrian Crossing Behaviour based on Human Factor." EDP Sciences. DOI:10.1051/matecconf/202030803003

[17] Papadimitriou, E., Yannis, G., & Golias J. 2009. "A critical assessment of pedestrian behaviour models." Transportation Research Part F 12, 242-255, https://doi.org/10.1016/j.trf.2008.12.004

[18] Rasouli, A., Kotsureba, I., K. Tsotsos, J.K., 2018. "Understanding pedestrian behavior in complex Traffic Scenes." IEEE Transactions on Intelligent Vehicles, volume 3, Issue:1, pages 61-70, http://dx.doi.org/10.1109/TIV.2017.2788193

[19] ISO PDTR 21934 (2017). Road vehicles — Traffic safety analysis — Prospective safety performance assessment of pre-crash technology by virtual simulation. Traffic accident analysis methodology.

[20] Schachner, M., Sinz, W., Thomson,R., & Klug, C. 2020. "Development and evaluation of potential accident scenarios involving pedestrian and AEB-equipped vehicles to demonstrate the efficiency of an enhanced open-source simulation framework." Accident Analysis and Prevention, 148. https://doi.org/10.1016/j.aap.2020.105831

[21] Soni, A., Robert, T., Rongiéras, F., & Beillas, P. 2013. "Observations on pedestrian pre-crash reactions during simulated accidents." Stapp car crash journal, 57, 157–183. https://doi.org/10.4271/2013-22-0006

[22] Teknomo, K., Takeyama, Y., & Inamura, H. 2016. "Review on Microscopic Pedestrian Model." Proceedings Japan Society of Civil Engineering Conference. https://doi.org/10.48550/arXiv.1609.01808

[23] Wakim, C.F., Capperon, S., & Oksman, J. 2004. "A Markovian model of pedestrian behavior." IEEE International Conference on Systems, Man and Cybernetics, 4, 4028-4033 vol. 4. https://doi.org/10.1109/ICSMC.2004.1400974

APPENDICES

Behavior profile parameter analysis results for seed with a value of 1. The parameters that were not being varied had the default value of 0.
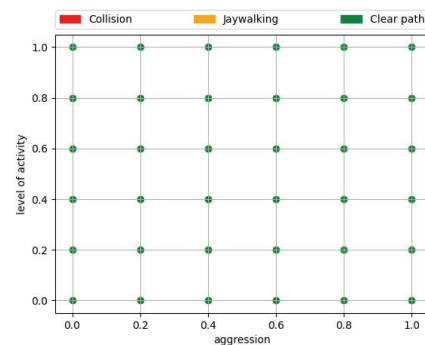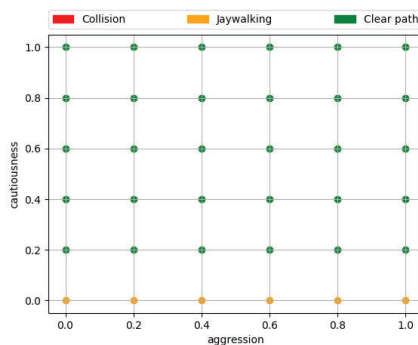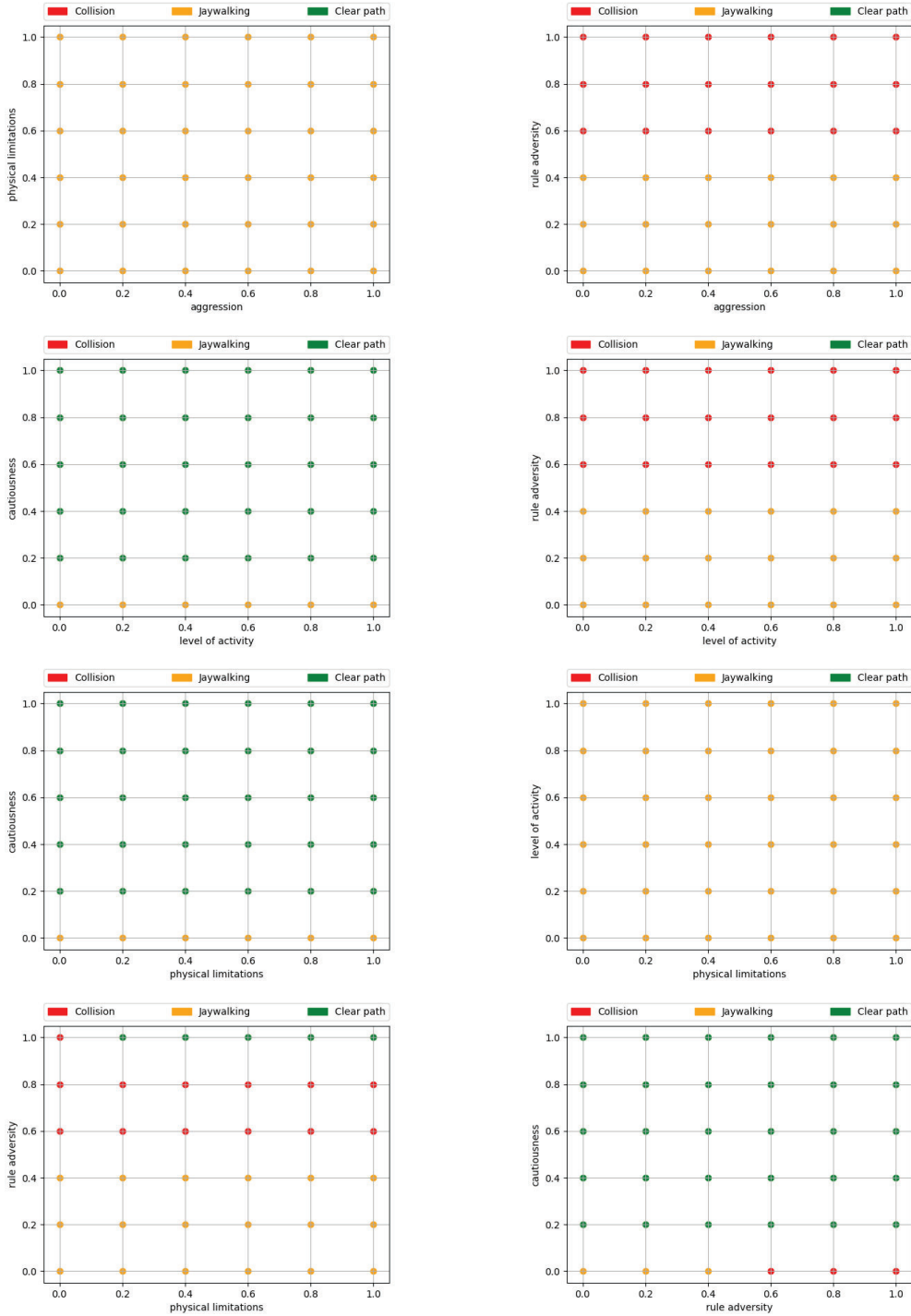
Figure 8*. Pedestrian behavior profile parameter analyses. Green means that the pedestrian waited the vehicle to pass, orange means the pedestrian tries to cross the road and reaches the other side of road without being hit by the vehicle and red means that there was a collision between the pedestrian and the vehicle.*

INVESTIGATION ON EFFECTS OF WHOLE-BODY KINEMATICS DURING COLLISION ON PEDESTRIAN INJURIES

Hidetoshi, Nakamura Hiroyuki, Asanuma Hyejin Bae
Honda R&D Co., Ltd.
Japan

ABSTRACT

Recently, pedestrian safety performance of vehicles has been improved by the modification of regulations and new car assessment programs (NCAPs). In particular, safety performance of the bonnet has been improved in terms of head protection by reducing HIC. According to the accident statistics, however, pedestrian fatalities account for a high percentage, and the causes of death include not only head injury but also thoracic and pelvis injuries. Therefore, pedestrian protection technologies need to include protection of these body regions in addition to the head. In order to reduce the number of pedestrian fatalities, this study aimed to investigate the effect of the whole-body kinematics on injury reductions of pedestrians.

In a collision between a bonnet-type vehicle and a crossing pedestrian, the whole-body moves in a chain reaction starting from the input to the legs, subsequently transmitted to the pelvis, the thorax, and the head. Therefore, it is expected that controlled pedestrian kinematics from the time of collision will have an effect on the injury to various body regions. In this study, the GHBMC 50th percentile male model and the vehicle model with general bonnet type was used to simulate car-pedestrian collisions. A model composed of spring and shell elements was affixed to the vehicle model to apply controlled loads to the center of gravity of the pedestrian model by changing the stiffness characteristics of the model, and the relationship between the whole-body kinematics of the pedestrian model and the injury values was investigated at a collision speed of 40 km/h.

The results confirmed that the angular velocity of the upper body around the center of gravity was reduced by the early input to the pedestrian pelvis, effectively reducing thoracic input and the head injury value.

Input to the pelvis depends on the input through the legs and the external force from the vehicle. Since the vehicle used in this study had a low bonnet height, there was little external force from the vehicle to the pelvic region, potentially diminishing the effect of restraining the center of gravity. Since this study used a specific collision speed and a pedestrian size, it is necessary to consider the influence of these factors in a future study.

This study clarified that pedestrian kinematics control technology may be one of the effective measures to further reduce pedestrian fatalities.

INTRODUCTION

The number of Traffic accident fatalities in Japan is are trending downward, fatalities in 2021 decrease by about 40% compared to that in 2011 [1]. However, the number of pedestrian fatalities accounted for 35% of overall fatalities in 2021, this rate has been continued to be the highest among the fatality groups for over 10 years. In terms of evaluation of pedestrian safety performance of vehicles, the head (HIC) and lower limb(the bending moment of the bones and the elongation of knee ligaments) injury evaluation using subsystem impactors are performed. Accidents in the real world include not only these injuries, but also brain injuries due to head rotation during collisions, thoracic injuries and pelvic injuries. However, current sub-system impactor is incapable of evaluating brain injury caused by head rotation and in addition, there is no evaluation method for thoracic and pelvic injuries. In many pedestrian accidents, the collision phenomenon starts with the input from the vehicle to the pedestrian's legs, upper body rotates toward the vehicle due to occur movement of the waist close to the pedestrian's center of gravity. Rotation of the upper body becomes rotational energy that causes thoracic injuries, and furthermore, it becomes a factor that causes brain injury due to head rotation. Finally, the head injury occurs when the head collides

with the vehicle. In a pedestrian accident, the injury region changes over time due to the input from the vehicle and the pedestrian whole-body kinematics. (Figure 1). Thus, the evaluation by entire body of a pedestrian is useful for investigating the mechanism of real-world pedestrian accidents. Nakamura et al. [2] investigated the effects of the input to the body regions on the whole-body trajectories and the brain injury by using the dummy model and a production car model with the restraint surface connected to the center of gravity of the vehicle model by the spring element. As the results of the study, it was found that the input to the pelvis influenced to the kinematics of the whole-body pedestrian and the brain injury. But, in order to reduce the number of pedestrian fatalities, it is also necessary to investigate the injury measures of the thorax and the pelvis. Since the pelvis of the dummy was rigid, the evaluation by using a human body model is needed to investigate in detail. In order to reduce the number of pedestrian fatalities, this study aimed to investigate the effects of the whole-body kinematics on the injury reductions of pedestrians.
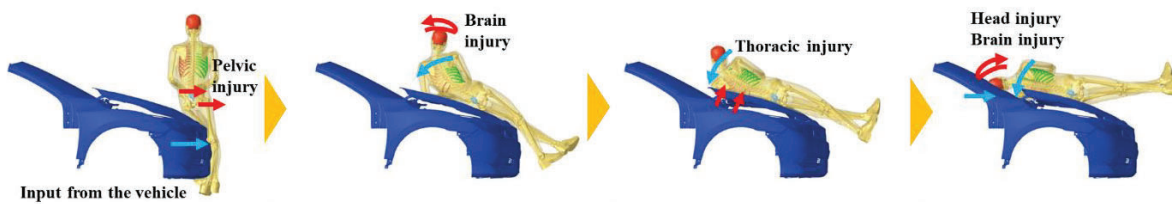

Figure 1. Pedestrian Collision Flow

METHODS

Verification of effects from waist restraint close to the pedestrian's center of gravity
In this study, a pedestrian human body model (HBM) capable of studying the whole-body kinematics was used. For verification, the 50th percentile male model of the simplified Global Human Body Models Consortium (GHBMC) ver1.4 pedestrian model. All simulations were performed by the LS-Dyna R9.2.0. As the pedestrian kinematics is thought to be influenced by depend on the restraint of the center of gravity, a sedan type vehicle model which exerts little force on the waist close to the center of gravity was selected in this study. In order to change pedestrian whole-body kinematics, a waist restraint surface was added to a standard sedan model vehicle. The restraining surface and vehicle were connected by a spring element with load-displacement properties. (Figure 2) (Table 1) The effect of changing pedestrian kinematics was verified by comparing models with and without waist restraint surface. Vehicle models with different restraint characteristics were made to collide with the pedestrian model at 40 km/h from the left side.
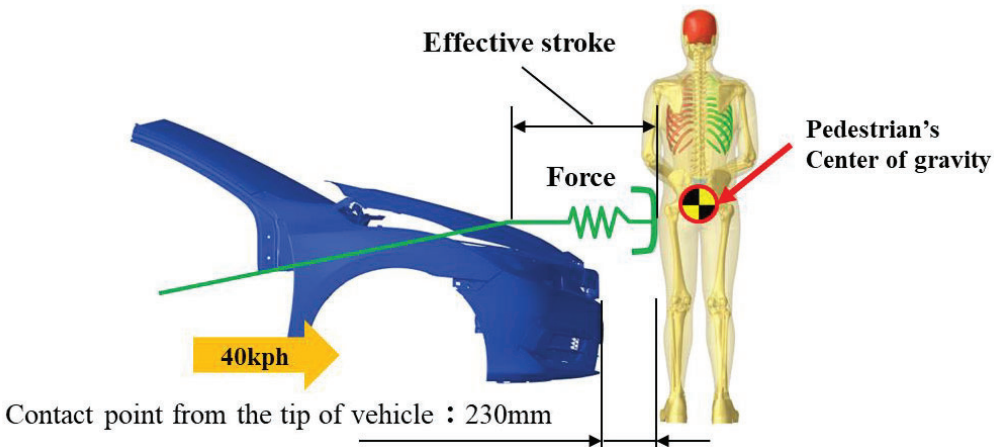

**Figure 2. Structure of vehicle model and evaluation method of pedestrian kinematics**

Table 1.
Restraint characteristics

	Spring characteristic		
	Force (N)	Effective stroke (mm)	Energy (J)
Original	N/A	N/A	N/A
Case (a)	2500	390	731
Case (b)	3000	390	878
Case (c)	3500	390	1024
Case (d)	4000	390	1170
Case (e)	4500	390	1316

Evaluation items

The effects of changing pedestrian kinematics were evaluated by the trajectory of the pedestrian, angular velocity around the pedestrian's center of gravity and injury criteria. Trajectories of the pedestrian were measured at the Head, T4, T8 and Pelvis relative to the vehicle models. The angular and translational velocity of the pedestrian's center of gravity were calculated based on the relative displacement of the waist and the T1 displacement in lateral and vertical directions. HIC was used as the injury criteria for the head injury. The brain injury was evaluated by using Convolution of Impulse Response for Brain Injury Criterion (CIBIC) developed by Takahashi et al. [3] In the past study, the multiple peaks of CIBIC were seen in both pre-impact (head swing) and impact (the head collides to the vehicle) phase in the simulation of the collision between the AM 50th percentile male pedestrian model and the vehicle models [4]. Thus, CIBIC was also evaluated in both pre-impact and impact phases in this study. In addition, in pre-impact phase, the relationship between CIBIC in pre-impact and the angular velocity around the pedestrian's center of gravity was calculated in order to investigate the effect of the angular velocity on CIBIC. In the impact phase, the relationship between the injury measures (HIC and CIBIC) and the impact velocity of the head were also investigated. The head impact velocity was calculated by the velocity of the head in x, y and z direction relative to the vehicle model.

The input to thorax was evaluated by the acceleration of the ribs of the left side. Pelvic injury was evaluated by the sacrum force and pubis force measured at the sagittal plane. Evaluation items are described in Figure 3.
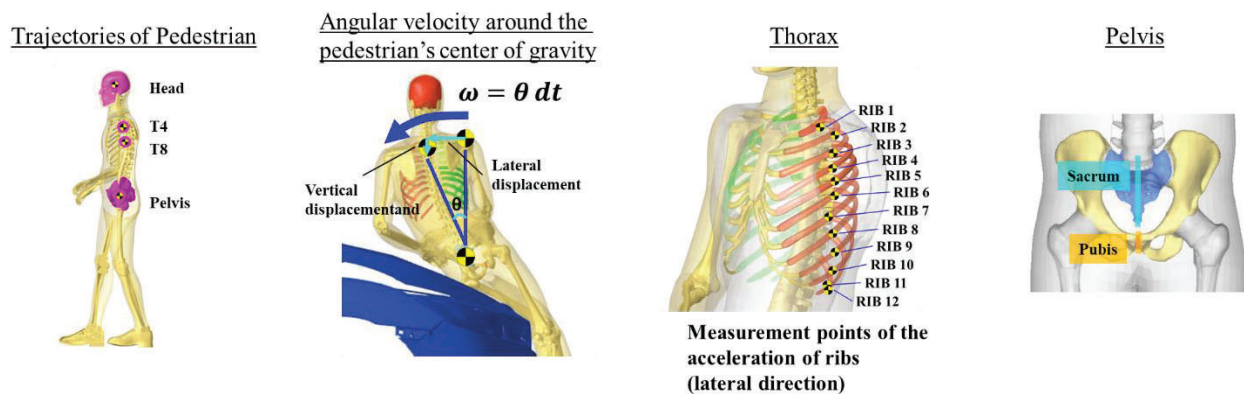
Figure 3. Evaluation items

RESULTS

Comparison of trajectories, angular and translational velocity
Figure 4 shows the trajectories of the landmarks (the head, T4, T8 and pelvis) of the pedestrian human models collided with the restraint characteristic vehicle models relative to the vehicle models. The wrap around distances of the head, T4, T8, and pelvis were decreased with increasing the input force to the waist of the pedestrian model. To analyze the pedestrian kinematics, figure 5 and 6 show the time histories of the angular velocity and translational velocity of the center of gravity of the pedestrian, respectively. The angular velocity at around 50msec increased and the angular velocity at around 100msec decreased as the input to the waist from the vehicle increased (Figure 5). The time of the beginning of increasing and the peak values of the translational velocity showed almost the same tendency as those of the time histories of the angular velocity (Figure 6).
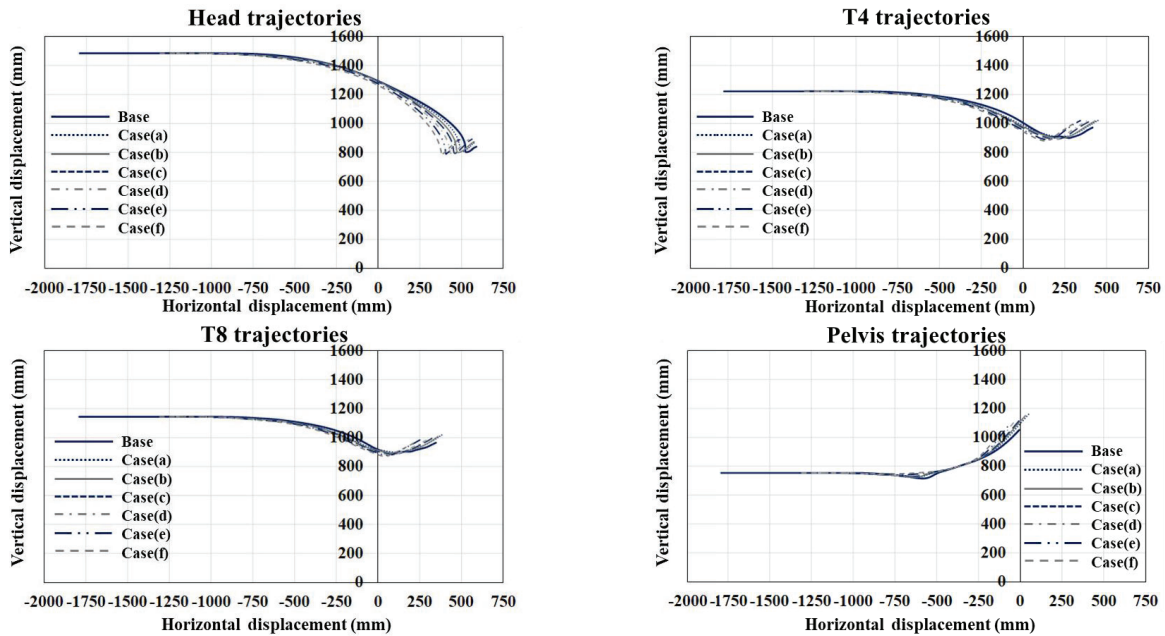

Figure 4. Trajectories of pedestrian with different restraint characteristics
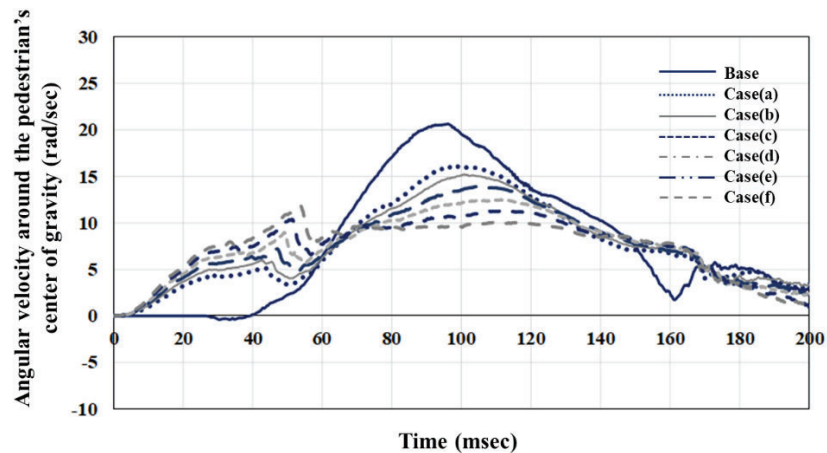

Figure 5. Time history of Angular velocity around the pedestrian's center of gravity
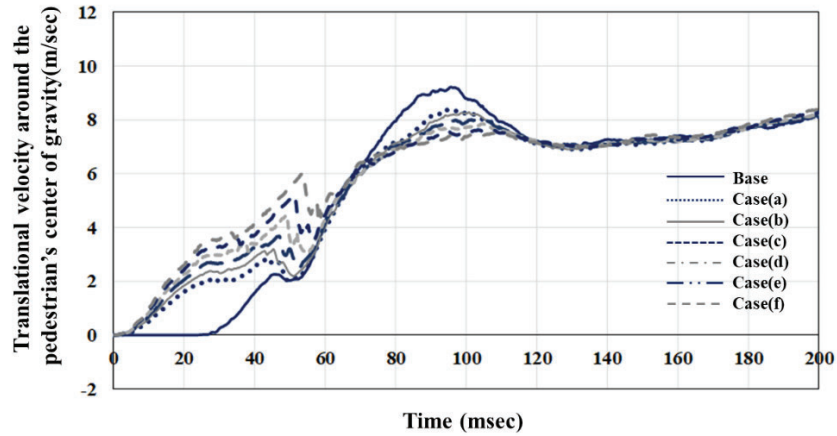
Figure 6. Time history of translational velocity around the pedestrian's center of gravity

Comparison of injury levels

Figure 7 shows the time histories of CIBIC calculated in all cases. The peak value of the strain in the brain occurred during both the pre-impact and impact phase in all cases.
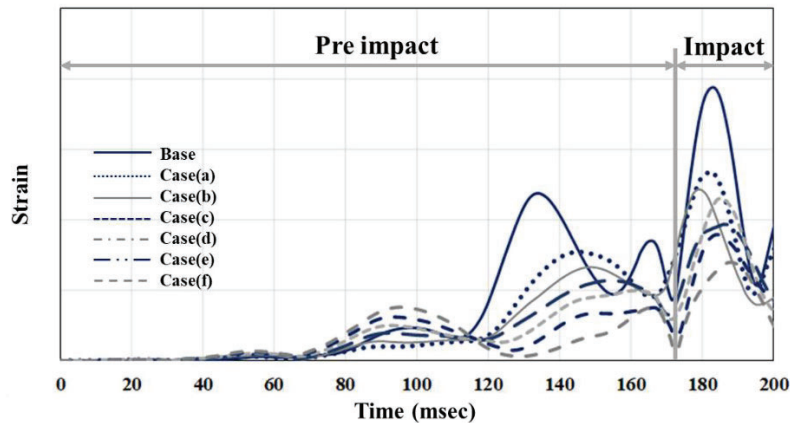

Figure 7. Comparison of CIBIC time histories

Figure 8 and 9 show the comparison of CIBIC in pre-impact by normalizing these values by that of the base model and the correlation between normalized CIBIC in pre-impact and the peak value of the angular velocity of the center of the gravity of the pedestrian model, respectively. Normalized CIBIC in pre-impact of case (a) was decreased to 64%. Normalized CIBICs in pre-impact were decreased with increasing the input force to the waist of the pedestrian model, showing the minimum value in case (e) (Figure 8). That of case (f) was equivalent to that of case (e). The coefficient of determination between normalized CIBIC in pre-impact and the peak value of the angular velocity was 0.9913 (Figure 9).

Figure 10 and 11 show the comparison of CIBIC in impact by normalizing these values by that of the base model and the correlation between normalized CIBIC in impact and the head impact velocity, respectively. Normalized CIBICs in impact of case (a), (b), (c) and (d) were decreased to about 50% (Figure 10). In addition, they were further decreased from case (d) to case (f). The coefficient of determination between normalized CIBIC in-impact and the head impact velocity was 0.9393 (Figure 11).

Figure 12 and 13 show the comparison of HIC by normalizing these values by that of the base model and the correlation between normalized HIC and the head impact velocity, respectively. The tendency of the comparison of normalized HIC was similar to that of normalized CIBIC in impact (Figure 12). That of case (f) with the maximum input to the pelvis showed minimum value. The coefficient of determination between normalized HIC and the head impact velocity was 0.9748 (Figure 13).

Figure 14 shows the comparison of the peak values of the accelerations of the ribs by normalizing these values by those of the base model. Except for the ribs between rib4 and rib9, the accelerations of the ribs with the restraint waist surface were lower than those of the base Model. In those of the ribs between rib4 and rib9, although they were also lower than those of the base model in most of cases, there are some cases that the accelerations were higher than those of base model. Figure 15 shows the comparison of the peak values of the sacrum force and pubis force by normalizing these values by that of the base model. The normalized sacrum force in case (a) was decreased to 86%. However, it was increased with increasing the stiffness of the waist restraint surface, exceeding that of base model in case (d). The normalized pubis forces showed almost the same tendency.
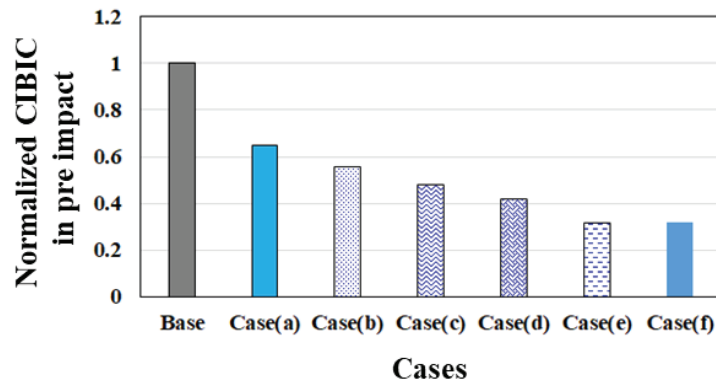

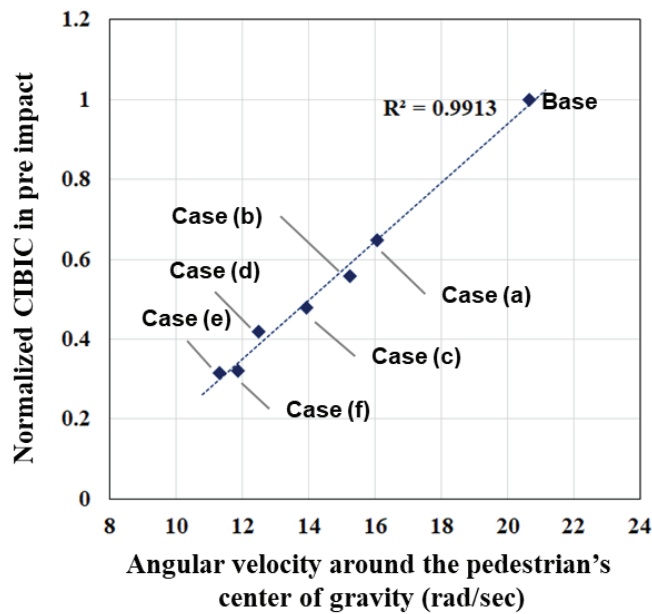**Figure 8. Comparison of CIBIC in pre-impact normalized by result from base model**

Figure 9. Correlation between normalized CIBIC in pre-impact and the maximum value of the angular velocity of the center of the gravity of the pedestrian model
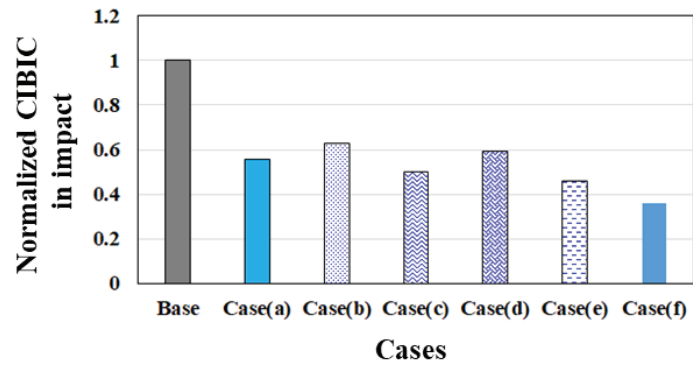

Figure 10. Comparison of CIBIC in impact normalized by result from base model
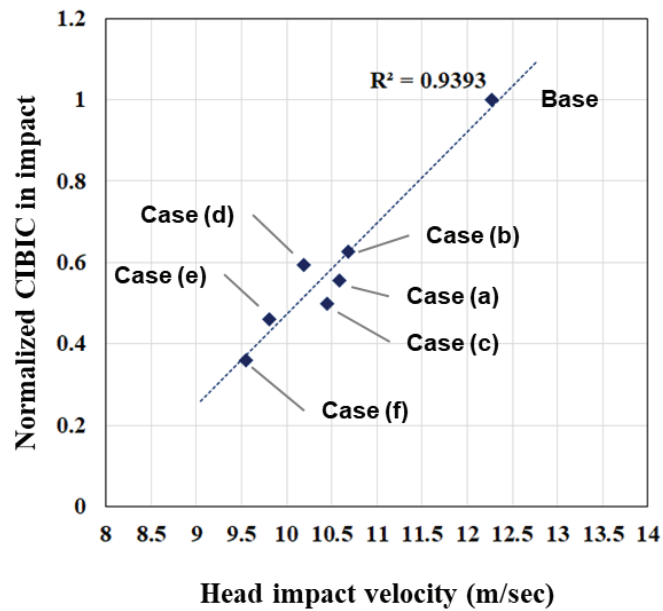
Figure 11. Correlation between normalized CIBIC in impact and the head impact velocity
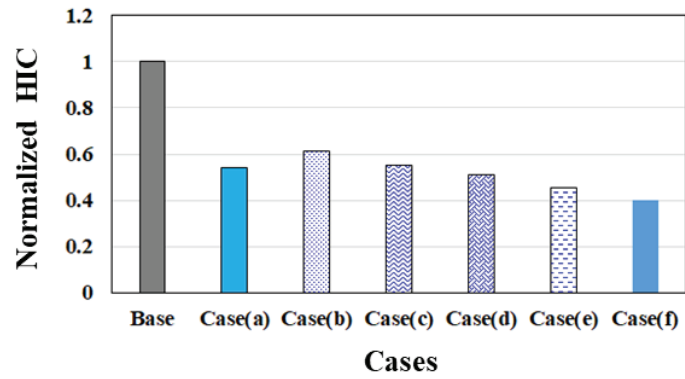
Figure 12. Comparison of HIC normalized by result from base model

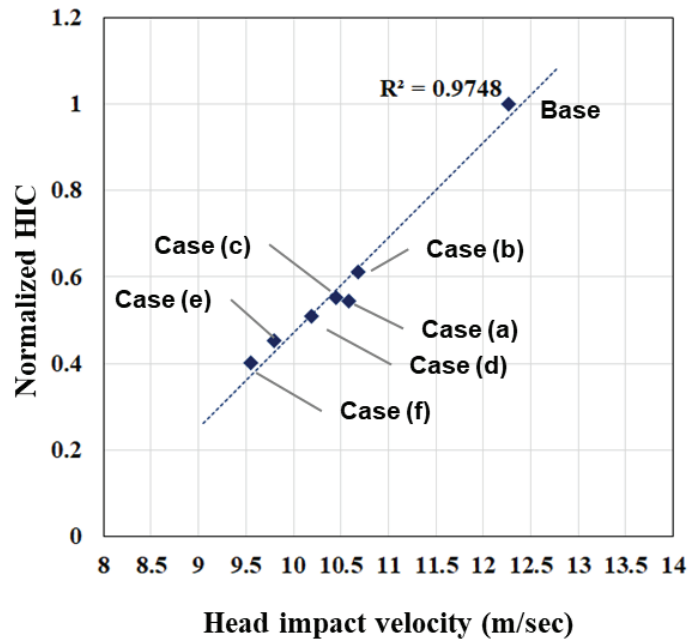**Figure 13. Correlation between normalized HIC and the head impact velocity**
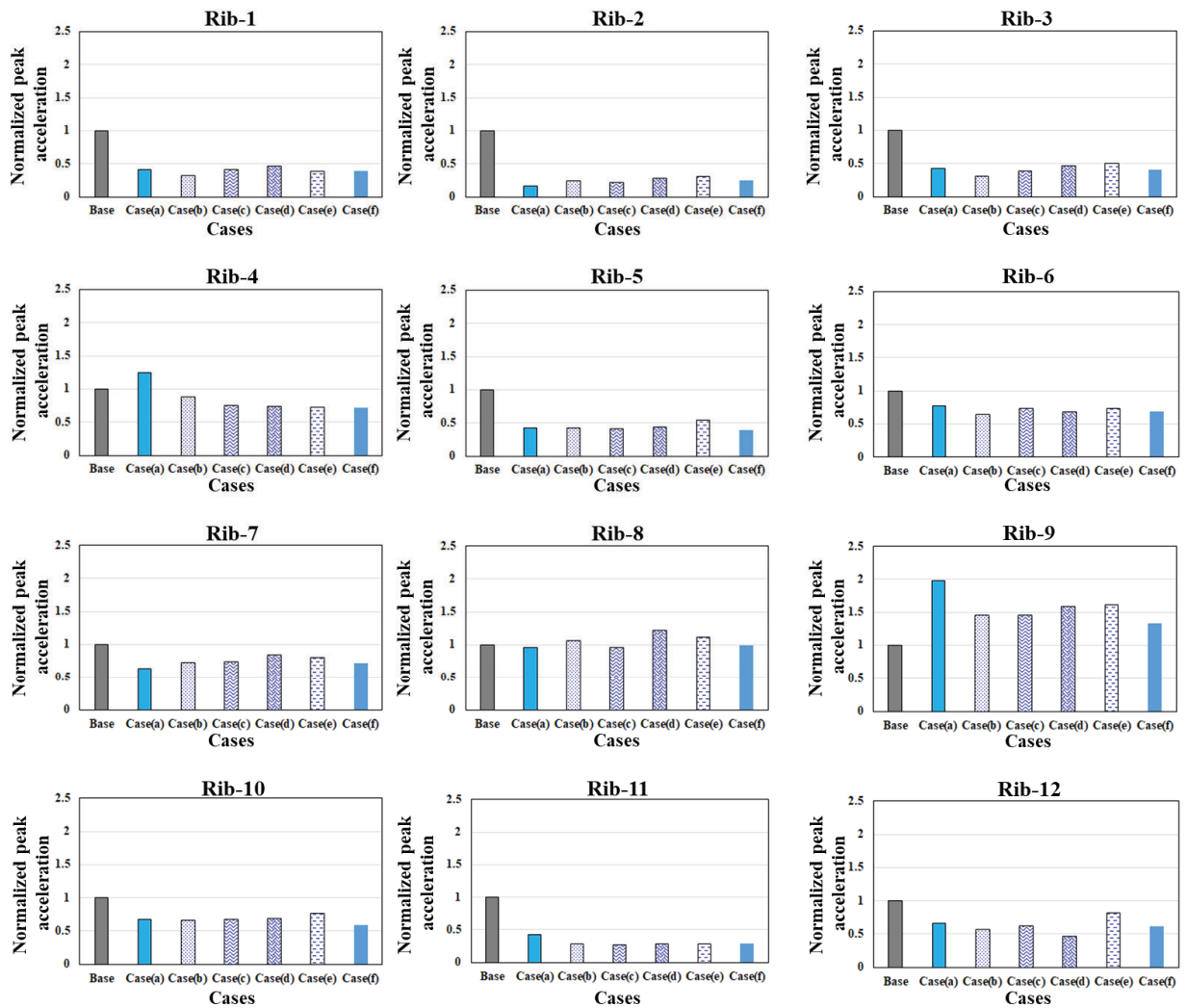
Figure 14. Ratio of the width between each rib and the spine at the timing of the maximum deflection to that of the original conditions from rib 01 to rib 12 of the impact side
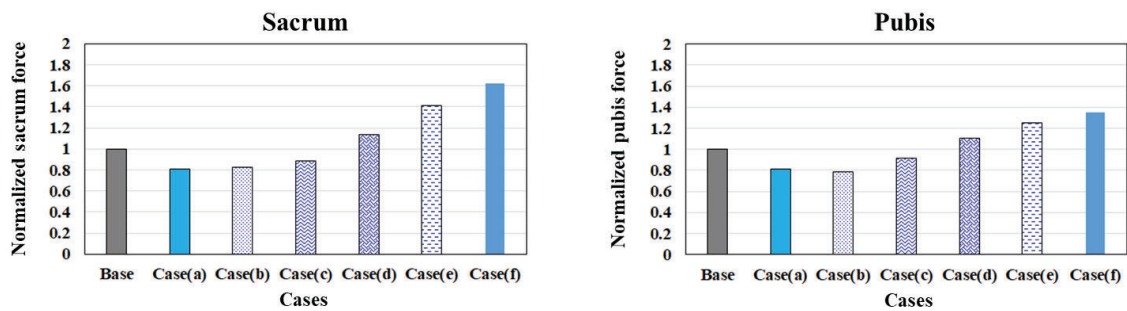

Figure 15. Comparison of the peak values of the sacrum force and the pubis force normalized by result from base model

DISCUSSION

 As the results of the simulations that the human body model was collided with the vehicle model adding the waist restraint surface, CIBIC (pre-impact and impact phase) and HIC were reduced, showing the minimum injury values about the maximum input force to the waist. As shown in the time histories of the angular and translational velocities of the center of gravity, the times of these starts were earlier by increasing the input force to the waist, decreasing the slopes of the time history of them. They led to the decrease of the angular acceleration of the upper body. By the influence of the upper body regions kinematics, the angular accelerations of the head were also reduced. Since CIBIC is calculated by the angular acceleration of the head, the values were reduced. By increasing the waist input, the velocity of the center of the gravity with respect to the ground is increased, so the velocity of the center of the gravity with respect to the vehicle is reduced accordingly. Due to the interaction of the upper body regions, lowering the velocity of the center of the gravity leads to lowering the velocity of the head relative to the vehicle, reducing HIC. Reducing HIC means reducing the reaction force from the surface of the vehicle to the head. Since in the impact phase, the head rotated around the shoulder that contacted with the vehicle, the angular acceleration of head in the impact phase increases with increasing the head velocity. Increasing the input force to the waist leads to decreasing the angular acceleration of the head. Thus, CIBIC was reduced by increasing the input force to the waist. As shown in above, CIBIC in both pre impact and impact phase and HIC was reduced by the larger input force to the waist. Generally, increasing the input force to the waist leads to increasing the risk of the fracture of the pelvis. In the case that showed the minimum value of CIBIC in both pre impact and impact phase and HIC, the sacrum and pubis forces were increased compared to the base model. In the most of cases with the restraint waist surface, the accelerations of the ribs were lower than those of the base model. However, in the region around the arm, those of the ribs were higher than those of the base model. It is thought that the contact between the arm and the thorax influenced the acceleration of the ribs,

A future study needs to focus on the compatibility of the injury measures of these body regions. As one way to do this, the methods the input force to the waist is changed from the concentrated to the distributed force.

CONCLUSIONS

In this study, the effects of whole-body kinematics from the phase of the first contract between the lower body of the pedestrian and the vehicle to that of the head impact were investigated by controlling the input to the pelvis. As the results of this study, the conclusions as shown in below are reached.

The injury measures in the phase of the head swing (CIBIC) and that of the head impact (HIC and CIBIC) can be reduced by controlling the value of the input to the pelvis. Investigation about compatibility of the injuries of the head and the pelvis is needed in order to reduce the injuries of these parts. These results will contribute to the reduction of the number of the pedestrian fatalities. The investigation was conducted by using the standard sedan model vehicle model and the 50th percentile male model in this study. However, the whole-body response is influenced by the geometry of the vehicle and the size of the pedestrian. It is necessary to investigate these influences.

REFERENCES

[1]   e-Stat Portal Site of Official Statistics of Japan, "Statistics about Road Traffic 2021".

[2]   Nakamura, H., Okamura, K., Umezawa, M., Ito, O., Asanuma, H., Sasaki, M., "RESEARCH OF PEDESTRIAN INJURY REDUCTION MECHANISM BETWEEN THE BEGINNING OF THE COLLISION AND FALL OF THE GROUND." 26th ESV conference, Paper Number: 19-0285

[3]   Takahashi, Y., Yanaoka, T. 2017. "A study of injury criteria for brain injuries in traffic accidents." Paper presented at: 25th ESV conference, Paper Number: 17-0040.

[4]   Yanaoka, T. and Takahashi, Y. and Sugaya, H. and Kawabuchi, T. 2019. "INVESTIGATION OF STRAIN-INDUCED BRAIN INJURY MECHANISM IN SIMULATED CAR ACCIDENTS." 26th ESV conference, Paper Number: 19-0070.

THE "TYPICAL" CAR-CYCLIST COLLISION UNDER THE MICROSCOPE: A GIDAS-BASED ANALYSIS OF THE PREVALENT CRASH SCENARIO

Niklas Puller
Gwendal Lucas
André Leschke
Volkswagen AG
Germany

Oliver Maier
Jörg Mönnich
Robert Bosch GmbH
Germany

Vittorio Rocco
Università degli Studi di Roma "Tor Vergata"
Italy

Paper Number 23-0270

ABSTRACT

In a world where reducing the carbon footprint is crucial, riding carbon-neutral vehicles such as bicycles or pedelecs is a sustainable and thus desired way of transport. Since motorized and unmotorized bicycles are missing any protective body, their riders are part of the vulnerable road users (VRUs). In order to increase the attractivity of transport by bicycle and pedelec, providing traffic safety for this group must be ensured.

To get a better understanding of cycle crashes, this paper's objective is to deduce the most important crash types of collisions of cyclists with passenger cars. By obtaining the characteristic details of these crashes, strategies for crash avoidance can be derived.

The **data source** used for the results presented in this paper is GIDAS (German In-Depth Accident Study). GIDAS is a unique database as the input data is provided by experts on crash reconstruction who join the police at the crash site and record the crash in great detail. 8497 relevant crashes involving bicycles, captured from 2000-2021, were evaluated.

The **methodology** consists of the evaluation of the two most common crash types regarding speed distributions and contact points of the crash opponents, street layout, driver intent, traffic density, and visual conditions.

The **results** show that the most common crashes are two crossing crash types accounting for nearly a third of all crashes between cyclists and drivers of motorized vehicles. Both of these crash types are characterized by the cyclist riding on the designated cycling infrastructure, while in the more common one, the cyclist goes against the expected direction for the crash opponent.

For the selected crash types, the results also show that more than half of crashes occur at junctions, predominantly where the driver has to yield. Most crashes occur during turning right maneuvers at low traffic densities and speeds below 13 kph. The evaluation of the car driver's maneuvers performed in the last second before the crash indicates a black spot in driving-off situations. In more than 70 % of the cases, the contact point with the cyclist is at the front. The data, analyzed in detail in the **discussion**, points towards the theory that drivers tend to "fail to look" at cyclists coming from the right and "look but fail to see" cyclists from the left. Furthermore, cyclists crossing from the right might not be expected in right-hand traffic.

A general **limitation** of official crash data sources based on police reports is a high underreporting rate of bicycle crashes. Using the German crash database, also certain bias towards countries with similar traffic infrastructure must also be assumed. This is further analyzed in the discussion.

The **conclusions** drawn from this study show that cycling infrastructure remains of the highest importance and needs to be designed in accordance with the human factor in traffic. Also, communication between involved parties can contribute largely to tackling the most dominating crossing crash types, i.e., virtually enhancing the cyclist's visibility for other traffic participants.

INTRODUCTION

In a world where reducing the carbon footprint is crucial, riding carbon-neutral vehicles such as bicycles or pedelecs is a sustainable and thus desired way of transport. Going by bike or pedelec also helps reduce traffic congestion in urban areas. Cycling in road traffic, however, involves dangers not present in other kinds of transport: crashes often lead to severe injuries due to the marginal to non-existing structural protection in collisions. As a consequence, cyclists are classified with the so-called vulnerable road users (VRUs) [1]. Due to the high crash risk, cyclists often tend to avoid certain routes or journey times [2].

Hence, preventing crashes and making cycling safer is an important step towards inclusive mobility. To prevent crashes, detailed knowledge about collisions and their causes is necessary. For example, to develop advanced driving assistance systems (ADASs) targeting crashes with VRUs, information about the expected speed of said VRU and the vehicle speed before impact is required.

Related Works

For a while, in crash research, car-cyclist collisions became a focus of attention, for example;

Summala et al. investigated car-cyclist crashes in Helsinki and found that the most dominant ones are those where the driver had to cross a cycle path while turning right and collided with a cyclist coming from the right [3]. They also showed that drivers turning right are focused on traffic from the left and fail to perceive cyclists coming from the right.

Car-cyclist crashes from the driver's perspective have also been investigated by Gohl et al. within the EU-funded PROSPECT project [4]. The authors defined use cases by analyzing the prevalent GIDAS crash types and ranked these based on frequency and injury severance. They identified the right turn subsets of two specific crash types, *UTYP 341 & 342*, as the fifth and first most relevant crashes. Referencing previous works (e.g., Summala et al.), they postulated that in crashes where the cyclist came from the right, the driver "failed to look", whereas in crashes where the cyclist came from the left, the driver "looked but failed to see" the cyclist.

The analysis of car-cyclist crashes for autonomous emergency braking (AEB) testing has been the subject of the CATS project. Within the project, Op den Camp et al. researched the main crash scenarios and demonstrated that the crossing scenarios are dominant throughout several European countries [5]. Uittenbogaard et al. later researched the crash parameters built on the selected crossing scenarios, showing, amongst others, that vehicle speed contributes to crash severity while cyclist speed does not [6].

During the European SAFE-UP project, Balint et al. determined safety-critical scenarios for VRUs in road traffic using the German In-depth Accident Study (GIDAS) pre-crash matrix (PCM) dataset [7]. The work contains an analysis of the last seconds of car-cyclist collisions, especially under the aspect of adverse weather conditions. They also identified the scenarios with cyclist crossing from the left and the right while the car approaches a junction as the most relevant.

Further studies outside of Europe are addressing the relevance of cyclist crossing crashes: E.g., MacAlister and Zuby demonstrated that straight-crossing crashes account for the highest number of car-cyclist crashes and the second highest number of fatalities in the USA [8]. Beck et al. analyzed cyclist crashes in Victoria, Australia, and found that crossing-path crashes are the second most common car-cyclist collision, just after crashes where both parties traveled in opposing directions [9].

Contribution

This work ties in with previous efforts to obtain more details about car-cyclist crashes. We aim to explore the most common crash scenarios between cyclists and cars using data from the GIDAS to be able to parametrize safety functions in later works. As already revealed in previous works, collisions where the car driver had to give way to a cyclist crossing on a cycleway are dominant in car-cyclist crashes: crashes where the cyclist came from the left (the far side in right-hand traffic) constitute 8 %, and crashes, where the cyclist came from the right 20.9 % of all collisions, making these the two most frequent crash scenarios.

In the following study, we focus on these two most common scenarios to not dilute the crash situation's characteristics with those of other scenarios. Yet, we differentiate the direction the cyclist is coming from as well as crash severity. In particular, we center on outlining the specifics of the "typical" crash, which occurs at junctions, in great detail to derive exact scenarios for developing and testing new ADASs. We reveal the similarities of car-cyclist crashes, for example, that most occur during the car turning right and into light traffic. We demonstrate that collisions

occur at relatively low speeds and that the car's speed increases the chance of severe injuries. Eventually, in accordance with previous works, we assume that drivers in turning maneuvers "fail to look" at cyclists coming from the right but "look but fail to see" cyclists from the left.

This work was inspired and influenced by the analysis of crashes in Europe performed within the SECUR project [10]. The SECUR publication focuses on identifying the main crash scenarios, aggregating similar crash types into groups, and analyzing characteristics of the identified scenarios, including but not limited to car-cyclist crashes. With the focus on describing the most common car-crash scenario for safety function development, we briefly share the methodology for identifying the characteristics of the relevant scenarios before focusing on a very particular subset of the car-cyclist crashes, the crash types *UTYP 341* and *UTYP 342*. The present work is, therefore, an extension of the SECUR study to provide further insights into two distinct and prevalent types of cyclist crashes and the differences between them.

The structure of the paper continues with Methodology, which contains a description of the GIDAS data set we used and the methodology we applied. Subsequently, in Results, we present the findings of our study. We discuss similarities and differences between the crashes as well as the applied methodology in Discussion. In Conclusions, we summarize our contribution and give an outlook on our follow-up research.

METHODOLOGY

The aim of the work is to sketch the "typical crash" between cars and cyclists as mentioned in Introduction. In the first step, we selected the most common crash scenario as described in Data source and scenario selection. Based on the selected subset, we analyzed the specifics of the most common crash scenario as described in Evaluation of selected crash cases. By fixating the analysis on a sole scenario instead of summarizing similar scenarios in groups, we aim to receive more precise results for the selected scenario. Since the study aims to get more insights into crashes for the development of novel safety functions, we mainly focused the evaluation on the car's perspective.

Data source and scenario selection

The analysis is based on the GIDAS database, containing a representative set of injury crashes in Germany since 1999 [11]. Experts who join the police at the crash site record extensive data about the crashes and reconstruct the course of events. Subsequently, the record containing up to 3500 data fields, including information about the crash type, vehicles, injuries, and environment, is saved in the database. For example, the crash type (GIDAS field *UTYP*) denotes the situational circumstances that led to the crash [12]. The level of detail in this database is considered unique in the world.

For our study, we focused on 8497 relevant crashes between 2000 and 2021, where the first collision of a passenger car, delivery van, or mini bus occurred with a cyclist (see also table 1). The crash types were then attributed to crash scenarios, combining collisions with a similar course of events. A first evaluation of the frequencies of the aforementioned scenarios showed that two very similar crash types are the most common: the collisions between cars in front of a junction that had to yield for crossing traffic with cyclists crossing on a cycleway (see also table 2). With a frequency of 1776 crashes (20.9 %), the cyclist coming from the right (*UTYP 342*) is the more common, while in 682 crashes (8 %), the cyclist comes from the left (*UTYP 341*) (compare fig. 1). In both cases, the cyclist has the right of way. Together, these account for 28.9 % of all car-cyclist injury crashes. Sorting instead by the highest share of crashes with killed and severely injured (KSI), *UTYP 342* also ranks 1st with 269 (14.6 %) out of 1837 KSI crashes, whereas *UTYP 341* ranks 4th with 127 (6.9 %) crashes.

Table 1.
Selected GIDAS crashes

Subset	Count	% of car-cyclist crashes
Car-Cyclist crashes	8497	100 %
... thereof UTYP 341 & 342	2458	28.9 %
... thereof urban crashes	2426	28.6 %
... thereof KSI crashes	392	4.6 %

Table 2.
Frequency distribution of the five most common car-cyclist crash scenarios

Rank	Rank KSI	Scenario	included UTYPEs	Count	Count KSI
1st	1st	before junction / car has to yield / cyclist from the right (on cycleway)	342	1776	275
2nd	4th	before junction / car has to yield / cyclist from the left (on cycleway)	341	682	127
3rd	10th	junction / turning right / cyclist in same direction on cycleway	242, 244, 275, 284, 285	560	61
4th	7th	junction / car has to yield / cyclist from left (on road)	301-303, 311, 312, 352	474	91
5th	2nd	junction / car has right of way / cyclist from the left (on road)	241, 243, 275, 284, 285	416	142
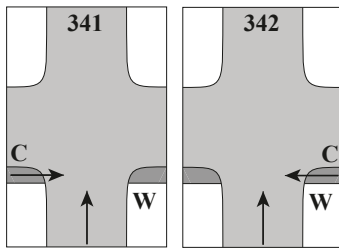
Figure 1. Schematic drawing of UTYP 341 and 342 as defined in [12]. C marks the cycleway and W marks that the car has to give priority to the crossing traffic.

Due to the similar nature of the crash scenarios *UTYP 341* and *UTYP 342*, we centered the following analyses on both types. Since 2426 or 98.7 % out of the 2458 crashes of the selected type and a predominant part of cyclist crashes, in general, occur in urban areas, we considered solely urban crashes in our evaluation.

Evaluation of selected crash cases

To get more details about the situational circumstances at the crash site, we performed a frequency analysis of the GIDAS data fields depicted in table 3 in *RStudio* [13] using the subset of cyclist crashes described in Data source and scenario selection. In each evaluation, non-applicable values or entries where no data was encoded were filtered out, reducing the size of the dataset. Furthermore, among the crash reconstruction data (REKO), we utilized the fields describing the speed over time in the last seconds before the crash (see also table 3). The data are split into sequences that denote a single action of one of the participants involved in the crash. For this, we linearly reconstructed the speed over time for each segment. After that, we attributed the labels *Accelerating* (Accel.), *Braking* (Brake.), *Constant speed* (Const.), and *Standstill* (Stand.) to each sequence, depending on the difference in speed of the last segment to the current segment. A speed below 3 kph is considered as *Standstill*. The sequences were then normalized so that they range from $t = -4s$ to the point of time of the crash, $t_0 = 0s$. Finally, we split the normalized sequences into intervals of 0.1 s duration.

We also considered using GIDAS PCM records which already provide time-sampled data for each road user involved in the crash. As we compared these to our reconstruction of speed profiles using the *REKO* record, it turned out that the speed profiles of the *REKO* data are a good approximation of the PCM data, so there is no benefit of using the PCM data instead. On the contrary, since there are more than twice as many records available in *REKO*, we gain better insights into the crash occurrence by using this source instead.

The fields *BRPX* and *BRPY* were used to reconstruct the collision points between cyclist and car.

<div align="center">

Table 3.
Evaluated GIDAS data fields

</div>

Records	Name	Description
BEFRAG	ABSICHT	Intention of action before crash
BETEIL	ANTSCH	Share of fault for the crash
	URSAMT1	Official cause of the crash
STRASSE	SICHTBV	Presence of permanent or non-permanent visual obstructions
	SICHTV	Kind of visual obstruction if present
UMWELT	STFUHO	Crash location
	TZEIT	Time of day regarding light conditions
	VKREG	Traffic regulation at crash site
	VSTUFE	Traffic density at time of crash
REKO	BRPX	Point of first contact of both opponents
	BRPY	
	SEQT	Duration of the sequence
	TREAKTV	Time in sequence until reaction
	TSYNC	Start of sequence regarding to global time
	V0	Speed at begin of the sequence
	VK	Speed at the end of the sequence / the collision

RESULTS

The first subsection of this chapter, Environmental circumstances, contains the analysis results using the records *BEFRAG*, *BETEIL*, *STRASSE*, and *UMWELT*, as introduced in Evaluation of selected crash cases. Subsequently, Collision speeds concentrate on the speeds at the time of the collision and the seconds before. Contact points finally addresses the point where the cyclist collided with the car.

### Environmental circumstances

The analysis of the **crash location**, depicted in fig. 2, shows that more than half of the crashes occur at junctions: with 52.7 %, the share of these crashes is just slightly higher for *UTYP 341* crashes than the 51.6 % corresponding to *UTYP 342* crashes. The same applies to KSI crashes, with 53.9 % and 51.5 %. The difference in crashes at crossings and property entrances is more notable: 30.6 % (KSI: 32.0 %) of the crashes where the cyclist came from the left occurred at crossings, as opposed to 24.1 % (KSI: 24.6 %) of cases where the cyclist came from the right. In contrast, 13.9 % (KSI: 10.2 %) of the *UTYP 341* and 21.7 % (KSI: 21.7 %) of the *UTYP 342* crashes occurred at property exits.
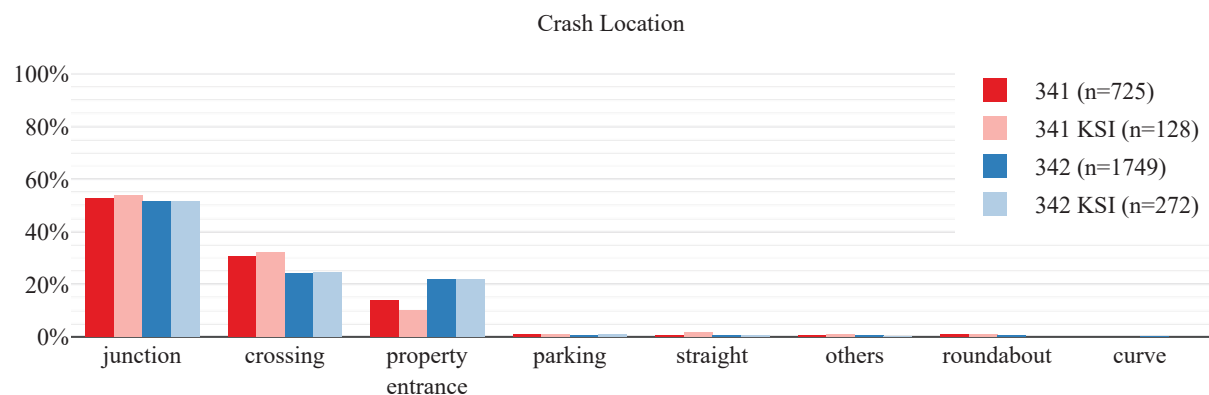
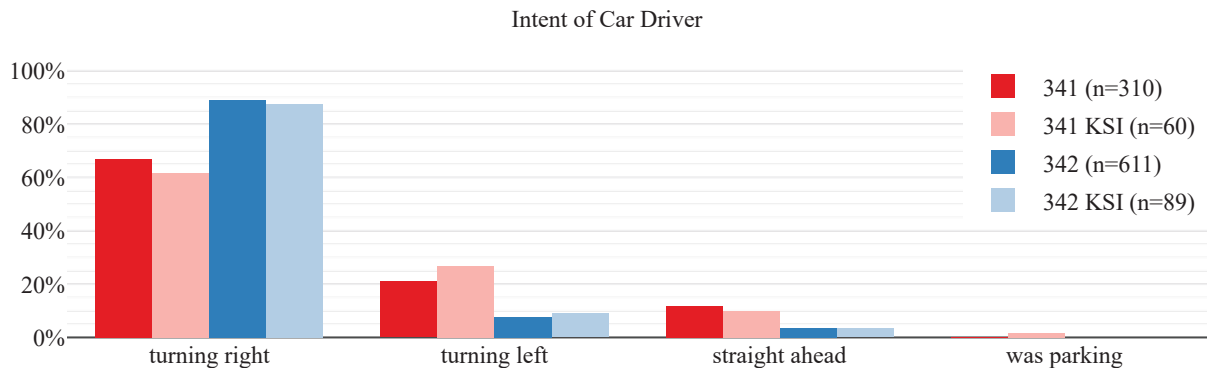*Figure 2. Frequency distribution of the crash location.*

Fig. 3 shows the frequencies of **rules of the road** at the crash site. With 74.5 % of crashes with the cyclist coming from the left (*UTYP 341*) and 68.5 % with the cyclist coming from the right (*UTYP 342*), in the majority of the

crashes, the car driver had to give way. The frequencies for *UTYP 341* and *342* KSI crashes differ slightly (74.2 %/64.9 %). 10.6 % (cyclist from left) and 13.3 % (cyclist from right) of the crashes occurred at property entries and exits with no significant difference in KSI crashes (9.7 %/13.5 %). Stop signs were present in 6.3 % and 9.9 %, respectively, of the crashes or 4.8 % and 11.6 %, respectively, of the KSI crashes. Traffic lights were present at 4.9 % and 4.3 % for crashes of all severities and 7.3 % and 5.4 % for KSI crashes.
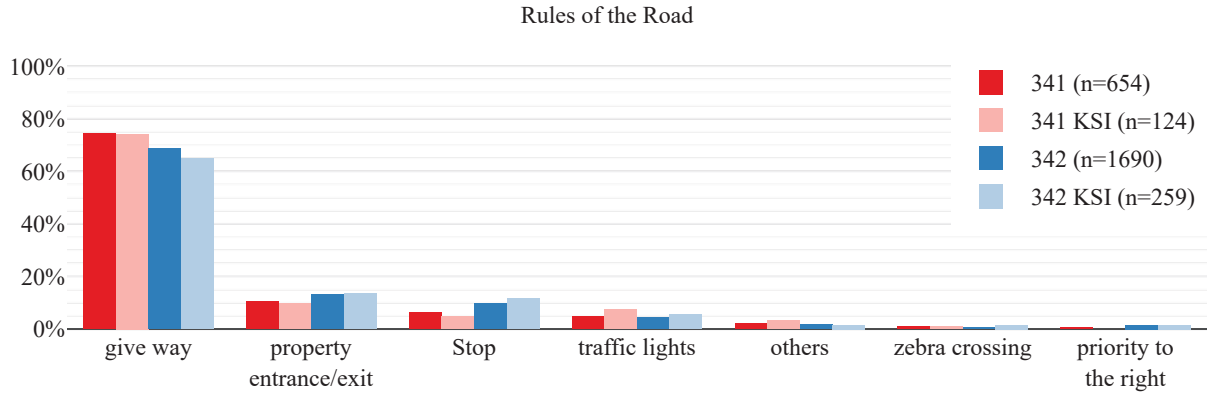
Rules of the Road

Figure 3. Frequency distribution of rules of the road at the crash site. Categories with a frequency of < 1% are not shown.

The **intent of the car driver** is depicted in fig. 4 for situations where the cyclist intented to go straight over the crossing. For other intents of cyclists, there are less than 1 % of cases for each *UTYP 341* and *UTYP 342*.
In most of the crashes and regardless of the *UTYP*, the car driver wanted to turn right: this was the car driver's intent in 66.8 % of the collisions with the cyclist coming from the left. This intent is even more pronounced for the collisions with the cyclist coming from the right, with 89.0 %. The KSI crashes' frequencies are distributed similarly (61.7 %/87.6 %). Turning left was the second most common intent of the driver with 21.0 % and 7.5 %, respectively, of all crashes and also 26.7 % and 9.0 %, respectively, of the KSI crashes. The car driver wanted to go straight in 11.9 % (KSI: 10.0 %) of the *UTYP 341* crashes and 3.4 % (KSI: 3.4 %) of the *UTYP 342* crashes. In a single KSI crash with the cyclist from the left (0.3 % of all; 1.7 % of KSI), the driver was parking.

Intent of Car Driver

Figure 4. Frequency distribution of the intent of the car driver before the crash when the cyclist intended to go straight ahead. Intents with a frequency of < 1% are not shown.

The evaluation of the **traffic density** at the time of the collision, as depicted in fig. 5, shows that most crashes occur in light traffic, with 42.4 % (*UTYP 341*) and 44.4 % (*UTYP 342*) of the crashes of any given severity. The numbers for KSI crashes are even slightly higher, with 45.4 % and 46.4 %. In 35.6 % of the collisions with the cyclist coming from the left and 35.1 % of the collisions with the cyclist coming from the right, there were cars on the street just occasionally. For KSI crashes, these numbers are slightly lower (32.8 % and 31.8 %). In 20.3 % (KSI: 21.0 %) of the

UTYP 341 and 19.0 % (KSI: 19.7 %) of the *UTYP 342* collisions, while there was dense traffic on the road, it was still possible to drive the maximum allowed speed. Collisions between cyclists and cars were rare when there was slow-moving traffic or traffic jam (all below 2 % each).
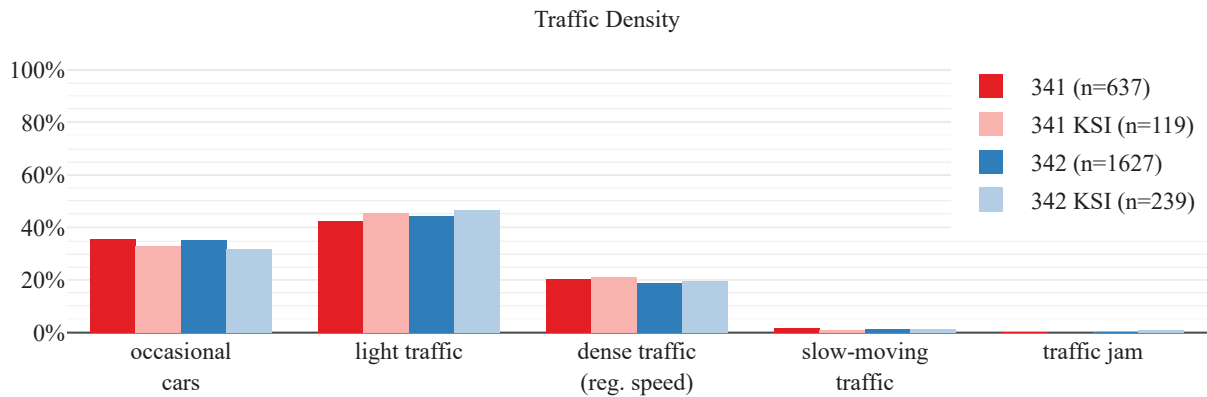
Traffic Density

Figure 5. Frequency distribution of the traffic density at the time of the collision.

As shown in fig. 6, most crashes between cyclists and cars occur during daylight, as the analysis of **daylight conditions** at the time of the crash indicates. While 76.1 % of *UTYP 341* crashes and 71.4 % of KSI crashes occurred during daylight, the percentage of these collisions is even higher within the *UTYP 342* scenario, with 88.5 % of crashes and 91.0 % of KSI crashes. A fraction of 15.9 % (KSI: 19.0 %) of *UTYP 341* crashes occurred at night, whereas only 5.7 % (KSI: 3.0 %) of *UTYP 342* crashes occurred without any daylight. Twilight conditions were present in 8.0 % of *UTYP 341* crashes and 5.8 % of *UTYP 342* crashes of any severity, and 9.5 % and 6.0 %, respectively, of KSI crashes.
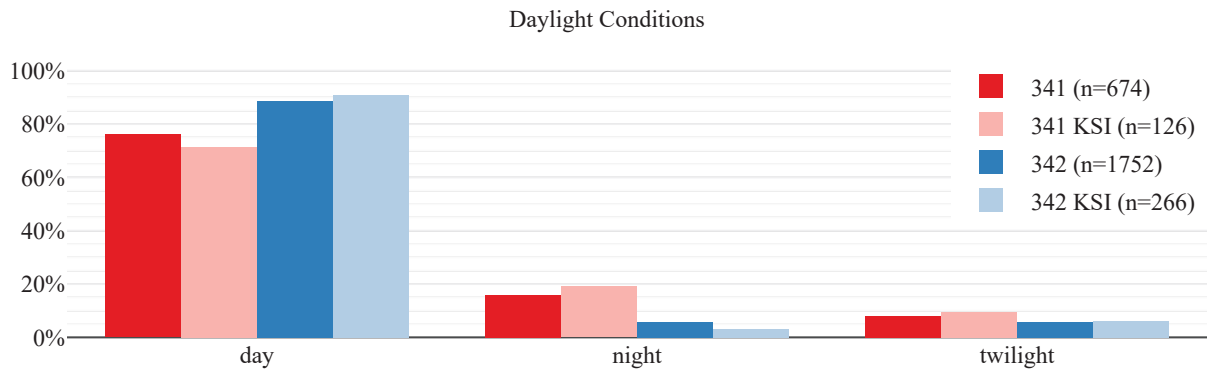
Daylight Conditions

Figure 6. Frequency distribution of daylight conditions at the time of the collision.

The evaluation of **visual obstructions** from the driver's perspective (depicted in fig. 7) shows that, in most cases, there was no obstruction in the line of sight. The fraction of crashes without obstruction is higher for those with the cyclist coming from the left (72.0 %) than for those with the cyclist coming from the right (62.1 %) and higher for all crashes than for KSI crashes only (64.5 % and 55.8 %, respectively). In the cases where the view was obstructed, the most common issues were structural circumstances, e.g., buildings, vegetation, or hills, with 19.0 % of collisions with the cyclist coming from the left and significantly more collisions with the cyclist coming from the right (32.3 %). In KSI crashes, these were present in 21.5 % and 35.1 % of the cases. Parking vehicles play a role in 4.4 % of *UTYP 341* and 4.0 % of *UTYP 342* injury crashes, as well as 5.4 % and 7.1 % of KSI crashes. Other circumstances are not of significant matter.

Visual Obstructions (POV: Car)
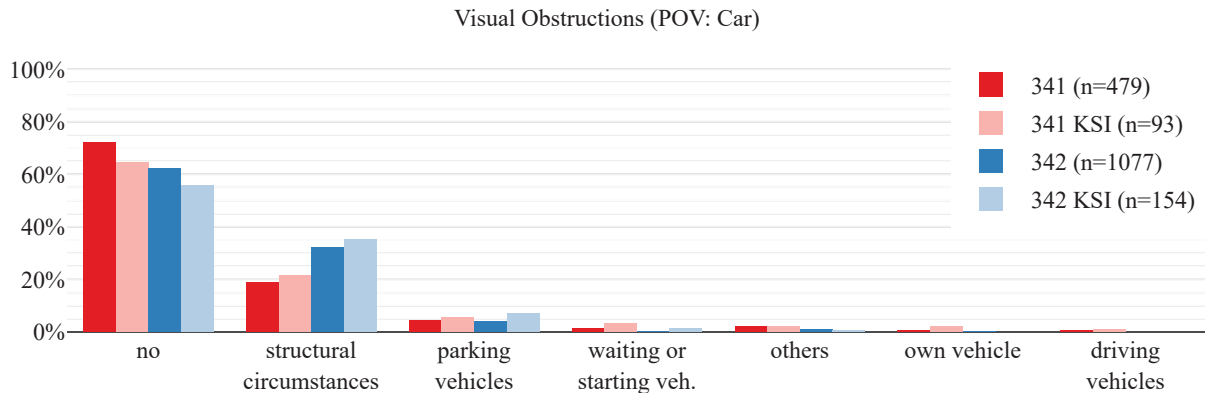
Figure 7. Frequency distribution of visual obstructions seen from the perspective of the driver.

The analysis of the **share of fault for the crash** (depicted in fig. 8) shows that in 87.2 % of crashes of *UTYP 341*, the cyclist had no responsibility for the crash. In contrast, in *UTYP 342* crashes, the cyclist was not even partially at fault in 35.6 % of crashes. The KSI crashes show similar numbers, with 91.7 % and 29.4 %. In only 10.0 %, the cyclist coming from the left was partially at fault for the crash, but in 60.2 %, the cyclist coming from the right was partially responsible. For the KSI crashes, again, the numbers are alike at 5.6 % and 65.2 %. When coming from the right, the cyclist was determined to be at the main fault in 3.2 % of crashes of all severities and 4.5 % of KSI crashes. Other constellations were present in less than 2 % each.

Subsequently, an analysis of the official cause of the crash yields further details: considering only the collisions where the cyclist's share of responsibility was not labeled as "not at fault" or no data was encoded, leaving only crashes where the cyclist was to blame partially, in 82.1 % of the *UTYP 342* collisions, the cyclist was wrongfully riding on the road or cycleway, e.g., riding in the wrong direction (not depicted). For *UTYP 341* crashes, in only 24.5 %, the cyclist was riding illegally on the road/cycleway.

Cyclist's fault for crash
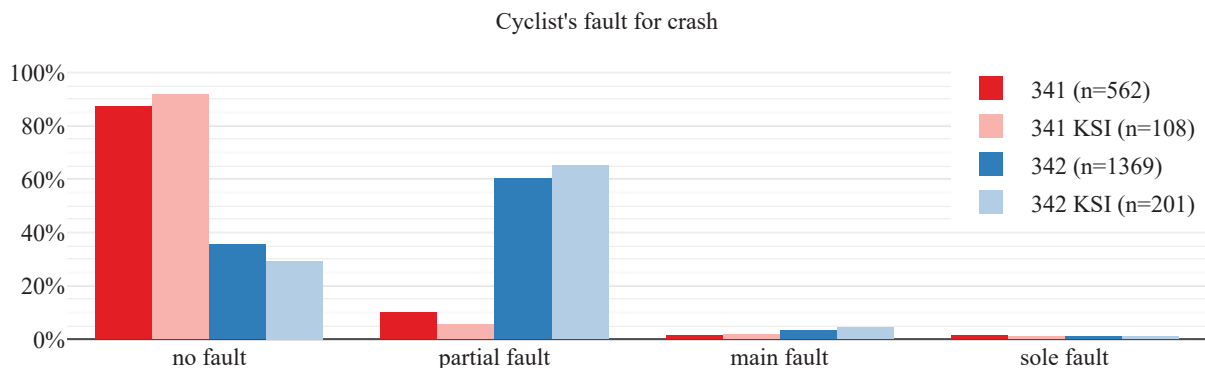
Figure 8. Frequency distribution of the cyclist's share of the fault for the crash.

Collision speeds

Fig. 9 shows the distribution of the **cars' speeds at impact**. More than half of the cars have a speed between 3 kph and 13 kph at the time of collision with the cyclist. In 95.9 % of the *UTYP 341* and 98.3 % of the *UTYP 342* crashes, the speed was 28 kph or less. Considering KSI crashes only, the speed was equal to or below 28 kph in 91.7 % and 95.5 % of the collisions, respectively.

Car Collision Speeds
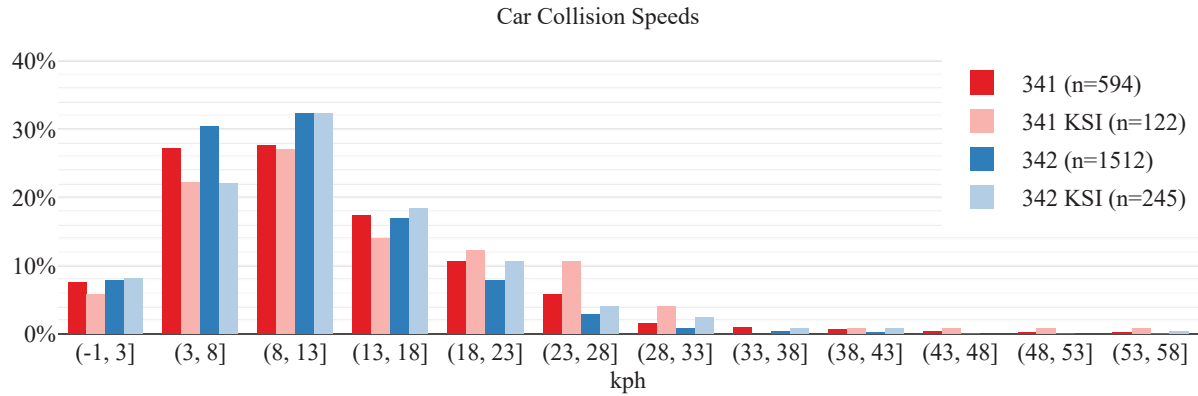
Figure 9. Frequency distribution of the cars' speeds at the time of the collision. One UTYP 341 and one UTYP 341 KSI crash each in bin [78, 83) are not shown.

In comparison, fig. 10 represents the distribution of the **cyclists' speeds at impact**. Compared to cars, the speed of cyclists is higher at the time of the collision: More than 60 % of the cyclists had a speed of 8 kph to 18 kph just before the collision. Above 90 % of cyclists were riding with a 23 kph maximum, and more than 97 % with a 28 kph maximum, both including the KSI cases. It is noticeable that the higher collision speeds are primarily present when the cyclist was riding along the usual driving direction: In ca. 26 % of *UTYP 341* crashes, the cyclist was going 18 kph to 28 kph, whereas in less than 13 % of *UTYP 342* crashes the cyclist was going this speed. The collision speeds of KSI crashes are similarly distributed as all injury crashes.

Cyclist Collision Speeds

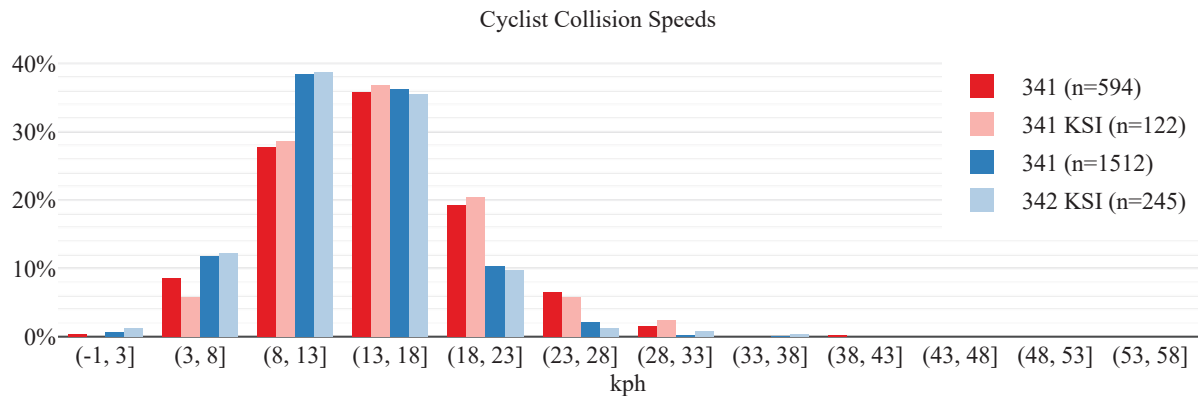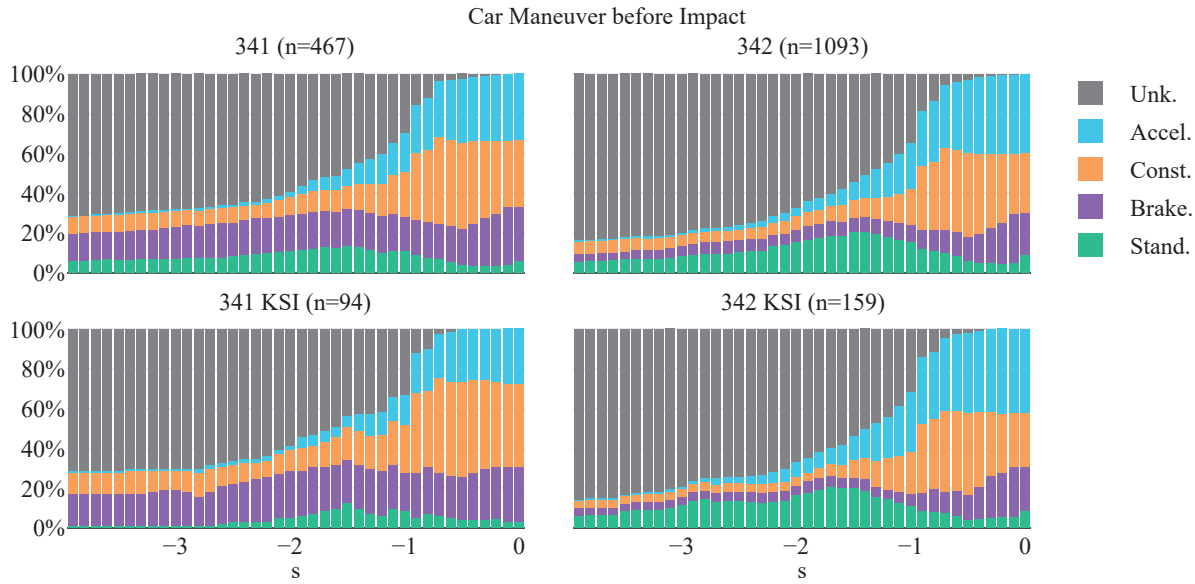*Figure 10. Frequency distribution of the cyclist speed at the time of the collision.*

Fig. 11 shows the distribution of **maneuvers conducted by the driver in the last four seconds** before the collision. The data originates from the crash reconstruction and subsequent assignment in intervals, as described in Evaluation of selected crash cases. If data was unavailable for this interval, the related interval is marked as "unknown". There is good data availability for the last 0.9 s before the impact: data could be reconstructed in more than 80 % of cases. Two seconds before the impact, not more than 40 % is available. For the *UTYP 342* crashes, only one fifth of the crashes had data recorded at $t = -3.9\,s$.

With 39.5 %, more drivers in *UTYP 342* crashes were accelerating in the last tenth of a second compared to the 33.2 % of *UTYP 341* participants. In contrast, more drivers were braking before colliding with the cyclist from the left (27.0 %) compared to crashes with the cyclist coming from the right (21.0 %). In both crash types, a rise in braking maneuvers can be seen in the last 0.5 s before impact. In *UTYP 342* crashes, more drivers stood still once in the last seconds before impact compared with *UTYP 341* crashes, with a maximum of 20.6 % vs. 13.7 % at $t = -1.5\,s$. At $t = 0\,s$, the constant velocity driving maneuver is slightly more frequent in *UTYP 341* crashes (33.6 %) than in *UTYP 342* crashes (30.6 %). The distribution of maneuvers of KSI crashes is similar to the distribution of all injury crashes except for more constant driving and less acceleration maneuvers in *UTYP 341* crashes.

Figure 11. Frequency distribution of the cars' maneuvers in the last four seconds before the collision.

Due to the declining availability of reconstructed speed for $t <= -1\ s$, the focus during the following analysis lies only on the last second before the collision. Fig. 12 depicts the analysis of the **cars' speeds during the last second** before the impact, clustered into the three maneuvers accelerating, constant speed drive, and braking.

For *UTYP 341* crashes where the car was **accelerating** in the actual interval, the median speed was 5.78 kph (Q1: 4.48 kph, Q3: 9.24 kph) at one second before the impact and 10.0 kph (Q1: 8.0 kph, Q3: 15.0 kph) at impact. Median speeds for *UTYP 342* are similar, while quartiles are lower with 5.33 kph (Q1: 4.0 kph, Q3: 7.13 kph) at $t = -1\ s$ and 10.0 kph (Q1: 7.0 kph, Q3: 12.0 kph) at $t = 0\ s$. There is no significant difference for acceleration crashes in speeds between KSI and all injury crashes.

In the group of the cluster of **braking** intervals before the crash, speeds are higher: the median for the interval at $t = -1\ s$ is 17.76 kph (Q1: 14.54 kph, Q3: 21.74 kph) for *UTYP 341* and 17.1 kph (Q1: 12.03 kph, Q3: 21.5 kph) for *UTYP 342* crashes. At $t = 0\ s$, the medians for intervals are 12.0 kph (Q1: 7.0 kph, Q3: 17.0 kph) for *UTYP 341* and 10.0 kph (Q1: 7.0 kph, Q3: 15.0 kph) for *UTYP 342*. KSI crashes show higher speeds over the last second before the impact: for *UTYP 341* collisions, especially at $t = -0.7\ s$, the speed is notably higher with 19.8 kph (Q1: 14.98 kph, Q3: 28.62 kph) compared to 16.4 kph (Q1: 12.6 kph, Q3: 22.4 kph) for all injury crashes. *UTYP 342* KSI crashes have similar speeds to all injury crashes.

The intervals with **constant speed** have the following properties: The reconstructed speed intervals of 341 crashes are slightly higher than for 342 crashes. For example, the speed at $t = -1\ s$ is 15.0 kph (Q1: 10.0 kph, Q3: 22.0 kph) compared to 12.0 kph (Q1: 9.0 kph, Q3: 20.0 kph) and the speed at $t = 0\ s$ is 13.0 kph (Q1: 8.0 kph, Q3: 20.0 kph) compared to 10.0 kph (Q1: 8.0 kph, Q3: 15.0 kph). The speeds for the KSI crashes exceed the speeds of their respective crashes of all injuries as well.
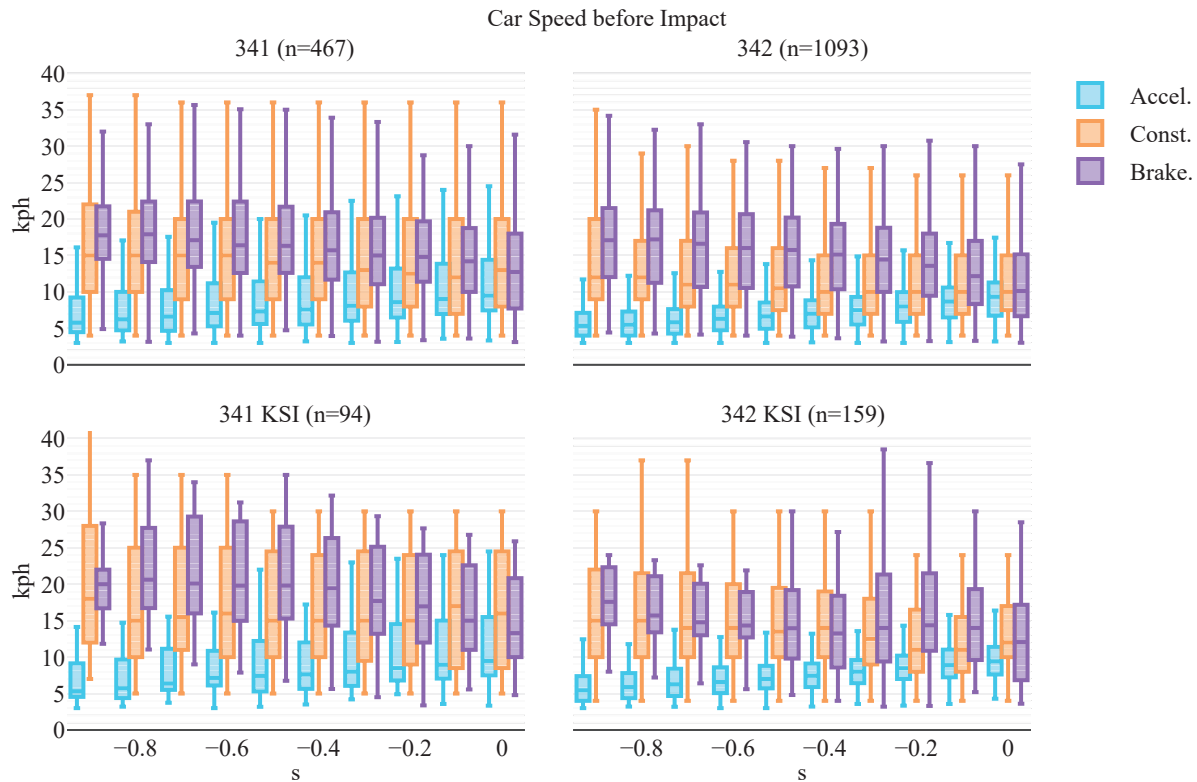
Figure 12. Box plots of the cars' speeds in the last second before the collision, grouped by maneuver performed in the particular interval.

Contact points

Fig. 13 represents the **first contact points** between cyclist and car for *UTYP 341 & 342* collisions. These are measured in centimeters from the point at the very front of the vehicle's longitudinal axis. Compared to the predominantly centered contact point in *UTYP 342* collisions, the majority of contacts in *UTYP 341* crashes are located more to the left with a maximum at −70 cm, which is where the headlight is located. Additionally, with 27.4 %, significantly more cyclists collided with the side of the car compared to 14.0 % in *UTYP 341* crashes. Most collisions into the side were recorded right at the front of the vehicle for *UTYP 342* crashes, but around 50 cm to the rear for *UTYP 341* crashes. KSI crashes occurred under very similar conditions regarding all aforementioned aspects. Only the share of contacts at the vehicle's side is slightly shifted towards the front.
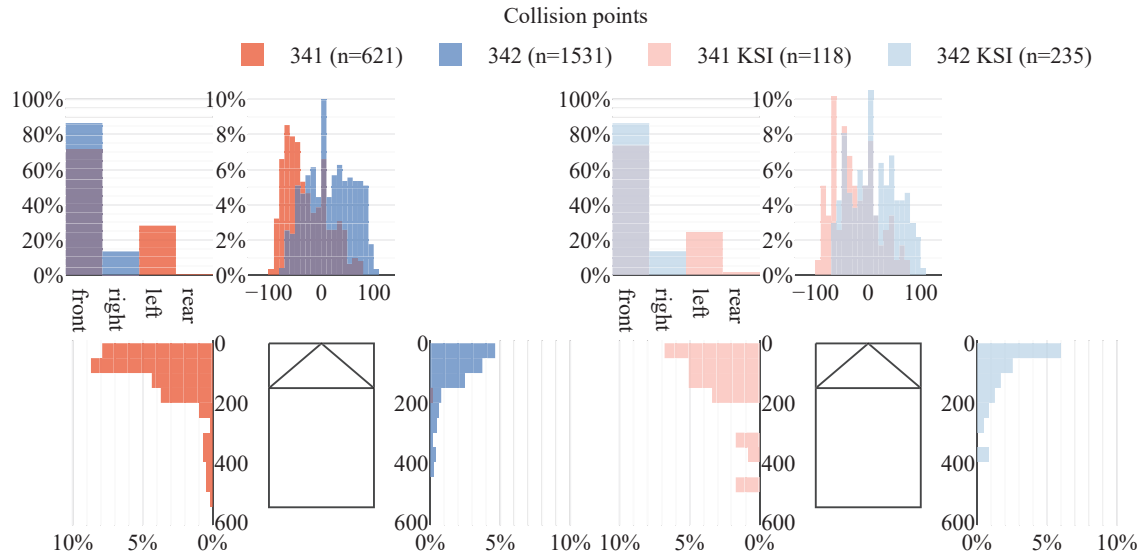
 Figure 13. Distribution of first contact points of the cyclist at the car. Two UTYP 341 collisions at the rear not displayed.

DISCUSSION

Discussion of results

Summarizing the findings in Results, we can draw a picture of the "typical crash" between cars and crossing cyclists at junctions with similarities, as well as notable differences between the collisions with the cyclist coming from the left (*UTYP 341*) and the right (*UTYP 342*):

Similarities between crashes **More than half of the crashes occur at junctions**. Next to that, for *UTYP 341* crashes, the share of crashes at crossings is more than twice as high for collisions at property entrances. However, *UTYP 342* crashes occur nearly as often at crossings as at property entrances.

"Give way" is the most dominant of the rules of the road at the crash site, with two thirds to three quarters of the collisions. Property entrances/exits, stop signs, traffic lights, and others play a minor role in these crashes. Between the *UTYP 341* and *UTYP 342* crashes, there is only little difference in the distribution. A slight shift toward more crashes at stop signs and property exits can be noticed for *UTYP 342* collisions.

Most crashes are turning right crashes: In nearly 90 % of the cases with the cyclist coming from the right, the car driver wanted to turn right at the junction. Other actions, therefore, only constitute slightly more than 10 % of the crashes. With the cyclist coming from the opposite side, the most common intent of the car driver is turning right as well, but here, in one third of the crashes, the driver intended to turn left or go straight ahead.

Nearly all crashes occur at low traffic densities: In about 4 out of 5 collisions, there was light traffic or only occasional cars on the road at the time of the crash, similarly distributed for crashes with the cyclist coming from left and right.

The crashes are mostly daylight crashes: While nearly 9 out of 10 *UTYP 342* crashes occur during daylight, the number for *UTYP 341* crashes is moderately lower, with 3 out of 4 crashes.

Visual obstructions are present in one third of collisions: In most crashes, no visual obstructions were on site. Yet, if there was an obstruction present, it is more likely to be in the crashes with the cyclist coming from the right than from the left, more likely for KSI crashes, and more likely to be a structural circumstance than a temporary obstacle such as a parking or waiting vehicle.

Collisions occur at relatively low speeds and while the car is accelerating: more than half of the crashes show a car's speed of 13 kph or below, and in more than 90 % of the cases, the speed is 28 kph or less. However, the analysis of the maneuvers performed in the last second before the collision shows that accelerating was the most common action.

Cyclists are most often hit by the car's front bumper: in 70.4 % of the *UTYP 341* and 85.2 % of the *UTYP 342* crashes, the collision point between cyclist and car was recorded at the car's front. In crashes where the cyclist came from the right, the share of impacts to the side of the vehicle is comparatively lower, and the contact point is more centered at the front bumper – both facts indicate that the car reached the cyclist at a later point in time compared to the crashes where the cyclist came from the left.

<u>Differences between crashes</u> **Crashes where the cyclist comes from the right are more frequent:** compared to the crash type *UTYP 341*, the related *UTYP 342* crash occurs 2.6 times more frequently.
The cyclist coming from the right might not be expected on this side: as shown in Environmental circumstances, in more than 60 % of the collisions, the cyclist was ruled to be at least partially responsible for the crash. In over 80 %, the reason was the wrongful use of the cycleway against the prescribed driving direction, meaning that the driver of the car could not have expected the cyclist to come from this direction.
Drivers "fail to look" at cyclists coming from the right and "look but fail to see" cyclists from the left: crashes, where data shows that reduced visibility could play a role, are more present in the *UTYP 341* group. For example, as seen in fig. 6, the collision ratio at night is nearly three times as high as in the *UTYP 342* crashes. It is also notable that *UTYP 342* crashes are almost entirely turning-right crashes. When the driver wanted to turn left or go straight over the crossing and therefore had to also look for traffic coming from the right, notably fewer crashes occur when the cyclist comes from the right. Following the work of Summala et al., we assume that once the driver is forced to look right to avoid collisions with other cars, the cyclist is perceived as well [3]. Visual obstructions are also more present in *UTYP 342* crashes, thus blocking the chance of seeing the cyclist coming from the right in time.
Crashes with the cyclist coming from the right occur at lower speeds: in *UTYP 342* crashes, the (collision) speed of the cyclist is lower compared to the opposite crash scenario. We suppose that cyclists might drive slower, purposely knowing that they are not expected by the cars' drivers when coming from that direction. The speed of the cars is also lower before and at the time of the collision, and drivers are more often accelerating again after standing still. The share of crashes at stop signs is higher compared to *UTYP 341* crashes, indicating that the driver had stopped or was about to stop before the collision. Additional time gained by slower maneuvers could have prevented the crash by decreasing the chance of overlooking the cyclist coming from the left, while in *UTYP 342* crashes, the two participants still collided, backing the thesis that the cyclist from the right is not seen at all due to visual obstructions or the drivers' omission to look right.
The cyclist's speed at the time of the collision does not affect the severity. In contrast, the car's speed does: A comparison of the speeds of both cyclist and car with the speeds for KSI crashes shows that there were not significantly more severe injuries or deaths when the collision speed of the cyclist was higher. However, the distribution of the collision speed of the car is visibly shifted to higher speeds for KSI crashes compared to all injury crashes.

Comparison to related works

As mentioned in Related Works, this work shares its methodology to some extent with the SECUR publication [10]. However, it focuses on a subset of a certain type of cyclists crashes within the group of crashes in the SECUR so-called "accident scenarios" *Straight Crossing Path – Left & Right Direction Bicyclist (SCP-LD-BC & SCP-RD-BC)*. It is obvious to compare the characteristics of the *UTYP 341* and *UTYP 342* crashes with these accident scenarios. Since the SECUR publication focuses on KSI crashes, only these are considered in the following comparison:
Compared to 50 % of the crashes in the SCP-LD-BC group and 55 % of crashes in the SCP-RD-BC group, in 74.2 % of the *UTYP 341* and 64.9 % of the *UTYP 342* KSI collisions, the car driver had to yield. Structural visual obstructions were present in 17 % (30 % presence of obstructions times 57 % structural obstructions) for SCP-LD-BC and 24 % (35 % times 69 %) for SCP-RD-BC compared to 21.5 % and 35.1 % in our analysis. Reported traffic densities were similar (sporadic or light traffic was present in 80 % for both SCP-LD-BC and SCP-RD-BC vs. 78.2 % and 78.2 %), as well as daylight conditions (80 % and 87 % vs. 71.4 % and 91.0 % crashes during daylight.) This indicates that the *UTYP 341 & 342* crashes are especially prone to visual obstructions in comparison to the larger group of crashes in similar constellations, and required yielding by the car driver is more common than other forms of rules of the road, such as stop signs or traffic lights.
The work's results align with the results of Summala et al., who analyzed car-cyclist crashes from 1987 to 1989 in Helsinki and found that the prevalent crash type is one where the cyclist came from the right and the car driver

wanted to turn right [3]. The crashes studied also showed low traffic densities. The authors also assumed that measures reducing the speed at the intersection and, thus, providing the driver more time increases the chance to see the cyclist and hence avoid the collision.

Gohl et al. state that in crashes where the cyclist came from the right, the driver "failed to look" into the cyclist's direction, whereas in crashes where the cyclist came from the left, the driver "looked but failed to see" the cyclist [4]. Our findings, for example, the high share of right-turning maneuvers in *UTYP 342* crashes and the comparatively higher proportion of visual obstacles confirm their statements. Their finding that drivers pay less attention when they expect the other party to comply with traffic regulations also backs up our result that the cyclist riding on the wrong lane and, therefore, crossing the car's path from the right might not be expected.

Using the data from several European countries, Uittenbogaard et al. highlighted that whether a cyclist is severely injured or killed is influenced by the car's speed at the time of impact, not by the cyclist's speed [6]. Our data also revealed similar results but for severe versus slight injuries.

Limitations of this study

In the present study, we solely used the famous GIDAS dataset as the basis for our evaluation. This data, collected in two cities in Germany, is as representative as possible of German crashes according to the data's providers due to sampling and weighting mechanisms [14]. Yet, the results cannot be projected directly onto other nations' crash occurrences. Especially the frequency of the selected crash scenarios, *UTYP 341 & 342* presumably differs from country to country, e.g., due to other road infrastructure, traffic rules, or driver education. Other works proved that, e.g., in Hungary, the most common crash scenarios are those in the longitudinal direction [15]. Though, there is also a high relevance of crossing scenarios in France, Italy, the Netherlands, Sweden, the UK [5], Australia [9], and the USA [8], as previous works have demonstrated. We, hence, suppose that the underlying principles of these crashes are similar in other countries. For example, it can be assumed that drivers turning right often focus on traffic from the left; therefore, cyclists from the right are not noticed. This has also been shown by similar works in Finland [3]. Since records are only added to GIDAS if the crash is rated as an injury crash, we do not have any information about the milder crashes without injuries. Also, due to the significant underreporting of crashes with cyclists [16, 17], data might be skewed toward the crashes that are reported. This includes especially crashes with low injury severity, while in contrast, crashes with pedelecs are relatively more often reported [2].

CONCLUSIONS

This work's goal lies in exploring the most common crash scenario between cars and cyclists and its characteristics. Therefore, using the GIDAS database, we first identified the crashes where the car collided with a crossing cyclist riding on a cycleway as the most significant crashes with a share of 28.9 % of all car-cyclist collisions. In the subsequent analysis, we then focused on these crashes but discriminated between the cases where the cyclist came from the left and the cases where the cyclist came from the right, as well as between crashes with all levels of injuries and crashes with killed and severely injured (KSI).

The most common crashes between cyclists and cars, as recorded in the GIDAS data set, can be described as crashes with light injuries at junctions where the car driver disregarded the right of way of the crossing cyclist. The car driver intended to turn right and merge into light traffic while the rules of the road required yielding. In the significantly more common case, the cyclist came from the right and was partially to blame for the crash for riding in the wrong direction. Most of the collisions occurred in daylight and without visual obstructions. The car's speed was less than or equal to 13 kph, and the cyclist's speed was less than or equal to 18 kph. In the last second before the collision, the car was accelerating or driving with nearly constant velocity. At the collision, the cyclist made first contact with the front of the car.

We demonstrate that besides similarities in environment and course of events of the crash, there are few features distinguishing the collisions with the cyclist coming from the left and the right: for instance, we assume that, in right-hand traffic, the driver "fails to look" at the cyclist from the right and "looks but fails to see" the cyclist from the left. The circumstance that a cyclist coming from the right might not be expected could contribute to these collisions. It is noticeable that comparatively fewer crashes occur in a situation where the driver had to look right, i.e., turning left or driving straight over a crossing. Our work also shows that the cyclist's severity of injuries is only influenced by the car's, not the cyclist's speed.

The present results highlight the need for measures reducing crashes with cyclists, especially in crossing situations. This includes well-designed traffic infrastructure protecting cyclists at junctions and crossings or avoiding crossing situations of these parties at all, but also novel in-vehicle safety applications making the driver aware of cyclists and, in general, VRUs in critical situations. Since Vehicle-to-everything (V2X) communication does not require line-of-sight conditions, systems based on this technology could support creating awareness of VRUs in the near future [18].

By means of the results presented, our follow-up work will consist of developing these novel safety applications based on vehicle-to-everything communication to avoid these types of crashes. The results will help us to understand the crash occurrence between cars and cyclists and allow us to determine requirements and derive parameters for aforementioned applications.

REFERENCES

[1] European Parliament, Council of the European Union. (2018, January 9). Directive 2010/40/EU of the European Parliament and of the Council of 7 July 2010 on the framework for the deployment of Intelligent Transport Systems in the field of road transport and for interfaces with other modes of transport (Text with EEA relevance) [OJ L 207 6.8.2010]. Retrieved June 4, 2021, from https://eur-lex.europa.eu/legal-content/EN/ALL/?uri=CELEX:02010L0040-20180109

[2] Maier, O., Hattula, S., Schneider, S., Mönnich, J., & Lich, T. (2021–November 12). Pedelec user study: Safety insights into an emerging vehicle [11]. *Proceedings of International Cycling Safety Conference 2021*.

[3] Summala, H., Pasanen, E., Räsänen, M., & Sievänen, J. (1996). Bicycle accidents and drivers' visual search at left and right turns [Journal Article]. *Accident Analysis & Prevention*, *28*(2), 147–153. https://doi.org/10.1016/0001-4575(95)00041-0

[4] I. Gohl, A. Schneider, J. Stoll, M. Wisch, & V. Nitsch. (2016–November 4). Car-to-cyclist accidents from the car driver's point of view. *Proceedings of International Cycling Safety Conference 2016*. https://doi.org/10.5281/zenodo.1135194

[5] Op den Camp, O. M., Ranjbar, A., Uittenbogaard, J., Rosen, E., & Buijssen, S. (2014–November 19). Overview of main accident scenarios in car-to-cyclist accidents for use in AEB-system test protocol. *Proceedings of International Cycling Safety Conference 2014*.

[6] Uittenbogaard, J., van Montfort, S., et al. (2016–November 4). Overview of main accident parameters in car-to-cyclist accidents for use in AEB-system test protocol. *Proceedings of International Cycling Safety Conference 2016*.

[7] Bálint, A., Labenski, V., Köbe, M., Vogl, C., Stoll, J., Schories, L., Amann, L., Sudhakaran, G. B., Huertas Leyva, P., Pallacci, T., Östling, M., Schmidt, D., & Schindler, R. (2021). SAFE-UP Deliverable D2.6: Use Case Definitions and Initial Safety-Critical Scenarios. Retrieved November 27, 2022, from https://www.safe-up.eu/s/SAFE-UP_D2_6_Usecasedefinitionsandinitialsafety-criticalscenarios_.pdf

[8] MacAlister, A., & Zuby, D. S. (2015–September 11). Cyclist Crash Scenarios and Factors Relevant to the Design of Cyclist Detection Systems. *2015 IRCOBI Conference Proceedings*, 373–384.

[9] Beck, B., Stevenson, M., Newstead, S., Cameron, P., Judson, R., Edwards, E. R., Bucknill, A., Johnson, M., & Gabbe, B. (2016). Bicycling crash characteristics: An in-depth crash investigation study [Journal Article]. *Accident; analysis and prevention*, *96*, 219–227. https://doi.org/10.1016/j.aap.2016.08.012

[10] Cornec, L., Unger, T., Rössler, R., Feifel, H., Hermitte, T., Page, Y., Puller, N., & Mousavi, M. (2023–April 6). Analysis of the European Car Road Accidents for the Identification of the Main Use Cases for a Significant Road Safety Improvement Through V2X. *Proceedings of the 27th ESV Conference*.

[11] *About GIDAS – Methodology*. (2022). Verkehrsunfallforschung an der TU Dresden GmbH. Retrieved December 10, 2022, from https://www.gidas.org/about-methodology-en.html

[12] Unfallforschung der Versicherer (Ed.). (2016). Unfalltypen-Katalog: Leitfaden zur Bestimmung des Unfalltyps. *Gesamtverband der Deutschen Versicherungswirtschaft e. V.* Retrieved October 8, 2022, from https://www.udv.de/resource/blob/80022/89b4d80028aacf8cab649d3a3c6157a0/unfalltypenkatalog-data.pdf

[13] R Core Team. (2018). R: A Language and Environment for Statistical Computing.

[14] *Welcome to GIDAS*. (2022). Verkehrsunfallforschung an der TU Dresden GmbH. Retrieved December 10, 2022, from https://www.gidas.org/start-en.html

[15] Glász, A., & Juhász, J. (2017). Car-pedestrian and car-cyclist accidents in Hungary [PII: S2352146517303666]. *Transportation Research Procedia*, *24*, 474–481. https://doi.org/10.1016/j.trpro.2017.05.085

[16] Maier, O., Pfeiffer, M., Wehner, C., & Wrede, J. (2015–September 16). Empirical Survey on Bicycle Accidents to estimate the Potential Benefits of Braking Dynamics Assistance Systems [09]. *Proceedings of International Cycling Safety Conference 2015*.

[17] Madsen, T. K. O., András Várhelyi, Evelien Polders, Sofie Reumers, Pau Hosta, Bibiloni, D. J., Alia Ramellini, Niels Agerholm, & Lahrmann, H. S. (2018). *Assessment of Safety of VRUs Based on Self-Reporting of Accidents and Near-Accidents*. European Commission * Office for Official Publications of the European Union.

[18] Feifel, H., Erdem, B., Menzel, M., & Gee, R. (2023–April 6). Reducing Fatalities in Road Crashes in Japan, Germany, and USA with V2X-enhanced-ADAS. *Proceedings of the 27th ESV Conference*.

FACTORS INFLUENCING UPPER NECK LOADING IN REGULATORY TESTS OF CHILD RESTRAINT SYSTEMS

Costandinos Visvikis
Christoph Thurn
Thomas Müller
CYBEX GmbH
Germany

Paper Number 23-0273

ABSTRACT

Potential neck force and moment limits in UN Regulation No.129 are part of on-going regulatory discussions. Pragmatic limits for the Q0, Q1 and Q1.5dummies were proposed to regulators in 2020, based on analyses of type-approval monitoring data. However, chin-to-chest contact was acknowledged as potentially skewing the analysis and undermining the proposed limits. The aims of this study were to: 1) investigate the effect of impact direction and child restraint orientation on neck tension force and 2) quantify the effect of chin-to-chest contact on a large study sample of child restraint type-approval tests, for all Q Series dummies (Q0 to Q10).

Over 200 official type-approval tests were collected from our internal database with data extracted for neck tension force and head vertical acceleration. The head vertical acceleration multiplied by the head mass was used to calculate the neck tension force due to inertial loading from the head. This was compared with the measured neck tension force to determine the frequency of chin-to-chest contact and its likely influence on neck tension force in type-approval tests. The data were then separated for each Q-Series dummy by impact direction and child restraint orientation to identify trends for each test or installation parameter

The inertial neck tension force calculated from head vertical acceleration was lower than measured neck tension force in almost all front impacts with forward-facing child restraints and in many rear impacts with rear-facing child restraints. Differences were in the region of 30-50 percent depending on the dummy and child restraint installation parameters. This indicated the presence of chin-to-chest contact in a large proportion of the tests in the sample. Forward-facing child restraints generated highest neck loads in front impact, whereas rear-facing child restraints generated highest loads in rear-impact.

Our analysis suggests chin-to-chest contact occurs frequently in child restraint type-approval tests with substantial influence on neck measurements. This confirms that pragmatic limits derived for regulation from type-approval data are likely to be skewed upwards by this contact. Subsequent measurements in future type-approval tests are also likely to be skewed upwards and hence mitigating chin-to-chest contact may be incentivised more than limiting inertial neck loading. Although large, our sample comprised tests from one child restraint manufacturer only. A larger sample, comprising a broad range of manufacturers, is needed to validate our findings fully. Nevertheless, this study has demonstrated a robust approach for such analyses.

Child restraints are very effective in reducing the risk of serious neck injury to children in collisions. Nevertheless, a relatively large range of neck loads can be measured in type-approval, which can be influenced by dummy chin-to-chest contact, as well as child restraint installation parameters. Quantifying these influences will contribute to ongoing regulatory discussions about the use of neck force and moment limits in UN Regulation No.129.

INTRODUCTION

United Nations (UN) Regulation No. 129 specifies Q-Series dummies to assess the performance of child restraint systems in dynamic impact tests. The upper neck tension force and flexion moment must be recorded for monitoring purposes, but thresholds are not currently applied to the measurements during type-approval. However, the UN Working Party on Passive Safety (GRSP) is considering introducing neck thresholds for the Q0, Q1 and Q1.5 dummies in frontal and rear impact tests in a future amendment of UN Regulation No. 129 [1]. To that end, the European Association of Automotive Suppliers (CLEPA) proposed pragmatic thresholds to GRSP for tension force and flexion moment, developed from a large sample of international type-approval monitoring data [2-3]. This approach was authorised by GRSP because previous efforts to derive child neck injury assessment reference values from accident reconstruction were unable to generate valid neck injury risk curves [4]. Prior to that, the European Enhanced Vehicle safety Committee (EEVC) proposed thresholds scaled from Hybrid III 50th percentile male (adult) dummy regulatory thresholds, and from Hybrid III child dummy neck injury assessment reference values [5]. However, these were not adopted by UN Regulation No. 129 because a very high proportion of child restraint systems on the market would have failed to meet them, which didn't reflect real-world neck injury risk [6].

During the regulatory discussions at GRSP, it emerged that chin-to-chest contact has the potential to increase the neck tension force measured by Q-Series dummies (i.e., beyond the level it would reach under purely inertial loading from the head) [7]. This means that the pragmatic thresholds developed from type-approval monitoring data may have been skewed upwards by chin-to-chest contact and that any subsequent regulatory test measurements might be similarly skewed [8-9]. Unfortunately, the frequency of chin-to-chest contact and its effect on the proposed thresholds was impossible to quantify in the type-approval monitoring sample because the data gathering exercise in [2] was limited to the peak neck tension force and flexion moment. Other parameters that might have revealed the presence and extent of chin-to-chest contact were not collected. Nevertheless, the implication of adopting thresholds skewed by chin-to-chest contact is that preventing such contact might be incentivised by regulation as a means of reducing the dummy neck force measurements, without real consideration of the true inertial loading to the cervical spine [8-9].

The Spanish delegation to GRSP proposed a method for calculating the inertial neck force using the head vertical acceleration multiplied by the head mass above the neutral axis of the load cell [7]. This method offered the potential to derive purely inertial neck loading, free from the influence of chin-to-chest contact. Research tests confirmed the method was capable of predicting the measured neck force up to the period of chin-to-chest contact, but it could also generate unexpected results, particularly when chin-to-chest contact occured at the same time as the peak inertial loading [9-10]. Furthermore, as head vertical acceleration was not included in the initial data gathering exercise, it was also impossible to apply this method to the type-approval monitoring data in order to determine its potential effect on the pragmatic thresholds.

The frequency and influence of chin-to-chest contact in UN Regulation No. 129 tests has been highlighted with relatively small research test studies [8-10]. The full extent to which chin-to-chest contact influenced the pragmatic thresholds proposed for the regulation is unknown and is impossible to determine from the monitoring data provided by type-approval authorities. There appears to be little appetite currently from regulators to repeat the collection of type-approval monitoring data with additional parameters (either to identify chin-to-chest contact and/or to calculate purely inertial neck force). Therefore, the aims of this study were to use an internal sample of type-approval test results to: 1) investigate the effect of impact direction and child restraint orientation on neck tension force and 2) quantify the effect of chin-to-chest contact on a large study sample of child restraint type-approval tests, for all Q-Series dummies (Q0 to Q10).

METHODS

This study followed the methods used by CLEPA in [2-3] to derive pragmatic neck tension force thresholds from type-approval monitoring data. However, in our study, the source was limited to CYBEX type-approval tests. No external data were used.

Data collection

Over 200 official type-approval tests were collected from our internal test database. These comprised front and rear impact tests carried out for new type-approvals and for extensions to existing approvals. Production qualification

tests, which are part of the type-approval process in UN Regulation No. 129, were excluded so as not to skew the sample with repeat tests. Research and development tests on prototype products were also excluded because they may not reflect real product performance and because most research and development tests will ultimately be repeated as an official type-approval test.

The sample was collected according to a template that included brief details of each test such as the dummy (Q0, Q1, Q1.5, Q3, Q6 or Q10), impact direction (front or rear), orientation of the child restraint (rear- or forward-facing) and its adjustment (where applicable, upright or reclined). The main test data extracted were the peak neck tension force (i.e. $+F_z$ channel) and the peak head vertical acceleration (i.e. $+a_z$). We extracted data for tests performed in our own crash test laboratory only because the correct sensor polarity was essential for the reliability of our study. This limited our sample to tests that were performed in 2019 and later (after our laboratory was installed), but it was our only means of guaranteeing that SAE J211 sign conventions had been used when the impact test was carried out. The sample included several tests with the same child restraint and dummy. This was due to the various test and set-up conditions required during the type-approval process. All such tests were included to maintain reasonable sample sizes for analysis.

Data analysis

As a first step, the data were separated for each Q-Series dummy by the impact direction and the child restraint orientation. The inertial neck force was then calculated according to the method proposed in [7] and set-out in Equation 1.

$$\textit{Inertial neck force (N) = Dummy head mass (kg) x Head vertical acceleration (ms}^{-2}) \qquad \text{(Equation 1)}$$

The inertial neck force was calculated for rear impact tests with rear-facing child restraints and front impact tests with forward-facing child restraints only. These are the only combinations of impact direction and child restraint orientation in which chin-to-chest contact can occur during the main laoding phase of the impact. The inertial neck force was not calculated for front impact tests with rear-facing child restraints because chin-to-chest contact occurs only in rebound and does not influence the overall peak neck tension force. Furthermore, as the head is in contact with the back of the child restraint from the outset, it seems likely that the calculation of the inertial neck force would not deliver a meaningful result. The intertial neck force was also not calculated for child restraints in which the child is restrained with an impact shield or in which an integrated child restraint airbag deployed. In both cases, chin-to-chest contact does not occur because the head comes into contact with the shield or with the airbag, before chin-to-chest contact can occur.

The percentage change from the measured neck tension force to the calculated inertial neck tension force was calculated for each applicable test. This was used to determine the presence of chin-to-chest contact and to estimate the level of neck force that might have been measured, if the contact had not occurred or had been mitigated. Substantial chin-to-chest contact was assumed to have occurred when the percentage change in the neck force was 10 percent or greater. This was a somewhat arbitrary figure chosen to ensure the level of difference was greater than that expected through normal test-to-test repeatability. To validate this approach, a selection of representative time histories were analysed to verify the presence, or not, of chin-to-chest contact for a given level of percentage change. In each case, the external head contact force was calculated and plotted with the neck force (measured and calculated inertial). The external head contact force was determined using the procedure specified in SAE J2052 [11]. The procedure uses the head mass (above the neutral axis of the load cell), the head acceleration components (a_x, a_y, a_z) and the neck force components (F_x, F_y, F_z) in a root sum square calculation. A contact is assumbed to have occurred when the external head contact force level has reached 500 N.

Worst-case combinations of impact direction and child restraint orientation from which to derive pragmatic thresholds were identified in [2] for each Q-Series dummy. No further separation by child restraint adjustment was made after an initial scan of the data revealed very low sample sizes for some combinations of dummy, impact direction and child restraint adjustment.Two statistical analyses were carried out on the results from these worst-case combinations: 95th percentile and the mean plus two standard deviations ("Mean +2SD"). We identified the same worst-case combinations and performed the same statistical analysis, in order to compare our sample with the larger study and to investigate how reduced data that avoided the influence of chin-to-chest contact might have influenced the pragmatic proposals.

RESULTS

Sample characteristics

Our study sample comprised around 20 child restraint systems and 210 type-approval tests with Q-Series dummies (Table 1). In UN Regulation No. 129, the stature range of the child restraint determines which dummies must be used in the dynamic tests. For a given dummy, impact direction and orientation, each child restraint is typically tested several times to cover different seat and/or support leg adjustments (where applicable). After the data were separated by impact direction and child restraint orientation, each sub-sample ranged from 7 tests (Q10, front impact, forward-facing) to 32 tests (Q0, rear impact, rear-facing). Tests with the Q6 were removed from the sample to avoid the specific model of child restraint being identified.

Table 1.
Child restraint system (CRS) type-approval sample characteristics

Test dummy	Impact direction	CRS orientation	Number of CRS	Number of tests
Q0	Front	Rear-facing	13	27
	Rear	Rear-facing	12	32
Q1	Front	Rear-facing	4	9
	Rear	Rear-facing	5	9
Q1.5	Front	Rear-facing	9	23
		Forward-facing	5	16
	Rear	Rear-facing	10	21
Q3	Front	Rear-facing	7	17
		Forward-facing	10	30
	Rear	Rear-facing	7	19
Q6	Front	Forward-facing	0	0
Q10	Front	Forward-facing	3	7
Total			**≈20***	**210**

*All child restraints cover more than one dummy/impact direction/orientation

Effect of test and child restraint parameters on neck tension force

The peak neck tension force measured by the upper neck load cell tended to increase with dummy size for any given impact direction and child restraint orientation (Figure1). A large spread in the neck tension force values was observed in most combinations of conditions and was substantial in the front impact tests with forward-facing child restraints. Although there were overlaps, the highest neck tension force tended to be measured in rear impact tests for both the Q0 and the Q1 dummies. The highest tension force was measured in front impact with forward-facing child restraints for the Q1.5, Q3 and Q10 dummies. These 'worst-case' combinations of impact direction and child restraint orientation for each dummy reflect those used in the development of pragmatic neck thresholds in [2].

The inertial neck tension force (calculated from the head vertical acceleration) followed similar overall trends to the measured force (Figure 2). However, there were some important differences. Firstly, the spread in the values reduced markedly for the forward-facing child restraints. This meant that the upper value, and the mean were also reduced greatly. More moderate effects were observed in the rear impact tests (i.e. with rear-facing CRS). Nevertheless, the spread in the values with the Q0 was visibly reduced. The inertial force was not calculated for the rear-facing child restraints in front impact, but the unchanged measurements were included on the chart for comparison with the other conditions. Despite these differences, the worst-case combinations of impact direction and child restraint orientation remained the same. In some tests with the Q0 (5 tests) and Q1.5 (10 tests), the calculated neck force increased compared with the measured force. It was unclear why this happened and until measurement errors could be ruled out these tests were excluded from subsequent analyses of the difference between the measured and the calculated force.
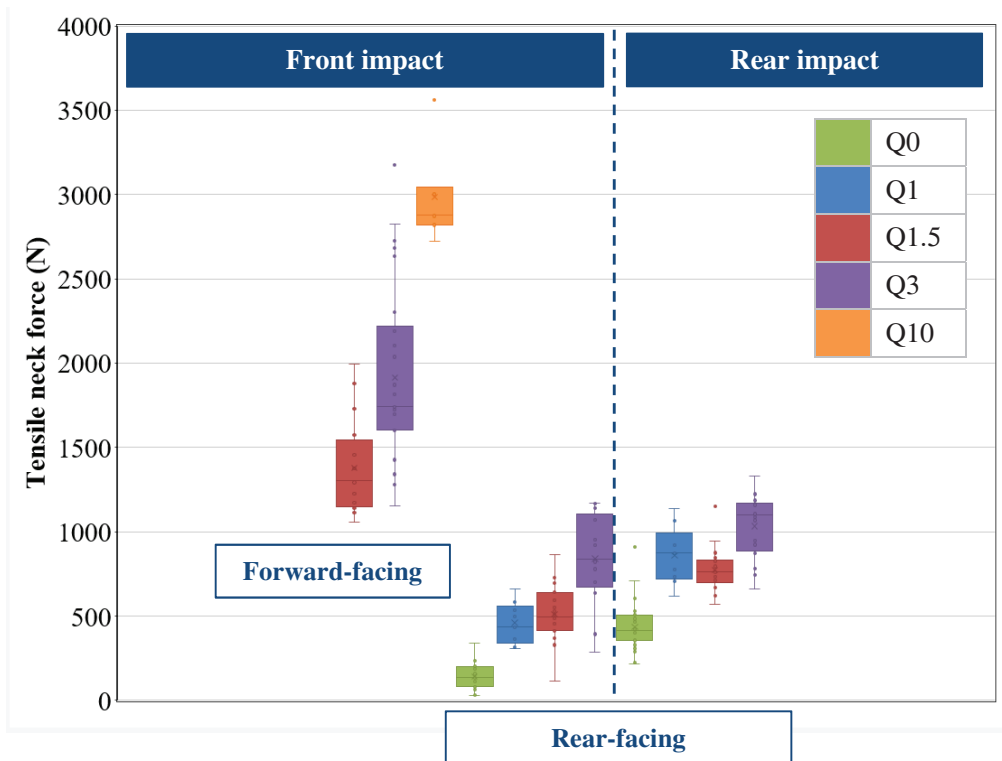
Figure 1. Peak measured neck tension force by impact direction and child restraint orientation
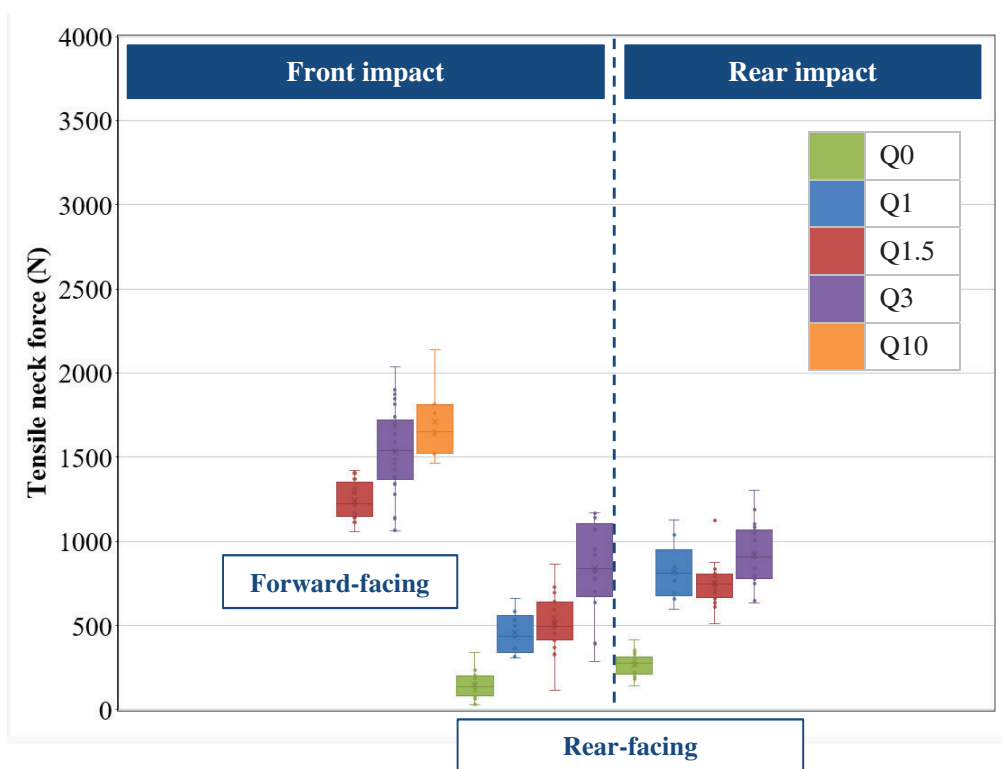

Figure 2. Peak calculated inertial neck tension force by impact direction and child restraint orientation

Effect of chin-to-chest contact on neck tension force

The percentage change from the measured neck tension force to the calculated neck tension force varied across each combination of impact direction and child restraint orientation (Table 2). The percentage change also varied to some extent within each combination. This suggests that chin-to-chest contact was more frequent in some combinations of impact direction and child restraint orientation than others, but that individual cases could occur in almost all combinations. For example, the greatest average percentage change was observed with the Q0 dummy in rear impact tests and the Q10 dummy in front impact tests, albeit with a very small Q10 sample. In the case of the Q0, 85% of tests displayed evidence of chin-to-chest contact (as defined by a percentage change of 10% or greater).

Relatively large differences were also observed with the Q1.5 and Q3 in forward-facing child restraints, which displayed average percentage changes of 18% and 26%. Although these average changes did not reach the level of those observed with the Q0, substantial proportions of each sample were affected, with 57% and 90% of applicable tests in each condition being affected by chin-to-chest contact. In contrast, the Q1 and Q1.5 (in rear impact) seemed least influenced by chin-to-chest contact and the Q1 in particular seeming to be unaffected in any of the tests, although the sample was small.
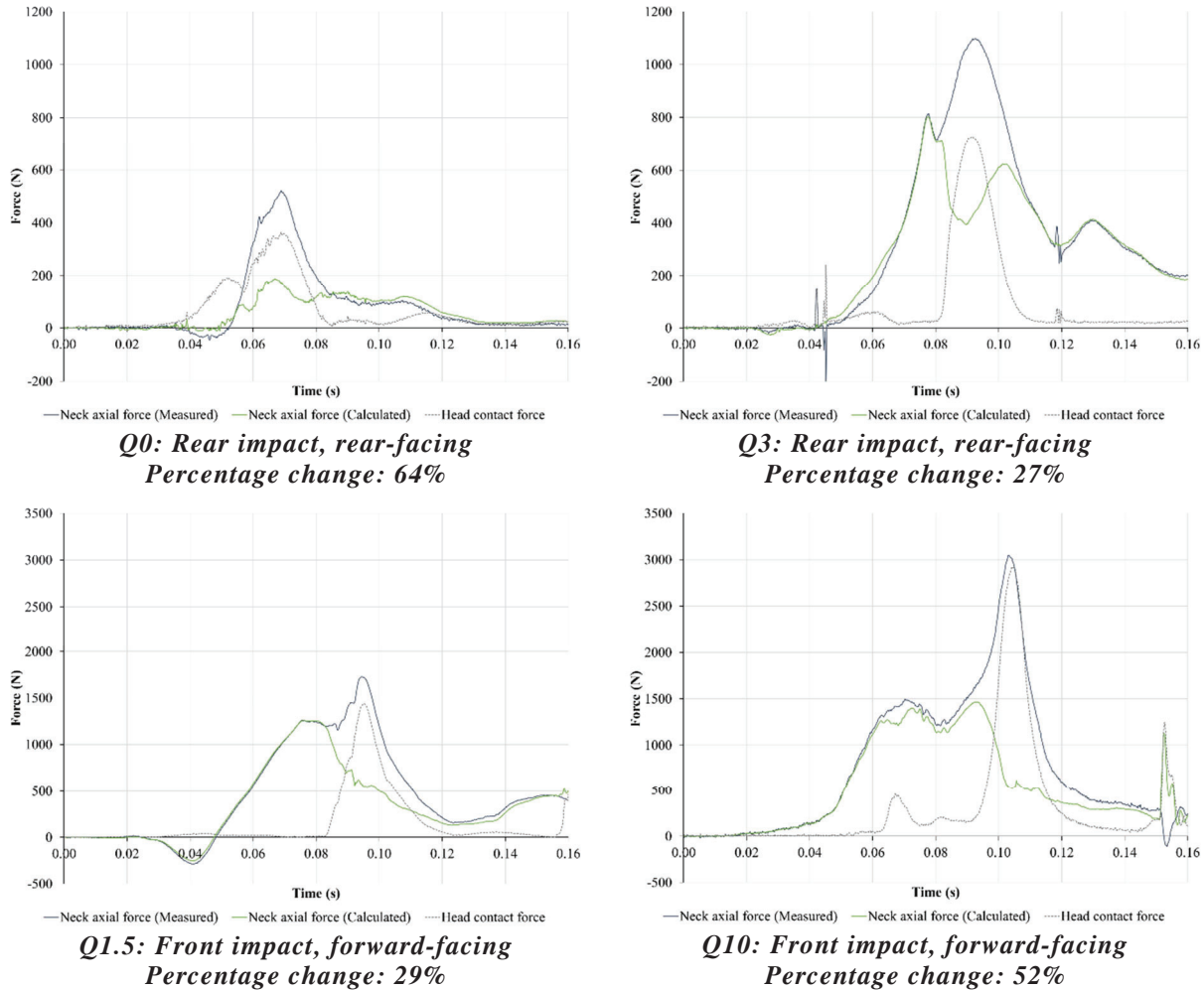
Table 2.
Percentage change in peak neck tension force from measured value to calculated value

Test dummy	Impact direction	CRS orientation	No. of tests	% change in neck tension (measured to calculated)		Proportion with chin-to-chest contact
				Average	Range	
Q0	Rear	RF	27	-43%	-64% to -29%	85%
Q1	Rear	RF	9	-4%	-9% to -1%	0%
Q1.5	Front	FF	7	-18%	-30% to -4%	57%
	Rear	RF	10	-6%	-33% to -1%	10%
Q3	Front	FF	20	-26%	-40% to -1%	90%
		FF – Integral	*15*	*-23%*	*-34% to -1 %*	*87%*
		FF – Boosters	*5*	*-32%*	*-40% to -27%*	*100%*
	Rear	RF	19	-11%	-29% to -2%	50%
Q10	Front	FF	7	-43%	-52% to -39%	100%

* RF: rear-facing; FF: forward-facing

A clear chin-to-chest interaction can be distinguished in representative time history plots in which the calculated force exceeded the measured force by a large margin (Figure 3). Two different responses are illustrated in the examples below. The Q3 (rear impact, rear-facing), Q1.5 (front impact, forward-facing) and Q10 (front impact, forward-facing) showed an initial, purely inertial, peak prior to chin-to-chest contact, followed by a second, much larger peak during the period of contact. The onset of this second peak corresponded with the time of engagement between the chin and chest, identified from the external head contact force. The second tensile peak, due to chin-to-chest contact, was the overall peak value. In each case, the calculated inertial neck force followed the measured force very closely up to the point of chin-to-chest contact at which point it diverged from the measured force over the period of contact. In some examples (i.e., the Q1.5 and Q3 in Figure 3), the inertial force fell away very rapidly.

The Q0 dummy (rear impact, rear-facing) displayed different behaviour. As shown in the example (Figure 3, top left), the calculated force diverged from the measured force earlier than the other examples, over the period of peak neck force. This behaviour was typical of the Q0 tests. The external head contact force did not reach the 500 N threshold specified in SAE J2502, however, the threshold was likely developed for adult dummies in mind. The external head force reached around 400 N with the Q0 and suggests some degree of contact occurred.

Q0: Rear impact, rear-facing
Percentage change: 64%

Q3: Rear impact, rear-facing
Percentage change: 27%

Q1.5: Front impact, forward-facing
Percentage change: 29%

Q10: Front impact, forward-facing
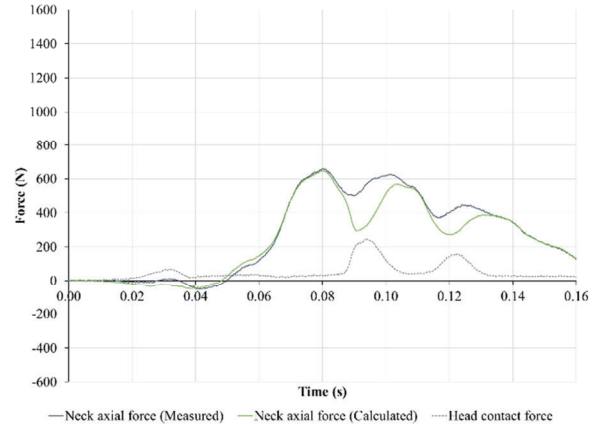*Percentage change: 52%*

Figure 3. Upper neck axial force and head contact force – representative examples with large percentage change from measured to calculated neck tension force

In tests where the peak calculated force was similar to the measured force, the representative time history plots showed that chin-to-chest contact was either marginal or occurred somewhat late in the impact event (Figure 4). In the examples with the Q1 and the Q3 (both rear impact, rear-facing), the external head contact force did not reach the 500 N threshold at which a significant contact is assumed to have occurred in SAE J2502, although it was quite close with the Q1 (400 N). In both cases, the inertial force followed the measured force very closely, but still diverged over the period of marginal contact. However, this did not influence the overall peak value. In the example with the Q1.5 (front impact, forward-facing), the external head contact force indicated a substantial chin-to-chest interaction, but although it increased the measured force compared with the inertial force, this second peak due to contact was only marginally larger than the inertial peak.

As mentioned above, there were some tests in which the calculated force exceeded the measured force (Figure 5). This was observed with the Q0 and Q1.5 dummies only (both rear impact and rear-facing child restraints). This occurred in cases where the contact was inconclusive or not sufficient to reach the threshold specified in SAE J2502. Further analysis is needed to understand what happened in these tests.
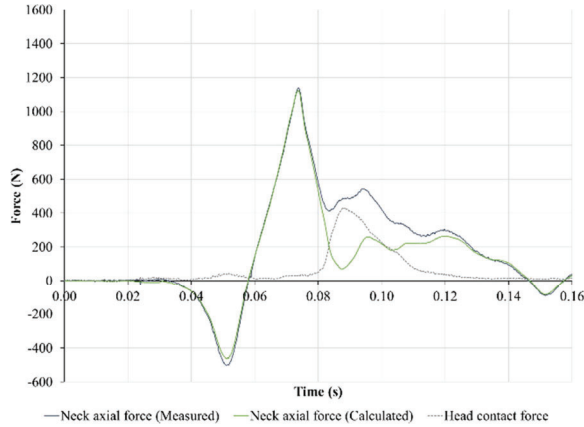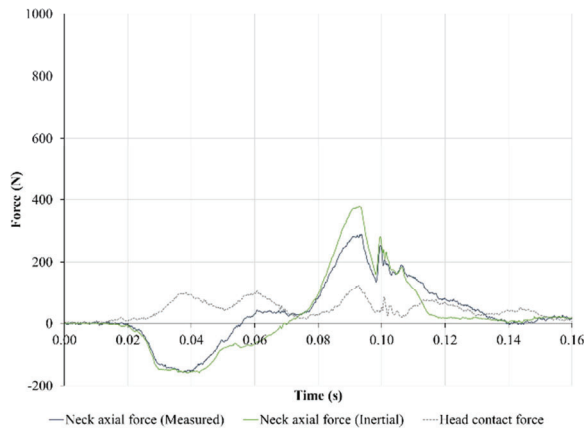
Q1: Rear impact, rear facing
Percentage change: 1%

Q3: Rear impact, rear-facing
Percentage change: 2%
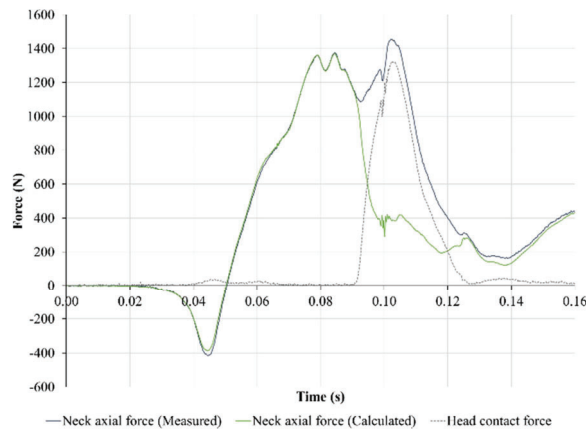
Q1.5: Front impact, forward-facing
Percentage change: 6%

Figure 4. Upper neck axial force and head contact force – representative examples with negligible percentage change from measured to calculated neck tension force
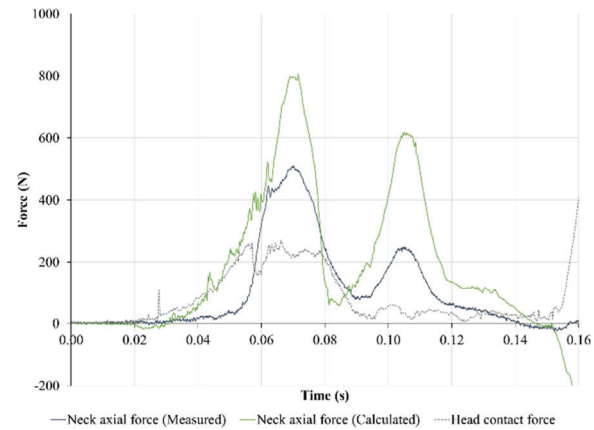

Q0: Rear impact, rear-facing

Q1.5: Rear impact, rear-facing

Figure 5. Upper neck axial force and head contact force – representative examples with large percentage change from measured to calculated neck tension force

Potential implications for the development of pragmatic neck tension thresholds

Despite fewer tests and less product diversity, the sample used in this study shared many characteristics with that used by CLEPA in [2-3] to derive pragmatic limits for the Q0, Q1 and Q1.5 (Table 3). Our sample featured slightly lower measurements overall for the Q0 and Q1.5 dummies, compared with the larger sample, but slightly higher measurements for the Q1. If the same approach used to derive pragmatic thresholds from the full type-approval monitoring data were used in our sample, it would yield similar thresholds for our measured neck force data (i.e. for the Q0, Q1 and Q1.5). However, if the method was used on our calculated inertial data, it would yield much lower thresholds than those proposed for UN Regulation No.129. In fact, the neck tension force thresholds proposed by EEVC in [6] for a 20% risk of AIS≥3 injury are quite similar to the upper range of the inertial force for the Q0, Q1 and Q10. However, the EEVC thresholds are somewhat higher than the upper range for the Q1.5 and Q3, and are closer to the mean value instead.

Table 3.
Measured and calculated neck tension force parameters and comparison with XXX

| Sample | Dummy | Impact direction | CRS orientation | n | Neck tension force | | | | | Threshold | |
					Min.	Max.	Mean	95th %ile	Mean + (2*SD)	CLEPA [2-3]	EEVC [6]
CLEPA [2-3]				*71*	*83*	*884*	*347*	*720*	*720*		
CYBEX	Q0	Rear	RF	32	217	911	437	656	656	700	498
CYBEX: inertial				32	140	415	263	343	343		
CLEPA [2-3]				40	242	1004	642	905	1018		
CYBEX	Q1	Rear	RF	9	620	1139	858	1110	1196	950	1095
CYBEX: inertial				9	597	1127	823	1092	1169		
CLEPA [2-3]				54	204	2914	1509	2122	2443		
CYBEX	Q1.5	Front	FF	16	1057	1996	1379	1909	1942	2000	1244
CYBEX: inertial				16	1057	1420	1242	1409	1468		
CYBEX	Q3	Front	FF	30	1154	3177	1913	2779	2906	-	1555
CYBEX: inertial				30	1065	2039	1535	1888	2063		
CYBEX	Q10	Front	FF	7	2725	3563	2986	3408	3539	-	2241
CYBEX: inertial				7	1467	2137	1712	2040	2160		

* RF: rear-facing; FF: forward-facing

DISCUSSION

The neck tension force measured by the upper neck load cell was highest in front impact tests with forward-facing child restraints. However, there were overlaps such that the lowest measurements in this 'worst-case' combination of conditions were consistent with the highest measurements in other conditions with the same dummies, notably rear impact with rear-facing child restraints. This was somewhat surprising given that the rear impact test in UN Regulation No. 129 is performed at a lower severity than the front impact test (i.e. 32 km/h, 14-21 g vs. 50 km/h, 20-28 g). Rear impact is not currently viewed as a high priority for child occupant protection, but that may change in the longer term, if automated vehicles lead to more frequent rear impact collisions as suggested by some studies [12]. Currently, consumer tests of child restraints encourage improved performance in front and side impact, but rear impact is left to the regulatory test.

Calculating the inertial neck tension force from the head vertical acceleration reduced the mean value and the spread of values for each combination of impact direction and child restraint orientation. Nevertheless, the same general trends were observed in terms of the worst-case combinations of impact direction and child restraint orientation. That said, compared with the measured force, the inertial force reduced the differences between the child restraint orientations in front impact, particularly with respect to the mean value. Ultimately, predicting non-contact, inertial neck injury risk is challenging. Aside from the complicating factor of chin-to-chest contact, the stiff thoracic spine of child dummies

results in high neck forces and moments that are not representative of the true injury potential [13]. Real-world data on the risk of neck injury in child restraints is inconclusive. The most recent studies suggest neck injury rates are very low [14]. Case studies with serious neck injury continue to be reported, but it is not always possible to rule out head impact, high collision speed or child restraint misuse as a factor [15]. Specifying a limit on (resultant) head acceleration likely provides some measure of control on tensile neck loading. However, UN Regulation No. 129 specifies thresholds for the head, chest and abdomen, and so adding thresholds for the neck could reduce the potential for uninstrumented load paths to be exploited.

Chin-to-chest contact occurred frequently in our sample of child restraint type-approval tests (as indicated by the discrepancies between the measured and the calculated neck tension force). It appeared to be particularly prevalent with the Q0 in rear impact, and with the Q1.5, Q3 and Q10 in front impact (with forward-facing child restraints). It was unclear why certain combinations of impact direction or child restraint orientation were more susceptible. Previous studies have highlighted that dummy posture and child restraint design can influence chin-to-chest contact characteristics [16-17]. A broad range in the effect of chin-to-chest contact was observed within each combination of impact direction and child restraint orientation in our sample (denoted by the percentage change from the measured to the calculated force). It seems plausible that dummy positioning and posture played a role, but a much larger study sample would be needed to investigate such influences. The prevalence of chin-to-chest contact in real-world collisions and its effect on child injury potential, if any, does not appear to have been reported. Chin-to-chest contact has been observed in child cadavers [13] and in human body models [18]. However, the severity of contact and its effect on neck forces seems to be much greater in dummies, primarily due to the stiffness of their components [19].

The calculated inertial neck tension force was used primarily as a means of identifying where significant chin-to-chest contact occurred. It was also used to comment on the likely neck tension force under purely inertial loading, for example, if chin-to-chest contact was not present. Although it was proposed for that purpose [7], the reliability of the calculation is unclear. The calculated neck force predicted the measured force up to the point of chin-to-chest contact very well in most tests; however, in some tests, the calculated force fell away very quickly when contact began. This might indicate that the chin-to-chest contact itself influenced the vertical head acceleration and consequently the calculated neck force. Similar findings were observed in an impact test study with prototype adapted heads with little chin structure [10] and in a large analysis of consumer tests of child restraints (under different impact conditions) [20].

Despite reservations over the reliability of the calculated neck force to predict the true inertial force in all tests, it was useful in confirming that the pragmatic neck tension force thresholds proposed for UN Regulation No. 129 were likely to have been influenced greatly by chin-to-chest contact (i.e., assuming our limited sample reflected the larger monitoring sample). Unfortunately, it is unknown whether the measured force (and thresholds derived from it) was skewed to the extent predicted by the calculated force, or whether chin-to-chest contact masked a more moderate increase in the tension force that the calculated force could not detect. However, if the calculated inertial force was meaningful, it suggests a marked influence on the pragmatic thresholds proposed for the Q0 and Q1.5 dummies. In fact, the inertial force reduced the values to such an extent that previously proposed thresholds scaled from Hybrid III child dummy injury assessment reference values appear to become more meaningful. That said, scaling with child dummies (from adult dummies, or between child dummy families and/or sizes) requires significant assumptions to be made about the difference in geometry, stiffness and failure stress between subjects [21]. Combinations of human and dummy ratios are used, which do not take account of differences in behaviour and performance between the dummies used [6].

Limitations

Our study sample comprised type-approval tests from CYBEX child restraint systems only. Although our data shared many characteristics with the larger type-approval monitoring sample used to derive pragmatic neck tension thresholds, child restraints from other manufacturers may be less susceptible to chin-to-chest contact (or even more susceptible). A larger sample, comprising a broad range of

manufacturers and products, is needed to validate our findings fully. Nevertheless, this study demonstrated a useful method for identifying and characterising chin-to-chest contact from a large dataset.

Similarly, the limited nature of our sample meant that some combinations of dummy, impact direction and child restraint orientation yielded very low sample sizes from our database. For example, there were very few tests with the Q1 dummy, and none with Q6. UN Regulation No. 129 requires that the smallest and the largest dummies corresponding to the stature range of the child restraint must be used in the dynamic tests. For most of our product range, these are 'intermediate dummies' and are consequently less likely to feature in our database.

Chin-to-chest contact can also influence Q-Series chest deflection [22-23] and abdomen pressure [24]. This study focussed on axial neck force only. We don't currently have a method to investigate the potential influence on these other measurements based on a simple analysis of peak type-approval measurement parameters. A detailed study of time history plots, possibly including the use of adapted dummies would be needed to investigate the effect of chin-to-chest contact on these other measurements.

CONCLUSIONS

Child restraints are very effective in reducing the risk of serious neck injury to children in collisions. Nevertheless, a relatively large spread of neck loads can be measured during type-approval. In our study, the neck tension force measured by the upper neck load cell of the Q-Series dummies was influenced primarily by the impact direction and the orientation of the child restraint. Front impact with forward-facing child restraints generated the higher neck forces than other scenarios. However, there were overlaps with rear impact tests with rear-facing child restraints, despite the lower rear impact severity. The calculated neck force (derived from the head vertical acceleration) displayed similar trends as the measured force in terms of the influence of the impact direction and child restraint orientation on the magnitude of the force. However, the level of difference between certain combinations of impact direction and child restraint orientation we reduced. This was likely due to the influence of chin-to-chest contact on the measured data, which was particularly pronounced with front impact tests on forward-facing child restraints.

Chin-to-chest contact occurred frequently throughout our study sample of internal child restraint type-approval tests. If the frequency and magnitude of chin-to-chest contact observed in our study was reflected in the larger type-approval monitoring sample in [2], it is likely that the pragmatic limits proposed for UN Regulation No. 129 are also likely to have been affected (i.e. increased). Subsequent measurements in future type-approval tests would also likely to be affected in the same way and hence mitigating chin-to-chest contact rather than inertial loading might become the priority for child restraint design. However, although the calculated inertial force was useful for identifying chin-to-chest contact and estimating its effect on the neck tension force measurement, it may also be influenced by chin-to-chest contact, such that encouraging contact at a certain time in the impact might be a means of reducing the vertical head acceleration and hence the calculated neck force value.

REFERENCES

[1] United Nations. 2019. Report of the Working Party on Passive Safety on its sixty-fifth session. Geneva, May 13–17.

[2] European Association of Automotive Suppliers (CLEPA). 2020. "Explanatory presentation to CLEPA neck load limits proposal". Informal Document GRSP-68-10, 68th session of GRSP, 7-11 December 2020.

[3] Visvikis, C., Pitcher, M., Bendjellal, F., Le Claire, M., Müller, T. 2020. "The development of pragmatic thresholds for upper neck tension force and flexion moment in Q-Series dummies in UN Regulation No.129 tests". Proceedings of the 18th International Conference Protection of Children in Cars, Munich, Germany.

[4] Johannsen, H., Trosseille, X., Lesire, P., Beillas, P. 2012. "Estimating Q-dummy injury criteria using CASPER project results and scaling adult reference values". IRCOBI Conference Proceedings; p. 580–596, Dublin, Ireland.

[5] Hynd, M., Pitcher, M., Hynd, D., Robinson, B., Carroll, J.A. 2010. "Analysis for the development of legislation on child occupant protection". TRL Client Project Report 821.

[6] Wismans, J., Waagmeester, K., Le Claire, M., Hynd, D., de Jager, K., Palisson, A., van Ratingen, M., Trosseille, X. 2008. "Q-dummies report. Advanced child dummies and injury criteria for frontal impact". European Enhanced Vehicle-Safety Committee (EEVC) Working Group 12 and 18 Report No. 514.

[7] Martinez Sáez, L. 2020. "Effect of Q1.5 chin-thorax contact in measuring upper neck forces". Informal Document GRSP-68-26, 68th session of GRSP, 7-11 December 2020.

[8] Visvikis, C., Thurn, C., Kettner, M., Müller, T. 2020. "The effect of chin-to-chest contact on upper neck axial force in UN Regulation No. 129 frontal impact tests of child restraint systems". Traffic Inj. Prev. 21(sup1):S173-S176. doi: 10.1080/15389588.2020.1829923.

[9] European Association of Automotive Suppliers (CLEPA). 2021. "R129 neck limits: effect of chin-to-chest contact and potential solutions". Informal Document GRSP-70-22, 70th session of GRSP, 6-10 December 2021.

[10] Visvikis, C., Thurn, C., Müller, T. 2021. "The effect of Q-Series dummy adaptation on the prevalence of chin-to-chest contact and its influence on upper neck tension force in UN Regulation No. 129 tests". Proceedings of the 19th International Conference Protection of Children in Cars, Munich, Germany.

[11] Society of Automotive Engineers (SAE) 2016. "Test device head contact duration analysis (SAE J2502)". https://www.sae.org/standards/content/j2052_201607/.

[12] Schoerrle, B. and Sivak, M. 2015. "A preliminary analysis of real-world crashes involving self-driving vehicles". University of Michigan Transportation Research Institute (UMTRI). Report No. UMTRI-2015-34.

[13] Sherwood, C.P., Shaw, C.G., Van Rooij, L., Kent, R.W., Crandall, J.R., Orzechowski, K.M., Eichelberger, M.R., Kallieris, D. 2003. "Prediction of cervical spine injury risk for the 6-year-old child in frontal crashes". Traffic Inj. Prev. 4(3):206–213. doi:10.1080/15389580309885.

[14] McMurry, T.L., Arbogast, K.B., Sherwood, C.P., Vaca, F., Bull, M,, Crandall, J.R., Kent, R. 2018. "Rear-facing versus forward-facing child restraints: an updated assessment. Injury prevention", 24, 55-59. doi: 10.1136/injuryprev-2017-042512.

[15] Gan, J.H., Davison, C., Prince, N., Gour, A. 2018. "Car seats: Facing backward is the way forward". Trauma, 21(1), 68-72. doi:10.1177/1460408618755811.

[16] Klinich, K.D., Reed, M.P., Ritchie, N.L., Manary, M.A., Schneider, L.W., Rupp, J.D. 2008. "Assessing child belt fit, volume II: Effect of restraint configuration, booster seat designs, seating procedure, and belt fit on the dynamic response of the Hybrid III 10YO ATD in sled tests". University of Michigan Transportation Research Institute (UMTRI). Report No. UMTRI-2008-49-2.

[17] Stammen, J.A., Sullivan, L.K. 2008. "Development of a Hybrid III 6yr. old and 10 yr. old dummy seating procedure for booster seat testing". National Highway Traffic Safety Administration (NHTSA) Technical Report. NHTSA Docket 2007-0048-0002.

[18] Maheshwari, J., Duong, N., Sarfare, S., Belwadi, A. 2018. "Evaluating the response of the PIPER scalable human body model across child restraining seats in simulated frontal crashes". Traffic Inj Prev. 19(sup2):S140–S142. doi:10.1080/15389588.2018.1532204.

[19] Stammen, J.A., Bolte, J.H., Shaw, J. 2012. "Biomechanical impact response of the human chin and manubrium". Ann. Biomed Eng. 40(3): 666–678. doi:10.1007/s10439-011-0419-x.

[20] Ratzek, A. 2022. "Influence of the chin-to-chest contact to the neck tension force". Proceedings of the 20th International Conference Protection of Children in Cars, Munich, Germany.

[21] Carroll, J.A., Pitcher, M., Hynd, M. 2011. "Extension of biofidelity and injury risk curve development for the Q10. EPOCh Project Report". Work Package 1, Task 1.3a and Task 3.2a.

[22] Visvikis, C., Carroll, J., Picher, M., Barrow, A., Cuerden, R., Broertjes, P. 2013. "Research findings for the optimised evolution of the new regulation on enhanced child restraint systems" Proceedings of the 11th International Conference Protection of Children in Cars, Munich, Germany.

[23] Pitcher, M., Carroll, J., Broertjes, P. 2015. "Research findings for setting dummy injury thresholds for Regulation 129 phase 2 regarding chest and abdomen loading". Proceedings of the 13th International Conference Protection of Children in Cars, Munich, Germany.

[24] Visvikis, C., Thurn, C., Müller, T. 2020. "Investigation of different methods of improving the assessment of booster seats in light of Dummy and sensor capabilities". IRCOBI Conference Proceedings; p. 487–498.

Title: Influence of Different Parameters of Vehicle and Pedestrian on Chest Kinematics Using Human Body Model (HBM)

Chinmoy, Pal
Shigeru, Hirayama
Nissan Motor Company Ltd,
Japan
Pratap Naidu, Vallabhaneni
Vimalathithan, Kulothungan
Renault Nissan Technology Business Centre India,
India

ABSTRACT

In Japan from 2000 to 2019, the number of motor vehicle occupant fatalities decreased significantly. Pedestrian road user type contributes to 37% of total traffic fatalities, the highest compared to other road user types since 2009. In pedestrian accidents, Head and chest body regions account for 51% and 40%, covering about 91% of the total AIS4+ injuries, respectively. So, head and chest protection are important elements for reducing pedestrian fatalities. At present, there are test procedures for head and lower extremities injury protection, but no test procedure exists for pedestrian chest protection. BAST has proposed a specific thorax injury prediction tool (TIPT) developed from side impact dummy ES-2. Based on their proposal, an adult chest impactor will be impacted by several predefined impact grid points covering a range from a child's lower rib height (WAD: 770mm) to a 95th-%ile male's upper rib height (WAD:1540mm). Injury criteria for TIPT were based on injury risk curves of 45 to 67 year-old adults. In this paper, the influence of different parameters of vehicles and pedestrians on chest injury using human body models (HBM) and TIPT modules are studied in detail. It can be concluded that (a) similar to the existing head injury evaluation impactors, child and adult TIPT impactors need to be different since the biomechanical characteristics are different (b) based on human body models' CAE simulation with the target generic vehicles models (GVM), the chest impact velocity is considerably lower than those recommended values of BASt and (c) it has been observed that BLE height, bumper lead upper, hood angle are the significant parameters for the chest impact velocity.

INTRODUCTION

Societies of advanced countries are aging demographically. Based on serious injury comparison among different body regions for the age group 25-64 and >65 year-old categories, the thorax body region ranks 3rd for the age group 25-64 and ranks 2nd for the age group >65 [Wisch et al., 2017]. Presently pedestrian regulations do not consider chest protection. Project SENIORS (Safety ENhanced Innovations for Older Road userS) aims to improve the safe mobility of the elderly and overweight persons, using an integrated approach that covers the main modes of transport.
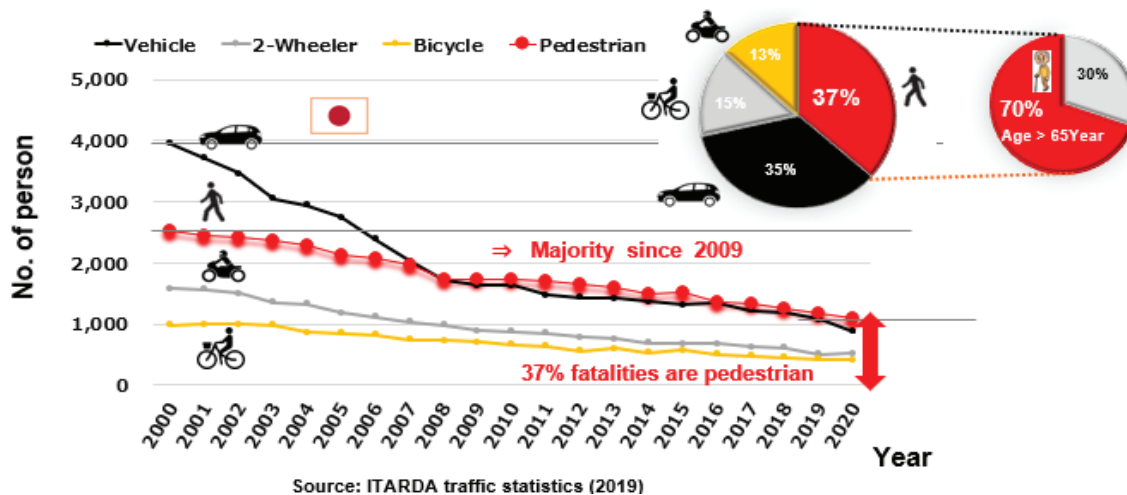

Figure 1. No. of fatalities based on the Japanese traffic accident database ITARDA, 2000-2020

According to International Transport Forum Report for Japan, pedestrians account for 37% of traffic fatalities in Japan for the year 2020. The road fatality rate per 100000 population for different age groups shows the risk for 65-74 & >75 year-old age groups is high compared to other age groups. Within 65-74 & >75 year-old age groups road fatality rate for different road user categories shows, pedestrian accidents account for a major share as shown in Figure 1.

The mission of BAST, a German organization for the Federal Highway Research Institute, is to improve the safety, environmental compatibility, economic efficiency, and performance of roads. It does Testing, certification, approval, and recognition activities in the field of road traffic. BAST's research activities have a considerable influence on EU-Regulation/ Euro-NCAP. BAST proposed a test tool for predicting thoracic injuries and assessment procedures as they did previously for bicyclist's head protection which was later included in EuroNCAP Roadmap 2021-2025. They have extracted the chest module from a side impact dummy EUROSID-2(ES-2), which has good capability in measuring chest injuries for side impact conditions. ES-2 dummy chest module was converted into an impactor TIPT (Thorax Injury Prediction Tool) which was designed to launch against the vehicle at the designed speed and angle. The test area was marked on the vehicle from WAD 770mm (height of lowermost rib of 6 year-old) to WAD 1540mm (height of uppermost rib of 95th-%ile male). Based on the half of the height of 160mm and width of 276mm of the chest module, evaluation impact points are marked with a pitch/interval of 80mm and 133.5mm as shown in Figure A1. Impact angle and velocity vary with the type of vehicle as shown in Figure 2 below and in Figure 4 of the method section. Scores are proposed based on the serious injury risk parameters for 45 year-old and 67 year-old PHMS test data. Nothing is mentioned about the child's chest injury criteria.
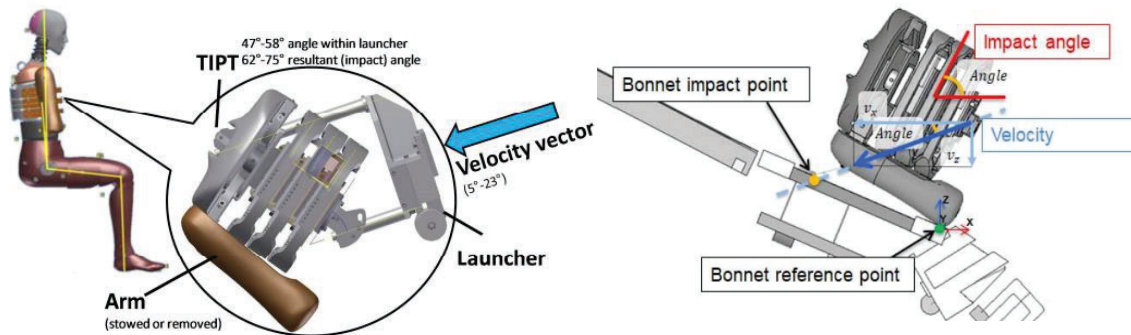

Figure 2. ES-II dummy chest-based TIPT module and a typical testing procedure (Oliver 2019)

This paper focuses on the following topics (i) to survey the chest injury characteristics of children and adults based on past published literature, (ii) to study the chest impact testing conditions using GHBMC pedestrian human model simulations against generic vehicles models (GVM), and (iii) to estimate the most influential front-end vehicle profile parameters contributing to a chest injury and impact conditions.

LITERATURE SURVEY

Children suffer fewer rib fractures and less blunt cardiac injury, but more lung contusions. Children's thoracic injuries are more often associated with head injuries and less often with spine injuries than those observed in adults. Notably, the majority of pediatric deaths were secondary to traumatic brain injury rather than thoracic injury. There was a significantly lower mortality rate in the pediatric group (16.7% v. 27.8%; p=0.037), despite Injury Severity Score ISS values in the two groups being similar [Skinner, 2015]. Osteopenic changes and co-existent underlying disease may also play a significant role in this process [Bass, 1990]. The overall outcome of child pedestrian casualties appears to be relatively constant across the pediatric stature range. However, pedestrian height seems to affect the frequency of injury to individual body regions, including the thorax and lower extremities. This suggests that vehicle safety designers need to account for the difference in injury patterns between adult and pediatric pedestrian casualties [Ivarsson, et al., 2007]. Based on Japan Trauma Data Bank 2004-12, the percentage of MAIS2+ thorax injuries in pedestrians of age 0-14 year-old children (M:16.3%, F:14.0%) are comparatively less than those of adults above 15 years (M:24.7%, F:22.6%) [Ito, et, al., 2015]. Due to the lower incidence of rib fractures, as mentioned in a number of past published literature[Ziegler1994], the patients in the pediatric age group need alternative criteria to identify patients with major chest injuries. The main focus of the present study is to identify the rationality of the chest protection proposal as recommended by BAST for adult pedestrian populations only.

METHOD

TIPT CAE Model Development

As per BAST recommendation, the CAE TIPT module was developed from an ES-2 dummy with a mass of 22.2kg as shown in Figure 3. ES-2 is already an authorized dummy for evaluating the side impact performance of existing vehicles. The mode of the impact of the pedestrian's chest is somewhat like that of a pure lateral impact for an occupant inside a car. Hence, there is an underlying basic assumption that the TIPT is expected to perform well in evaluating pedestrian chest injuries when impacted with the front end of a car also.
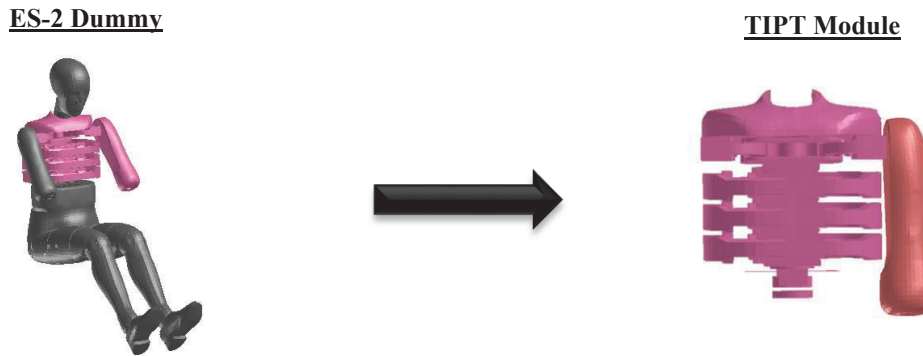
ES-2 Dummy   **TIPT Module**

Figure 3. TIPT CAE module derived from ES-II dummy

TIPT impact conditions with vehicles (BASt proposal)

BAST recommended impact locations for chest protection, ranging from 6 year-old(YO) children to 95th-%ile male adult pedestrians as shown in Figure A1. Testing conditions such as orientation, impact speed, and impact angle vary for different types of vehicle categories based on BLE height and front-end profiles. Scoring for each impact location is decided based on the amount of maximum rib deflection. A five-level scoring method was recommended based on the injury risk curves of 67-YO & 45-YO as shown in Figure 4. A separate impactor was not proposed for child chest protection. Rather the same scoring system as adult injury risk conditions is indicated for evaluation in child impact zones near WAD>770mm with the TIPT chest module of 22kg mass.

TIPT	Vehicle	FCV BLE<835	SUV BLE>836	MPV/VAN
FRD of BLR-RL*	Impact Angle (deg)	15(75)	20(70)	28(62)
	Velocity Angle(deg)	19	23	5
	Impact speed(kph)	27	15	21
FRD to BLR-RL*	Impact Angle (deg)	90		
	Velocity Angle(deg)	0		
	Impact speed(kph)	40		
* Bonnet Leading Edge Reference Line				

Color	Max deflection (mm)	Injury Risk	Score
Green	<28	5% of AIS3 **(67YO)**	1
yellow	28 - 35	20% of AIS3 (45YO)	0.75
orange	35 -40	30% of AIS3 (45YO)	0.5
brown	40-44	40% of AIS3 (45YO)	0.25
Red	>44	50% of AIS3 (45YO)	0

Figure 4. TIPT Evaluation proposed by BAST and injury score criteria

Pedestrian evaluation condition with different vehicle types

The present study used Generic Vehicle Models (GVMs) for standard vehicle categories (Family Car, SUV & MPV). In line with real-world pedestrian safety evaluation methodology as proposed by Euro-NCAP, CAE models of HBMs (GHBMC, AM50, AF05 & AM95) as mentioned in "Euro-NCAP Technical Bulletin TB 024" was chosen for this study. Refer to Figure 5 and Euro-NCAP technical bulletin [TB-024, 2022].
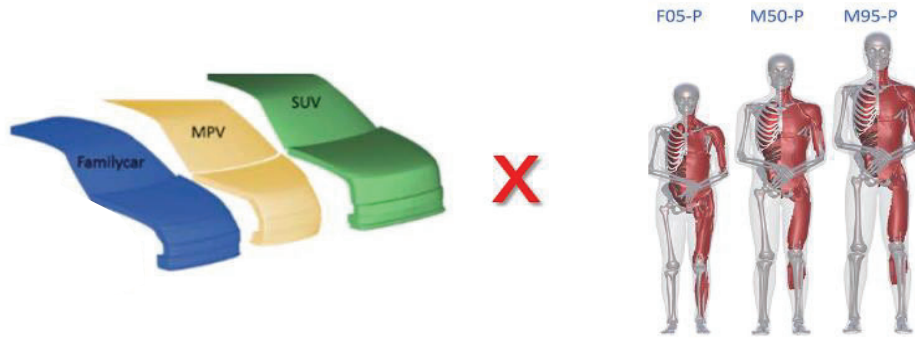
Figure 5 GVMs and different pedestrian human body models (GHBMC, AM50, AF05 & AM95).

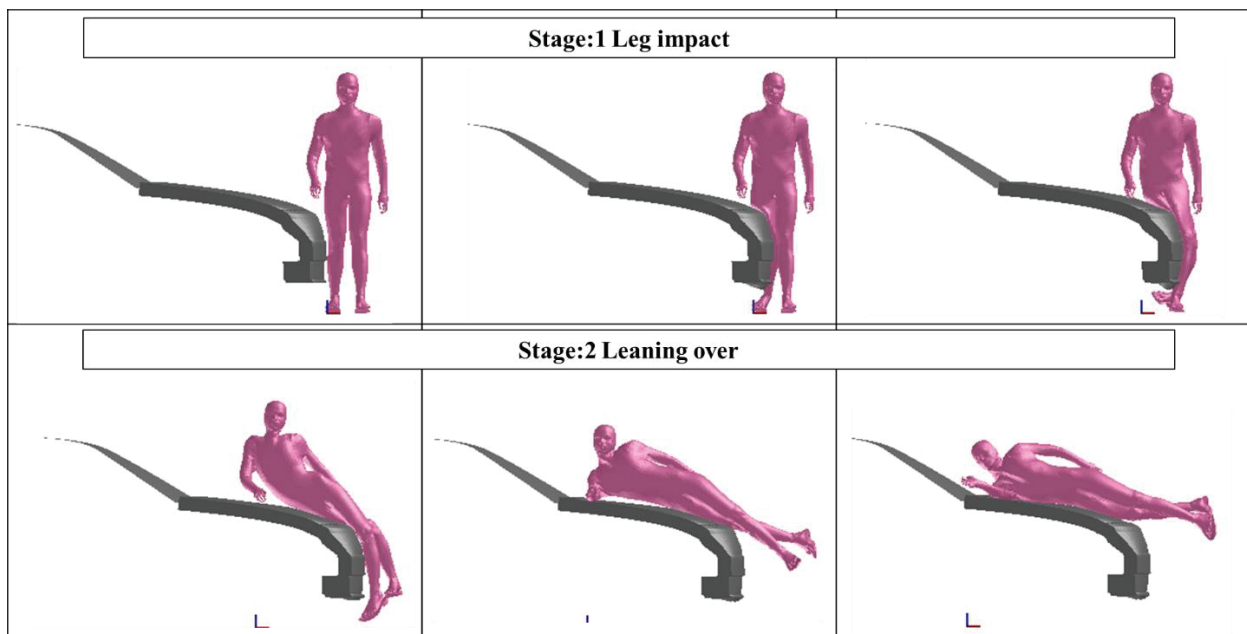**RESULTS**

HBM interaction with GVM

Figure 6 Evaluation of a typical SUV at the hood region with TIPT "with-arm & without arm" condition

This study simulated the different vehicle categories of GVM with different sizes (AM95, AM50 & AF05) of human body models (HBMs) at 40kph as shown in Figure 6. There are two stages of pedestrian-vehicle interaction; i) at first, the vehicle impacts the pedestrian's legs and causes injuries to leg bones (femur, tibia, fibula, etc.) and if the velocity is more, then the second stage will start ii) pedestrian slips and slides over the vehicle, which cause injuries to arms, chest, and head. At 40kph impact, AF05, AM50 & AM95 HBMs were impacted against different GVMs and the chest velocity is monitored at the time of contact between the vehicle and chest skin as shown in Table 1. The study reveals that

a) Chest impact velocity for a small family car (FCV) category is high, followed by MPV and SUV categories, It shows a similar trend recommended with BASt.
b) However, chest impact velocities identified are lower than those of BASt recommendations

Table 1: Chest impact velocity for FCV, SUV and MPV/VAN at 40kph impact speed

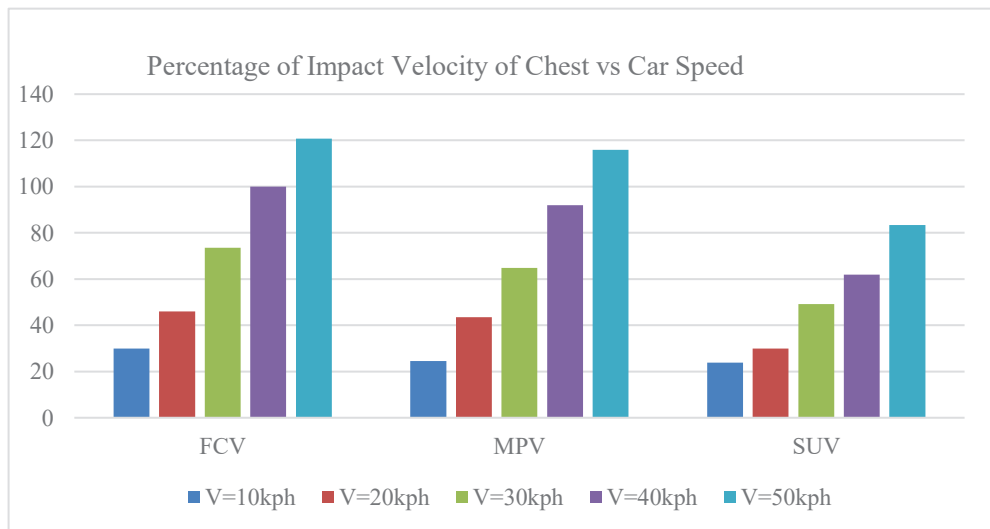| Chest impact velocity (kph)			
Category	FCV	SUV	MPV/VAN
BAST (Recommendation)	27	15	21
AM95	21.6	14.4	19.1
AM50	17.8	10. 1	14.4
AF05	18	6.1	11.9

Based on this limited case of the simulation studies, the proposed BAST impact velocities are high in all vehicle categories compared to the present simulation results which are tabulated in Table 1.

Effect of vehicle front-end profile

To understand the effect of different dimensional parameters of a vehicle's front-end profile (refer to Figure A2-1) on pedestrians' chest impact velocity on the hood, the morphing technique is used in this present study. Morph volume-based method was used to develop a series of new front-end profiles created from the original base vehicle. The front-end profile dimensions, such as BLE height, hood angle, bumper profile heights at different locations, etc., are some of the top influential parameters having a higher degree of sensitivity with respect to the chest impact velocity of AM50 HBM. Among all geometric parameters, the position of the BLE with respect to the pedestrian's CG location, which is located near the sacrum of the pedestrian, is the most influential parameter (relative sensitivity of 72%) in determining the kinematics of the chest as shown in the sensitivity chart of Figure A2-1. As the BLE height increases to a level of 120% of the BLE of the reference vehicle (BLE:100%, chest velocity:100%, as shown by the red dot of Figure A2-2), the CG of the pedestrian will be almost equal to the BLE height. The gradient of chest impact velocity becomes flat as highlighted by the blue segment in Figure A2-2.

DISCUSSION
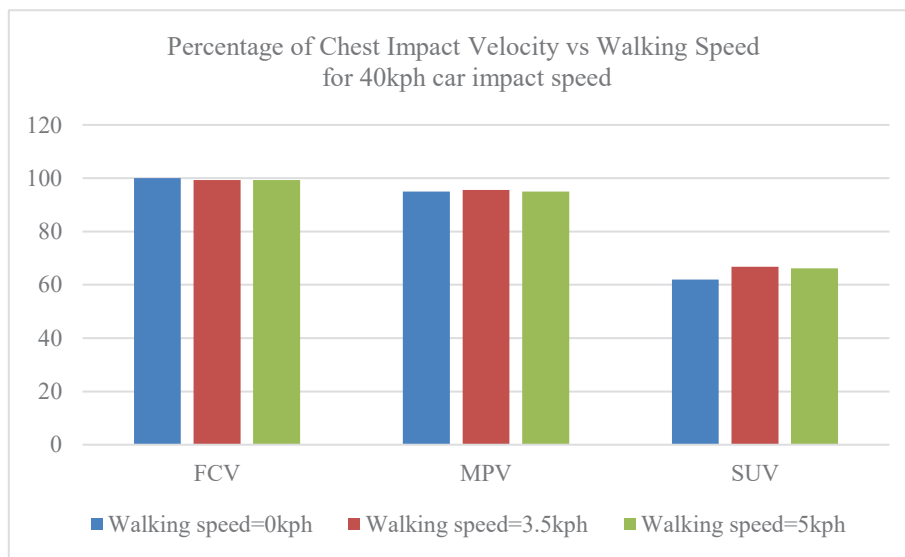
Effect of impact velocity

Figure 7. Impact velocity influence on chest velocity (normalized with FCV, V40kph as 100%)

Encompassing a wider range of real-world traffic accidents, the AM50 human model was impacted against different GVMs at different velocities ranging from 20 to 50 kph (Figure 7). Chest impact velocity is positively correlated with

impact velocity. Linear relationships exist between chest impact velocities and the corresponding impact velocities for different GVM. Irrespective of the initial impact velocity of the car, the chest impact velocity for sedan/small (FCV) cars is higher compared to those of other types of GVM. As the height of the bonnet leading edge (BLE) increases, the overlap portion and the initial contact area of the lower part of the pedestrian with the vehicle front end will be increased. As a result, the vehicle will exert more horizontal force to throw or push the pedestrian forward further. Consequently, there will be more forward translational movement causing a delay in the start of the rotational movement of the upper part of the pedestrian. Hence, the impact velocity of the chest just before it touches the hood will be significantly reduced.

Effect of walking speed

In general, walking speed significantly decreases as age increases. Walking speed decreases slightly each year as one gets older. This averages out to a difference of 1.2 minutes slower for every kilometer at age 60 than at age 20. However, the walking speed changes over time, with smaller velocities in the first, and larger velocities in the second half of the crossing time at the intersection [Asano, 2017]. The AM50 human model was impacted against different GVMs at 40kph impact velocity and a walking speed of 3.5kph and 5kph. Pedestrian walking speed has less influence on chest impact velocity, as the lateral walking speed component near an intersection is much less than the impact

Figure 8. Influence of walking speed on chest impact velocity (normalized by FCV, AM50 walking speed 0kph)

velocity of the vehicle (refer to Figure 8). However, the situation will be different, in the case of bicyclists who travel at a relatively higher speed of an average of 15 kph than a pedestrian. Refer to the paper by Pal, et al. [Pal, 2020] for a detailed study of bicyclist kinematics which shows the effect of the speed of the bicycle.
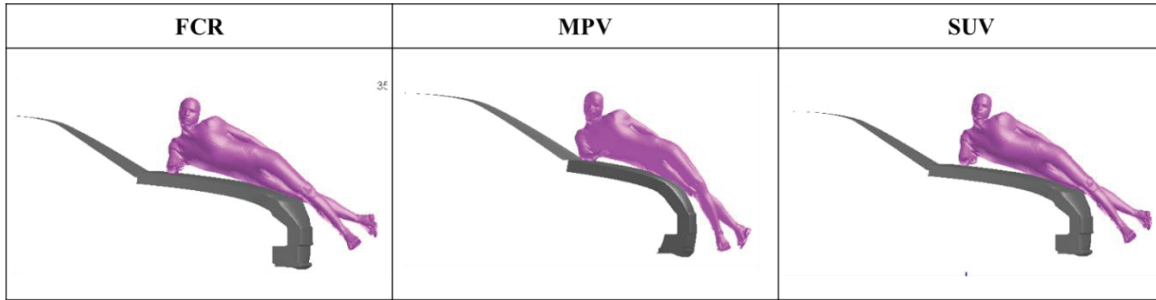
Pediatric injury protection

The thoracic cage of a child is more elastic and flexible than that of an adult. Age-related bone diseases like osteoarthritis, osteoporosis, osteomalacia, and osteopenia are very less likely in children compared to adults and the elderly >65 year-old population. Children have significantly lower mortality than adults, despite having similar Injury Severity Scores, ISS. Compliance of the pediatric thorax is much greater than that of the adult thorax, because of the pliability of the cartilage and bony structure. With the same level of mortality, ISS=15 for adults is equivalent to ISS=25 for children [Skinner 2015, Brown 2017].

Based on human body models (Figure A3), the approximate child chest mass is 5-7 kg (height =178 mm, width =195 mm, depth = 111mm) and it is quite different from TIPT characteristics (mass=22.2kg, height =272 mm, width = 302mm, depth = 268mm). TIPT was derived from an adult side impact dummy with 22.2kg mass and injury criteria based on 67-year-old and 45-year-old populations (Figure 4). It may be a debatable issue whether such an adult dummy-based TIPT chest module can be used for predicting pediatric chest injury accurately.

TIPT evaluation with or without arm

The arm and shoulder will play an important role in rib deflection. In most real-world scenarios, a pedestrian's arm and shoulder will influence the level of chest injury. As a rational approach, the TIPT module should be evaluated with arms for more accurate chest injury estimation. From Figure 9, it is evident that the pedestrian arm interacts with the vehicle before the chest impact. From Figure 10, it is also evident that the 'TIPT with arm' rotation behavior is different from TIPT 'without arm'.
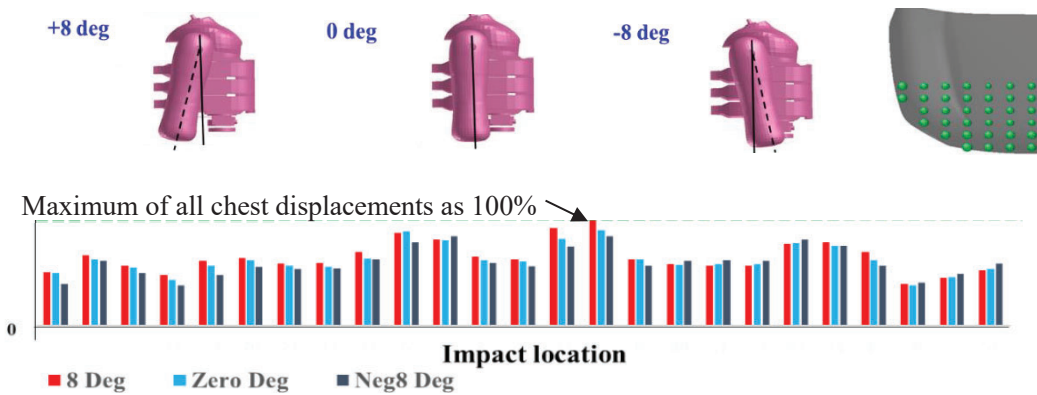
FCR	MPV	SUV

Figure 9. Typical arm interaction just before chest impact with the hood for different GVMs

Initial stage	Impact Stage	Rebound stage

TIPT without hand

TIPT with hand

TIPT with hand: rotation behavior is different
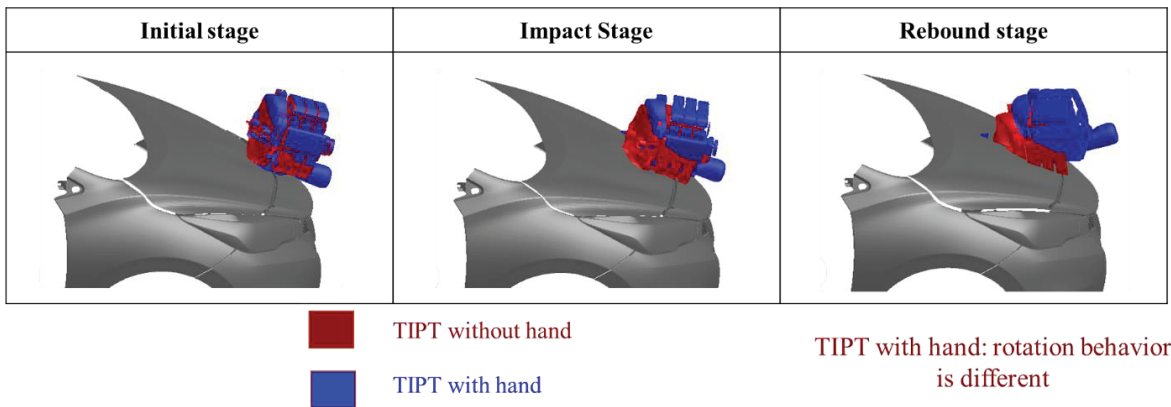
Figure 10. TIPT kinematic impact behavior with-arm and without-arm after hood contact

Effect of TIPT arm angle

+8 deg   0 deg   -8 deg

Maximum of all chest displacements as 100%

Impact location

■ 8 Deg   ■ Zero Deg   ■ Neg8 Deg

Figure 11. Arm angle influence on TIPT displacement for a typical SUV vehicle hood based on BAST test evaluation procedure at different locations as marked green on the hood.

TIPT with 3 different arm angle positions (-8 deg, 0 deg, +8deg) were impacted against the typical SUV vehicle as shown in Figure 11. Irrespective of TIPT arm angle positions, rib deflection for all impact locations will vary in the order of 12% for TIPT arm angle variations -8 deg. to +8 deg with respect to its corresponding values at 0 deg. vertical arm position. Hence, the arm angle is not a significant influential parameter for TIPT chest displacement.

Effect of vehicle speed on impact chest-spine angle before impact
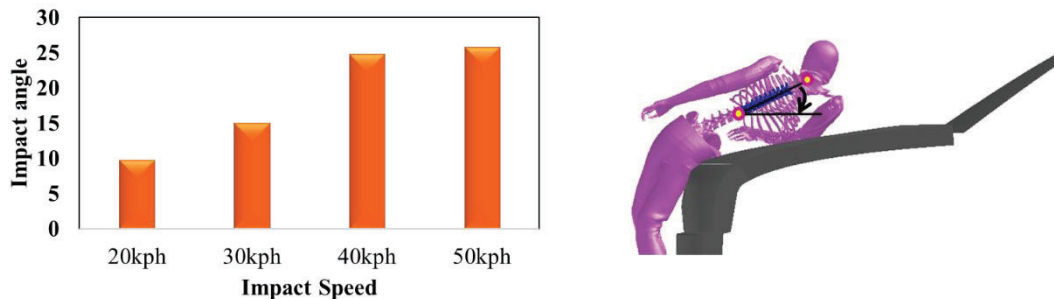
Figure 12. Variation of chest-spine angle for AM50 HBM impacted with SUV GVM with different speeds.

Figure 12 shows the variation of the chest-spine angle of AM50 HBM impacted with an FCV GVM for different vehicle speeds of initial impact. There is a positive increasing linear relationship between the chest-spine impact angle of HBM AM50 and vehicle impact speed. However, above 40kph vehicle speed, the gradient of change of chest-spine angle is decreased. The values of TIPT impact angles (refer Figure 4, FCV:15deg., SUV: 20 deg. and MPV:28deg.) as proposed by BAST [Oliver, 2019] are slightly different from the respective GVM-based simulations results of chest-spine angles (FCV:16.7deg., SUV: 25deg. and MPV:18.5deg.). As shown in Figure A4, the kinematics of the upper extremity above the pelvis undergoes three stages, i) initial state ii) intermediate hand interaction state and iii) final chest interaction state. However, at a high speed of 50kph impact, there will be no distinct separation between the intermediate hand interaction state and final chest interaction state. Due to the higher inertia effect at 50kph, the leaning/deformation patterns of the spine and head are different when compared with those of the 20kph kinematics. As a result, the chest impact angle is high for a 50kph impact.

Considerations for future evaluations

In the future, in regulations and NCAP evaluation procedures, if such test procedures are necessary to be introduced to ensure better chest injury protection to address the issue of increasing elderly pedestrian population using existing dummy chest modules, one needs to keep in mind the following point also.

A detailed accident data analysis is necessary to identify the actual benefits of new evaluation procedures [Henrik Liers, 2009] and to establish relevant detailed test procedures with a sufficient level of confidence related to repeatability and reproducibility. Further, detailed basic research is necessary before it is to be implemented in actual vehicle safety performance evaluations in the future to include findings from real-world accident data and associated effectiveness studies in the development of passive safety measures, legislation tests, or ratings like NCAP.

Based on the outcome of ongoing European HBM4VT WG activity and the trend of roadmaps of Euro-NCAP, from 2026 onwards, the NCAP evaluations will have more focus on using digital virtual testing procedures. Hence, it may be a more rational approach to incorporate the present TIPT based pedestrian chest injury evaluation procedure within the above framework.

CONCLUSION

To check the impact velocity conditions of TIPT test procedures as mentioned by BASt in the 2019 ESV paper, Euro-NCAP recommended GVMs and detail GHBMC HBMs are used in the present study to check the impact velocity conditions of TIPT test procedures as mentioned by BASt in the 2019 ESV paper, It is observed that, the chest impact velocities are lower than those proposed by BASt.

Chest impact velocity for a family small car (FCV) is highest, followed by MPV and SUV. The height of the BLE of a vehicle will be inversely proportional to the chest impact velocity of the thorax on the hood. Based on the present

sensitivity study of vehicle front-end profile parameters, it is more appropriate to define the impact speed of TIPT more precisely as a function of the height of the BLE of the vehicle under consideration instead of defining it approximately by a broad category definition of the vehicles.

Unlike a faster bicyclist's travel speed, a slower pedestrian walking speed will have negligible influence on chest impact velocity.

Based on accidents in real-world scenarios, TIPT with arms should be considered for chest injury evaluation. Arms will interact with the thorax before hitting the hood as observed in all simulations of the present study. A detailed TIPT model is developed to check the kinematics of TIPT in "with arm" and "without arm" impact conditions. However, the position or angle of arm has marginal effect.

However, for child chest protection evaluation criteria, a separate impactor should be considered to represent not only the chest geometry (size, shape, etc.) but also, appropriate chest injury criteria which are very different from those of adults [Brown, 2017].

REFERENCES

Wisch M., Vukovic E., Schäfer R., Hynd D., et al., (2017). "Road traffic accidents involving the elderly and obese people in Europe including investigation of the risk of injury and disabilities." SENIORS Deliverable D 1.2.

Wisch M., Zander O., Vukovic E., Schäfer R., Hynd D., Fiorentino A., et al., (2017), "Road traffic crashes in Europe involving older car occupants, older pedestrians or cyclists in crashes with passenger cars – results from SENIORS." Paper no. 17-0398 of 25th ESV conference proceedings, Detroit, 2017.

Ito, et al, (2015), "Analysis of pedestrian and bicycle rider injury occurrence using JTDB", Journal of the Japanese Council of Traffic Science Vol.15 No.2 2015.

D L Skinner, et al., (2015) "Severe blunt thoracic trauma: Differences between adults and children in a level I trauma center", South Africa Medical Journal 2015;105(1):47-51.

Joshua B. Brown, et al., (2017), "The value of the Injury Severity Score in pediatric trauma: Time for a new definition of severe injury?", Journal Trauma Acute Care Surgery. 2017 June; 82(6):995–1001. doi:10.1097/TA. 0000000000001440.

Lowne R., Janssen E. "Thorax injury probability estimation using production prototype EUROSID." ISO/TC22/SC12/WG6 document N302.

European New Car Assessment Programme 2018-2. "Assessment Protocol – Pedestrian Protection Version 9.0.4" Euro NCAP, September 2018. www.euroncap.com.

Oliver Zander, Marcus Wisch, et al., (2019), "Development and Evaluation of A Thorax Injury Prediction Tool (TIPT) and Possibilities for Incorporation Within Improved Test and Assessment Procedures – Results From Seniors", paper no. 19-0014, 26th ESV conference proceedings,

Ziegler DW, Agarwal N.N. (1994), "The morbidity and mortality of rib fractures", J Trauma 1994;37(6):975–979.

RB, Bass SM, Morris JA, MacKenzie E., (1990), "Three or more rib fractures as an indicator for transfer to a level I center: A population-based study", J Trauma 1990;30(6):689–694.

"Pedestrian Human Model Certification Euro-NCAP pedestrian TB024", https://cdn.euroncap.com/media/66108/tb-024-pedestrian-human-model-certification-v301.pdf.

Chinmoy Pal, et al., (2020), "Comparison of Head Kinematics of Bicyclist in Car-to-Bicycle Impact", paper number 2020-01-093, SAE 2020 World Congress.

B. Johan Ivarsson and Jeff R. Crandall, (2006), Influence of Age-Related Stature on the Frequency of Body Region Injury and Overall Injury Severity in Child Pedestrian Casualties, Traffic Injury Prevention, 7:290–298, 2006.

HBM4VT (2022), https://projectvirtual.eu/2022/10/31/virtual-testing-with-human-body-models-global-initiatives/

Henrik Liers, (2009), "Benefit Estimation of the EURONCAP Pedestrian Rating Concerning Real World Pedestrian Safety", Paper 09-0387 ESV2009.

M. Iryo-Asano et.al. (2017), "Modeling pedestrian crossing speed profiles considering speed change behavior for the safety assessment of signalized intersections," Accident Analysis & Prevention, vol. 108, pp. 332–342, 11 2017

NOMENCLATURES

ADAS: Advanced Driver-Assistance Systems
AM95, AM50 & AF05: Male 95%ile, Male 50%ile, Female 05%ile population
BLE: Bonnet Leading Edge,
BLR-RL: Bonnet Leading Edge Reference Line
EUROSID-2(ES-2): European Side Impact Dummy
GVM: Generic Vehicle Model
HBM: Human Body Model
HBM4VT: Human Body Model for Virtual Testing
ISS: Injury Severity Score
TIPT: Thorax Injury Prediction Tool,
WAD: Warp Around Distance

APPENDIX

- WAD770 (height of lowermost rib of 6YO)
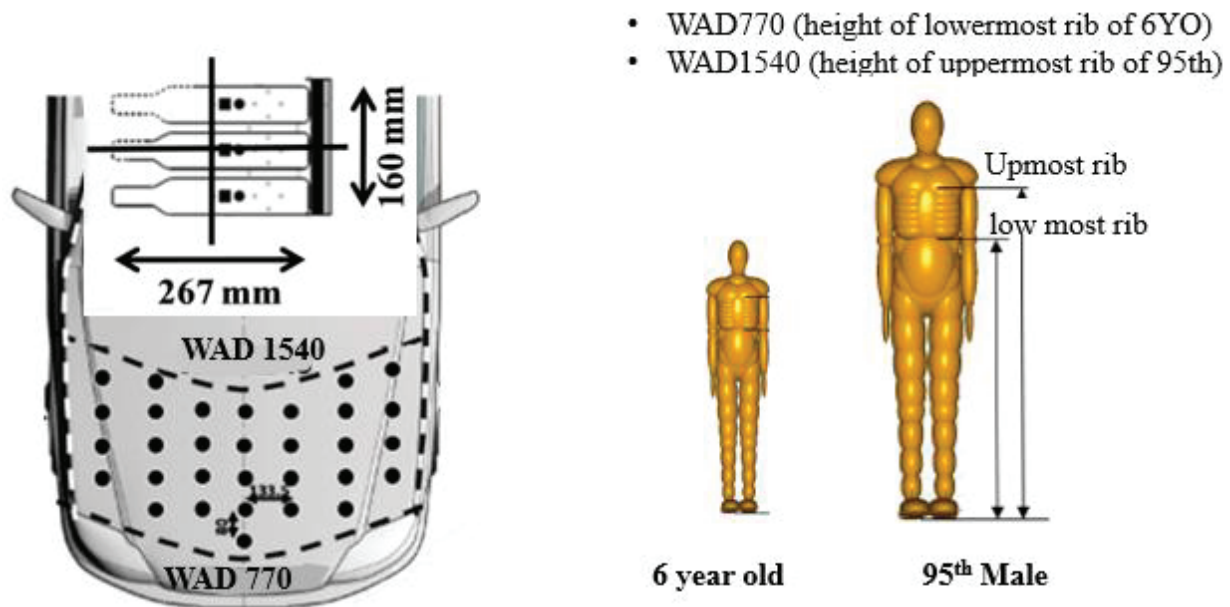- WAD1540 (height of uppermost rib of 95th)

Figure A1. TIPT evaluation Grid map locations with all impact target locations at the intersection of the TIPT middle rib and vertical rib center planes (Oliver, 2019)
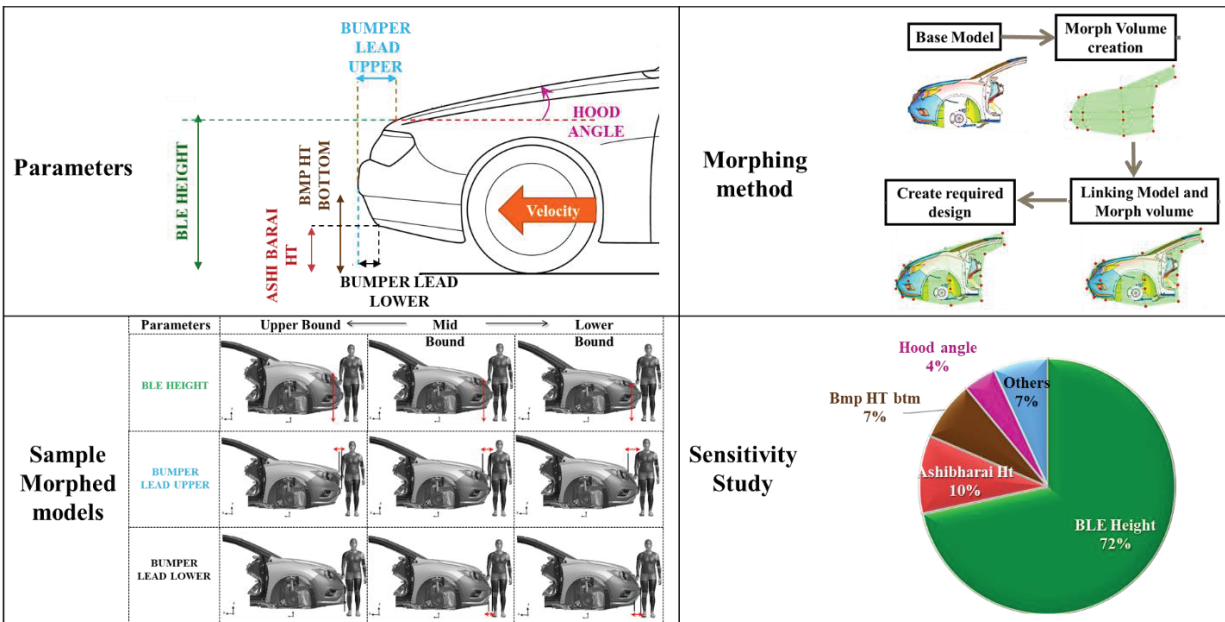
Figure A2-1. Morphing parameters, morphing method, morphed models and sensitivity chart of influential parameters for HBM AM50 chest velocity.
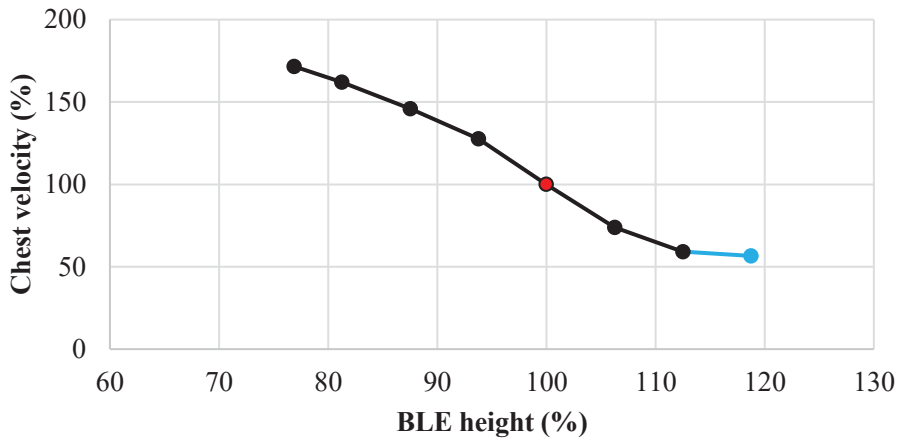

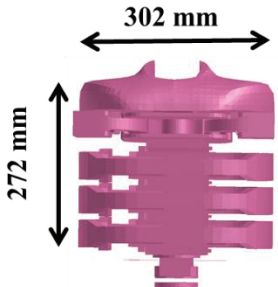**Figure A2-2. Sensitivity of chest impact velocity w.r.t BLE height of the original vehicle (100% as reference).**
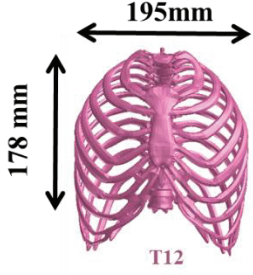
Figure A3. Comparison of chest size (TIPT vs Child)
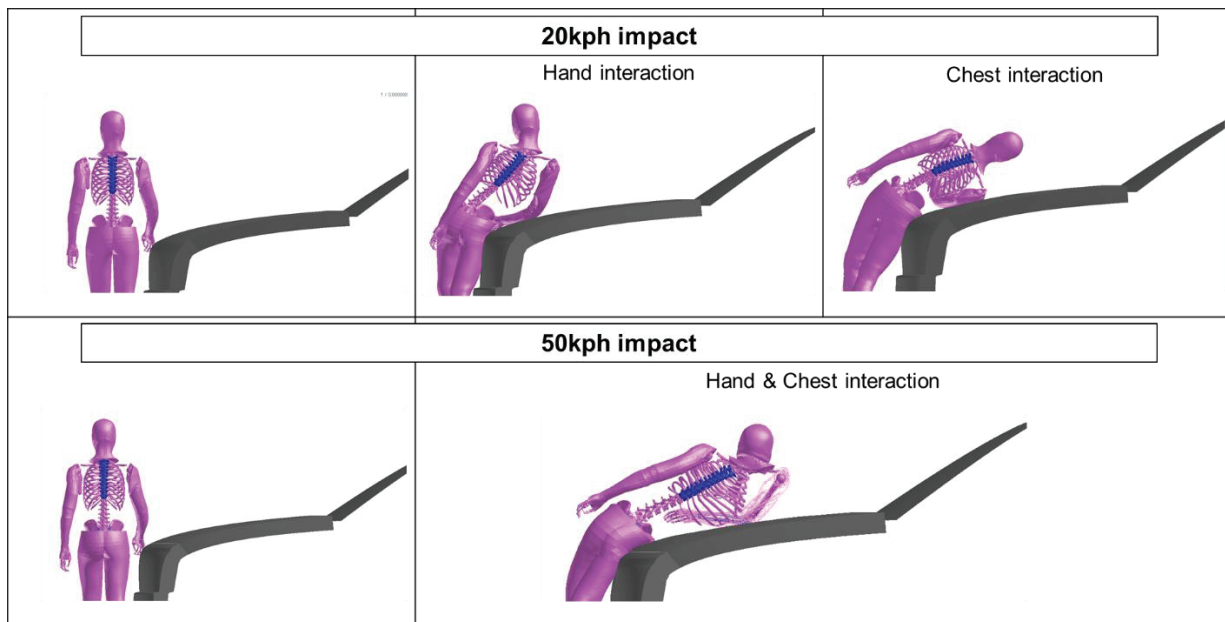

Figure A4. Impact velocity influence in chest spine angle

PRELIMINARY STUDY ON CRASH PULSE INFLUENCE FOR CHILD ATD RESPONSE IN CHILD RESTRAINT SYSTEMS

Hans Hauschild
Brian Stemper
Medical College of Wisconsin
United States of America

Ian Hall
Allison Louden
National Highway Traffic Safety Administration
United States of America

ABSTRACT
Different vehicle crash scenarios may produce different crash pulses dependent on several variables. Crash simulations utilizing a sled system are more repeatable but may subject anthropomorphic test devices (ATDs) to different input pulse levels depending on sled type and its settings. Those different input pulses may influence the test device's response. The goal of this current study examined different sled pulse inputs and their influence on child ATDs. ATDs were secured in child restraint systems on the proposed updated frontal test bench for Federal Motor Vehicle Safety Standard (FMVSS) No. 213 and subjected to three input pulses with the same target delta-v (48 kph). All three input pulses were within the FMVSS No. 213 boundaries. Hybrid III 10-year-old and 6-year-old test devices were tested using four belt positioning booster seats and one forward facing harness seat. Head, chest, neck, and belt load metrics were examined for coefficient of variation, trends related to input pulse acceleration increases, and any significant differences. Examination of the study results indicate that increased acceleration pulse inputs had the most influence on head accelerations, chest accelerations, and neck tensions but had little effect on chest deflections or head and knee excursions.

INTRODUCTION
Many studies have examined the effect of crash pulses on occupant kinetics. Crash pulse shape or characteristics can be influenced by vehicle structure, crash delta-v, and collision partner [1], [2], [3], [4], [5]. One study examining full scale crash tests of 1998 to 2002 model year vehicles including full frontal (48 kph), offset deformable (40 kph), and underride guard barriers (64 kph) demonstrated distinctly different pulse shape during the vehicle deceleration from the three types of crash tests [1].

Results from a study by Locey [2] examining crash pulse characteristics (CPC) of model year vehicles from 1997 - 2010 found new vehicle crashes within the same vehicle group and under the same conditions have become more homogenous as the model years increased. They found the range of peak acceleration was greater for the model year 1997 – 1999 vehicle group (17.1 G) vs the model year 2009 – 2010 vehicle group (10.7 G) [2]. That study also noted the same trend for maximum acceleration time and pulse duration was reduced from group to group for the newer model year vehicles. One conclusion was that as crash pulses become more homogenous, restraint system design can become more universal.

Most studies have examined effects to adult occupants or adult sized anthropomorphic test devices (ATD). One modelling study using a HIII 50th male ATD model found different pulses with the same delta-v affected HIC and chest Gs [6]. Another adult modelling study concluded that the CPC influences the occupant kinematics and the timing of potential injury [7]. One study of four different sled pulse effects on the spine response of a HIII 50th% found changes to the thoracic load, lumbar load, pelvis accelerations, and belt loads [8]. One field study reported that long-term neck injury consequences were more likely as mean and peak accelerations increased [9].

A previous NHTSA study reviewing test procedures found that drivers subjected to a stiffer pulse had a higher frequency and risk of serious to fatal injuries [3]. The NHTSA study defined a "soft pulse" as having a duration longer than 125 ms and a peak deceleration below 20 Gs, while a "stiff pulse" was defined as short duration, under 110 ms, and higher peak decelerations, approximately 25 Gs.

One recent study examined pulse effects on a Hybrid III 6-year-old, Hybrid III 5th% adult female, Hybrid III 95th% adult male, and THOR ATDs [4]. In that study the authors used a soft and severe pulse based on NHTSA New Car Assessment Program (NCAP) crash tests conducted at 56 kph. The severe pulse had an approximate peak of 57 Gs and duration of 85ms while the soft pulse had an approximate peak of 28 Gs and 110 ms duration and same delta-v. This study [4] concluded sled pulse changes from a soft to severe pulse resulted in increased HIC, neck tension, chest Gs, and chest deflection.

Most of the pulse influence studies have used adult ATDs and models. There is limited data for the influence of pulse on child occupants and child occupants using add-on child restraint systems. It is known that adult and child injuries differ in vehicle crashes [10], [11]. This study's goal was to analyze any response differences of child ATDs in child restraint systems (CRS) secured on the Federal Motor Vehicle Safety Standard (FMVSS) No. 213 proposed updated frontal standard seat test bench [12] subjected to different sled acceleration pulse inputs. The current FMVSS No. 213 sled pulse peak acceleration corridor extends from 19 G to 25 G with a duration between 75 and 90 ms. The tests conducted in this research targeted three pulses peaking at 21.5 G, 23.0 G and 24.5 G and a pulse duration less than 90 ms [13].

METHODS AND DATA SOURCE
Four belt positioning booster (BPB) seats and one forward-facing CRS with an internal harness (FFH) (n = 5 CRS models) were tested using three different frontal acceleration pulses at a 48-kph change in velocity (delta-v) (n = 15 test configurations). The CRSs tested included no-back BPB (NB-BPB), high-back BPB (HB-BPB) and forward-facing harness CRS. Hybrid III 6-year-old (HIII-6YO) and Hybrid III 10-year-old (HIII-10YO) ATDs were used for testing on each type of BPB, and the FFH was tested only with a HIII-6YO.

The three pulses had target peak accelerations of 21.5 G, 23.0 G and 24.5 G (low, mid, and high-pulse respectively) while remaining within the FMVSS No. 213 frontal pulse upper and lower acceleration boundaries and targeting a 48 kph delta-v (Figures 1 & 2). Tests were conducted on a Seattle Safety accelerator type sled. FMVSS No. 213 research test setup procedures [13] were followed. ATDs and CRS were secured on the proposed updated frontal standard seat assembly per the FMVSS No. 213 research procedures [12], [13], [14] and the CRS manufacturer supplied instructions. A 3-point fixed belt was used for the BPB seats (tensioned at 2-4 pounds) and the LATCH was used for the FFH CRS (tensioned at 12-15 lbs).

All data were collected and post-processed according to SAE J211 [15] specifications. A total of 41 sled tests were used for analysis. Collected data included head and chest accelerations, chest deflections (not regulated in FMVSS No. 213), upper neck axial forces (not regulated in FMVSS No. 213), head and knee excursions, and seat belt webbing loads (not regulated in FMVSS No. 213). Additional data for two BPBs was downloaded from the NHTSA database for three low-pulse tests.

The ATDs' triaxial head and chest accelerometers, chest potentiometer, upper neck force transducer, and belt webbing load cells were collected at 20,000 Hz. utilizing a DTS (Seal Beach, CA) data acquisition system. Seat belt webbing loads were measured with Denton seat belt load cells (Denton, Michigan, United States) installed on the shoulder and lap belt, and when possible, on the lower anchors and top tethers. Head and knee excursion data were calculated from video analysis using TEMA (Specialised Imaging, United Kingdom) software using the 4-point target method [13].

Final ATD measurements were done with a coordinate measuring machine (CMM). Generally, head, thorax, belt and CRS positions were within 15 mm of each test for same CRS and ATD set up. Belt tensions were set per the FMVSS No. 213 research procedures [13]. Comparisons between corresponding peak metrics for each ATD-CRS combination and the acceleration inputs were analyzed. When data for more than one test was available, the results were averaged in each pulse group and a coefficient of variation calculated. Generally, each individual CRS pulse group had good repeatability for the metrics in this research.

Regression analysis was conducted to determine trends related to the changing pulses. R^2 greater than 0.8 was considered an excellent fit, and an R^2 greater than 0.7 was considered a good fit. Single factor ANOVA was computed for each CRS-ATD group to determine if there was a significant difference between the pulse groups. P-values less than 0.05 were considered as being significantly different. Post hoc Tukey tests were performed to determine if a specific group in each metric was related to causing the difference. Coefficient of variation (CV) was

calculated for the metrics and pulses for each CRS-ATD-Pulse group when more than one sled test was available, 10% or less was considered a low degree of variation and good test repeatability. For each metric with a CV, the team calculated the substantiveness of the variation relative to the IARV or performance limit. Sigma-to-Limit (StL, σ_L) (Equation 1) results above 2.0, would indicate at least two standard deviations between the average response and the IARV or performance limit.

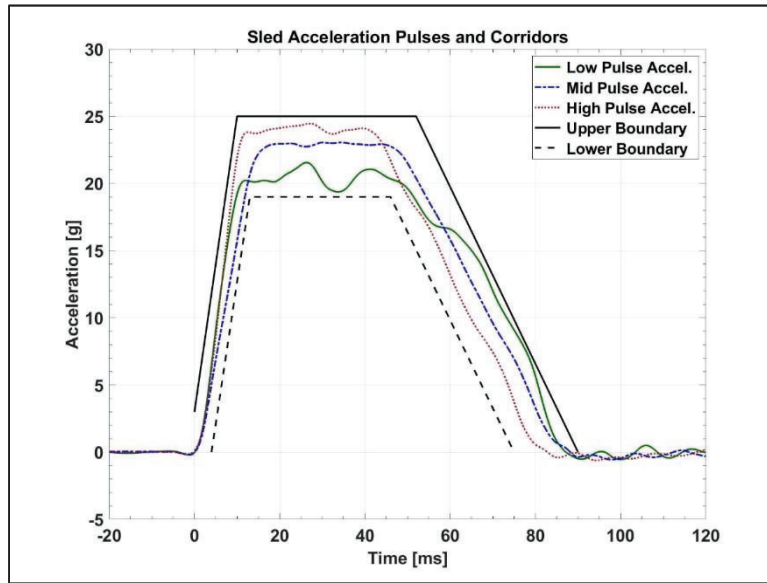$$Sigma - to - Limit\ (STL, \sigma_L) = \frac{(Limit - \bar{x})}{\sigma}$$ **Equation 1**

Figure 1. Average acceleration vs time with FMVSS No. 213 upper and lower boundaries
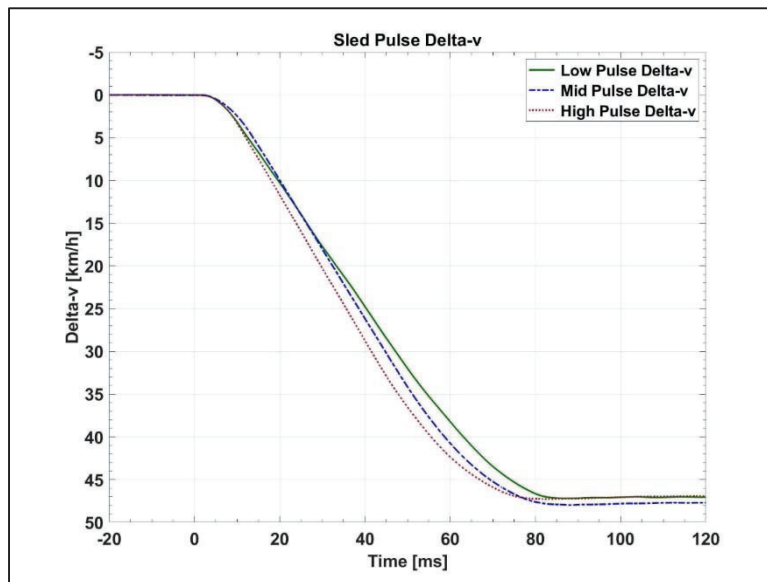

Figure 2. Average delta-v vs time of three input pulses.

RESULTS

The five different CRS models were evaluated comparing each CRS results from each pulse group. Results include analysis of HIC36, 3ms chest acceleration, chest deflection, neck tension, head excursion, knee excursion and belt loads. Averages were calculated from each pulse group and used to determine any correlation of increases or decreases between pulse inputs. Single factor ANVOA statistical results were calculated for each metric of the whole CRS group and pulses, and regression analysis was done comparing each metric relative to the pulse acceleration change. For this study p-values less than 0.05 are significant and R^2 values over 0.8 are considered excellent correlation. Tukey post hoc test were conducted for any metric found to be significantly different. Sigma-to-limit was calculated for each CRS / ATD group, and responses greater than two identify "good" levels of variation that are unlikely to cross the IARV or performance limit. Detailed results are presented in tables 1, 2, 3 and 4. IARV and performance values are included for reference only, some metrics are not regulated by the FMVSS No. 213 such as neck tension, chest deflection, belt loads and HIC36 for the HIII 10YO.

Head Acceleration

Thirty-six millisecond head injury criteria (HIC36) were calculated for each test. All five CRS had increased HIC values as the peak sled pulse acceleration was increased ($R^2 = 0.88$-0.96). Three of the CRS had significant HIC36 differences between the low- and high-pulses (all p<0.004). The NB-BPB with the HIII-10YO had the largest increase from the low to high peak pulse ranging from 502 to 831, and there was significant difference between pulses (P = 0.004). The FFH CRS with the HIII-6Y0 had the greatest significant difference (P = 0.0001) with average HIC36 values ranging from 389 to 625. Generally, the CV for HIC values within CRS pulse groups demonstrated good repeatability. Calculated CVs across all three pulses demonstrated high variation and ranged from 6.2% to 26.7%. Only the HB-BPB with HII-6YO had a CV less than 10% across the three pulses. The HIC values did not exceed IARV or performance limits for any test (Figure 3). The NB-BPB HIII-10YO sigma-to-limit calculation was 1.8, all other combinations were over 2.
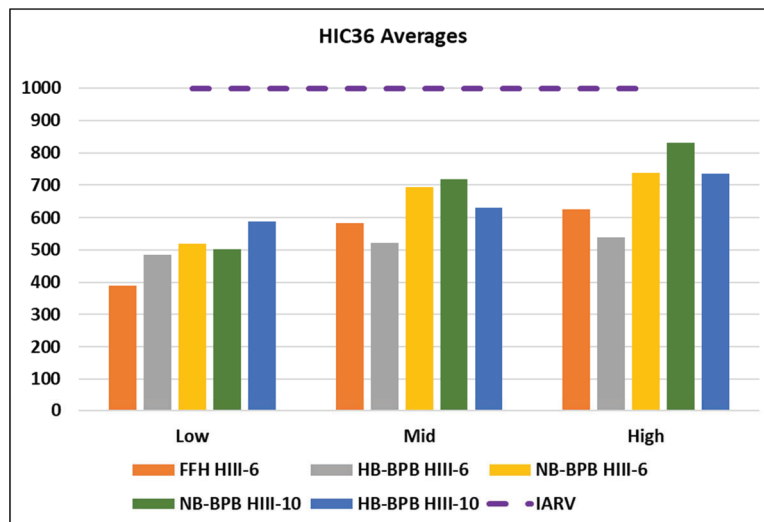
Figure 3. HIC 36 averages across pulses and IARV [16].

Chest/Thorax

ATD peak chest deflections (not regulated) were measured for each test. The HB-BPB with the HIII-6YO chest deflection recorded the largest increasing difference (8.2 mm) from low- to high-pulse ($R^2 = 0.85$) and was significantly different between pulses (P = 0.001). The HB-BPB with the HIII-6YO chest deflection ranged from -37 to -45 mm. The HB-BPB with a HIII-10YO also had significant differences between pulses (P = 0.03) but did not have any correlation nor trend related to pulse inputs and only recorded a 2 mm difference between the three pulses. Post hoc test of the results found that the significance differences were between the low- and mid-pulses. Other CRS chest deflections only varied about 1.0 mm. The chest deflections exceeded IARV values for the HIII-6YO in BPB seats for some tests in low-, mid- and high-pulse inputs [16].

Three millisecond chest accelerations (CLP3) were calculated from the thoracic resultant acceleration. All the CRS tested had increases of the calculated CLP3 with increasing pulse severity. Four of the CRS CLP3 calculations correlated well to the pulse increases ($R^2 = 0.82 - 0.99$) and one correlated good ($R^2 = 0.77$). The NB-BPB with HIII-10YO, had the lower correlation ($R^2 = 0.77$) due to the calculated average CLP3 for the mid and high-pulses being almost identical (47.9 G and 48.0 G respectively) while the low-pulse average was 42.7 G. The two BPBs with the HIII-10YO did not have significant CLP3 differences between the pulse inputs (P = 0.06 and 0.07), although the HB-BPB with HIII-10YO demonstrated a good correlation to pulse increases ($R^2 = 0.99$). All CRS tested with the HIII-6YO had CLP3 values that were significantly different between pulses (P = 0.0001 – 0.001). Post hoc analysis indicated that all the CRS with the HIII-6YO were significantly different between the low-pulse and both the mid and high inputs. The 6YO in BPBs had average CLP3 values near the maximum performance values (59.4 and 59.5 G) both during the high-pulse.

Both chest deflection and CLP3 demonstrated good repeatability and low variation across each CRS pulse group and across all the CRS pulse groups, ranging from 2.7% to 6.6% for chest deflection and 5.2% to 9.3% for CLP3. All sigma-to-limit values for chest deflections were over two. CLP3 sigma-to-limit calculations were under two for both BPBs with the HII 6YO. Average results are presented in Figures 4 and 5.
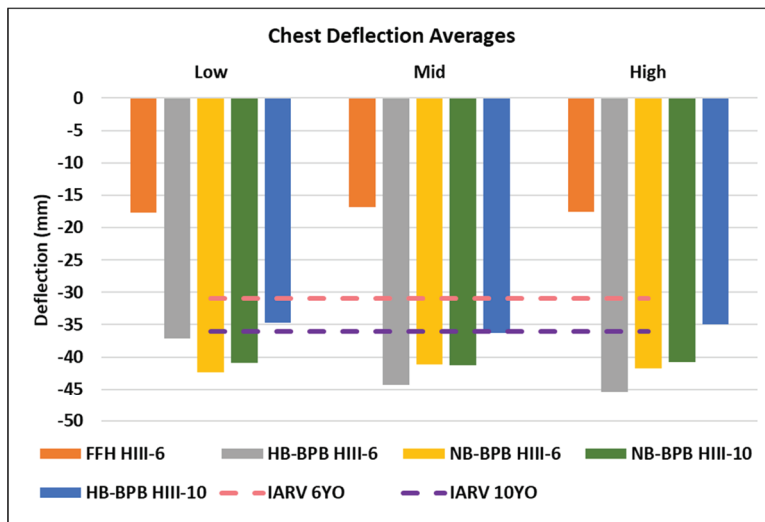

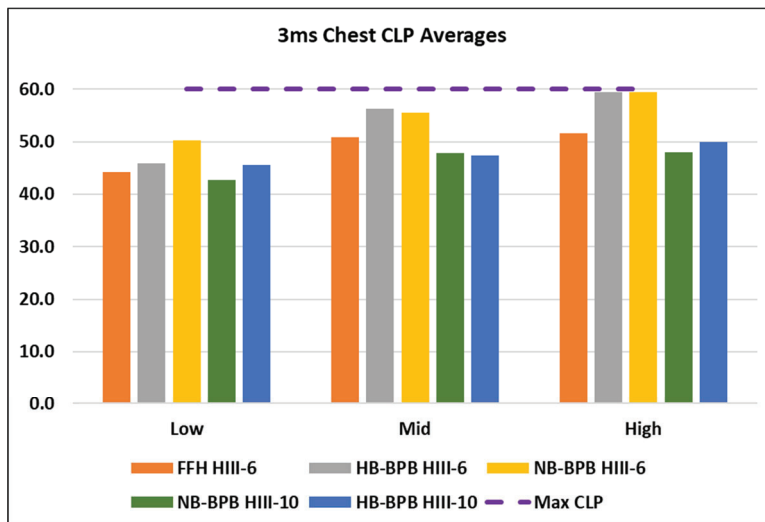*Figure 4. ATD Chest Deflection averages across pulses and IARV [16].*

Figure 5.ATD Chest 3ms CLP averages across pulses and performance limit.

Neck Tension

Neck tension values (not regulated) were measured for each test and CRS-ATD combination. Four of the CRS had increasing neck tension values as the pulses were increased, three of which correlated well ($R^2 = 0.81 - 0.99$) and the fourth was good ($R^2 = 0.77$). One CRS did not have increasing neck tension with the increasing pulse, HB-BPB with HIII-10YO ($R^2 = 0.08$). The HB-BPB with HIII-10YO had a lower average peak neck tension during the three mid-pulse tests (2.7 kN) compared to the low-pulse (3.1 kN) and high-pulse (3.3 kN). Only three of the CRS had significant differences between the pulse inputs; HB-BPB with HIII-10YO, NB-BPB with HIII-6YO, and FFH with HIII-6YO (all P $\leq$.04). Calculated CVs within the CRS pulse groups varied from 1.8% for a HB-BPB with HIII-10YO during the high G pulse to 17.7% for the NB-BPB with HIII-6YO during the high G pulse. Only the HB-BPB with HIII-6YO had a CV less than 10% across all tests, the other CRS ranged from 11.2% to 20.4% indicating variations between the lower and higher pulses. Neck tension calculated sigma-to-limit values were less than two for all CRS except the HB-BPB with the HIII 6YO. Average neck tension results are presented in Figures 6.
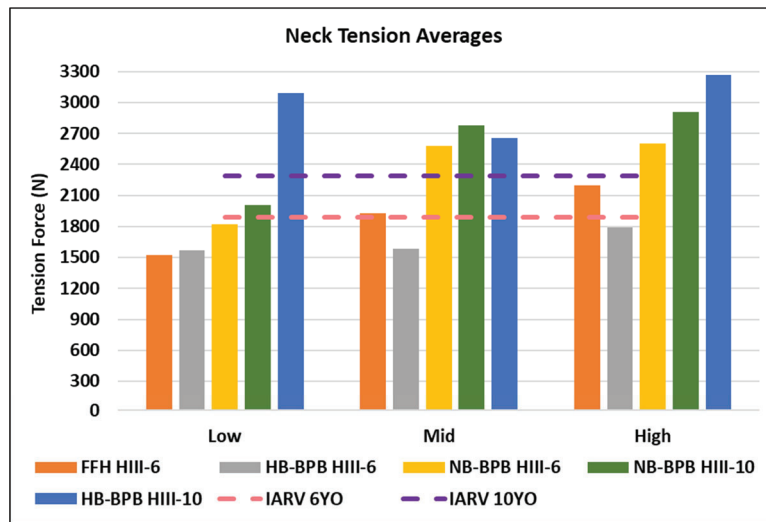

Figure 6. ATD Neck Tension averages across pulses and IARV [16].

Head / Knee Excursion

Measured head excursions between pulse groups were not significantly different for any CRS (P > 0.05). Both HB-BPB with HIII-10YO and HIII-6YO had increased head excursion which correlated with the increased pulse inputs ($R^2 = 0.97$ and 0.96 respectively). The measured increases were small, HB-BPB with HIII-10YO was 9 mm difference, and the HB-BPB with HIII-6YO was 18 mm difference from low to high-pulses. The FFH with HIII-6 had the greatest excursions (628 to 671 mm). The lowest excursions were the NB-BPB with the HIII-6YO (453 to 472 mm)   There was a reduction of head excursion for the FFH CRS of 23 mm ($R^2 = 0.95$). There was no correlation of pulse inputs to changes of head excursion for the NB-BPB HIII-10YO and HIII-6YO ($R^2 = 0.01$ and 0.22 respectively).

Three CRS did not have any correlation to the pulse differences ($R^2 < 0.8$) for the measured average peak knee excursions for HB-BPB HIII-10YO, NB-BPB HIII-10YO and NB-BPB HIII-6YO. The NB-BPB with HIII-6YO knee excursion did demonstrate a significant difference (P = .01) between the pulse inputs which ranged from 567 to 598 mm ($R^2 = 0.7$). The average knee excursion during the mid-pulse test was only 2 mm larger than the high-pulse but was 31 mm larger than the low-pulse. The FFH HIII-6YO had a decreasing trend for average peak knee excursion ($R^2 = 0.75$) and resulted in 2 mm differences, between the low- to high-pulses. The greatest excursions occurred with the FFH with HIII-6YO (779 to 801 mm) while the lowest excursions were with the NB-BPB with HIII-6YO (551 to 607 mm).

Head and knee excursions were very repeatable and had low variation across the individual pulse groups and across the three pulse groups. CVs were very low across the three CRS pulse groups (< 3%). No excursion performance

requirements were exceeded for any test (head < 720 mm and knee < 813 mm) (Figures 7 and 8). Sigma-to-limit calculations were over two for both head and knee excursions for all CRS groups.
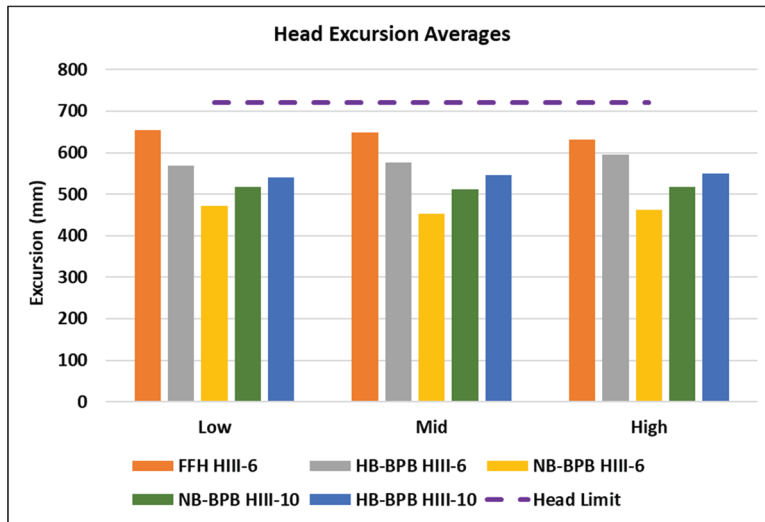
Figure 7. ATD Head Excursion averages across pulses and lower performance limit.
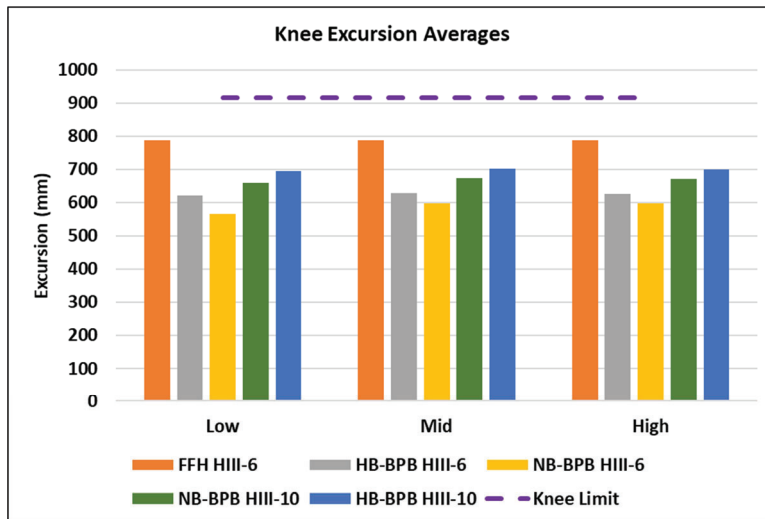
Figure 8. ATD Knee Excursion averages across pulses and performance limit.

Belt Webbing Forces

Measured peak shoulder belt loads (not regulated) for the HB-BPB and NB-BPB increased as the pulses increased ($R^2 > 0.8$) (Figure 9). Shoulder belt loads had significant differences for three of the BPB (P = 0.001 to 0.05), while the NB-BPB HIII-10YO calculated significant difference was P = 0.06.

The peak lap belt loads for the HB-BPB and NB-BPB increased as the pulses increased. Three of the CRS had an excellent correlation ($R^2 > 0.80$) and the HB-BPB with HIII-10YO had a good correlation ($R^2 = 0.76$) (Figure 10). Only the NB-BPB with HIII-6YO had a significant difference (P = 0.001) for the lap belt load with a 1.1 kN difference from the low to high-pulses. The HB-BPB with HIII-10YO lap belt loads was significantly different and while only presenting a 0.3 kN difference from the low- to high-pulse, while the mid- and high- pulse demonstrated nearly the same values (4.0 kN) for the lap belt loads (P = 0.05, $R^2 = 0.76$). Post hoc tests of this group indicated most significant differences were due to the low-pulse tests as compared to both the mid- and high-pulse tests.

The FFH CRS with the HIII-6YO was secured with lower anchor and tether webbing. The lower anchor and tether webbing peak loads did not have an increasing or decreasing trend as the pulse acceleration peaks became higher (R^2 = 0.57 and 0.05 respectively). The lower anchor and tether loads were significantly different across the pulse inputs (P = 0.01 and 0.0001 respectively). The lower anchor loads recorded a difference of 1.2 kN between the pulses with the highest average peak measured during the mid-pulse (5.3 kN). The tether only recorded a 0.4 kN peak difference between the pulses, while the low-pulse had the highest average peak load (3.1 kN).

Within each CRS pulse group, the belt webbing forces calculated CVs demonstrated good repeatability, CV<10% for all except one group which was 11.1%. For the combined three groups shoulder belt force CVs ranged from 3.3% to 10.6% and the lap belt force differences ranged from 3.8% to 16.5% for the BPBs. The LATCH lower anchors and tether forces CVs were 12.0% and 6.1% respectively across the three pulses for the FHH.
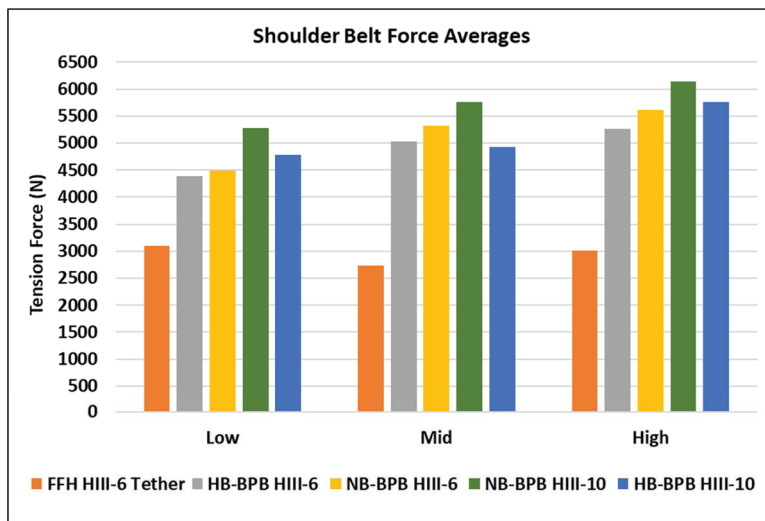

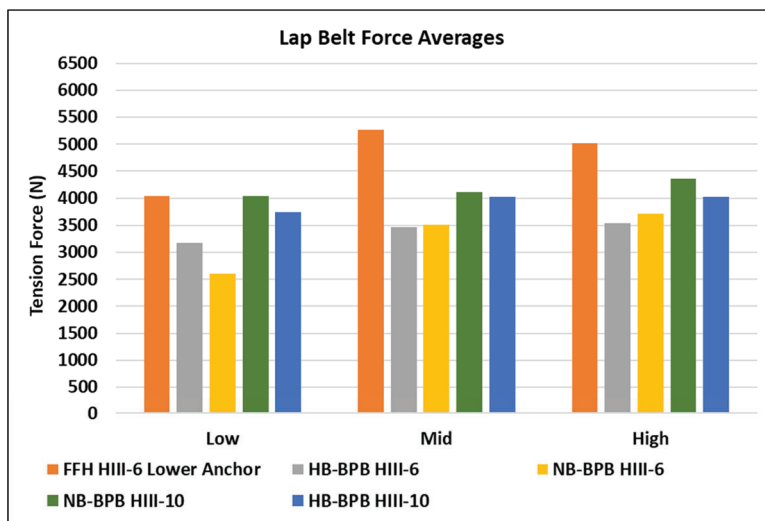*Figure 9. Shoulder/Tether Belt Webbing Force averages across pulses.*

Figure 10. Lap/Lower Anchor Belt Webbing Force averages across pulses.

Table 1. ATD metric increases correlation to sled acceleration increases.

| | | | | | | | | Shoulder / Tether | Lap / LA |
Type	ATD	HIC36	Chest Deflec	Chest CLP	Neck Tension	Head Excursion	Knee Excursion	Belt Force	Belt Force
HB-BPB	HIII-10	0.94	0.02	0.99	0.08	0.97	0.35	0.86	0.76
NB-BPB	HIII-10	0.97	0.08	0.77	0.85	0.01	0.64	0.99	0.91
NB-BPB	HIII-6	0.89	0.24	0.99	0.77	0.22	0.70	0.92	0.88
HB-BPB	HIII-6	0.96	0.85	0.91	0.81	0.96	0.39	0.93	0.90
FFH	HIII-6	0.88	0.02	0.82	0.99	0.95	0.75	0.05	0.57

Table 2. ATD metric increase or decrease trend related to input pulse.

| | | | | | | | | Shoulder / Tether | Lap / LA |
Type	ATD	HIC36	Chest Deflec	Chest CLP	Neck Tension	Head Excursion	Knee Excursion	Belt Force	Belt Force
HB-BPB	HIII-10	increase	none	increase	none	increase	none	increase	increase
NB-BPB	HIII-10	increase	none	increase	increase	none	none	increase	increase
NB-BPB	HIII-6	increase	none	increase	increase	none	none	increase	increase
HB-BPB	HIII-6	increase	increase	increase	increase	increase	none	increase	increase
FFH	HIII-6	increase	none	increase	increase	decrease	decrease	none	none

Table 3. ATD metric p-values related to differences across all pulses.

| | | | | | | | | Shoulder / Tether | Lap / LA |
Type	ATD	HIC36	Chest Deflec	Chest CLP	Neck Tension	Head Excursion	Knee Excursion	Belt Force	Belt Force
HB-BPB	HIII-10	0.002	0.03	0.06	0.04	0.36	0.70	0.05	0.24
(F-value)		22.163	6.38	4.687	5.54	1.23	0.31	6.03	1.94
NB-BPB	HIII-10	0.020	0.98	0.07	0.13	0.92	0.22	0.004	0.54
(F-value)		11.570	0.02	5.45	4.35	0.08	2.29	30.16	0.71
NB-BPB	HIII-6	0.004	0.69	0.001	0.04	0.06	0.01	0.001	0.001
(F-value)		16.642	0.40	24.506	5.68	4.65	11.41	23.372	23.541
HB-BPB	HIII-6	0.07	0.001	0.0001	0.13	0.26	0.41	0.009	0.20
(F-value)		4.199	81.214	29.810	3.54	1.92	1.11	19.430	2.43
FFH	HIII-6	0.0001	0.67	0.0005	0.00001	0.18	1.00	0.0001	0.0078
(F-value)		55.896	0.427	36.022	133.66	2.27	0.04	73.791	12.15

Table 4. Sled and ATD minimum, maximum, min-max differences, average, standard deviation, coefficient of variation, and sigma-to-limit across all three pulse groups and performance limits and/or IARV [16].

CRS Type	ATD		Peak Accel	HIC36 (10 YO*)	Chest Deflec. (mm)*	Chest CLP (Gs)	Neck Tension (N)*	Head Excursion (mm)	Knee Excursion (mm)	Shoulder Belt Force (N)*	Lap Belt Force (N)*
IARV or Performance Criteria (10YO / 6YO)			n/a	1000	belt only (36/31)	60	(2290/1890)	720 /813	915	n/a	n/a
HB-BPB	10	Min	21.1	589	-36	45.5	2658	541	695	4785	3749
		Max	24.5	734	-35	50.0	3266	549	702	5761	4024
		Diff	3.4	146	2	4.5	608	9	7	976	275
		Avg.	22.9	651	-35	47.6	3004	548	699	5206	3954
		SD	1.5	69	1	2.5	336	7	11	551	191
		CV	6.4%	10.6%	2.7%	5.2%	11.2%	1.3%	1.5%	10.6%	4.8%
		StL, σ_L		5.0	78.9	5.0	-2.1	37.3	20.6		
NB-BPB	10	Min	21.1	502	-41	42.7	2003	511	658	5280	4042
		Max	24.1	831	-41	48.0	2904	518	674	6136	4363
		Diff	3.0	330.0	1	5.3	901	7	16	856	321
		Avg.	22.6	674	-41	45.7	2583	516	666	5716	4190
		SD	1.5	180	2	3.3	524	12	9	443	381
		CV	6.9%	26.7%	5.1%	7.3%	20.3%	2.3%	1.6%	7.7%	9.1%
		StL, σ_L		1.8	36.6	4.3	-0.6	25.6	26.8		
NB-BPB	6	Min	21.2	518	-42	50.2	1821	453	567	4485	2611
		Max	24.6	737	-41	59.4	2603	472	598	5611	3713
		Diff	3.3	218	1	9.2	782	19	32	1126	1103
		Avg.	23.0	650	-42	55.0	2334	462	587	5141	3277
		SD	1.5	109	2	4.2	476	11	17	539	539
		CV	6.3%	16.8%	3.7%	7.7%	20.4%	2.3%	2.9%	10.5%	16.5%
		StL, σ_L		3.2	49.8	1.2	-0.1	33.2	19.0		
HB-BPB	6	Min	21.2	485	-45	45.9	1570	576	626	4385	3176
		Max	24.6	538	-37	59.5	1794	594	629	5256	3540
		Diff	3.4	53	8	13.7	225	18	3	871	364
		Avg.	23.4	524	-44	56.2	1674	583	626	5032	3455
		SD	1.3	32	3	5.2	141	16	5	324	174
		CV	5.5%	6.2%	3.0%	9.3%	8.4%	2.7%	0.9%	6.4%	5.0%
		StL, σ_L		14.9	26.6	0.7	4.4	14.4	56.7		
										Tether (N)	Lower Anchor (N)
FFH	6	Min	21.3	389	-18	44.2	1526	632	786	2738	4041
		Max	24.6	625	-17	51.6	2200	655	788	3094	5264
		Diff	3.3	236	1	7.4	674	23	2	355	1223
		Avg.	23.0	532	-17	48.9	1885	645	787	2949	4775
		SD	1.4	112	1	3.7	297	15	8	180	571
		CV	6.3%	21.0%	6.6%	7.5%	15.8%	2.4%	1.0%	6.1%	12.0%
		StL, σ_L		4.2	43.9	3.0	0.02	4.9	16.8		

Notes: Three tests from another other lab were included for low pulse tests; data includes HIC 36 and Chest CLP, Chest Deflection, Belt Forces and excursions NB-BPB with HIII10YO, and HB-BPB with HIII 6YO.

* HIC36 for HIII-10, chest deflection, neck tension, and belt webbing forces are not regulated by FMVSS No. 213.

DISCUSSION

This preliminary study examined different sled pulse inputs influence on child ATD biomechanics secured using CRS on the proposed FMVSS No. 213 updated frontal standard seat assembly test bench fixture using three different peak acceleration pulses (targeting peak 21.5 G, 23.0 G, and 24.5 G) utilizing the same delta-v (48 kph). This research evaluated the measured metrics for trends, repeatability, and significant differences across the different pulses. The test set up during this research included the same CRS and belt configurations in each group with only the acceleration pulse changing.

In this research, while the peak sled pulse acceleration values, approximately 21.5 G to 24.5 G, from the three test groups demonstrated a CV less than 7%, ATD metrics had higher CV values, increasing trends, some variations, and differences. While the delta-v remained consistent with less than 0.8 kph difference across the differing pulses, some occupant metrics were influenced by the pulse changes. This research found the small increases in peak pulse had the most influence on the head accelerations, chest acceleration, neck tensions and shoulder belt webbing tension. Results indicated only small increasing or decreasing trends for the chest deflections, head excursions and knee excursions. Chest deflections, head excursions and knee excursions generally did not demonstrate significant differences, any large variations, and appear be affected little by pulse changes.

Test device data differences may be attributed to lab set up processes, test fixtures, material types, restraint material characteristics, CRS design, CRS variability, and/or ATD instrumentation or construction variances. Sled systems input pulses are controlled with several methods such as computer-controlled braking, air pressure modulation, or hydraulic or mechanical deceleration control. Each producing their own CPC. Repeatability and reproducibility testing can account for differences in test methods, test labs, test pulses (within the specified boundary conditions) and ATDs with a calculated CV.

Vehicle CPC vary from one vehicle model to another model. Objects impacted can also change a CPC. As vehicle structure and CPC may influence injury it is important to examine the standard test methods to evaluate the different influences on the ATDs. This investigation is important to ensure the test methods, ATDs and crash pulses are robust enough to capture different crash scenarios. Additionally, as lab differences can be encountered, this research can identify CRS and ATD sensitivities related to the acceleration changes.

Other studies have examined the crash pulse influence on occupant kinetics. Most studies were conducted examining the influence on adult occupants, or supplemental restraint systems ([1], [3], [4], [6], [8], [17], [18]. Research has also been conducted to analyze the vehicle structure for crashworthiness [5] and studies found an increase of thoracolumbar spine fractures increased with newer model year vehicles [17], [18]. Pintar [17] suggested that the possibility of stiffer vehicle structure may influence injury patterns, and that study also concluded the struck object had an influence on the crash pulse and subsequent injuries.

Locey's [2] research found that the newer vehicle fleets, including all vehicle types, have a more homogenous pulse. Their research reported that the latest vehicle group in their dataset (2009 – 2010) only had a peak acceleration difference of about 11 Gs and pulse duration difference of about 13 ms. Across all three pulse variations, the average sled acceleration peaks in our research had a 3 G difference and about a 10 ms difference in pulse duration (Figure 1).

As vehicle CPC become more homogenous it will be advantageous for CRS design and regulatory performance requirements. The FMVSS No. 213 pulse used in this research allows for a range peak acceleration from 19 G to 25 G and a 75 to 90 ms duration. The current FMVSS No. 213 small pulse variations presented in this study are more homogenous than the current vehicle fleet but did present some differences of some measured metrics.

The small peak acceleration changes in pulse during this preliminary study found minimal effect on the ATDs chest deflections, head excursions and knee excursions. Our study used the fixed 3-point belt system specified in the FMVSS No. 213 procedures for the BPB. The FFH CRS used the child restraint manufacturer lower belt webbing and a tether attached to the LATCH anchors. The fixed belt and LATCH webbing likely limited the head and knee motion during the different pulses.

There were strong correlations of increased head acceleration, chest acceleration, and neck tension as the peak pulse acceleration increases for most of the CRS. The head injury and chest injury values are measured with accelerometers; it would be expected that there would be an increasing trend since pulse acceleration was increased.

Force is based on mass times acceleration and therefore the neck force trend increase would also be expected. Of those which had a good correlation, only three CRS in each metric demonstrated significant differences between pulses.

Seat belts and CRS belts with load limiters may have more influence on head and knee excursions and chest deflections, particularly as ATD or occupants become heavier. Load limited seatbelts and CRS or other advanced restraints may decrease the head and chest accelerations and neck tensions during increased accelerations as described in another study [4]. The Hu study [4] results are similar to our study except for the chest deflection. That study [4] used a production rear vehicle seat and belt system, and other advanced restraint systems.

Limitations in this study include that only two ATDs, HIII-10YO and -6YO, were examined. Only five models of CRS were tested which included NB-BPB, HB-BPB, and FFH CRS types. Two groups of data had only one test and three tests were data collected at a different facility (Table 5). Although these limitations exist the results are similar to other research conducted.

CONCLUSIONS

This preliminary study concluded that a small increase in peak sled acceleration, while maintaining constant delta-v, influenced ATD head acceleration, chest acceleration and neck tension values most. The change in pulse did not significantly affect chest deflection, and head and knee excursion of ATDs restrained in most CRS, although there may have been slight changes. Many metrics increased with the pulse changes and resulted in differences, but they only had small variations, which included belt webbing forces, chest accelerations, and other individual CRS-ATD metrics. Generally, CV results and ANOVA calculations both demonstrated the pulse influence for head accelerations and neck tensions, while other metrics varied across both analysis methods. This study includes new research related to child ATDs and CRS sensitivity during different test conditions.

Table 5. CRS and ATD test notes

Model	Type	ATD	Number Low Pulse Tests	Number Mid Pulse Tests	Number High Pulse Tests	Notes
Evenflo Amp	HB-BPB	HIII-10	3	3	3	
Chicco GoFit	NB-BPB	HIII-10	3 *	1	3	Limited data, only 1 test 23 G pulse tests
Harmony Youth	NB-BPB	HIII-6	3	3	3	
Graco Turbobooster	HB-BPB	HIII-6	1**	3	3	Limited data, only 1 test 21.5 G pulse tests
Evenflo SureRide	FFH	HIII-6	3	3	3	Tether and lower anchor forces

    * Two tests from the NHTSA database   ** One test from the NHTSA database

Low-pulse = peak approximately 21.5 G / 48 kph
Mid-pulse = peak approximately 23.0 G / 48 kph
High-pulse = peak approximately 24.5 G / 48 kph

ABBREVIATIONS
ATD - Anthropomorphic Test Devices
CPC - Crash Pulse Characteristics
CRS – Child Restraint System
CV - Coefficient of Variation (CV)
FMVSS – Federal Motor Vehicle Safety Standard
HB-BPB – high-back belt positioning booster seat
NB-BPB – no-back belt positioning booster seat
HIC – Head Injury Criteria
LATCH – Lower Anchors and Tether for Children
NHTSA – National Highway Traffic Safety Administration
FFH – Forward-facing-harness child restraint system
HIII-10YO – Hybrid III 10-year-old ATD
HIII-6YO - Hybrid III 6-year-old ATD

REFERENCES

[1] Comeau, J. L., German, A., & Floyd, D. (2004). Comparison of Crash Pulse Data from Motor Vehicle Event Data Recorders and Laboratory Instrumentation. *Proc. CMRSC-XIV*, 27-30.

[2] Locey, C. M., Garcia-Espana, J. F., Toh, A., Belwadi, A., Arbogast, K. B., & Maltese, M. R. (2012, October). Homogenization of vehicle fleet frontal crash pulses from 2000–2010. In *Annals of advances in automotive medicine/annual scientific conference* (Vol. 56, p. 299). Association for the Advancement of Automotive Medicine.

[3] Hollowell, W. T., Gabler, H. C., Stucki, S. L., Summers, S., & Hackney, J. R. (1999). Updated review of potential test procedures for FMVSS No. 208. *NHTSA Docket*, 6407-6.

[4] Hu, J., Fischer, K., Lange, P., & Adler, A. (2015). *Effects of crash pulse, impact angle, occupant size, front seat location, and restraint system on rear seat occupant protection* (No. 2015-01-1453). SAE Technical Paper.

[5] Gu, L., Tyan, T., Li, G., & Yang, R. J. (2004, January). Vehicle structure optimization for crash pulse. In *International Design Engineering Technical Conferences and Computers and Information in Engineering Conference* (Vol. 46946, pp. 945-951).

[6] Mark, S. (2003). Effect of frontal crash pulse variations on occupant injuries. In *Proceedings: International Technical Conference on the Enhanced Safety of Vehicles* (Vol. 2003, pp. 7-p). National Highway Traffic Safety Administration.

[7] Grimes, W. D., & Lee, F. D. (2000). *The effect of crash pulse shape on occupant simulations* (No. 2000-01-0460). SAE Technical Paper.

[8] Hauschild, H. W., Halloway, D., & Pintar, F. A. (2015). ATD spine response as a function of crash pulse input. *Traffic Injury Prevention*, *16*, S237-S240.

[9] Kullgren, A., Krafft, M., Nygren, Å., & Tingvall, C. (2000). Neck injuries in frontal impacts: influence of crash pulse characteristics on injury risk. *Accident Analysis & Prevention*, *32*(2), 197-205.

[10] Rao, R. D., Berry, C. A., Yoganandan, N., & Agarwal, A. (2014). Occupant and crash characteristics in thoracic and lumbar spine injuries resulting from motor vehicle collisions. *The Spine Journal*, *14*(10), 2355-2365.

[11] Bilston, L. E., Clarke, E. C., & Brown, J. (2011). Spinal injury in car crashes: crash factors and the effects of occupant age. *Injury Prevention*, *17*(4), 228-232.

[12] NHTSA. (2019b). NHTSA Standard Seat Assembly; FMVSS No. 213, NHTSA-213-2016 Drawings. Child Frontal Impact Sled – V2. May 2019. Docket No. NHTSA-2020-0093-0004

[13] NHTSA. (2020). NHTSA Research Procedure for the Proposed FMVSS No. 213 Frontal Impact Test. Nov 2020. Docket No. NHTSA-2020-0093-0016

[14] NHTSA. (2019a). Federal Motor Vehicle Safety Standard (FMVSS) No. 213 Updated Frontal Standard Seat Assembly. Solicitation no. 693JJ919R000042. July 19, 2019

[15] SAE International Surface Vehicle Recommended Practice. Instrumentation for Impact Test, SAE J211. 2014.

[16] Mertz, H. J., Irwin, A. L., & Prasad, P. (2003). Biomechanical and scaling bases for frontal and side impact injury assessment reference values (No. 2003-22-0009). *SAE Technical Paper*.

[17] Pintar, F. A., Yoganandan, N., Maiman, D. J., Scarboro, M., & Rudd, R. W. (2012, October). Thoracolumbar spine fractures in frontal impact crashes. In *Annals of Advances in Automotive Medicine/Annual Scientific Conference* (Vol. 56, p. 277). Association for the Advancement of Automotive Medicine.

[18] Doud, A. N., Weaver, A. A., Talton, J. W., Barnard, R. T., Meredith, J. W., Stitzel, J. D., ... & Miller, A. N. (2015). Has the incidence of thoracolumbar spine injuries increased in the United States from 1998 to 2011?. *Clinical Orthopedics and Related Research®*, *473*(1), 297-304.